

2006-01-01

An Investigation into the Behaviour of Sheet Metal Workpieces when Subjected to Simultaneous Double Bending

Arthur Henry
Technological University Dublin

Follow this and additional works at: <https://arrow.tudublin.ie/engmas>



Part of the [Engineering Commons](#)

Recommended Citation

Henry, A. (2006). *An investigation into the behaviour of sheet metal workpieces when subjected to simultaneous double bending*. Technological University Dublin. doi:10.21427/D7K90K

This Theses, Masters is brought to you for free and open access by the Engineering at ARROW@TU Dublin. It has been accepted for inclusion in Masters by an authorized administrator of ARROW@TU Dublin. For more information, please contact arrow.admin@tudublin.ie, aisling.coyne@tudublin.ie, vera.kilshaw@tudublin.ie.

An investigation into the behaviour of sheet metal workpieces when subjected to simultaneous double bending

by

Arthur T. Henry

Submitted in fulfilment of the requirements for M. Phil.

2006

Supervisor: Dr. Gerry Woods

The work presented in this thesis was conducted at The Dublin Institute of Technology, Ireland.

This is to certify that all the work described in the following document is the sole work of the author, with the exception of LabView interface programming, which was performed by Mr. John Kealy M.Sc.



Arthur T. Henry



Date

Acknowledgement

I would like to sincerely like to thank Dr. Gerry Woods of the Dublin Institute of Technology for his guidance throughout the duration of this project.

Abstract

Simultaneous double bending, where two 90° bends are formed in a single workpiece, in close proximity to each other and in alternate directions, are common in the metal forming industry, especially so in small production batches where press brakes and their associated tooling is extensively used. This bending process, resulting in what is commonly called a 'joggle' bend, is executed using specially shaped forming dies. The geometry of these dies determines the geometry of the bend and also the amount of sliding and / or stretching that takes place in the workpiece during the forming process. This in turn determines the forces and therefore the stresses experienced by the dies, and the strains experienced by the workpieces.

The objectives of this research were as follows:

- To determine by experiment the relationship between the displacements of metal forming dies, the forces that they are subjected to at particular displacements and the geometry of the forming dies.
- To observe and record, via the use of etched grid circles, the strain distribution on the surfaces of chosen experimental test pieces.
- To compare the experimental results with results predicted by Finite Element Analysis (FEA) using Deform PC Pro, a commercially available elasto-plastic capable FEA package.
- To determine, using the same FEA package, the elastic stresses in the dies and the plastic strain in the workpieces at various stages throughout the forming process.
- Having considered both experimental and analytical data, to determine whether general conclusions can be drawn that have not been observed previously and which would allow for better understanding and control of the process.

In order to complete the objectives, a test rig was designed and built; forming dies of various profiles were manufactured; experimental work was conducted and compared with FE predictions. A number of conclusions were noted that can improve the forming process and component design. The principal conclusions are:

- Interference of strain fields on adjacent bends is a function of geometry of the die, with no interference occurring at die step heights of 10.5 mm and above, for workpiece materials of 3 mm thickness, whether aluminium or steel. No useful experimental or finite element work was done on material thicknesses other than 3mm.
- Workpiece thinning occurs when the die step height is less than twice the material thickness.
- Incremental force required for incremental strain in the workpiece is a function of displacement and has a continually rising characteristic.
- Incremental force required for incremental strain in the workpiece is also a function of the geometry of the die, and the profile of the applied force – displacement curve changes significantly with die geometry.
- It is difficult to identify a relationship between die step height and total energy required for deformation, for workpieces made from either steel or aluminium.

Table of Contents

| | Section : |
|---|---------------|
| | Page |
| <i>Declaration</i> | i |
| <i>Acknowledgements</i> | ii |
| <i>Abstract</i> | iii |
| <i>Table of contents</i> | v |
| 1. Introduction | 1 : 1 |
| 1.1. Motivation | 1 : 1 |
| 1.2. Mechanics and measurement of the bending process | 1 : 2 |
| 1.2.1. Plasticity. | 1 : 2 |
| 1.2.2. Forces required to produce a bend. | 1 : 2 |
| 1.2.3. Material allowance for bending | 1 : 5 |
| 1.2.4. Spring-back. | 1 : 6 |
| 1.2.5. Grid circle strain analysis. | 1 : 6 |
| 1.2.6. Forming limit diagrams. | 1 : 7 |
| 1.3. Bending of sheet metal: general description of common processes | 1 : 9 |
| 1.3.1. General principles. | 1 : 9 |
| 1.3.2. Force generation equipment. | 1 : 10 |
| 1.3.3. Air-bending and V-bending | 1 : 12 |
| 1.3.4. Wiping | 1 : 13 |
| 1.3.5. U-Bending | 1 : 14 |
| 1.3.6. Joggle Bending | 1 : 15 |
| 1.4. Objectives of the study | 1 : 17 |
| 2. Literature review and associated theory | 2 : 1 |
| 2.1. Theory of finite element | 2 : 1 |
| 2.2. Review of papers published on sheetmetal forming | 2 : 13 |
| 2.2.1. Elastic and plastic deformation of metals | 2 : 14 |
| 2.2.2. Finite element analysis: Theoretical background | 2 : 14 |
| 2.2.3. Current research: metal bending and metal forming | 2 : 15 |
| 2.2.3.1. Introductory papers | 2 : 15 |
| 2.2.3.2. Sheet metal bending | 2 : 16 |
| 3. Experiment design and testing | 3 : 1 |
| 3.1. Design and manufacture of the bending rig | 3 : 1 |
| 3.2. Die design and manufacture | 3 : 4 |
| 3.2.1. Tooling manufacture | 3 : 5 |
| 3.3. Instrumentation and calibration | 3 : 6 |
| 3.3.1. Load transducer calibration | 3 : 6 |
| 3.3.2. Displacement transducer calibration | 3 : 8 |
| 3.4. Material properties of the workpieces | 3 : 9 |
| 3.4.1. Steel | 3 : 9 |
| 3.4.2. Aluminium | 3 : 9 |
| 3.5. Workpiece design and manufacture | 3 : 10 |
| 3.5.1. Geometry | 3 : 10 |
| 3.5.2. Material | 3 : 11 |
| 3.5.2.1. Steel | 3 : 11 |
| 3.5.2.2. Aluminium | 3 : 11 |
| 3.5.3. Workpiece manufacture | 3 : 11 |
| 3.5.3.1. Steel | 3 : 11 |
| 3.5.3.2. Aluminium | 3 : 12 |
| 3.5.4. Grid circle marking | 3 : 12 |
| 3.6. Description of testing | 3 : 17 |

| | | |
|-------------|--|--------------|
| 3.6.1. | Experiment operation | 3 : 18 |
| 3.7. | Measurement and recording | 3 : 23 |
| 3.8. | Finite element software and setup | 3 : 23 |
| 4. | Results and discussion | 4 : 1 |
| 4.1. | Experimental and FEA results, AISI 1010 Steel | 4 : 1 |
| 4.1.1 | Exp. vs. FEA results, 3mm AISI steel, 4.5 mm dies | 4 : 2 |
| 4.1.2 | Exp. vs. FEA results, 3mm AISI steel, 6.0mm dies | 4 : 3 |
| 4.1.3 | Exp. vs. FEA results, 3mm AISI steel, 7.5 mm dies | 4 : 4 |
| 4.1.4 | Exp. vs. FEA results, 3mm AISI steel, 9.0 mm dies | 4 : 5 |
| 4.1.5 | Exp. vs. FEA results, 3mm AISI steel, 10.5 mm dies | 4 : 6 |
| 4.1.6 | Exp. vs. FEA results, 3mm AISI steel, 12.0 mm dies | 4 : 7 |
| 4.1.7 | Exp. vs. FEA results, 3mm AISI steel, 16.5 mm dies | 4 : 8 |
| 4.2. | Experimental and FEA results, 6062 Aluminium | 4 : 9 |
| 4.2.1 | Exp. vs. FEA results, 3mm 6062 aluminium, 4.5 mm dies | 4 : 10 |
| 4.2.2 | Exp. vs. FEA results, 3mm 6062 aluminium, 6.0 mm dies | 4 : 11 |
| 4.2.3 | Exp. vs. FEA results, 3mm 6062 aluminium, 7.5 mm dies | 4 : 12 |
| 4.2.4 | Exp. vs. FEA results, 3mm 6062 aluminium, 9.0 mm dies | 4 : 13 |
| 4.2.5 | Exp. vs. FEA results, 3mm 6062 aluminium, 10.5 mm dies | 4 : 14 |
| 4.2.6 | Exp. vs. FEA results, 3mm 6062 aluminium, 12.0 mm dies | 4 : 15 |
| 4.2.7 | Exp. vs. FEA results, 3mm 6062 aluminium, 16.5 mm dies | 4 : 16 |
| 4.3. | Discussion of experimental and FEA results. | 4 : 17 |
| 5. | Conclusion | 5 : 1 |
| 5.1. | Relationship between displacement, force and geometry | 5 : 1 |
| 5.1.1 | Forces vs. displacements | 5 : 1 |
| 5.1.2 | Forces vs. die geometry | 5 : 2 |
| 5.2. | Observation of strain distribution via grid circles | 5 : 4 |
| 5.3. | Comparison of experimental and FEA results | 5 : 5 |
| 5.4. | Elastic stresses in dies, plastic strain in workpieces | 5 : 8 |
| 5.5. | General conclusions | 5 : 11 |
| Appendix 1 | Hydraulic circuit | |
| Appendix 2 | Die profiles | |
| Appendix 3 | Calibration of load and displacement transducers | |
| Appendix 4 | Correlation of standards for steel | |
| Appendix 5 | Verification of Young's modulus for workpieces | |
| Appendix 6 | Transducer Characteristics | |
| Appendix 7 | FEA outputs | |
| Appendix 8 | Drawings of test rig | |
| Appendix 9 | FE analysis method | |
| Appendix 10 | Bibliography | |

1. Introduction

1.1 Motivation

Manufacturers in the sheet metal processing industry are subject to a number of commercial and market forces, few of which are within their control. With the exception of the automotive and white goods industries, specialist sheet metal processors are an insignificant group in terms of processed tonnage. This puts suppliers to these companies, e.g., steel suppliers, in a powerful position to influence profitability. Often buyers specify the product entirely by reference to the engineering drawings and therefore are in a position to anticipate manufacturing costs and change suppliers with minimal switching costs. Modern purchasing strategies are such that customers may buy a significant proportion of their requirements from one or two suppliers, meaning that suppliers seeking to enter the market may have to cut costs severely to gain entry. In addition there is the continual threat of substitute products, for example plastics, in order to reduce costs. Finally, there is an ever-increasing demand for product quality.

All of these factors force manufacturers to focus increasingly on the application of manufacturing technology. The requirement for flexible manufacturing in terms of smaller production batches, diverse materials and shorter cycle times has led to the increasing use of air bend tooling, with its associated risk of unpredictable bending behaviour. This has subsequently motivated research workers to investigate the response of sheet materials to the air bending process.

Although considerable research has taken place in an attempt to predict the behaviour of material during the bending process [1,2,3,4], it has until very recently been on the basis of unidirectional constant velocity relative motion between the punch and die. Researchers are now beginning to recognise the fact that so many parameters influence the result of the bending process that a new manufacturing strategy must be employed. Hence, the most recent research papers work on the basis of closed loop control systems [5,6,7], where the input parameter to the system is not the relative punch and die motion, but the bent up angle of the workpiece.

Many of the difficulties encountered in the forming of sheet metals can be categorised into four major groups as follows:

| | |
|----------------------|--|
| Material parameters: | Thickness variations, (intra-batch and inter-batch), anisotropy, change in material behaviour with respect to strain or strain rate. |
| Process parameters: | Machine deflection, accuracy, precision, repeatability and control. In addition to these parameters, further errors can be introduced by prior |

processing, e.g., inaccurate cutting of the workpiece blanks, poor handling causing material damage, improper inspection etc.

Modelling inaccuracies: Mathematical or empirical models may make incorrect assumptions, and may be required to be extremely complex in an effort to reflect material behaviour. Care must be taken to ensure boundary conditions, load cases, material constants and element choices are correct. In addition, these models often require specialist interpretation.

Output requirements: The requirements for accuracy, low cost production, repeatability etc. are ever increasing.

1.2. The mechanics and measurement of the bending process.

1.2.1. Plasticity.

The extent to which a material exhibits plasticity is significant in evaluating its suitability for bending. Plasticity is the ability of a material to sustain permanent deformation due to the application of a force. Metals may be plastically anisotropic depending on their deformation history, i.e. the material exhibits differing physical properties in different directions at a point in the material.

1.2.2. Forces required to produce a bend.

For the purposes of this investigation, the following assumptions are made:

- Bends occur about a straight axis, independently of other bends and the bent surface is part of a cylinder. This correlates with the linear nature of press brake tooling and with the fact that adjacent bends are usually multiples of material thickness away from each other. A constant radius (bend considered to be part of a cylinder) simplifies calculations in terms of bend deduction and bend allowance.
- Final (permanent) deformation of the sheet is limited to the region of the bend. This correlates with the fact that bending moments large enough to cause plastic deformation are restricted by the geometry of the tooling to the region of the bend. In effect no bending moment is applied to the workpiece flanges.
- During bending, plane sections of the workpiece remain plane, and converge to a centre of curvature. This is due to the fact that the strain experienced by any particular lamina

parallel to the neutral plane is considered to be a linear function of its distance from the neutral plane.

- The principle directions of stress and strain coincide with the radial and circumferential directions of the bends. Because the load applied to any element on the bend is perpendicular to the bend axis, i.e., parallel to the direction of increasing curvature as the bend progresses, the direction of the load will be the first principal direction, i.e., in the circumferential direction of the bend. The second principal direction will be normal to this, i.e. the radial direction, and the third principal direction will be parallel to the axis of the bend.
- There are no stress or strain *gradients* in the circumferential direction. This is assumed in order to simplify the mathematical treatment of the system.

In order to approximate the bending moment required to produce a bend in a particular work piece, we consider a simplified analysis of the stresses experienced by an ideal, non-strain hardening material, subject to constant moment M , all elements of which behave plastically, with reference to Figure 1.1.

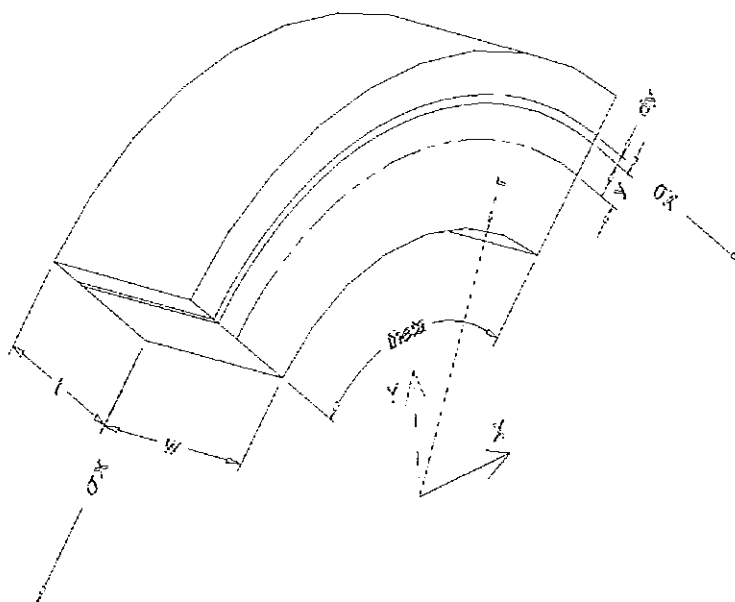


Figure 1.1 A workpiece undergoing bending

Considering any plane section normal to the neutral surface and parallel to the axis of the bend, the total moment resisting the applied moment is given in equation (1.1).

$$M = \int_{-\frac{t}{2}}^{\frac{t}{2}} w \sigma_x y dy = 2 \int_0^{\frac{t}{2}} w \sigma_x y dy \quad (1.1)$$

For a perfectly plastic material with no elastic core, $\sigma_x = \sigma_o =$ flow stress; i.e., the stress required to produce plastic flow. Then,

$$M = 2w\sigma_o \int_0^{\frac{t}{2}} y dy = \frac{w\sigma_o t^2}{4} \quad (1.2)$$

Consider the bending moment produced on a workpiece in a V-bending process, referring to figures 1.2 and 1.3.

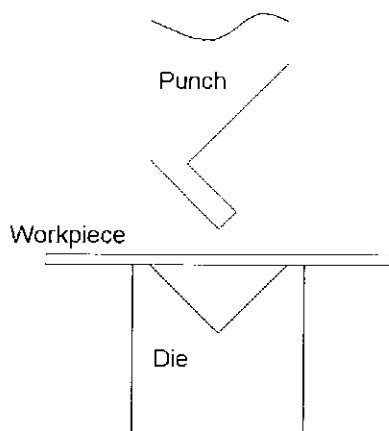
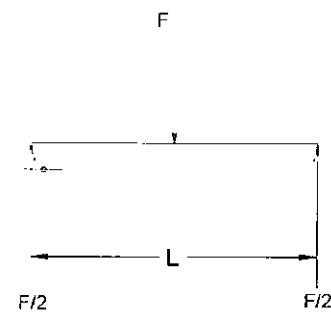


Figure 1.2. Schematic diagram of bending device

This can be modelled as



Max bending moment = $FL/4$

Figure 1.3. Body force diagram of workpiece at commencement of bending.

It can be seen, referring to Figure 1.3 that the maximum bending moment available at the centre of the workpiece is $FL/4$, hence

$$\frac{FL}{4} = \frac{w\sigma_o t^2}{4} \Rightarrow F = \frac{w\sigma_o t^2}{L}, \text{ where} \quad (1.3)$$

F = Force required to just initiate the bend

w = length of bend

σ_o = yield stress of the material

t = material thickness

L = V-die width

This formula usually needs to be corrected to allow for work hardening, friction, anisotropy, etc.

1.2.3. Material allowance for bending.

The un-deformed length of material for a bend, or the bend allowance (BA) is usually made on the basis of length of the arc along the shifted neutral plane as follows:

$$BA = (\theta / 360) (2\pi (r + kt)), \quad (1.4)$$

where r is the radius of the inner surface of the bend or punch radius, θ is the angle of the bend in degrees and k is a dimensionless factor usually between 0.3 and 0.5 depending on the material in question, and delineates the displacement of the neutral plan during bending. Since the neutral axis shifts toward the centre of curvature, the last term, kt , varies from $0.3t$ to $0.5t$. This bend allowance is used to determine the length of the flat strip before bending by adding l_1 , l_2 and BA as shown in figure 1.4.

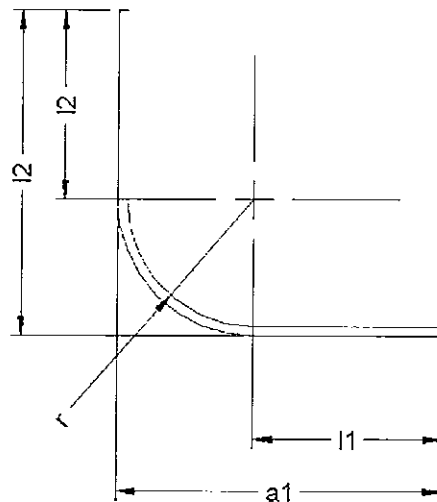


Figure 1.4. Bend allowance for material

In practice it is difficult to measure l_1 or l_2 , especially when the bend radius is large compared to the material thickness. In addition, the curvature of the workpiece may not be a constant radius. In these cases the length of the flat strip is determined by experiment, and a *bend deduction* (BD) is used, where total length before bending = $a_1 + a_2 - BD$. This method is inherently more accurate as measurements are easier to make, and as material similar to the workpiece is used in the corresponding tooling setup, previous deformation history, anisotropic behaviour and other material and tooling properties are reflected accurately. This method is important in precision sheet metal fabrication, i.e., for the computer industry.

1.2.4. Spring-back.

During bending, the outer surface of the bent sheet is placed in tension and the inner surface is placed in compression (the applied tensile load is assumed to be zero in this case). As bending progresses, the neutral surface shifts from the centre of the cross section of the sheet towards the centre of curvature or the compression side. On removal of the load, the material partially elastically recovers, and the final angle of the bend is less than the angle that obtains when the tooling is in its limiting position. This partial elastic recovery is called spring-back, and the spring-back error is defined as:

$$\text{Spring-back error} = (\theta_1 - \theta_2) / \theta_1 \quad (1.5)$$

where θ_1 and θ_2 are the bend angles before and after bending load is removed.

Determination and correction of spring-back error is a significant problem in the sheet metal industry. Two approaches to correcting the problem are *over-bending* and *setting*. During over-bending, the punch and die angles are reduced to about 88° when a 90° bend is required and the material is air bent. This means that careful setting of the tooling is necessary and accurate control of the downward stroke of the press is required. During setting, the punch is allowed to come into hard contact with the material in the die, causing local plastic flow (and occasionally material thinning) in the region of the bend. The punch radius may be small, i.e., 0.5 times the material thickness or less, to facilitate this process.

1.2.5. Grid circle strain analysis.

During the forming operation various areas within the material workpiece may be subjected to differing strain modes by stretching, compression, bending, torsion etc. Hence the simple consideration of the bending process above may not explain bending behaviour fully.

Grid circle strain analysis is used to indicate maximum tensile and compressive strains on different areas of the workpiece during deformation. A grid consisting of an array of chemically etched circles (usually 2.5 millimetres in diameter) is produced on the blank workpiece. The workpiece is subject to deformation and removed from the die. The grid is then examined in the areas of large strains. The etched circles have been transformed to ellipses due to tensile or compressive strains, as shown in figure 1.5 below.

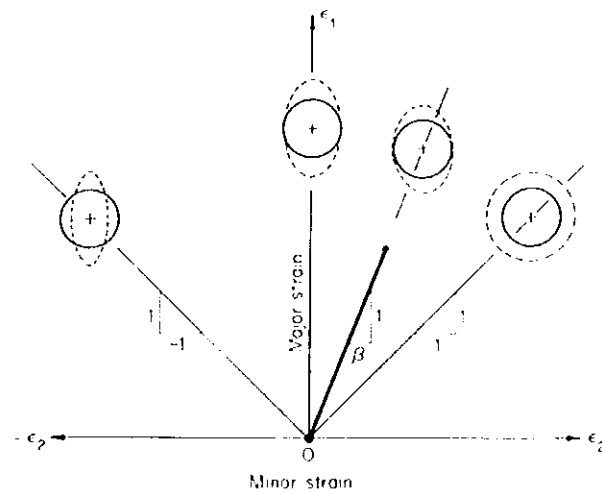


Figure 1.5 Transformation of grid circles to ellipses during strain

from *Mechanics of Sheetmetal forming*, Z. Marciniak and J. Duncan

Edward Arnold 1st Edition 1992 p. 35

The major and minor axes of the ellipses are compared with the original circle diameters and the strain at local areas can be determined with reference to figure 1.6. Strain magnitude and type i.e., compression or tension, can be determined locally. These strains and the combinations of them are compared with forming limit diagram strains, see section 1.2.6. to determine how close the material is to failure. Many bends may be close to failure, but not yet at the point at which they tear. During tool trials slow press speeds, additional lubrication, careful operation of the press etc., will allow the production of all these bends without failure. However during normal production these carefully controlled conditions may not apply. Therefore the use of grid circle analysis will allow the identification of critical areas in the component and preventative measures may be taken during die manufacture.

1.2.6. Forming limit diagrams.

The forming limit diagram gives a graphical representation of behaviour of a sheet material when subject to biaxial stress. Grid circle strain analysis techniques are used and individual pieces of material are subject to loading, i.e., (biaxial tension – tension) or (biaxial tension – compression) stresses, until the material fails and cracks result.

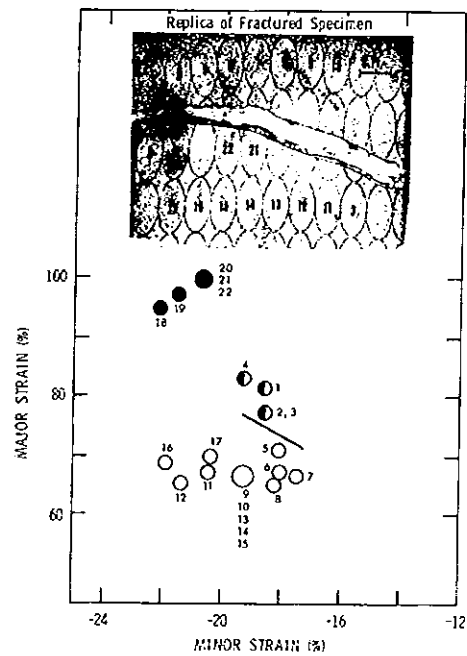


Figure 1.6 Material marked with grid circles and loaded to fracture

From Manufacturing and Engineering Technology, Serope Kalpakjian
Addison-Wesley 3rd 1995 Edition p. 458

After plastic deformation, the major and minor axes of the ellipses at the failure site are observed and strain is evaluated. These *limiting* major and minor engineering strains are plotted against each other on two perpendicular axes of the forming limit diagram (FLD) as shown in figure 1.7 below.

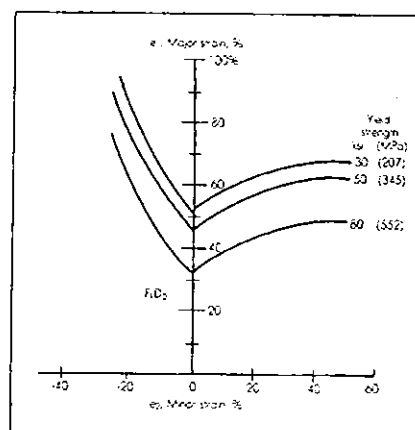


Figure 1.7 A forming limit diagram for three materials

From Manufacturing and Engineering Technology, Serope Kalpakjian
Addison-Wesley 3rd 1995 Edition p. 457

The vertical axis is used to plot the major engineering strain, the horizontal axes is used to plot the minor engineering strain, as a matter of convention. The left-hand portion of the diagram indicates states of stress in the material that would be encountered in deep drawing operations, the right hand portion of the diagram indicates the type of strain that would be encountered in stretch forming. The plot is the critical strain band that separates the failure from the non-failure states of material.

In order to produce a forming limit diagram a number of workpieces are prepared for biaxial loading by etching them with a matrix of circles. Each workpiece is subjected to a known strain in the first principal direction, and then, while held in the strained condition, subjected to a strain in the second principal direction. This second principal strain is increased until the test piece fractures. The test piece is then reassembled and the principal strains recorded as a series of co-ordinates. A second workpiece is subjected to a higher first principal strain and the process repeated, establishing a second set of co-ordinates. This complete cycle is repeated until enough co-ordinates are available to produce a smooth profile, the forming limit diagram.

When a forming limit diagram is available for a particular material type, it is used in conjunction with the grid circle analysis technique for a given formed component to determine how close to failure the various areas are within the component.

1.3. Bending of Sheet Metal: General description of common processes.

1.3.1. General principles.

Bending may be described as the application about a linear axis of a moment to a material, causing alternate sides about the neutral plane of the material to exceed the yield strength of the material, resulting in a permanent angular deformation of the material. Sheet metal can be bent by an imposed moment, by stretching over a cylindrical form or by a combination of both moment and tension. When bending by imposed moment, equal, opposite and axially displaced forces are applied to the material via punches and dies. The axial distance between the effective edges of the punches and dies is large compared to the thickness of the material, and the forming die edges are normally radiused. The material properties and geometric arrangement of the tooling is such that its deflection is negligible compared to the workpiece, and that it remains elastic, i.e., at all points in the tooling the applied stress is well below the elastic limit of the tooling material. This discussion concentrates on bending methods using applied moments only, for materials at ambient temperature.

In order for bending as described to take place, the following features are required.

- A method of applying a force (press).
- A method of directing a force or converting the force to a moment (tooling).
- A workpiece that will deform plastically.

1.3.2. Force generation equipment.

Presses provide a method to move a force through a distance, realised by a slide moving relative to a fixed frame. The slide displacement provides the action force that is transmitted through the punch, workpiece and die to the frame. Presses can therefore be classified on the basis of both the maximum available force (usually specified in terms of tonnes force) and the maximum stroke of the press (usually specified in millimetres). Note that for mechanically actuated presses the force available at any specific stroke position may vary with position or time, whereas hydraulically operated presses will normally have a fixed available force regardless of stroke position or time.

For sheet metal bending *press brakes* are normally used. This press type is characterised by a pair of side frames connected to a long narrow bed and a reciprocating slide, as shown in figure 1.8, which includes a view of typical press brake tooling. The type of press shown is a hydraulically actuated down-acting press, i.e., the slide or ram moves down on to the workpiece, relative to the fixed frame.

Note also the fact that the press in this instance controls the alignment of the punch and die, i.e., no die set is used. This leads to a requirement for accurate machining and fitting of press components to ensure movement of the ram parallel to the bed and accurate setting of the punch and die positions.

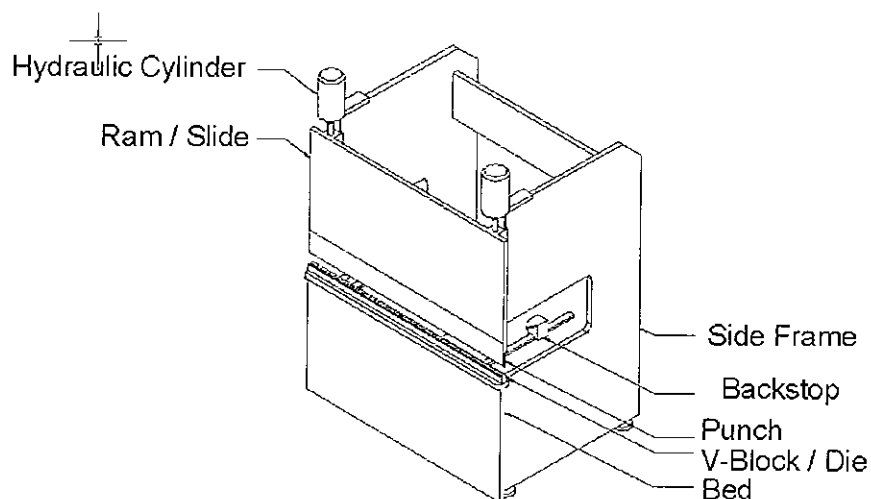


Figure 1.8 A Press Brake

Because the action forces are vertically applied to each end of the ram and the workpiece is usually in the middle of the ram, this can lead to distortion of the ram under the applied loads. The deflection profile is shown in figure 1.9.

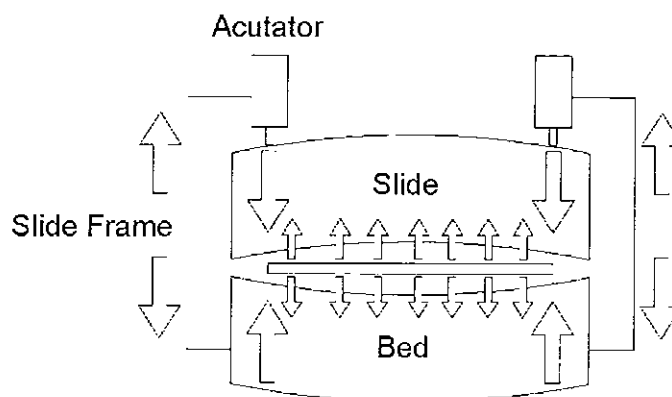


Figure 1.9 Deflection profile of a down-acting press

As can be seen from this deflection profile, the distance between the slide and bed increases towards the centre of the press. This means that the workpiece will be over-bent at each end and under-bent in the middle. Press operators often use shim material between the press bed and the bottom die to reduce this error, but this is a difficult, arbitrary and time-consuming process.

An up-acting press, shown in figure 1.10, partially alleviates this problem by maintaining a similar distance between the bed and the ram of the press. Long press brakes are more likely to be up-acting presses, or to have some mechanical compensation for deflection in the press members.

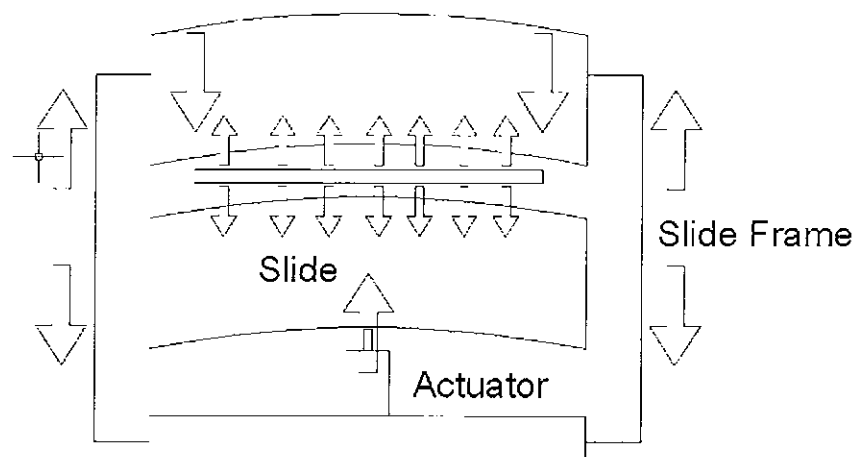


Figure 1.10 Deflection profile of an up acting press

In addition to the main force generating or constraining members, press brakes will also incorporate a set of movable, usually computer numerically controlled backstops to position the workpiece relative to the tooling, a control system to govern the position of the ram and mechanical or opto-electronic guards.

Among the methods used to apply moments to sheet-metalwork pieces are the following;

- Air bending
- V-bending
- Wiping
- U-bending
- Joggle bending

1.3.3. Air-bending and V-bending.

Both of these bending processes convert the longitudinal motion of the press to a bending moment by supporting the workpiece using a fixed, v-shaped die at either side of and beneath the descending punch. The punch and die are aligned axially so that when the punch descends through its full stroke, it will mate with the die without lateral loading.

V-die bending is a non-steady process. With punch motion, the parameters that are constantly affected are workpiece geometry, bending moments and force directions, material response caused by elasto-plastic strain, and strain hardening. Several consecutive processes are involved in V-die bending as shown in the figure 1.11. Initially, the workpiece passes through the *air bending* stage, (a, b, c). At the outset bending is elastic. Plastic

deformation sets in when the stress in the outer fibre exceeds its elastic limit. As the bending progresses, it reaches a stage when the legs of the bent sheet or plate become tangent to the sides of the die near both support locations (d).

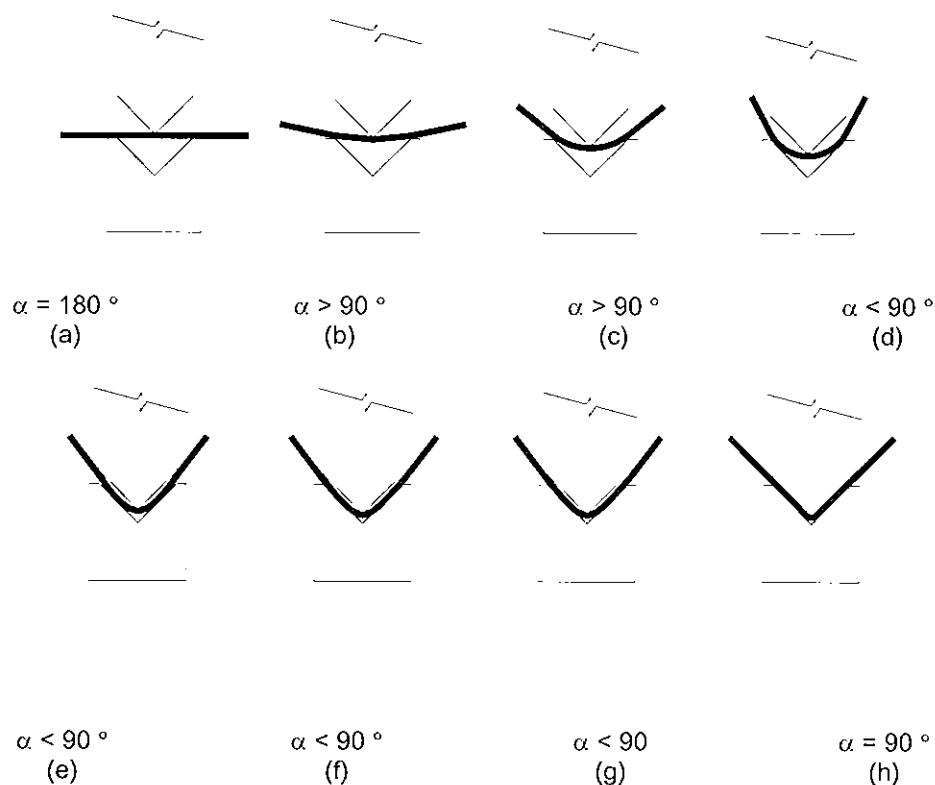


Figure 1.11 Consecutive processes in V-bending

At this instant (e) the transition from air bending to *V-bending* or *setting* begins. Additional downward motion of the punch causes the ends of the workpiece to lift off from the die faces. With still further downward motion of the punch, the bend angle opens up again (f, g). The bending angle is then forced to approach the die angle, and the inner radius of curvature of the workpiece adjusts to the curvature of the punch (h). One limitation with the V-bending process is that the required bend radius will affect the minimum size of the bend flange.

1.3.4. Wiping.

During this process the bending moment is supplied by clamping one side of the workpiece between the die and a spring or hydraulically loaded pressure pad and applying a force via a moving punch on the other side, as shown in figure 1.12. One of the difficulties of this method is that it causes a lateral force to be developed between the punch and the die, which must be resisted by the supporting members of a die set, which involves additional cost. In addition, it requires the geometry of the tooling to be such as to permit relative motion between the pressure pad and the punch and a method to supply the pressure pad force. This leads to

additional design complications. This design is also problematic in terms of control of elastic spring-back; determining the amount of relief on each side of the punch or die to allow for over-bending is an empirical and time consuming process. This type of tool setup is however useful for producing multiple bends in a single press cycle, is quick to install in the press and requires limited skill to operate.

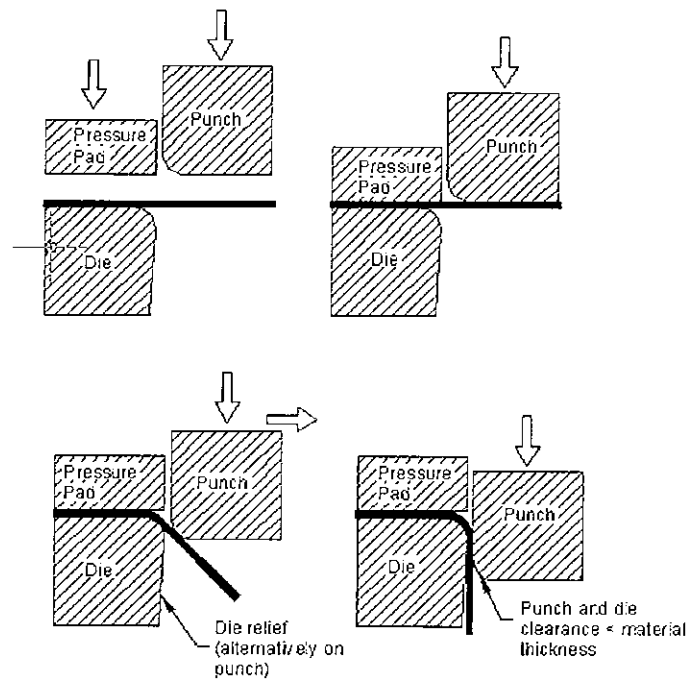


Figure 1.12 Wiping

1.3.5. U-Bending.

U-bending, shown in figure 1.13, is very similar to wiping, except that the material is bent in at least two places at the same time and the bends are positioned relative to each other so as to balance the lateral forces developed during the operation. In addition, there may be a form of ejection system incorporated in the tooling to remove the workpiece from the punch. Normally the pressure pad ejects the component from the die. In common with the wiping process, tool relief for over-bending is empirically designed and the process can produce multiple bends in one press cycle. Note, however, that the directions of the bends are the same, i.e., both in the upward (or downward) direction.

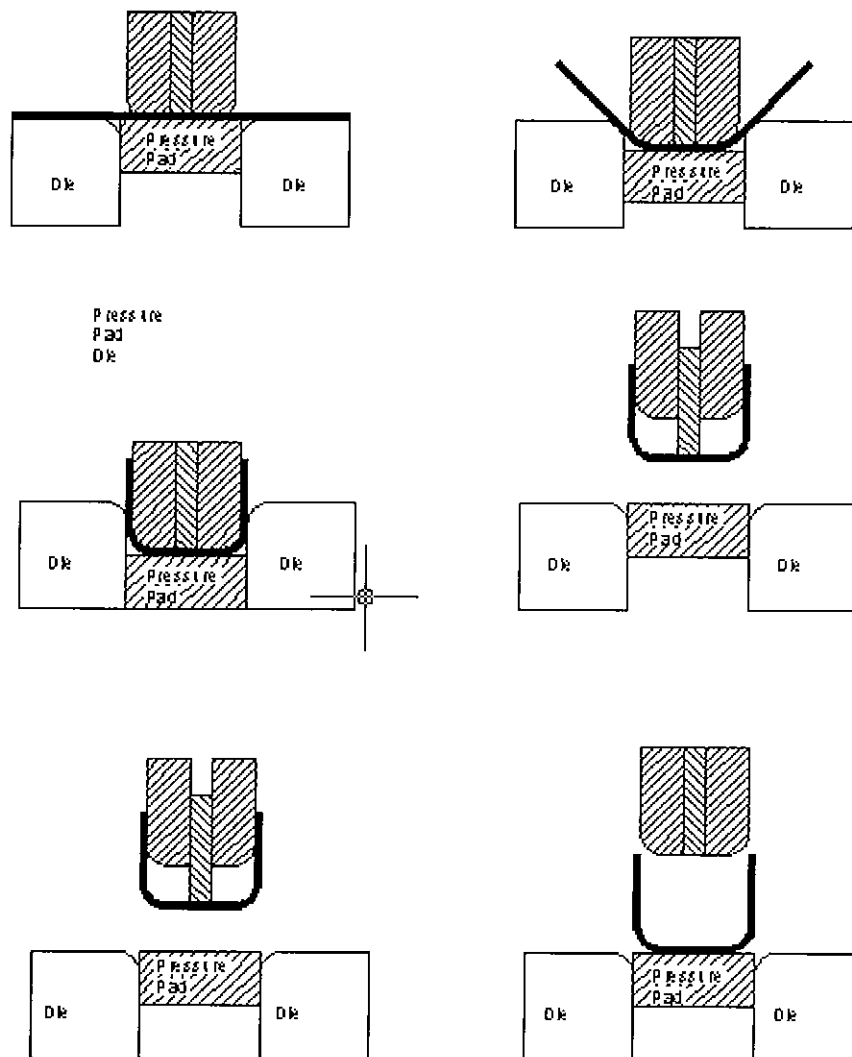


Figure 1.13 U-bending

1.3.6 Joggle Bending.

When forming sheet metal components, there is often a requirement for two ninety-degree bends in close proximity to each other, and in alternate directions. This is known as a *joggle* bend. Forming two v-bends back-to-back cannot usually produce this particular profile. This is because the minimum distance between any two v-bends is normally a little more than half of the v-width, as shown in figure 1.14.

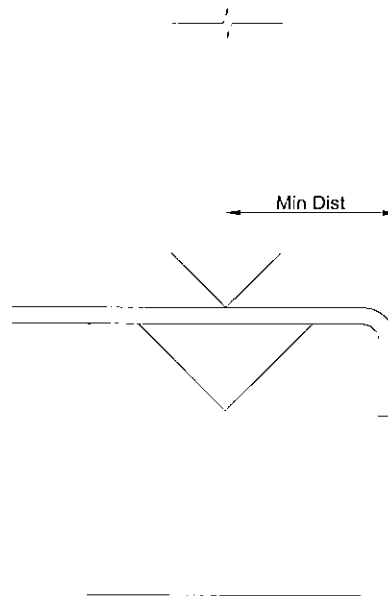


Figure 1.14 Minimum distance to centre of bend using V-die

This leads to the use of special joggle profile tooling, shown in figure 1.15. The step height x and angle α shown depend upon the material thickness and the required step height of the component. Therefore there is no standard stepped tooling normally available and it is usually manufactured on a per-job basis. This in turn means that this tooling is normally in a soft or toughened condition, as opposed to being fully hardened, as is the case for commercial tooling. The tooling is left unhardened as the hardening, tempering and grinding of this type of tooling, where the length dimension is often orders of magnitude greater than the other two dimensions, requires special techniques and equipment. A particular problem with the heat treatment of these types of geometries is the maintenance of straightness and flatness of the tool during and after processing.

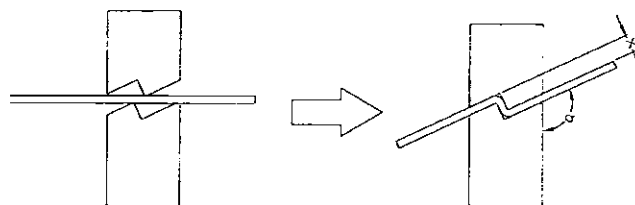


Figure 1.15. Joggle bending

As can be seen from the profile of this tooling, material between the areas undergoing bending is forced to undergo strain to a certain degree. In addition, material may flow over the tool radii and into the area undergoing a high longitudinal strain. The ratio of material strain to

material flow is likely to depend upon the tool radius, the material thickness, the material hardness, lubrication and tooling angle. However, the success of the bending action will also depend upon some of these parameters. For example if the tool radius were too large then there would not be enough plastic strain within the depth of the material to offset any of the effects of elastic spring back. This will be true regardless of the press force used, unless the force is large enough to overcome the yield stress of the material in the normal-to-plane direction. As the tooling will be in a soft condition more often than not it is unlikely that a force of this magnitude would be used.

Joggle bending will be the primary focus of this study in order to increase understanding of the joggle bending process, and hence establish a knowledge base upon which the manufacturing process may be improved.

1.4 The objectives of this study are as follows:

- i. To determine by experiment the relationship between the displacements of metal forming (joggle) dies, the forces that they are subjected to at particular displacements and their geometry. This will necessitate the design, manufacture and calibration of a workpiece test rig. This rig must provide sufficient force and displacement to allow experiments to be conducted on common materials and thicknesses. It must allow the recording of real time data and allow the data to be organised and presented in a meaningful way. A series of dies (upper and lower) are required, with varying geometries, to allow for a range of experiments to be executed.
- ii. To observe and record, via the use of etched grid circles, the strain distribution on the surfaces of chosen experimental test pieces.
- iii. To compare the experimental results with results predicted by Finite Element Analysis using Deform PC Pro ®, a commercially available elasto-plastic capable FE package. This will involve the study of output data from both the experimental rig and the FE package, noting both the comparisons and contradictions in the data sets.
- iv. To determine, using the same FE package, the elastic stresses in the dies and the plastic strain in the workpieces, at various stages throughout the forming process. This would check that the dies remained elastic throughout the experimental process and that the workpiece materials were not exposed to excessive strain.
- v. Having considered both experimental and analytical data, to determine whether general conclusions can be drawn that have not been observed previously and which would allow for better understanding and control of the process.

The proposed outcome of the study will be a theoretically and experimentally correlated model of the behaviour of work hardening materials undergoing this type of bending process.

2. Literature review and associated theory

2.1. Theory of finite element

Finite element analysis or the finite element method is a computer based numerical technique, started in the early 1950s, as a tool for the structural and stress analysis of complex shapes. This method of solution has become well established in the complex problems of stress analysis, vibrations, heat transfer etc. The system employs a method of solution whereby bulk materials subject to forces, temperature, and displacement etc. are divided into small discrete elements, whose properties are known, and individually described. These individual descriptions are then combined to find an overall description of the problem, to which may be applied a numerical method of solution. The finite element method has thus been defined as a method of piecewise approximation in which the approximating function is formed by connecting simple functions, each of which is defined over a small region (element). (Cook, et.al., (10))

The finite element method is versatile, in that it can model arbitrary shapes and loading conditions. In addition, the model resembles the physical entity. Finite element software packages are commercially available, and can now run on desktop PCs and workstations. One of the limitations of the method is that a specific result is obtained for a specific problem, (i.e., it is non-parametric and does not allow general conclusions to be drawn). In addition, it may have voluminous inputs and outputs.

The finite element method fulfils the three basic requirements of modelling elastic and plastic materials, i.e.

- I. It complies with the relevant material laws, e.g. Young's modulus, Poisson's ratio, etc.
- II. It conforms to the requirement of compatibility of displacements, i.e. deformed element profiles will contact other profiles at all points
- III. It conforms to the requirement of the matching of reaction and applied forces and moments

Finite element software has three distinct parts:

The pre-processor.

The pre-processor is used to model the physical object that will be subject to analysis, for example, a nut and bolt assembly or a beam and also to define and apply the loads or displacements to be modelled. During this stage of the process, the engineer works interactively with the computer. Some CAD vendors supply pre-processing software.

The solver.

The solver uses the input file prepared by the pre-processor and applies numerical solution techniques to this input file, generating an output file of data.

The post processor.

The post-processor operates on the data supplied by the solver and transforms it into a visual output, normally in the form of the stress or temperature distribution, which can be viewed on the screen, or copied to a printer, plotter etc.

Basic description of the finite element method for stress analysis.

Degrees of freedom.

In a continuous elastic or plastic medium, there are infinite number of points to which a mathematical analysis may be applied. The purpose of the finite element method is to apply the method of solution to a finite number of points or nodes within the bulk material. In a three-dimensional material where, for example, we are analysing the displacement of the material point in three directions, the point in question is termed a node, and the node has three degrees of freedom (DOF), for example in the x, y, and z directions. This point has therefore three unknowns, and if we choose to analyse 2,500 points within the medium, and then we will have 7,500 unknowns. This means we in turn have 7,500 equations for solution. In practice the terms DOF number and equation number are used interchangeably.

Degrees of freedom per node.

During the formulation or modelling of a problem, the analyst may determine the number of degrees of freedom to be modelled. However the number of degrees of freedom per node is fixed. Depending on the element type there may be one or more degrees of freedom per node. For example when modelling a three-dimensional bulk solid, the analyst can choose to model simply the orthogonal displacements, giving three degrees of freedom per node, or displacements and rotation so giving six degrees of freedom per node. The number of degrees of freedom per node is fixed during the element formation; therefore it is up to the analyst to choose the correct element type for the problem in question.

The finite element.

Finite elements are the small discrete regions into which the problem domain is divided. This is known as discretisation of the domain. The boundaries of these elements do not have to be parallel to be orthogonal axes, and therefore a wider variety of shapes can be modelled. The area or volume within the element is also taken into account. If, for example, we are considering the elastic displacements of the nodes of an element, then any point within the element will be displaced according to functions of the displacements of the nodes. These functions are normally simple polynomials, because they are a good approximation locally inside any element. The study of the type of polynomials to use, the shape of the elements, the degrees of freedom associated with nodes, the number of nodes in an element, etc., constitute the finite element sub-discipline of element technology.

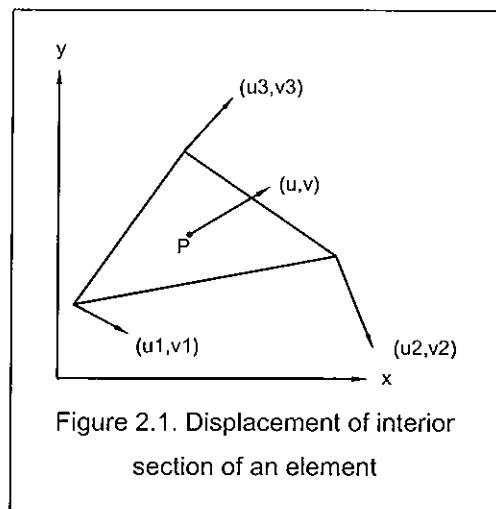
The basic steps in finite element analysis are as follows.

Discretisation

This involves breaking up the main problem domain into smaller discrete elements. These are in fact the finite elements. A problem domain can be a mixture of the required type of elements, i.e., triangular rectangular, etc. The elements may have straight sides, curved sides and nodes along the edges. If required each element may have different material properties. The software prepares an input file that contains the coordinates of all the nodes, the element types, the element connectivity, any applicable constants, and the material properties.

Interpolation of displacements.

Although the displacements of the nodes of an element are used in the analysis, it is also necessary to formulate the displacement of the interior section of the element. This is the case even though these nodal displacements are not yet known. Consider the two-dimensional triangular element as shown in figure 2.1, with each vertex is displaced (u_1, v_1) , (u_2, v_2) , (u_3, v_3) , an (as yet) unknown amount and any point p within the element displaced (u, v) , (after Krishnamachari, (13)).



A relationship is established between (u, v) and (u_1, v_1) , (u_2, v_2) , (u_3, v_3) as such that:

$$\left. \begin{aligned} u &= N_1 u_1 + N_2 u_2 + N_3 u_3 \\ v &= N_1 v_1 + N_2 v_2 + N_3 v_3 \end{aligned} \right\} \text{where, } \begin{cases} N_1 = f_1(\text{coordinates of } u, v) \\ N_2 = f_2(\text{coordinates of } u, v) \\ N_3 = f_3(\text{coordinates of } u, v) \end{cases} \quad (2.1)$$

Thus, the displacement of the general point (u, v) within the element is a weighted average of the displacements $(u_1, v_1), (u_2, v_2), (u_3, v_3)$ at the nodes. The values N_1, N_2, N_3 are the interpolation functions of the element. Thus, the displacements of the point within an element can be described as:

$$\begin{Bmatrix} u \\ v \end{Bmatrix} = \begin{bmatrix} N_1 & 0 & N_2 & 0 & N_3 & 0 \\ 0 & N_1 & 0 & N_2 & 0 & N_3 \end{bmatrix} \begin{Bmatrix} u_1 \\ v_1 \\ u_2 \\ v_2 \\ u_3 \\ v_3 \end{Bmatrix} \quad (2.2)$$

which can be abbreviated as

$\{u\} = [N]\{u\}^e$ where $\{u\}$ = the internal displacement within the element, $[N]$ = the interpolaton function matrix, and $\{u\}^e$ = the displacements of the nodes.

The form of the interpolation functions is now found. Consider the triangular element shown below. The general internal point P divides the element into three areas, 12P, 13P, 23P, whose areas are A_1, A_2 and A_3 respectively. Three ratios are defined L_1, L_2, L_3 such that

$$L_1 = \frac{A_1}{A}, L_2 = \frac{A_2}{A}, L_3 = \frac{A_3}{A} \quad (2.3)$$

By virtue of the fact that the position of point P defines a unique L_1, L_2, L_3 the natural coordinates of the point P can be states as $L_1, L_2,$ and L_3 . Since an interpolation function must be expressed as a function of co-ordinates:

$$\left. \begin{aligned} N_1 &= f_1(L_1, L_2, L_3) \\ N_2 &= f_2(L_1, L_2, L_3) \\ N_3 &= f_3(L_1, L_2, L_3) \end{aligned} \right\} \begin{cases} \text{that is, the value of any N is function of} \\ \text{its postion within the element} \end{cases} \quad (2.4)$$

Since the N_s are polynomials in L_s , and picking the simplest available functions, i.e.,

$$\left. \begin{aligned} N_1 &= L_1 + 0L_2 + 0L_3 \\ N_2 &= 0L_1 + L_2 + 0L_3 \\ N_3 &= 0L_1 + 0L_2 + L_3 \end{aligned} \right\} \text{i.e., } N_1 = L_1, N_2 = L_2, N_3 = L_3 \quad (2.5)$$

For these functions it is observed, referring to figure 2.2, that when the general point is coincident with a node, its displacement is identical with that of the node and when the general point is half way along one edge its displacement is the average of the displacements of the nodes defining that edge. This is one (linear) method of interpolating internal displacements within elements. There are many more.

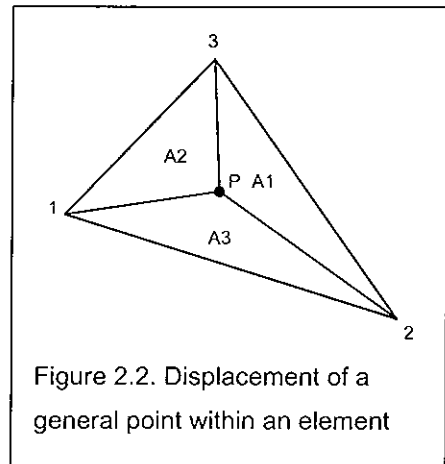


Figure 2.2. Displacement of a general point within an element

It is now necessary to convert the displacements of P from natural co-ordinates to Cartesian co-ordinates. P is given the general co-ordinates (x, y) , and the vertices of the finite element co-ordinates (x_i, y_i) , (x_j, y_j) , (x_k, y_k) , for the nodes i, j and k respectively. The area of a triangle is a function of the determinant of its co-ordinates, i.e.,

$$A_i = \frac{1}{2} \begin{vmatrix} 1 & x & y \\ 1 & x_j & y_j \\ 1 & x_k & y_k \end{vmatrix} = \frac{1}{2} \left\{ (x_j y_k - x_k y_j) + x(y_j - y_k) + y(x_k - x_j) \right\} \quad (2.6)$$

$$= \frac{1}{2} (a_i + b_i x + c_i y), \text{ where,} \quad (2.7)$$

$$a_i = (x_j y_k - x_k y_j), b_i = (y_j - y_k), c_i = (x_k - x_j)$$

By cyclic permutation we have:

$$A_i = \frac{1}{2} (a_i + b_i x + c_i y), A_j = \frac{1}{2} (a_j + b_j x + c_j y), A_k = \frac{1}{2} (a_k + b_k x + c_k y) \quad (2.8)$$

$$\text{and } \begin{cases} a_i = (x_j y_k - x_k y_j), b_i = (y_j - y_k), c_i = (x_k - x_j) \\ a_j = (x_k y_i - x_i y_k), b_j = (y_k - y_i), c_j = (x_i - x_k) \\ a_k = (x_i y_j - x_j y_i), b_k = (y_i - y_j), c_k = (x_j - x_i) \end{cases} \quad (2.9)$$

This yields

$$L_i = \left(\frac{A}{A_i} \right), L_j = \left(\frac{A}{A_j} \right), L_k = \left(\frac{A}{A_k} \right) \quad (2.10)$$

giving

$$L_i = \frac{(a_i + b_i x + c_i y)}{2A}, L_j = \frac{(a_j + b_j x + c_j y)}{2A}, L_k = \frac{(a_k + b_k x + c_k y)}{2A}. \quad (2.11)$$

For the linear triangle we have

$$N_i = L_i, N_j = L_j, N_k = L_k. \quad (2.12)$$

Given that the displacements at i, j and k are $(u_i, v_i), (u_j, v_j), (u_k, v_k)$ and the displacement p is (u, v) , then,

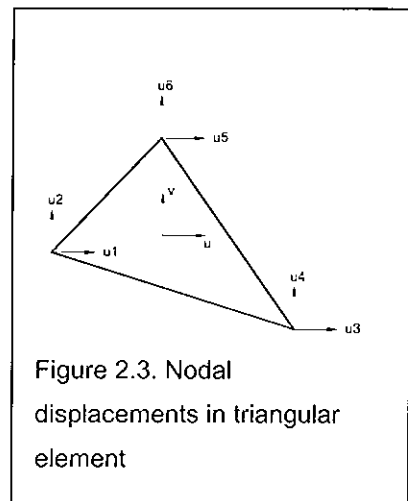
$$\begin{aligned} u &= N_i u_i + N_j u_j + N_k u_k \\ v &= N_i v_i + N_j v_j + N_k v_k \end{aligned} \quad (2.13)$$

(after Krishnamachari, (13)).

Calculation of element stiffness

Consider the triangle shown in figure 2.3. The nodal displacements are labelled as $u_1 \dots u_6$ for ease of computation. The convention that displacements are the causes of forces is adopted, and the effect of the displacement in a given direction and on a given node, in terms of the forces that it induces in a given direction on another node is considered. Since force = displacement \times stiffness, the displacement in a direction of u_2 for example, will produce a force in the direction u_5 , of the value

$F_2 = k_{25} u_5$, where k_{25} is a constant whilst the material is



elastic, and is yet to be evaluated. It is known as the stiffness co-efficient.

As can be seen in the diagram, each of six displacements can cause six forces (the force in each of two directions, at all three nodes). Hence there are $6 \times 6 = 36$ individual values of k to be evaluated. The calculation of the K matrix requires two additional matrices as discussed below.

The B Matrix

The B matrix is also known as the gradient matrix and is a property of the element shape. As described above, the internal displacement of any point within an element is denoted by:

$$\{u\} = [N]\{u\}^e \quad (2.14)$$

To evaluate the internal strains within the element using

$$\varepsilon_x = \frac{\partial u}{\partial x}, \varepsilon_y = \frac{\partial v}{\partial y} \quad \text{and} \quad \gamma_{xy} = \gamma_{yx} = \frac{\partial v}{\partial x} + \frac{\partial u}{\partial y}, \quad (2.15)$$

Then since

$$\begin{Bmatrix} u \\ v \\ u+v \end{Bmatrix} = \begin{bmatrix} N_1 & 0 & N_2 & 0 & N_3 & 0 \\ 0 & N_1 & 0 & N_2 & 0 & N_3 \\ N_1 & N_1 & N_2 & N_2 & N_3 & N_3 \end{bmatrix} \begin{Bmatrix} u_1 \\ v_1 \\ u_2 \\ v_2 \\ u_3 \\ v_3 \end{Bmatrix} \quad (2.16)$$

gives

$$\begin{Bmatrix} \varepsilon_x \\ \varepsilon_y \\ \gamma_{xy} \end{Bmatrix} = \begin{bmatrix} \frac{\partial N_1}{\partial x} & 0 & \frac{\partial N_2}{\partial x} & 0 & \frac{\partial N_3}{\partial x} & 0 \\ 0 & \frac{\partial N_1}{\partial y} & 0 & \frac{\partial N_2}{\partial y} & 0 & \frac{\partial N_3}{\partial y} \\ \frac{\partial N_1}{\partial y} & \frac{\partial N_1}{\partial x} & \frac{\partial N_2}{\partial y} & \frac{\partial N_2}{\partial x} & \frac{\partial N_3}{\partial y} & \frac{\partial N_3}{\partial x} \end{bmatrix} \begin{Bmatrix} u_1 \\ v_1 \\ u_2 \\ v_2 \\ u_3 \\ v_3 \end{Bmatrix} \quad \text{i.e., } \{\varepsilon\} = [B]\{u\}^e \quad (2.17)$$

The D Matrix

The D matrix is also known as the elasticity matrix, and its properties are dependent on the material properties in question. It simply relates stresses and their corresponding strains, as follows:

$$\begin{Bmatrix} \sigma_x \\ \sigma_y \\ \tau_{xy} \end{Bmatrix} = \frac{E}{1-\nu^2} \begin{bmatrix} 1 & \nu & 0 \\ \nu & 1 & 0 \\ 0 & 0 & \frac{1-\nu}{2} \end{bmatrix} \begin{Bmatrix} \varepsilon_x \\ \varepsilon_y \\ \gamma_{xy} \end{Bmatrix} \quad \text{i.e., } \{\sigma\} = [D]\{\varepsilon\} \quad (2.18)$$

The element stiffness matrix.

The stiffness matrix for an (elastic) element is defined as:

$$[K]^e = \int_V [B]^T [D][B] dV \quad (2.19)$$

for three dimensional elements and

$$[K]^e = \int_V [B]^T [D][B] dA \quad (2.20)$$

for two dimensional elements.

Assembly of the Global Stiffness Matrix.

The elemental stiffness and force matrices must be assembled into one global stiffness matrix and one global force matrix. The unknown global matrix of displacements $\{u\}$ is related to the other two by the equation

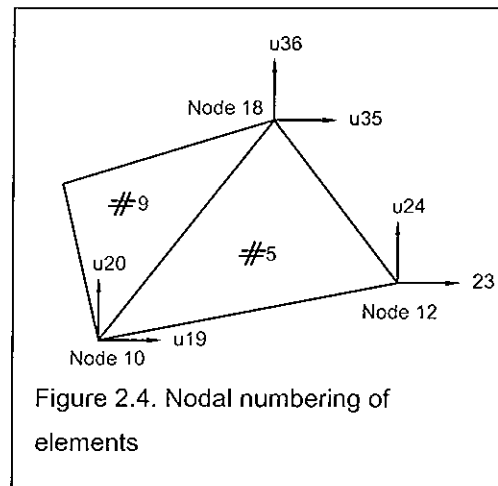
$$[K]\{u\} = \{f\} \quad (2.21)$$

The stiffness for the entire assembly is equal to the sum of the element stiffnesses, and the global force matrix is equal to the sum of the elemental force matrices, providing that both are expressed in terms of global co-ordinates. Consider two adjacent elements as shown below. Considering first element number 5 only. Its stiffness co-efficients are placed in the global stiffness matrix as shown,

$$\begin{bmatrix}
 \dots & \dots & \dots & \dots & \dots & \dots & \dots & \dots & \dots & \dots \\
 \dots & k_{19,19} & k_{19,20} & \dots & k_{19,23} & k_{19,24} & \dots & k_{19,35} & k_{19,36} & \dots \\
 \dots & k_{20,19} & k_{20,20} & \dots & k_{20,23} & k_{20,24} & \dots & k_{20,35} & k_{20,36} & \dots \\
 \dots & \dots & \dots & \dots & \dots & \dots & \dots & \dots & \dots & \dots \\
 \dots & k_{23,19} & k_{23,20} & \dots & k_{23,23} & k_{23,24} & \dots & k_{23,35} & k_{23,36} & \dots \\
 \dots & k_{24,19} & k_{24,20} & \dots & k_{24,23} & k_{24,24} & \dots & k_{24,35} & k_{24,36} & \dots \\
 \dots & \dots & \dots & \dots & \dots & \dots & \dots & \dots & \dots & \dots \\
 \dots & k_{35,19} & k_{35,20} & \dots & k_{35,23} & k_{35,24} & \dots & k_{35,35} & k_{35,36} & \dots \\
 \dots & k_{36,19} & k_{36,20} & \dots & k_{36,23} & k_{36,24} & \dots & k_{36,35} & k_{36,36} & \dots \\
 \dots & \dots & \dots & \dots & \dots & \dots & \dots & \dots & \dots & \dots
 \end{bmatrix} \quad (2.22)$$

where $k_{20,36}$ for example, relates the force global degree of freedom (DOF) number 26 due to a displacement DOF number 36, (after Krishnamachari, (13)).

Consider now figure 2.4, which shows the element number 9, which is adjacent to element number 5, and shares edge 10-18. This element has stiffnesses associated with the nodes numbered 10 and 18, i.e., the stiffnesses of element 9 pertaining to shared nodes are $k_{19,19}$, $k_{19,20}$, $k_{19,35}$, $k_{19,36}$, $k_{36,19}$, $k_{36,20}$, $k_{36,35}$ and $k_{36,36}$. These stiffnesses are different in value to the corresponding stiffnesses of element 5, (due to the different size of element number 9), but are in the same position in the global stiffness matrix.



Thus, the stiffnesses at corresponding locations in the matrix, due to adjacent elements, are added. Hence, for a node shared by n finite elements, there are n entries in the corresponding matrix element, in the global stiffness matrix.

The same procedure applies to the global force matrix, which is a single column vector of nodal forces. However, there is only need to supply forces here where the nodes are subject to loading. These are called static boundary conditions. Generally this means that the global force matrix consists largely of zero value entries.

By virtue of the fact that the global stiffness matrix consists of N_d rows by N_d columns, (N = number of nodes in the model (element assembly), and d = the number of degrees of freedom per node) and a displacement of a particular node causes a reaction force only in the nodes of elements that are attached to it, stiffnesses can only be determined for corresponding entries in the global stiffness matrix. Therefore the global stiffness matrix consists of largely zero value entries.

The node-numbering pattern thus determines the position of entries in the global stiffness matrix. Node numbering algorithms have been developed to ensure that the matrix is filled with non-zero values in such a way as to ensure minimum bandwidth, i.e., the distribution of non-zero values along the main diagonal, itself a requirement of minimisation of computational resources when solving the general equation.

For linear elastic elements, where no energy is lost from the system, since $k_{ij} = k_{ji}$ (Maxwell Betti theorem (41), displacement at position i caused by a force at position j is equal to a displacement at position j caused by a force at position i), then the global stiffness matrix must be symmetric, i.e., elements mirrored in the leading diagonal will have equal values.

The global stiffness matrix is singular, i.e., the determinant of $[K]$ is zero, and hence the equation $[K]\{u\} = \{f\}$ has no solution in its present state. The support structures of the assembly of elements have not yet been applied to the equation $[K]\{u\} = \{f\}$, hence the body is free to undergo a rigid translation. It is necessary to restrain the body in term of rotation and displacement by kinematic boundary conditions before the equation can be solved, (after Krishnamachari, (13)).

Computational steps in the finite element method.

Refer to table 2.1

| Operation performed | Mathematical Equivalent |
|-----------------------------|---|
| Discretisation | None |
| Interpolate displacements | $\{u\} = [N]\{u\}^e$ |
| Gradient Matrix | $[B] = \frac{\partial [N]}{\partial \{x\}}$ |
| Elasticity Matrix | Construct $[D]$ |
| Element Stiffness | $[K]^e = \int_V [B]^T [D] [B] dV$ |
| Element Load | $\{f\}^e = \int_V [N]^T \{f_b\} dV + \int_S [N]^T \{f_s\} dS$ |
| Global Stiffness | $[K] = \sum_e [K]^e$ |
| Global force vector | $\{f\} = \sum_e \{f\}^e$ |
| Global displacement vector | Obtained by Gauss elimination. |
| Element displacement vector | Retrieved by book keeping. |
| Element Strain | $\{\varepsilon\}^e = [B]\{u\}^e$ |
| Element stress | $\{\sigma\}^e = [D]\{\varepsilon\}^e$ |

Table 2.1, computational steps in the finite element method, (after Krishnamachari, (13)).

In order to evaluate strains within an element, the values within the $[B]$ matrix are required. But these values are dependent upon interpolation functions, and these functions may differ element to element. Thus, although the values of the interpolation functions are unique within the any given element, their values on the element nodes may be different depending upon which element is used to evaluate them. For example, in the figure above, the value of the interpolation function at node 18 will change depending on whether element 9, or element 5 is used to evaluate it. Therefore finite element analysis packages avoid the calculation of the nodal strains, and corresponding nodal stresses and calculate these at the element centroids or other useful points within the element. The software then interpolates the values of the required parameter, centroid to centroid, or Gauss point to Gauss point, ignoring the nodal values.

The above discussion describes the sequence of events for elastic deformation of the finite elements, where no energy is lost to the system. A different method is required for the construction of $[K]^e$ when the element is subject to plastic strain. The plastic $[D]^e$ matrix is obtained from:

$$[D^p]^e = \frac{E}{1+\nu} \begin{bmatrix} \left(\frac{1-\nu}{1-2\nu} - \frac{\sigma_x'^2}{S} \right) & 0 & 0 \\ \left(\frac{\nu}{1-2\nu} - \frac{\sigma_x' \sigma_y'}{S} \right) & \left(\frac{1-\nu}{1-2\nu} - \frac{\sigma_y'}{S} \right) & 0 \\ \left(-\frac{\sigma_x' \tau_{xy}}{S} \right) & \left(-\frac{\sigma_y' \tau_{xy}}{S} \right) & \frac{1}{2} - \frac{\tau_{xy}^2}{S} \end{bmatrix} \quad (2.23)$$

where

σ' = the deviatoric stress,

$$S = \frac{2}{3} \bar{\sigma}^2 \left(1 + \frac{H'}{3G} \right)$$

$\bar{\sigma}$ = the equivalent, effective or representative stress, described above

$H' = \frac{d\bar{\sigma}}{d\bar{\epsilon}^p}$, the slope of the equivalent stress - plastic strain curve.

Once $[D^p]^e$ is defined, then the elemental plastic stiffness matrix can be evaluated as

$$[K^p]^e = \int_e [B]^T [D][B] dA = [B]^T [D][B] \Delta \quad (2.24)$$

where Δ = the area of the triangular element.

For each step in the finite element evaluation process, the new plastic stiffness matrix is substituted for either the original elastic stiffness matrix if the yield stress of the material in the element has been exceeded for the first time, or the old value of the plastic stiffness matrix if the element is continuing to yield.

Guidelines to finite element modelling.

In order to set up a finite element model, the user must have an understanding of the physical behaviour occurring, and an understanding on the physical behaviour of individual element

types. The user must check and choose the correct element type, must understand the boundary conditions to be applied to model, and the type of loads, and their magnitudes and positions as applied.

The aspect ratio of individual elements must be considered. The aspect ratio of an element is the ratio of its longest dimension to its shortest dimension. The solution accuracy generally decreases with increasing aspect ratio. Corner angles of quadrilateral elements should be as close to 90 degrees as possible and not less than 45 degrees.

Appropriate use of symmetry, where part of the problem is modelled and is representative of the entire problem, reduces computational resource requirements. This helps on the basis of reducing the actual problem size and also allowing finer meshes to be used on the part of the problem that is of significance, for the same resources requirement. At the plane(s) of symmetry the deflection normal to the plane(s) must be zero. Care should be taken because symmetry of geometry does not necessarily imply symmetry of loading or other fields.

Natural sub-divisions of element types can be used where the properties of the model or loads change abruptly. For example, nodes are required at the points of application of point nodes, or at load discontinuities. Nodal lines can be defined by abrupt changes in model thickness, or at the interface between two model materials.

The mesh density will vary both with the model geometry, and the loading conditions. Mesh density should be high where high stress gradients are expected, for example holes, sharp or re-entrant corners, or small fillets.

The model should be checked carefully before the computation process begins. The restraints and forces must be in the correct propositions and at the proper orientations, consistent units must be used and correct element types and mesh densities must also be used.

After the solution has been obtained, the boundary conditions should be checked. For example if a given boundary condition was that the horizontal displacement at a given position was to be zero, then this must be checked, to ensure it actually occurred. If symmetry exists then stresses and displacements should exhibit this symmetry. Often approximate analytical results can be obtained, and these can be used to check the order of magnitude of the finite element results.

2.2. Review of texts and research papers published on sheetmetal forming

In order to commence the study of the behaviour of sheetmetal workpieces subject to simultaneous double bending, various texts were evaluated. The object of this evaluation was

twofold: first to review background theory on elastic and plastic behaviour of metals, and also the finite element method, and secondly to determine the current state of research in this area.

2.2.1 Elastic and plastic deformation of metals: theoretical background.

Various authors, including DeGarmo (1) describe the double bending of sheet metal workpieces in press brakes. The author describes three main problems associated with bending, i.e., the minimum permissible bend radius, the determination of blank size for given component dimensions and the minimum flange size. Kalpakjian (2) also describes some of the features of bent metals, including the possibility of cracking due to excessive strain (insufficient bend radius). He also describes Poisson's effect, resulting in the narrowing of the material being bent, and springback, the tendency of the material to return to its original shape after the bending forces have been removed. Simultaneous double bending, or joggling, is also illustrated.

The elastic behaviour of materials is described by Urry and Turner (3), and Timoshenko and Goodier (4) and various standard solutions are presented for common elastic problems. In addition, and of particular relevance to the current project, the common theories of failure, i.e., Von Mises and Tresca are presented.

Anderson, Leaver, Alexander and Rawlings (5) present the molecular theories behind elastic, anelastic (time dependent) and plastic deformation of metals, including descriptions of the role of dislocations in the strain hardening of materials. They also discuss strain in both mono-crystalline and bulk metals. Additional descriptions are provided by Higgins (6).

Calladine (7) presents general mathematical descriptions of the plastic deformation in bulk metals and pays particular attention to the basic principles of this type of deformation. The author also introduces the concept of true strain and the true stress-strain diagram. Johnson and Mellor (8) suggest a number of models for material behaviour, including perfectly elastic, [rigid – perfectly plastic], [rigid – linear work hardening], [elastic – perfectly plastic] and [elastic – linear work hardening]. They also introduce the concept of a yield locus. Marciniak and Duncan (9) describe the theory of sheet metal bending, and introduce grid circle strain analysis to assist in the physical measurement strain during experimental bending. They also describe the creation and use of forming limit diagrams.

2.2.2 Finite element analysis: Theoretical Background.

Various texts were studied in order to gain an insight into the setup and use of the finite element method, including texts by Cook (10), Spyrakos (11), and The National Agency for

Finite Element Methods and Standards (12). Krishnamachari (13) provides a good introduction to the FE method, and also provides the mathematical background such as analysis of stress at a point, transformation of axes, matrix algebra, etc. In addition, the author provides a clear description of the FE method and its use in the elastic analysis of materials. He also provides information on the practical modelling of material and loading systems.

Bajpai, Mustoe and Walker (14), Jefferey (15) and Sokolnikoff and Refheffer (16) describe some of the mathematical background techniques used in the descriptions of both the FE method and elastic and plastic analysis of materials.

2.2.3 Current research: metal bending and metal forming.

Various technical papers were studied to determine the current status of research into sheetmetal bending processes. Although few papers described the double bending or joggling process specifically, many of the papers described work done by researchers that would have a direct bearing on the study of the joggle process, based either on a finite element approach or on an experimental approach.

2.2.3.1 Introductory Papers

Kroeze, Streppel and Lutters (17) reiterate the reduction in time required from design to manufacture, in particular with regard to product life cycle and decreasing lot sizes. They also describe in particular the problems associated with the use of press brakes for sheet metal forming, in terms of press bed deflection.

Tekaya (18) describes the requirements of industry in terms of design cycle time reduction and the iterative process of design – analyse – redesign relating to sheet metal components. He suggests appropriate FE elements as being membrane, plate, shell and continuum.

Hollander (19) describes the chemical properties of steel, and notes that once the properties are fixed, the physical properties are fully determined by the grain structure and the material on the borders of the grains. Grain size depends upon the magnitude of the last strains applied, the cooling rate, and the coiling temperature of the steel. The author explains the importance of various parameters such as strip temperature, workpiece velocity and roll geometry accuracy in the determination of the workpiece properties and geometrical accuracy.

2.2.3.2 Sheet Metal Bending

Klingenberg, Singh and Urquhart (20) describe the three point or air bending operation, using a variable width die and various punch displacement velocities. During their experimental work, measurements were taken including punch displacement, displacement rate and reaction forces due to the workpiece. They claim good correlation between experimental results and FE predictions for force – displacement, force – die width and punch displacement – bent up angle curves.

The three point bending model is also described by DeVin, Klingenberg and Singh (21) with particular reference to the effect of the punch radius on the radius of the workpiece. They note however that for large radii (compared to sheet thickness), the experimental and theoretical models that they use diverge considerably with regard to bend allowance, possibly due to the bend profile being parabolic rather than constant radius.

Hagenah and Backes (22) recognise that the position and accuracy of any one bend will depend on the position and angular accuracy of the previous bend(s), and have proposed a statistical analysis of the inter-influence of bends upon one another. In the event that joggle tooling is used, (as investigated in this research), inter-bend influence should be reduced.

Heckel (23) has completed experiments on the phenomenon of springback in air bent components, and has drawn various conclusions, classifying materials in order of sensitivity to springback, and demonstrating that springback is linearly proportional to bent up angle, and is independent of grain direction. In addition, he has demonstrated a method of closed loop control by the real time measurement of bent up angle of the workpiece with respect to punch position.

Devin, Urquhart and Singh (24) describe the difficulties encountered when using both closed die forming (fully shut out dies), i.e., a reduction in process flexibility, as compared to the air bending process. They also describe the difficulties encountered in the air bending process, i.e., the effects of machine and material variability. They note that previous research on [force – displacement] curves is incomplete and subject to various difficulties, and propose a modified model.

Lutters, Streppel and Kroeze (25) disagree with the use of hydraulic pressure transducers for punch force detection, (see reference 28) citing inaccuracy of the sensors. They describe a new method for bent up angle detection using rotating laser sensors, and also propose an algorithm to be used in closed loop control of an air bending system.

Perduijn and Hoogenboom (26) have performed experimental work on the bending process by producing a pure bending moment (no shear) via the use of a special rotating clamp and

frame system. However, due to the physical requirements of non-interference of tooling when the bending occurs, the clamps were of lighter than optimal construction. In addition, there were large variations between theoretical bent profile and experimental results, especially at large bent up angles.

Sheetmetal Forming

Anokye-Siribor and Singh (27) completed a series of forming experiments (on aluminium and titanium), and noted that the experiments indicated that Young's modulus and the work hardening index are rolling direction dependent, i.e., the material behaves in an anisotropic fashion. In addition, lubrication does not have much effect on punch force, nor does dwell time. In this research the authors used a pressure – voltage transducer in the hydraulic circuit to determine punch force.

Leacock, Gilmour, Laurenson and Urquhart (28) have proposed a simple empirical model for the production of strain data in the context of sheet forming processes.

Siegert (29) describes advances in metal forming and drawing technology for complex formed components. These advances include the use of pins with individually controllable heights in order to be able to vary pressure plate force for individual positions. This leads to the ability to reduce the influence of variation in lubrication, thickness and other material parameters.

Ferreira, Duarte, dos Santos and da Rocha (30) describe the material testing equipment available for sheet metal formability testing.

Shirvani and Daniels (31) describe a qualitative approach to metal forming analysis using the FE method, and describe some experimental work they have completed using the deep drawing process.

3. Experiment Design and Testing

3.1. Design and manufacture of the bending rig

The test rig design was based on two main considerations. These were (1) the physical requirements of the experimental process, and (2) the available resources. The sizes of the test pieces were chosen such that their dimensions would closely match the industrial components that they were intended to model. This also enabled the experiments to be completed using available equipment.

The experimental process required a test rig capable of producing enough force to plastically deform the workpiece. A hydraulic power pack of capacity 138 MPa (2000 PSI) was available, including an 11.0 kW 380V 3-phase motor. This power pack was permanently wired into an electrical supply, using a triple fused spring-loaded isolator switch. A hydraulic cylinder was purchased from Redwood Hydraulics, and various laboratories supplied load cells and displacement transducers.

Initially the test rig was designed as shown in figure 3.1. The design intent was to measure the load on the workpiece via a hydraulic pressure transducer, but perusal of the literature (7) demonstrated that this was not a feasible method. In addition, it was intended that the design should be simple to manufacture, i.e., that the effort and expense of manufacture should be minimised, hence the use of parallelepiped and cylindrical components. However, examination of this initial design shows that the forming load would be resisted inter-alia by the four assembly bolts in each of the upper and lower ends of the main uprights. In the event that the bolts or the threads into which they are screwed failed, a sudden release of strain energy would result, and the system would fail in a dangerous manner.

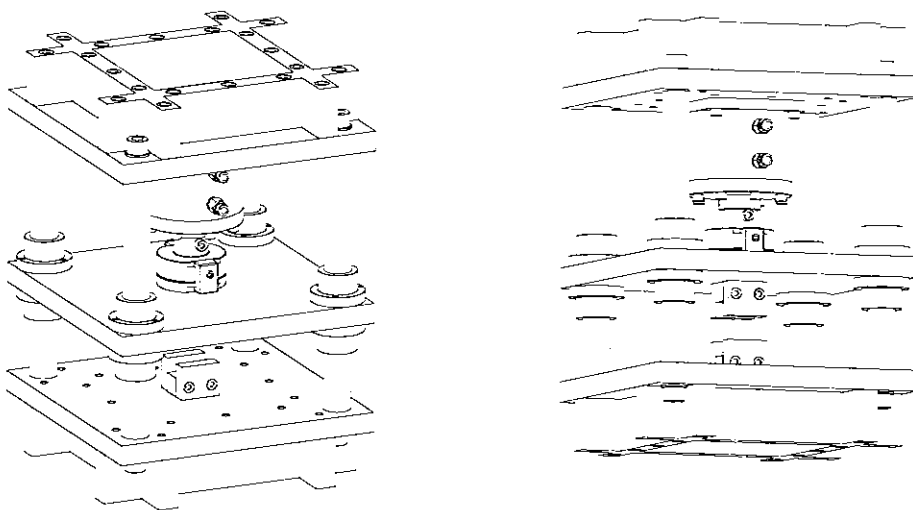


Figure 3.1 Initial design of test rig

In addition, a rig of this design would need to have accurate positioning of the holes in the fixed and moving platens, in order to ensure free running of the moving platen on the pillars.

Based on the above considerations, the entire test rig was redesigned, the concept of which is shown in figures 3.2 and 3.3. As can be observed, the load bearing elements of the test rig are such that the fasteners are exempt from forming loads and in fact are used only to locate the main load resisting elements. Hence, based on design calculations and the available force from the hydraulic cylinder, the test rig was deemed operable in a safe condition. The relative positions of the top and bottom forming tools were maintained in their correct positions by the use of a commercially available die set, eliminating the need for jig boring of pillars and bushes.

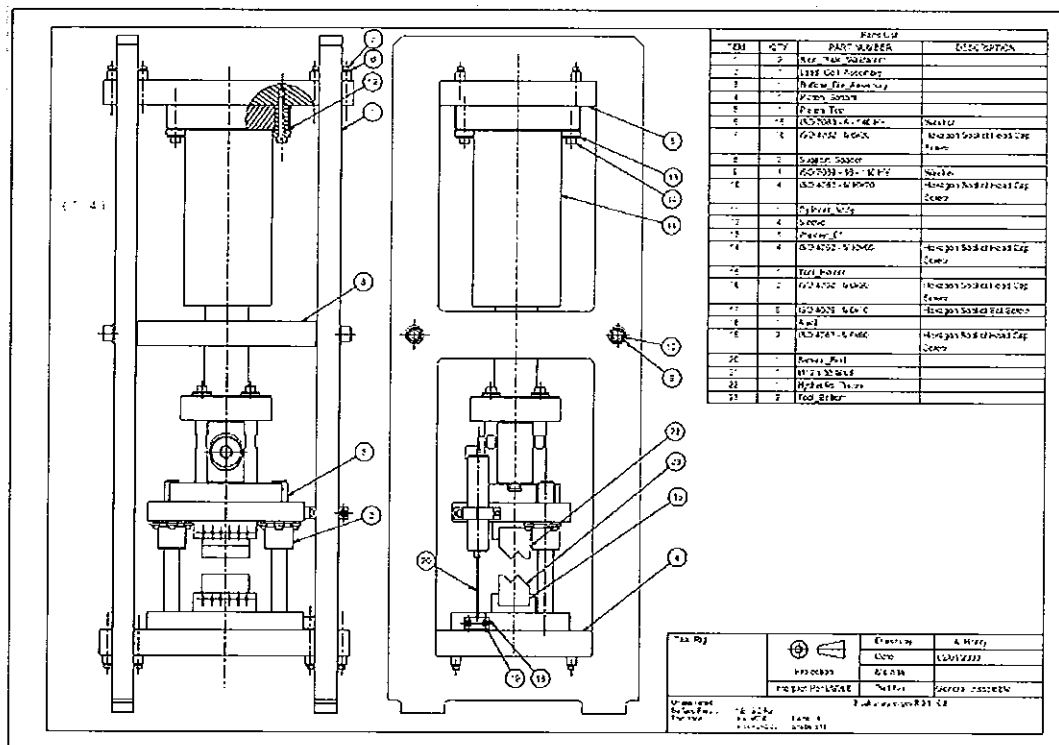


Figure 3.2 Orthographic view of final rig design

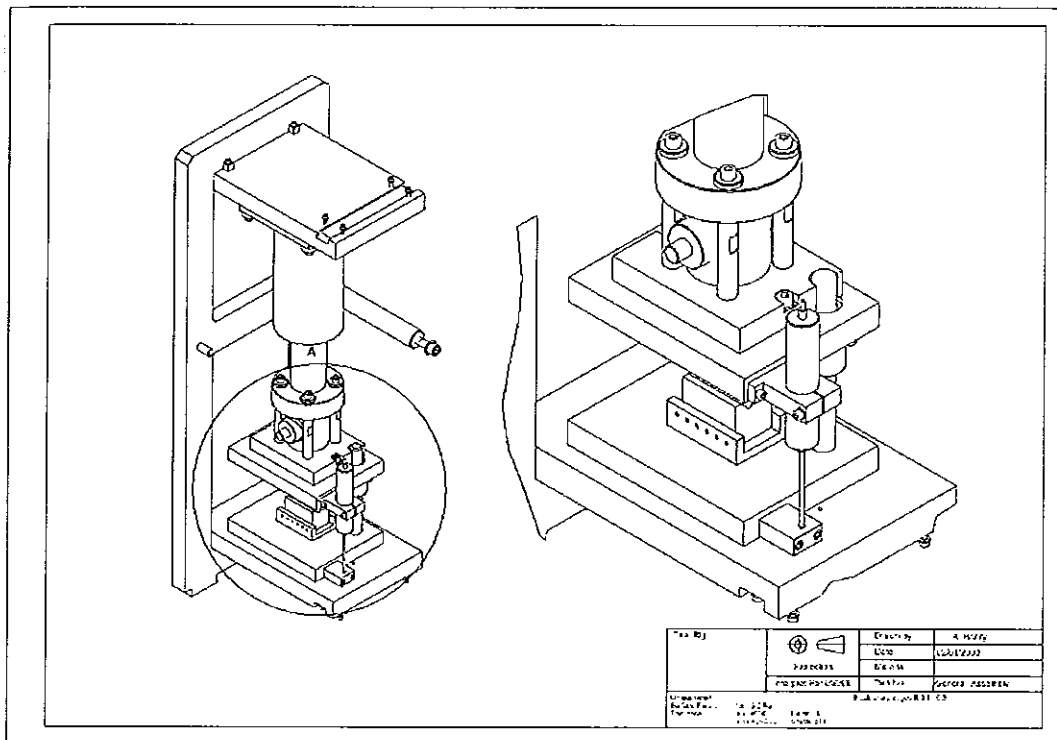


Figure 3.3 Isometric view of final rig design

The test rig was manufactured over a number of months. The main load bearing frame elements were purchased flame cut from 40 mm plate, and the contact surfaces were machined using a combination of high speed steel and tungsten carbide cutters. Due to the physically large nature of the machine elements, they proved difficult to work with and assembly of the main frame proved a physically difficult task due to the mass of the assembly. Transport of the assembly from the workshops to the laboratory where the machine now resides was also problematical. A number of the exposed machine elements were painted to enhance corrosion protection. Location, transportation, repair and commissioning of the hydraulic power pack used to supply the test rig hydraulic cylinder also proved difficult, as did the installation of a three phase 380 V correctly rated electrical outlet for it.

The hydraulic cylinder on the rig was filled with oil, and the rig cycled for several hours to ensure that the hydraulic system contained no air. The completed Test rig is shown in figure 3.4 below. The hydraulic circuit for the rig is shown in Appendix 1. A set of working drawings for the test rig is shown in Appendix 8.



Figure 3.4 The completed test rig.

3.2 Die Design and manufacture

Since tool design is necessarily a function of workpiece geometry, it must be considered first. The workpieces have two ninety-degree bends in close proximity to each other as shown in figure 3.5. This is a common requirement in the sheet metal industry. Under normal circumstances two bends can be made by two separate forming operations using either air bending or coining in a v-die. However, as can be seen in figure 3.6, there is a minimum limit to the dimension 'x' that can be achieved due to the geometry of the v-die. Occasionally a dimension that is smaller than that which can be achieved using a v-die and top tool is required. In this case a special set of tools is necessary to facilitate the process, see figure 3.5. The geometry of this tooling is such that the top and bottom dies are not subject to a resultant bending moment when the workpiece is loaded, i.e., the die set (if used) will only be subjected to axial loads, and no strain energy due to bending is stored in the die set or press. In addition, the geometry dictates that there is no tendency for lateral displacement (i.e., displacement normal to the loading axis). This leads to a safe and controllable bending process.

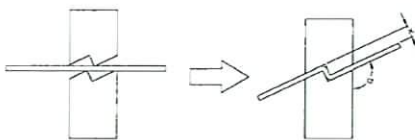


Figure 3.5 Workpiece profile

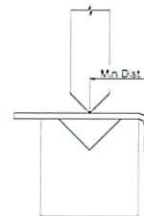


Figure 3.6 Workpiece size limit

Due to the fact that in project seven different sets of tooling were required and each set consists of a matching pair, a parametric CAD system (AutoCAD Mechanical Desktop) was used to produce the tool drawings. This proved convenient for the tool manufacture. In addition, the tool profiles were exported as .iges files for use in Deform PC Pro finite element software.

The tool profiles are as shown in Appendix 2. These profiles were chosen to generally match tools often used for component production in industry which are often made on a one-off or per-job basis. This is because it is difficult to anticipate the required profiles and / or material thicknesses that are likely to be used on any given job, and hence standard tools are unavailable. The tools usually have a flat rather than radiused profile due to the lack of availability of radiused cutters, and the difficulty of producing long lengths of tooling. The tooling produced for use in the experiments described had a flat profile of dimension 0.5 mm.

3.2.1 Tooling Manufacture

The first set of tools was manufactured using mild steel, as is often the case in industry for short run components in thin materials. However these tools proved to be easily damaged by the thick (8mm) workpieces used in the first experiments, and were discarded in favour of a second set manufactured from a heat treatable steel.

This second set of tools was manufactured from AISI 01 oil hardening tool steel, standard stock size of 50mm x 50mm x 500 mm cut to the appropriate lengths and machined. The machining process was executed using 20 mm diameter end mills and a specially radiused end mill to give the internal fillet on the tool profile. This internal radius was essential to prevent cracking of the tooling during hardening and also to prevent cracking during use. The tools were heat treated as follows: Heated to 820°C and soaked at this temperature for 30 minutes to ensure through heating. They were then quenched in oil, and tempered for one hour at 300°C to bring the material to a Rockwell hardness of 54-56Rc, a typical hardness for forming tools.

A number of difficulties were encountered during the manufacture of the tooling. Heat treating a full set of tools together caused the cooling oil to overheat and the process needed to be repeated for individual tools.



Figure 3.7. Set of tools after machining and heat treatment, prior to experimental use.

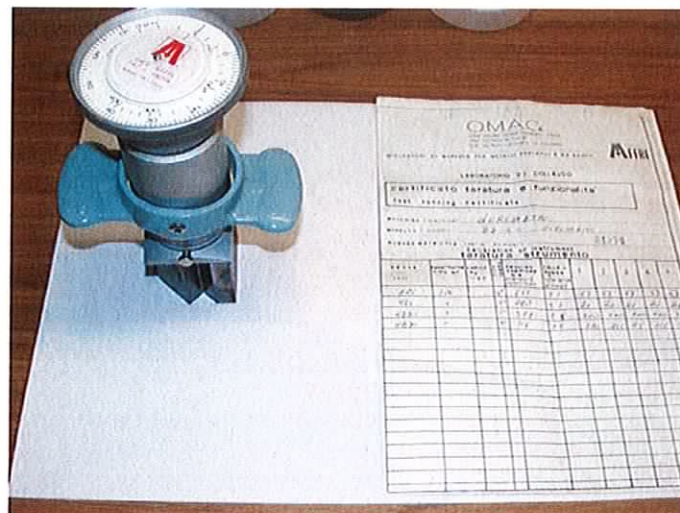


Figure 3.8. Hardness testing of sample tooling, showing calibration certificate of hardness tester.

3.3. Instrumentation and calibration

In order to ensure that the load displacement graphs yielded by the experiments were accurate, the test rig was calibrated. This was executed as follows:

3.3.1 Load transducer calibration

Because the load cell that measures the workpiece load during the experiment is physically connected to the test rig and the data acquisition card whilst the card is connected to the PC, it was impossible to calibrate the rig load cell independently. The approach taken was to calibrate a second (intermediate) load cell and apply a load from the test rig to this cell. The

test rig load was adjusted via the hydraulic bypass valve on the power pack, so that known series of loads (as measured by the intermediate cell and strain readout device) were passed through the load cell in the rig. The slope and intercept values on the data acquisition card were then adjusted so that the rig load cell output matched the calibrated cell output. This ensured that the rig output readings from the data acquisition card were correct.



Figure 3.9

Calibration of intermediate load cell



Figure 3.10

Taking intermediate load cell readings



Figure 3.11

Test Rig ready for calibration

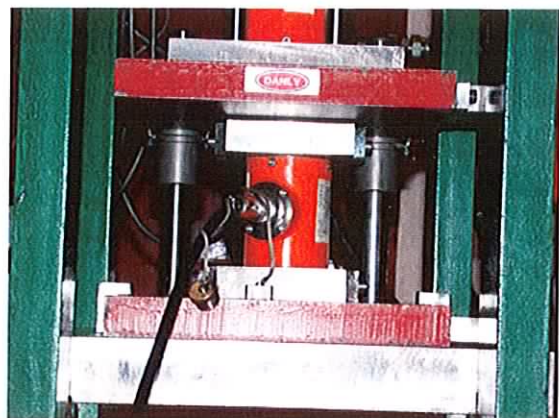


Figure 3.12

Intermediate load cell in place

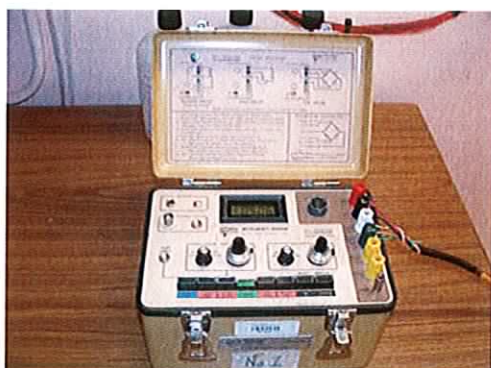


Figure 3.13

Reading taken from load cell

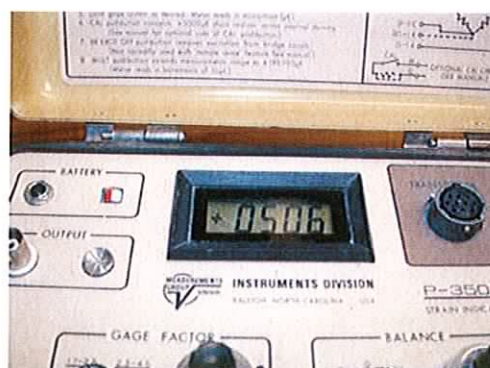


Figure 3.14

Calibration at 5.0 tonnes force

The calibration output for the load calibration test is shown in Appendix 3.

3.3.2. Displacement transducer calibration.

Displacement transducer calibration was completed using gauge blocks, in order to produce known displacements. The slope and intercept constants on the data acquisition card interface were then adjusted so that the displacement transducer outputs were correct.

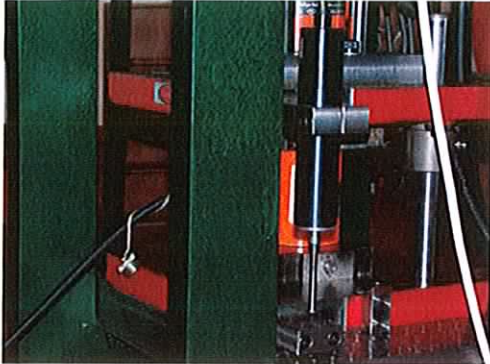


Figure 3.15
Displacement transducer



Figure 3.16
Gauge blocks ready for use

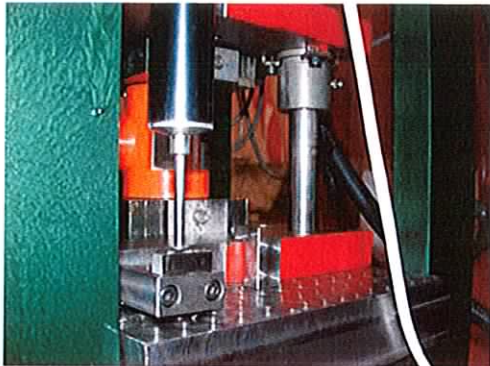


Figure 3.17
Displacement calibration at 0 mm

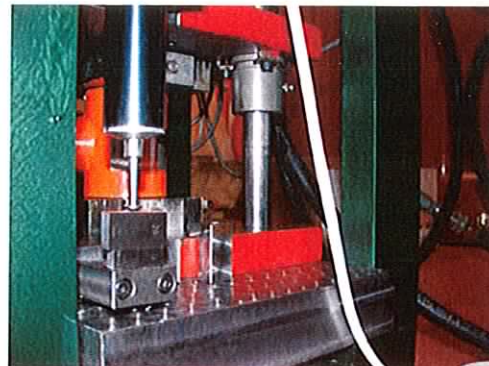


Figure 3.18
Displacement calibration at 20 mm

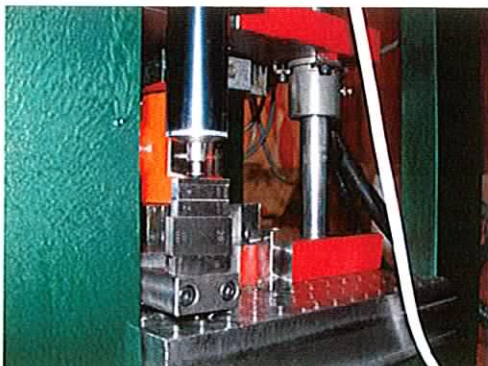


Figure 3.19
Displacement calibration at 40 mm

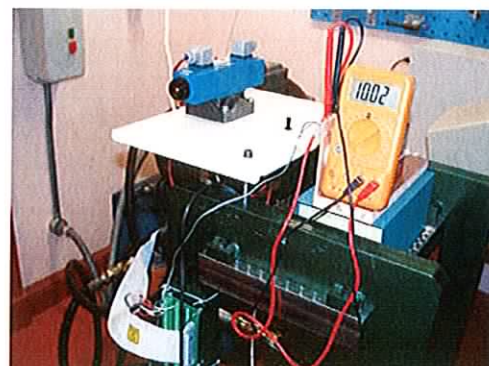


Figure 3.20
Potential divider supplying 10V to DAC

The calibration output for the displacement calibration test is shown in Appendix 3.

3.4. Material properties of the workpiece

3.4.1. Steel.

In order to ensure correspondence between the flow stress curves for various workpiece materials available in the Deform PC Pro database and the actual material properties of the workpiece in use, it was necessary to research comparative international standards for material specification. This proved more difficult than expected, due to the multiplicity of international standards, and the lack of data available to correlate them. In the end, Chorus steel was able to correlate the standards as shown in Appendix 4.

CR4 is the common purchase specification for general-purpose steels for use in the metal forming industry in Ireland, and this was the steel type used in the experimental work. The material flow curve for AISI 1010 was available in the Deform PC Pro package, hence it was necessary to show equivalence between AISI 1010 and CR4. This has been established as shown in the Appendix 4.

3.4.2 Aluminium.

The flow stress curve available in Deform PC Pro for aluminium is for type 6062. The material commercially available and commonly used in production of sheet metal products in Ireland is 6082 T6. The designation is explained as follows:

| | |
|----|---|
| 6 | The alloy group |
| 0 | Modification (0 = no modification) |
| 82 | The purity rating, i.e., 82 means that the aluminium is 99.82% pure |
| T6 | The aluminium is not cold worked after heat treatment |

Table 3.1

It can therefore be seen that the aluminium workpieces are very similar in properties to the material flow curves in the software database, and were therefore considered suitable for use.

As with the tooling materials, see Appendix 5, the author sought to verify the materials Young's Modulus and Poisson's Ratio for the steel and aluminium in question.

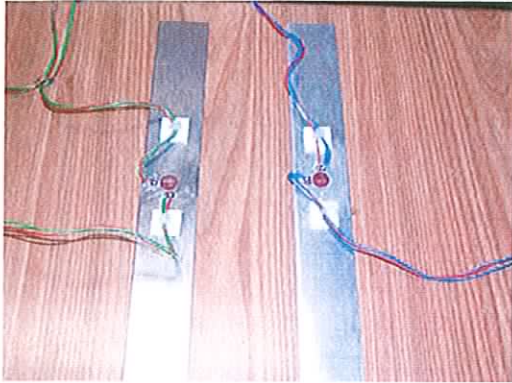


Figure 3.21

Aluminium and Steel workpieces with strain gauges attached

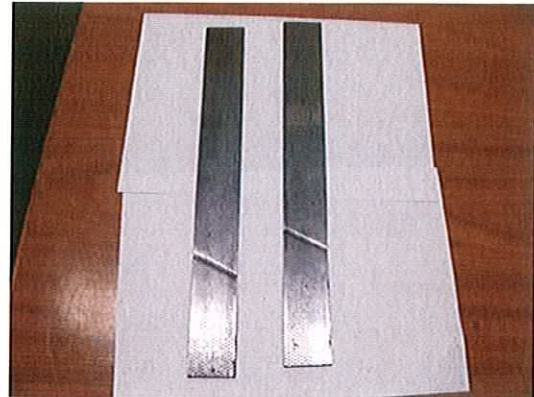


Figure 3.22

Additional workpieces loaded to fracture.

3.5. Workpiece design and manufacture

3.5.1. Geometry

Consideration of the geometry of the workpiece suggests that the force required for forming will be directly proportional to the *length* of the bend. If we speculate that end effects will not be pertinent to the experimental outcomes at a distance of two or three times the material thickness from either end of the bend, (St. Venant's Principle), then a bend length that will yield results that are indicative of longer bends can easily be determined. The minimum flange displacement x (see fig 3.23) was determined from dimensions found commonly in industrial components, and the maximum displacement is that determined by the capability of single bend v-dies.

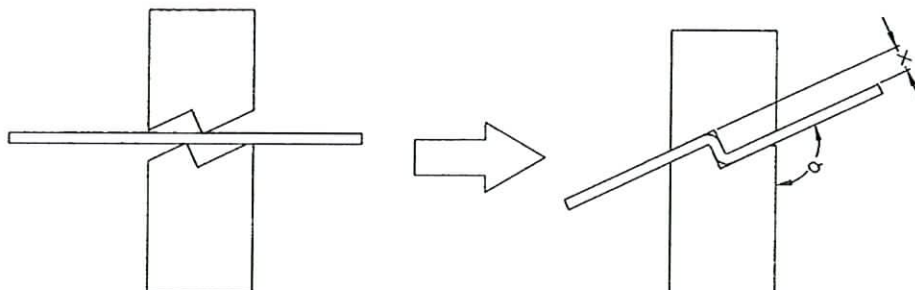


Figure 3.23

3.5.2. Material

3.5.2.1. Steel:

In order to compare the physical experimental results with the finite element analysis performed on Deform PC Pro, it was essential to ensure that the material mechanical properties of CR4 were substantiated. This proved difficult to achieve: there are many standards for the specification and description of the chemical, mechanical and bulk properties of steel. Each country seems to have its own standard, e.g., USA, Japan, etc. In fact, even within Europe, there is a European standard, and also individual standards including France, Germany, Italy, Spain, etc. After some considerable research, documentation was identified (see Appendix 4) correlating the CR4 standard of the actual workpieces with the AISI 1010 steel flow curve available in the Deform PC Pro Package.

3.5.2.2. Aluminium

The initial geometry of the aluminium workpiece was the same as that for the steel workpieces described in 3.5.1.

3.5.3 Workpiece Manufacture

3.5.3.1. Steel

A first series of workpieces (25mm x 8mm) were cut from stock using a power band saw. They were surface ground, and chemically etched with 6.0 mm grid circles. This size of workpiece was discarded after the first trial as it damaged the mild steel tooling used in the trial.

A second series of workpieces (40 mm x 3mm) were cut from stock using a power band saw, and surface ground. These workpieces, because they were made from a thinner material, were therefore expected to form to smaller bend radii, of the order of the material thickness. These workpieces were therefore grid circle etched with circles of 2.5 mm diameter in order to identify differential strains over a smaller bend radius. Again, these workpieces were discarded as the material fractured as its bend radius approached the material thickness.

A third series of workpieces were cut using the shear proof method on a CNC punch press from a 1250 mm x 1250 mm x 3 mm sheet of CR4. This ensured consistency in size from workpiece to workpiece. The surface finish on these workpieces was such that it was unnecessary to surface grind them before grid marking.

3.5.3.2. Aluminium

In common with the manufacturing method for the steel workpieces, the first series of aluminium workpieces (25 mm x 6 mm) were cut from stock using a band saw. They were not grid marked as the first forming trial indicated the problems with brittle fracture of the material and their use was discontinued.

The second series of workpieces were punched using the shear proof method on a CNC punch press. As with the CRS, the surface finish was such that surface grinding was not required before grid circle marking.

3.5.4. Grid Circle Marking.

In order to determine strain patterns on the surface of the workpieces, a grid circle pattern was used. The basic principle of the process is that a piece of initially unstrained material is etched to produce indelible circles of a suitable size and pattern. The diameter of the circles is known. The material in question is then strained via the manufacturing process being modelled. This results in the grid circles becoming ellipses whose major and minor axes lie in the directions of maximum and minimum principal strains respectively. The circles are usually formed by an electrochemical etching process.

The electrochemical etching process is relatively easy to execute.



Figure 3.24

The blank workpiece is cleaned in order to remove any oil or other residue that might affect its conductivity. In this case Radionics Fast Dry Precision Cleaner (Part number 203-0716) was used and found to be very effective.

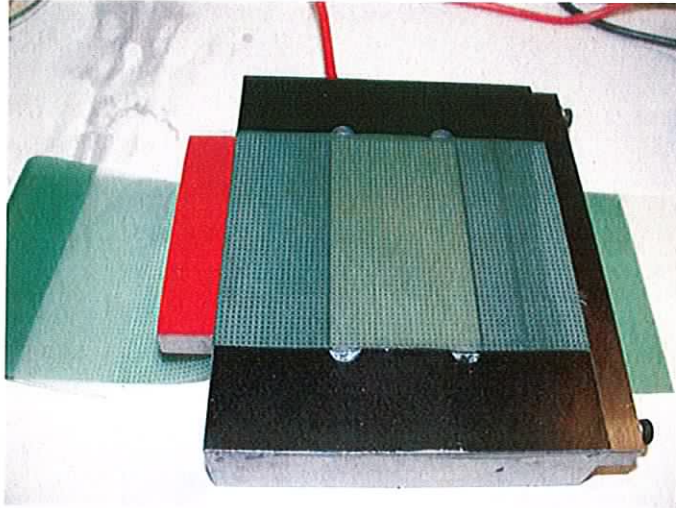


Figure 3.25

The correct grid stencil is placed on the workpiece. In this case, a fixture was designed and manufactured to ensure that the stencil remained in place during the etching process. This fixture also provided an effective grounding connection for the electrochemical etching current, as initial experiments showed that poor connections result in the generation of considerable heat.

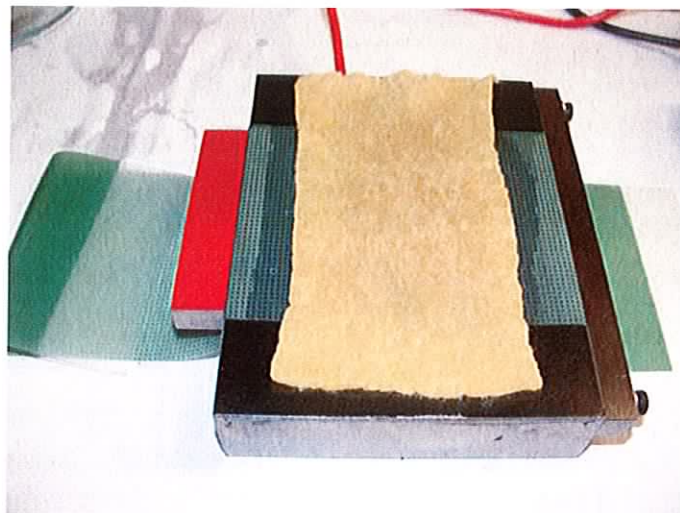


Figure 3.26

A felt pad soaked in the appropriate electrolyte (Lectroetch Electrolyte No. SC82 for aluminium, and Lectroetch Electrolyte No 39E for Steel) is placed over the workpiece as shown.

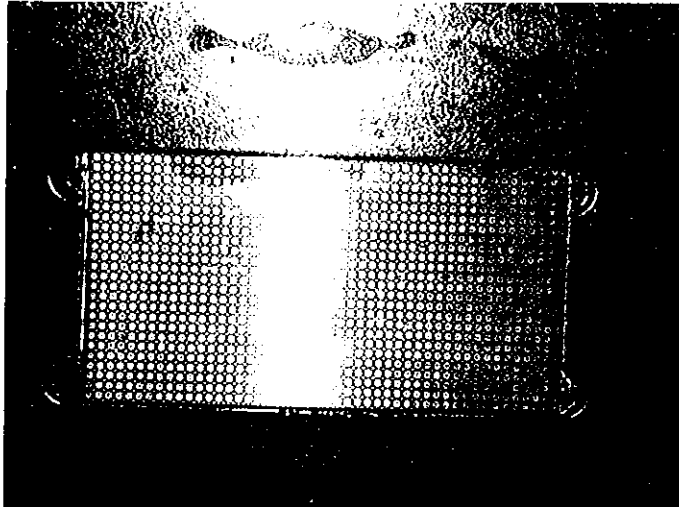


Figure 3.29

The final result of the process is shown here, (steel workpiece shown).

Although this is a process often described in texts concerning sheet metal forming, it was initially very difficult to locate specific information on the marking process and even more difficult to locate suppliers of the equipment used. This problem was resolved with the assistance of Corus. The proposed suppliers were:

Etch-Mark Limited,
Unit 5
Romford Road
Astonfields Industrial Estate
Stafford
ST16 3DZ
Tel: 0044 1785 253143
Fax: 0044 1785 223282

Universal Marking Systems Limited
Mount Road
Feltham
TW13 6EP
Tel: 0044 181 8984884
Fax: 0044 181 8989891

Lectroetch Company
5342 Evergreen Parkway
Sheffield Village
Ohio 44054
USA
Tel: 001 440 934 1249

Lectroetch Company was chosen as a supplier, based on price and availability of small diameter circles ($0.0625'' = 1.58\text{mm}$), essential to determine the form of strain fields on small radius bends.

3.6. Description of testing

The purposes of the experiments were to determine the actual force – displacement curves for the workpieces under consideration.

In normal sheetmetal bending processes, the radius of curvature of the bend is of the same order of magnitude as the thickness of the material undergoing bending. However, the length of the bend is usually several orders of magnitude larger than the material thickness. This leads to large force requirements for bends, especially bends with relatively small radii or relatively thick materials.

The first set of experiments used mild steel workpieces with the bend length: material thickness ratio in the order of 2.5:1, i.e., workpieces of 20mm x 8 mm cross section. By using a ratio of this magnitude, it was hoped that it might have been possible to measure strains through the thickness of the workpiece, on the outer surfaces, i.e., the sides of the workpieces. Figure 3.30 shows that some progress was made. Note however that at this stage of the experimental work it had not yet been possible to purchase grid-marking stencils, and the workpiece was marked out using marking blue, a surface coating used to increase the contrast of scribed lines on the workpiece, and a height gauge. This led to surface stress raisers, and figure 3.31 shows the fracture as a result of this. In addition, the forces required to complete the bending operation with this material thickness caused excessive stress for the mild steel tooling as shown in figures 3.32 and 3.33. This line of experimentation was abandoned.

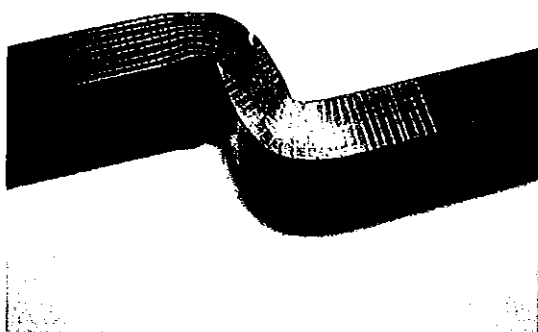


Figure 3.30

Through depth strain pattern, 8.0 mm thick workpiece.

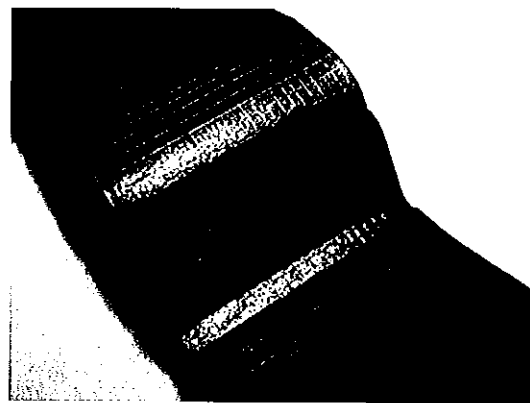


Figure 3.31

Fracture caused by stress raisers on 8.0 mm workpiece.

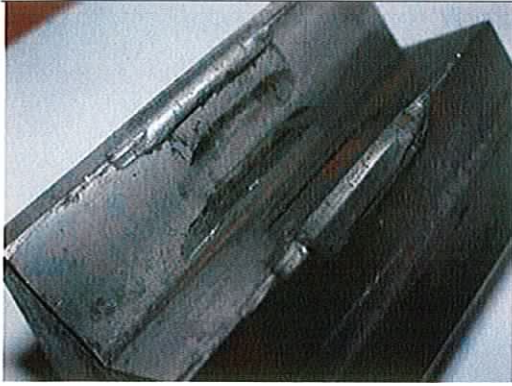


Figure 3.32

Tool damage caused by 8.0 mm workpiece.

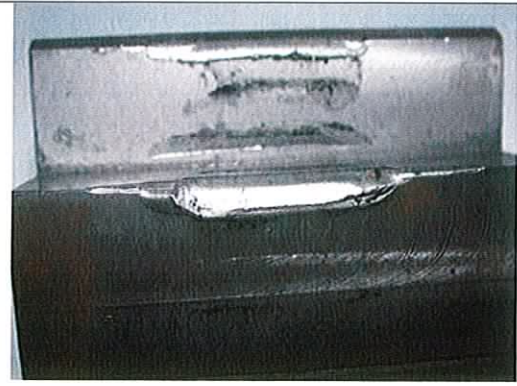


Figure 3.33

Tool damage caused by 8.0 mm workpiece.

In order to reduce the total required forces for experimental work, it was decided to use a workpiece with the bend length: material thickness ratio of about 13.

3.6.1. Experiment Operation

The following set of figures (3.34 to 3.42) show the general behaviour of the tooling and workpiece during the forming process:

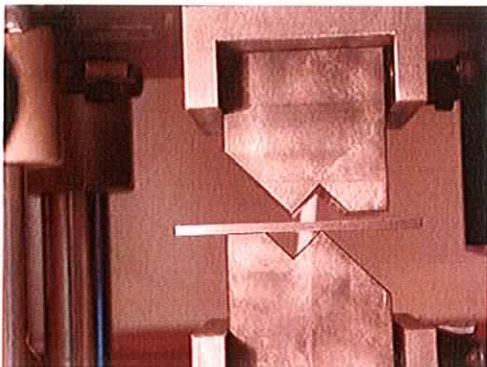


Figure 3.34

Test piece at start of forming process.

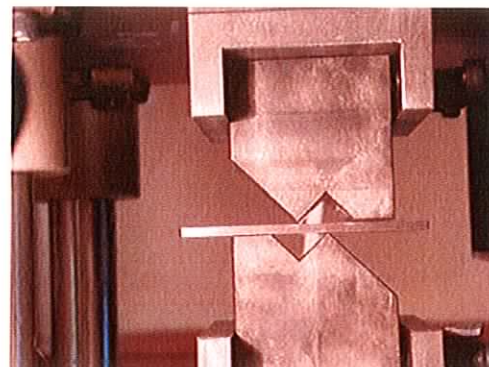


Figure 3.35

Stage 1 forming: Tool contact.

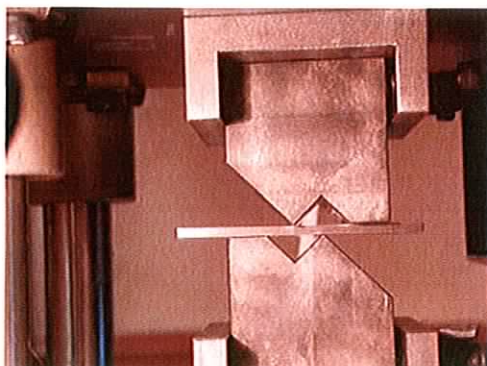


Figure 3.36
Stage 2 forming.

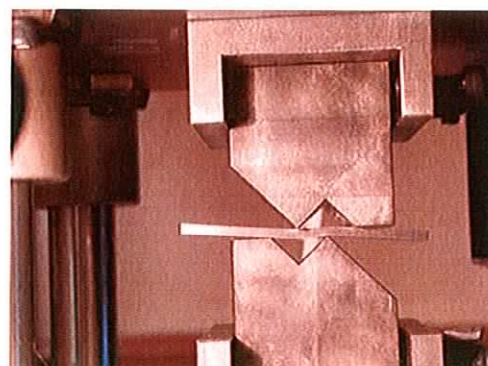


Figure 3.37
Stage 3 forming.

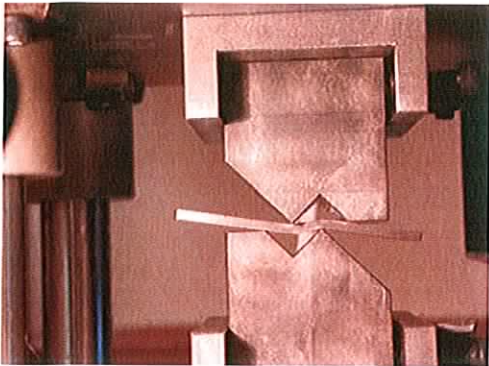


Figure 3.38
Stage 4 forming.

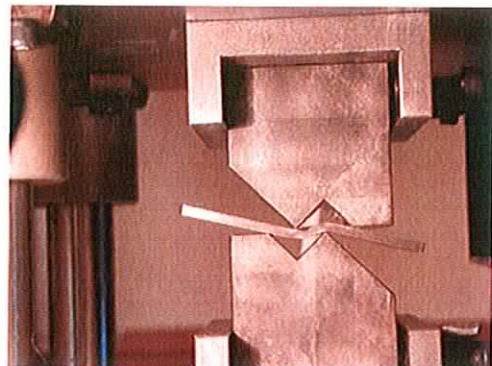


Figure 3.39
Stage 5 forming.

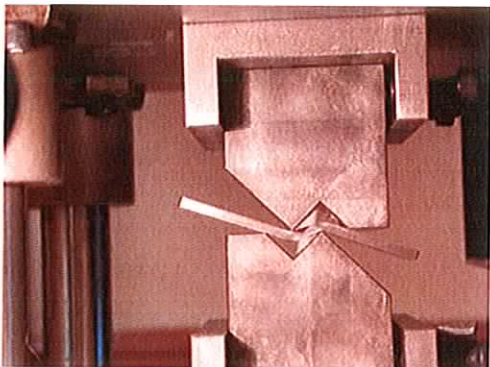


Figure 3.40
Stage 6 forming

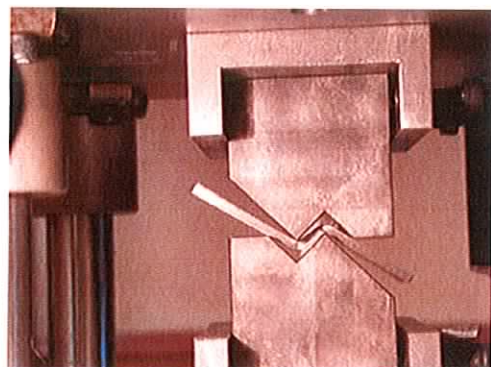


Figure 3.41
Stage 7 forming (fracture initiation).

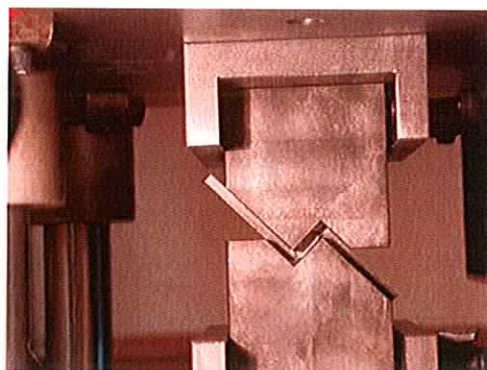


Figure 3.42
Stage 8 forming: Note fracture of workpiece.

Initially, the experiments were executed using mild steel tooling on a mild steel cold rolled strip workpiece. The logic for this approach was that mild steel tools are often used in industry

in these circumstances, in order to allow small production runs of non-standard components. However, due to the fact that extremely thick material was to be formed in the first experiments and in order to study through thickness distortion of the grid circles, the compressive loads were excessive and the mild steel tooling was plastically deformed under load. This led to this tooling being discarded and to the production of hardened tooling.

As can be seen from figures 3.41 and 3.42, the workpiece started to fracture before the completion of the forming stroke. This was due to the heavily work-hardened nature of the workpiece. As can be seen from the deformation of the grid circles in figures 3.43 and 3.44, the strain at fracture was small in the context of metal-forming processes.

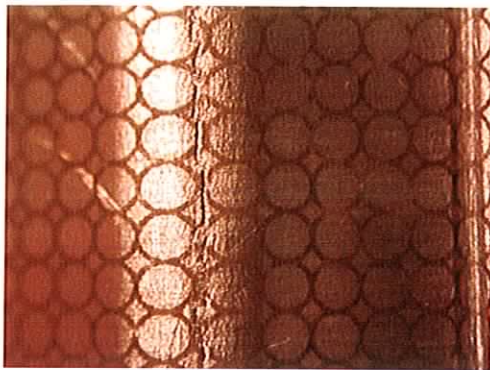


Figure 3.43
Fracture of workpiece

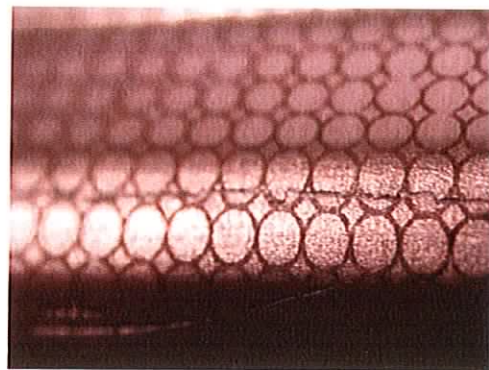


Figure 3.44
Fracture of workpiece

It was on this basis that forming grade (AISI 1010 or CR4) steel and Aluminium 6062 was used for further forming experiments. The results of the forming process are shown in the figures 3.45 to 3.56.

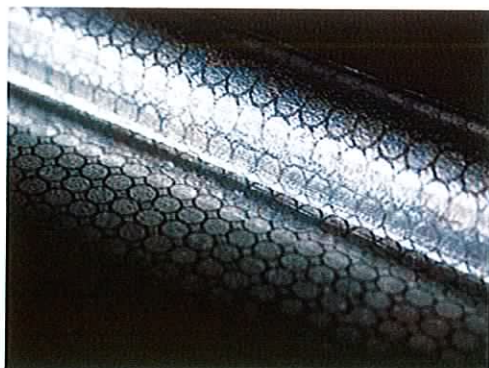


Figure 3.45
6.0 mm Die, 3.0 mm CR4.



Figure 3.46
6.0 mm Die, 3.0mm Al 6062.

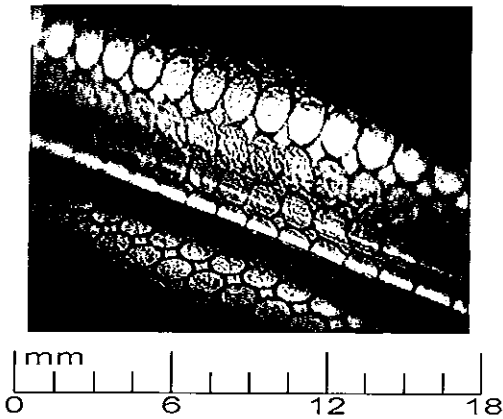


Figure 3.47
7.5 mm Die, 3.0 mm CR4.

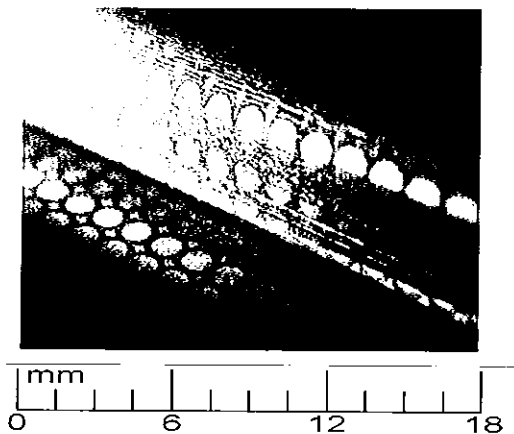


Figure 3.48
7.5 mm Die, 3.0mm Al 6062.

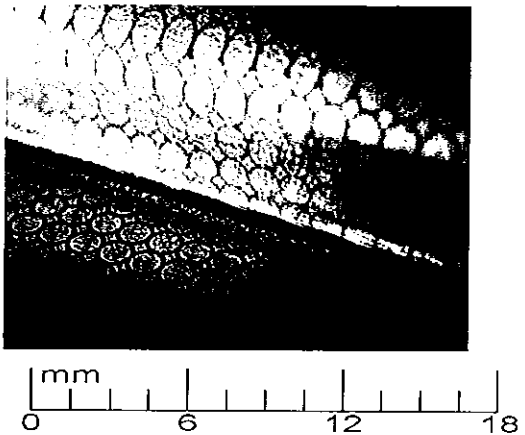


Figure 3.49
9.0 mm Die, 3.0 mm CR4.

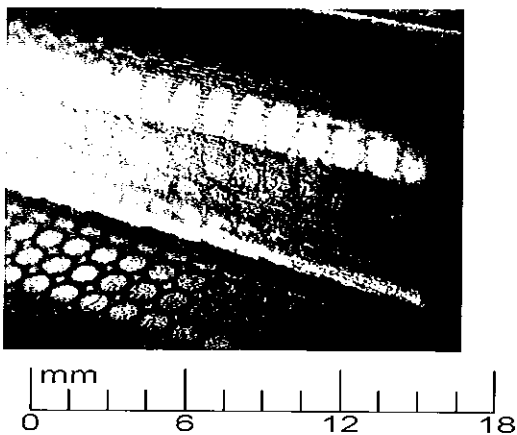


Figure 3.50
9.0 mm Die, 3.0mm Al 6062.

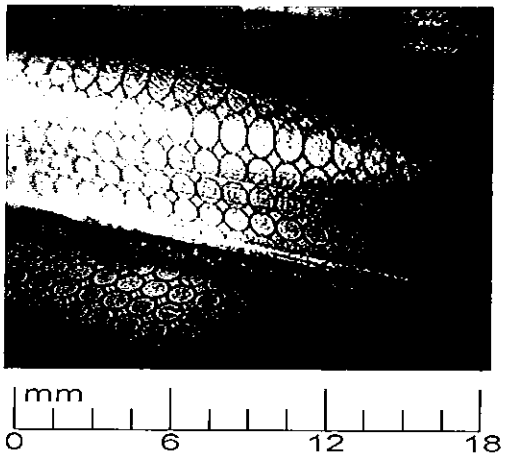


Figure 3.51
10.5 mm Die, 3.0 mm CR4.

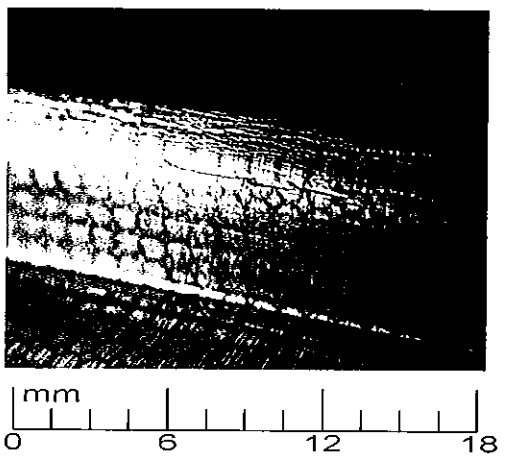


Figure 3.52
10.5 mm Die, 3.0mm Al 6062.

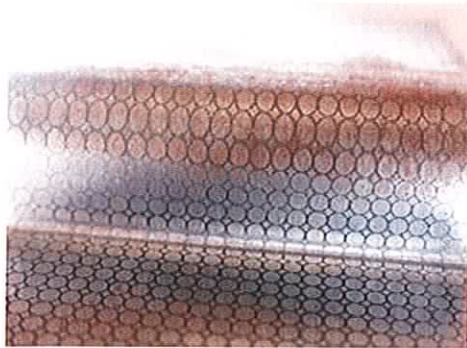


Figure 3.53

12.0 mm Die, 3.0 mm CR4.

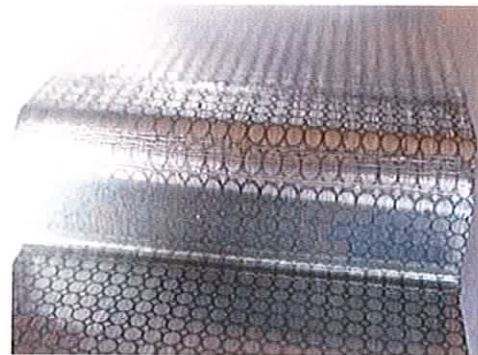


Figure 3.54

12.0 mm Die, 3.0mm Al 6062.

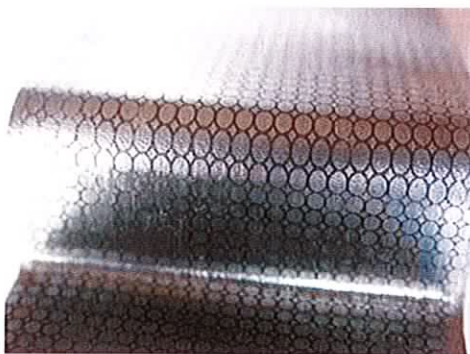


Figure 3.55

16.5 mm Die, 3.0 mm CR4.

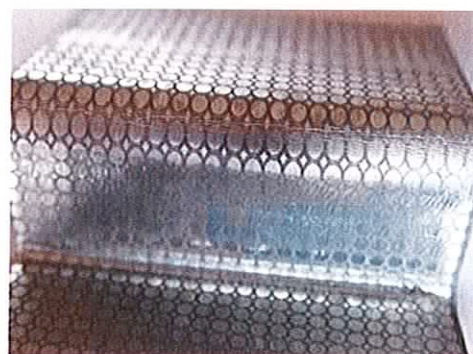


Figure 3.56

16.5 mm Die, 3.0mm Al 6062.

As can be seen from the figures above, the majority of the strain indicated by the change in shape of the grid circles is positive, i.e., there is very little if any compressive strain shown on the inner radii of the workpieces.

Comparing the steel and aluminium workpieces, it can be seen that there is more strain on the aluminium workpieces in the region of the bend than there is on the steel workpieces. Careful measurement with a digital calliper yields engineering strains of about 0.3 for the steel workpieces on the 6.0 mm dies, compared with engineering strains of about 0.6 for aluminium workpieces on the same dies. This rises to engineering strains of approximately 1.2 for steel and engineering strains of approximately 0.9 for aluminium on the 16.5 mm dies. It is thought

that the higher range in strain readings from the steel components may be a function of the difference in influence of both work hardening and friction between the steel workpieces and the aluminium ones.

It should be noted also that the aluminium workpieces exhibited surface fractures on all but the 6.0 mm dies. The reason for this is unclear, but a possible cause may have been variations in contact surface conditions, for example surface finish or unintentional lubrication differences in the workpieces. The principal axes are parallel and perpendicular to the long dimension of the workpiece.

3.7. Measurement and recording

Experimental data (Load – Displacement, Load – Time and Displacement – Time) data was acquired in real time. Load data was acquired via a calibrated load cell type Tokyo Sokki Kenkyujo CLC-30A, the characteristics of which are shown in Appendix 6. Displacement data was acquired via a Tokyo Sokki Kenkyujo CDP-50 50mm displacement transducer, again the characteristics of which are shown in Appendix 6. The data was logged and analysed by a National Instruments PCI-1200 data acquisition board, running National Instruments LabView on a PC under Microsoft Windows 95.

3.8. Finite Element software and setup

A finite element (FE) analysis of and physical deformation of 7 workpieces was carried out, in order that the reaction forces determined by experiment could be correlated with the FE predictions. This strengthens the case that the predicted FE stress and strain distributions, within the dies and workpieces respectively, are correct. The step height of the dies (i.e., the distance between corresponding faces of the workpieces, dimension x in figure 3.57), was as follows: 4.5 mm, 6.0 mm, 7.5 mm, 9.0 mm, 10.5 mm, 12.0 mm and 16.5 mm. This series of heights corresponded with the step heights on the tooling manufactured for the experimental work.

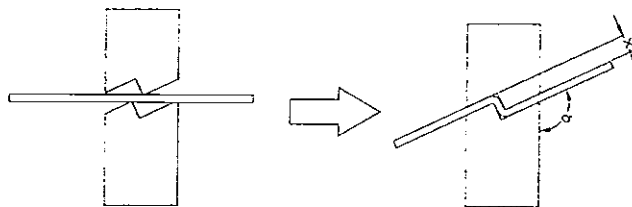


Figure 3.57
Workpiece and die profile

The geometry of the workpieces was drawn in AutoCAD and imported into the finite element program, Deform PC Pro, via the .iges file format. The material properties of the workpieces and materials were chosen from the material database that is integral with the program, having first confirmed that the material standards corresponded with the actual material that would be used in the experimental work. Additional criteria, e.g., the co-efficient of friction between the workpieces and the tooling etc., were chosen from the recommended values in the program, i.e., shear friction, $\mu=0.08$ for both the steel and aluminium workpieces.

Initially, the strain distributions in the material were computed first, and the stress in the tooling computed using the die stress analysis option in the program. This allows the die stress to be computed at any defined position in the deformation cycle. However, consideration of this method showed that it would be very time consuming, and it was decided to execute the analysis via the coupled problem method, i.e., compute the deformation of the workpiece, its strain patterns and the die stress analysis, all at the one time.

The analysis cycle takes approximately 4 to 6 hours to complete, depending on the die profile, and taking account of multiple analyses of independent workpiece strain and tooling stress analysis and a considerable number of practice runs, there totalled over 100 hours of analysis time.

A mesh density of 5000 elements was chosen for the workpiece model, as this is the area of primary concern in the analysis. The mesh density was kept constant. A mesh density of 2900 elements was chosen for the tooling, and the mesh density increased at areas of contact between the tool and the workpiece, as this is the area likely to be subject to increased stress. The Deform PC pro program facilitates variable mesh densities in both workpiece and tooling geometry.

A notable feature of the program is the automatic re-meshing of elements, when required. During the deformation analysis, the aspect ratio of an element may change to such an extent that the accuracy of the output may be compromised. In the event that this happens, the workpiece is automatically re-meshed, transferring the current material properties to the new elements, ensuring that material property changes in flow stress, density etc. are preserved. This ensures a more accurate model.

The method used to perform the FE analysis is described in Appendix 9.

4. Results and discussion

4.1. Experimental and FEA results: AISI 1010 Steel.

Experimental results were collated from a series of 7 trials of each workpiece produced in AISI 1010 Steel. These results were graphed and compared both with each other and with the corresponding FEA predictions. The total energy to deform each workpiece was calculated, and also compared on the same basis.

It can be seen from the general shape of the graphs that an increasing joggle displacement (distance x in figure 3.59) leads to a more convex rather than concave load – displacement curve. For the larger displacements (distances x), the curves are almost horizontal for the majority of their length and are close to the horizontal axis. This clearly indicates that the forces are comparatively low and steady at the earlier stages of deformation. The forces are likely to be of small magnitude due to the fact that the larger distances between contact points of the dies on the workpiece lead to greater bending moments for given forces. They increase steadily for the following reason. As strain occurs in one local area of the workpiece, work hardening takes place in this area, calling for an increase in stress to maintain the straining process. However, this increase in stress affects an adjacent, previously unstrained and hence softer area, which now becomes deformed and hence work hardened. This process takes place throughout the workpiece in one location after another leading to an overall smooth rise in reaction stress. For the tooling with smaller displacements x , larger forces are required to produce moments capable of forming the material and the predicted and experimentally measured forces are larger in the earlier stages of forming. These larger forces will in turn cause larger direct stresses, and therefore larger strains, in the region of the bends in the workpieces. In addition, there is likely to be an overlap of strain fields between one bend and the next in the smaller displacement experiments. This theory was verified by the finite element strain distribution results, see Figures 4.1 to 4.14 which show the load – displacement profiles of each experiment, followed by the corresponding FEA prediction, for comparison purposes. The 3.0 mm displacement dies were not used as the step height was found to be ineffective in producing a joggle bend. The strain hardening relationships that were used in the finite element analysis were those available as part of the software package, after verification that the material used in the experiments was the same as that modelled in the software.

4.1.1. Experimental vs. Finite Element results: 3mm AISI 1010 Steel, 4.5mm displacement dies.

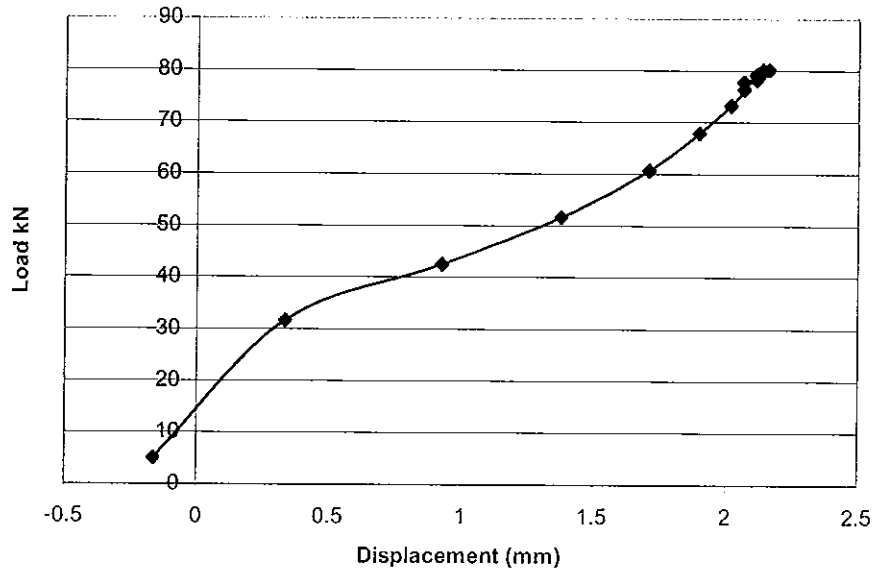


Figure 4.1
Load – Displacement 4.5 mm Die, 3.0 mm AISI 1010
(Experimental Result)

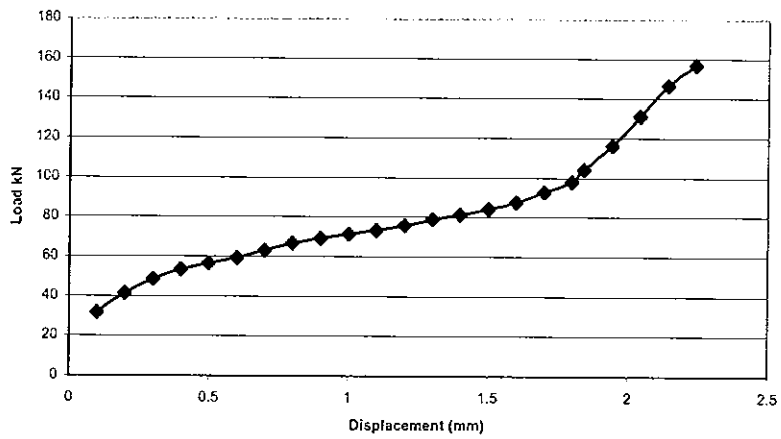


Figure 4.1
Load – Displacement 4.5 mm Die, 3.0 mm AISI 1010
(Finite Element Result)

4.1.2. Experimental vs. Finite Element results: 3mm AISI 1010 Steel, 6.0mm displacement dies.

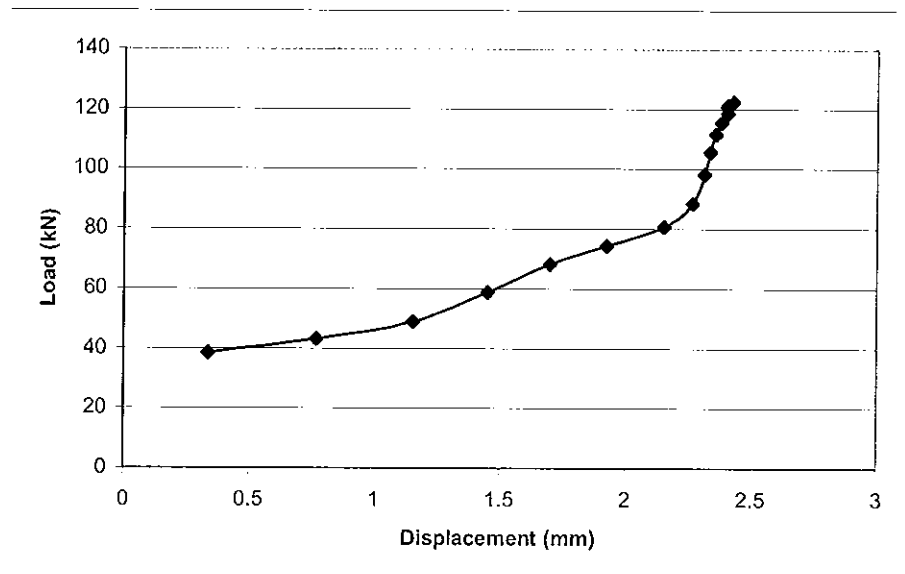


Figure 4.3

Load – Displacement 4.5 mm Die, 3.0 mm AISI 1010
(Experimental Result)

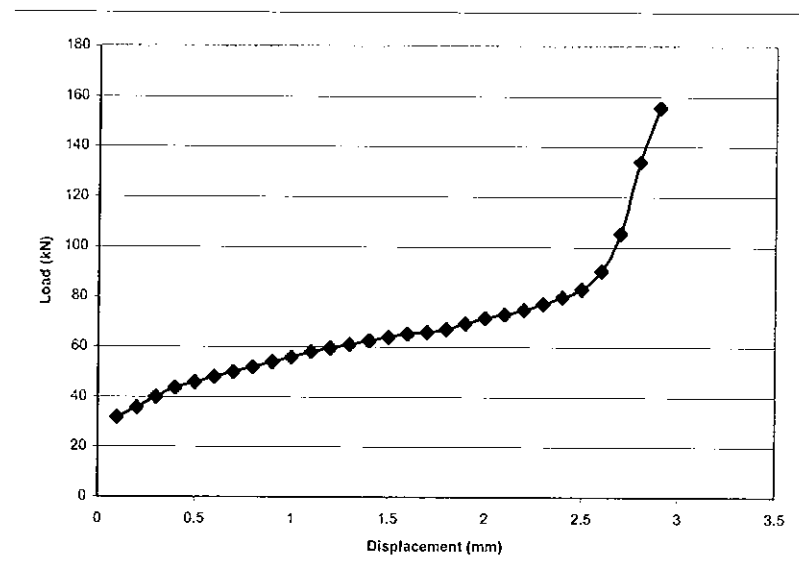


Figure 4.4

Load – Displacement 6.0 mm Die, 3.0 mm AISI 1010
(Finite Element Result)

4.1.3. Experimental vs. Finite Element results: 3mm AISI 1010 Steel, 7.5mm displacement dies.

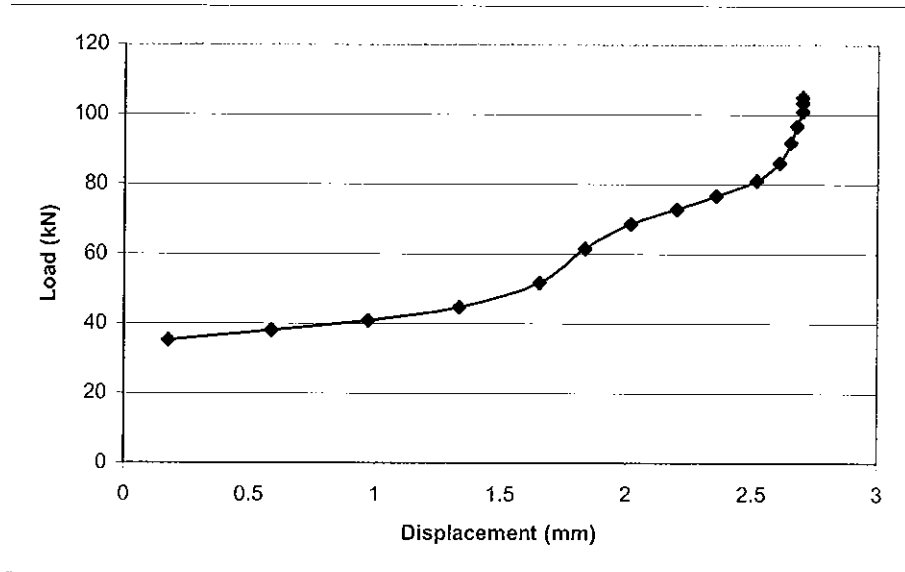


Figure 4.5
Load – Displacement 7.5 mm Die, 3.0 mm AISI 1010
(Experimental Result)

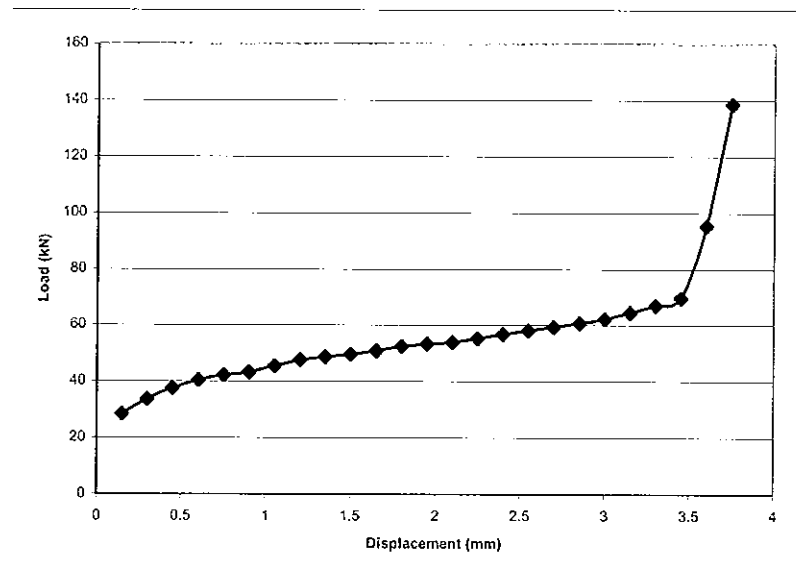


Figure 4.6
Load – Displacement 7.5 mm Die, 3.0 mm AISI 1010
(Finite Element Result)

4.1.4. Experimental vs. Finite Element results: 3mm AISI 1010 Steel, 9.0mm displacement dies.

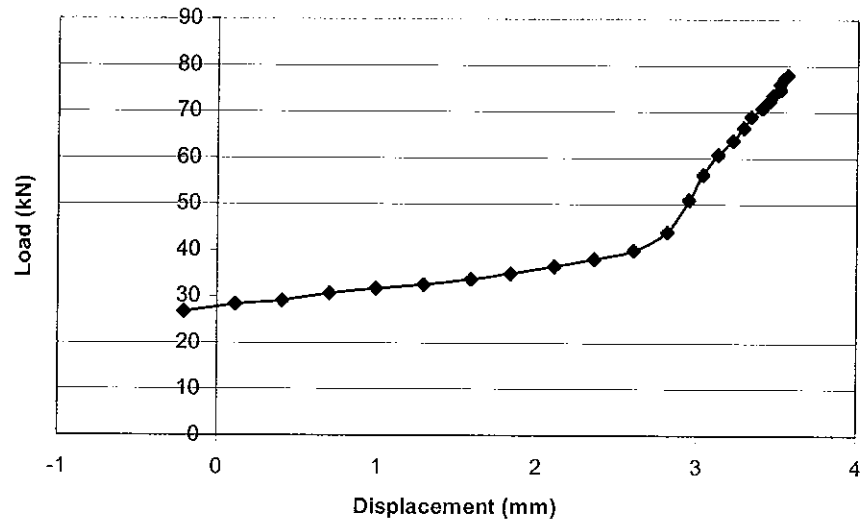


Figure 4.7

Load – Displacement 9.0 mm Die, 3.0 mm AISI 1010
(Experimental Result)

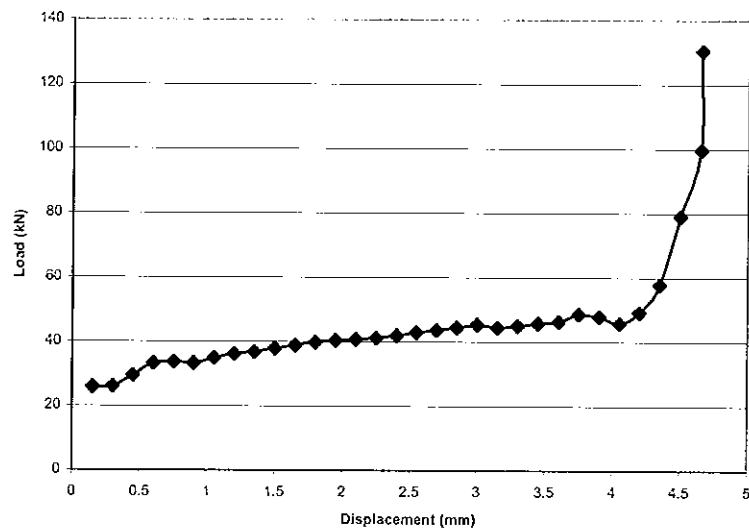


Figure 4.8

Load – Displacement 9.0 mm Die, 3.0 mm AISI 1010
(Finite Element Result)

4.1.5. Experimental vs. Finite Element results: 3mm AISI 1010 Steel, 10.5mm displacement dies.

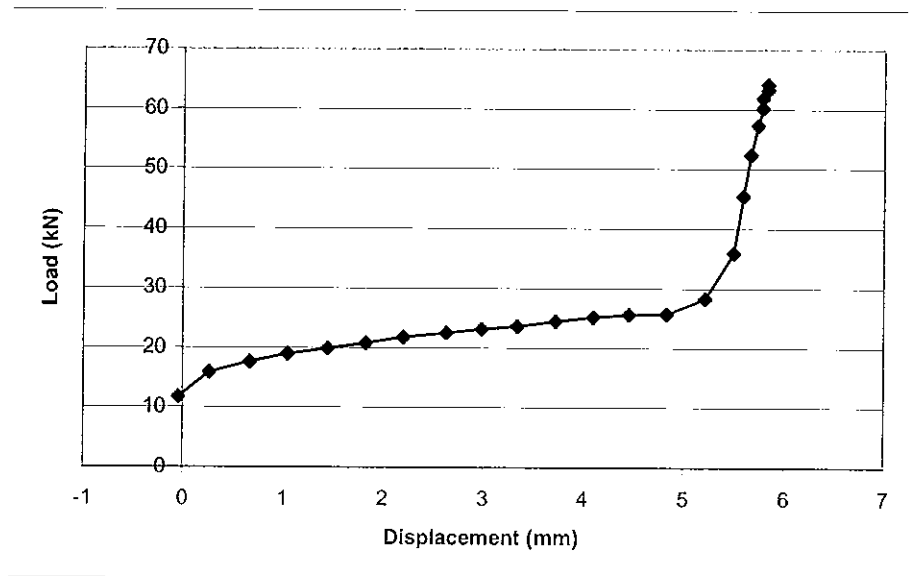


Figure 4.9
Load – Displacement 10.5 mm Die, 3.0 mm AISI 1010
(Experimental Result)

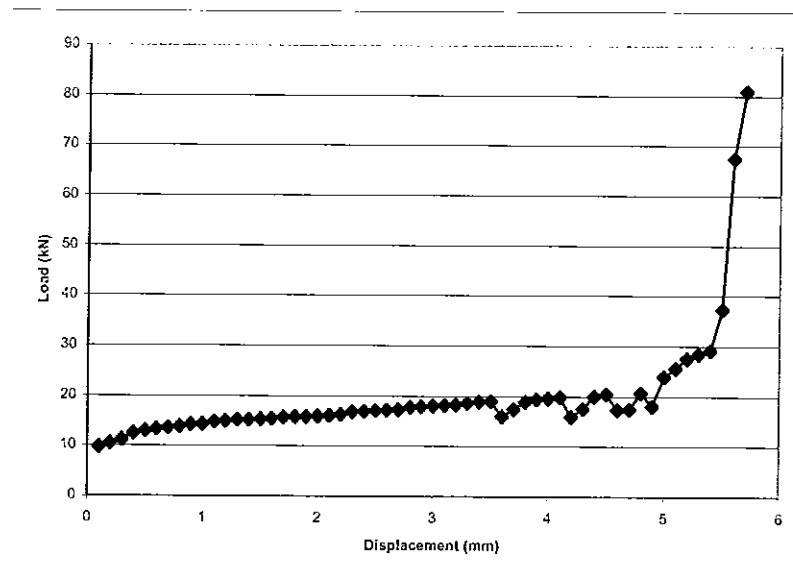


Figure 4.10
Load – Displacement 10.5 mm Die, 3.0 mm AISI 1010
(Finite Element Result)

4.1.6. Experimental vs. Finite Element results: 3mm AISI 1010 Steel, 12.0mm displacement dies.

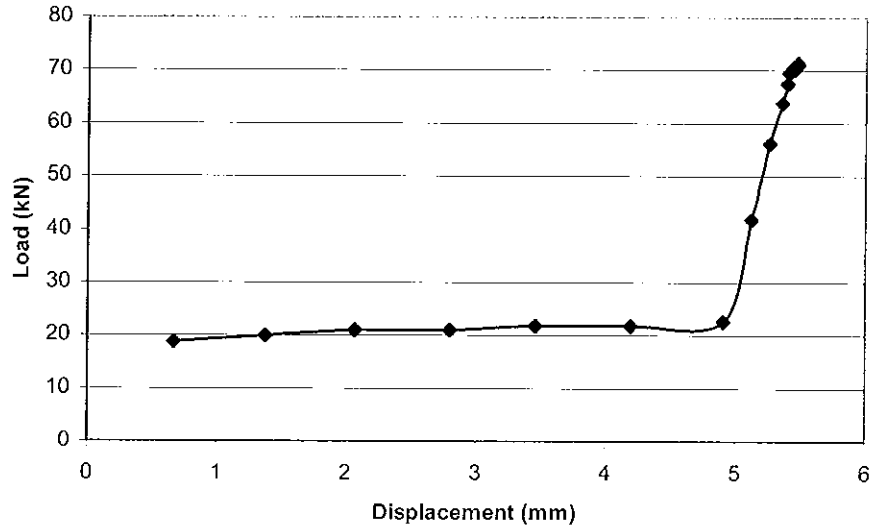


Figure 4.11
Load – Displacement 12 mm Die, 3.0 mm AISI 1010
(Experimental Result)

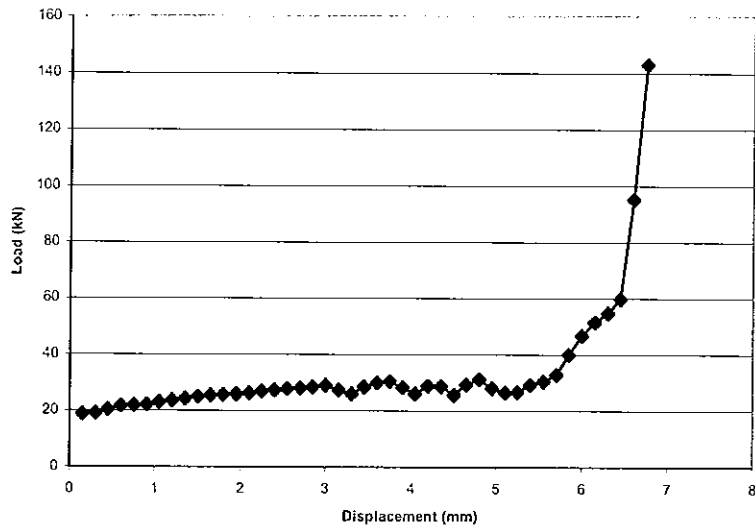


Figure 4.12
Load – Displacement 12.0 mm Die, 3.0 mm AISI 1010
(Finite Element Result)

4.1.7. Experimental vs. Finite Element results: 3mm AISI 1010 Steel, 16.5mm displacement dies.

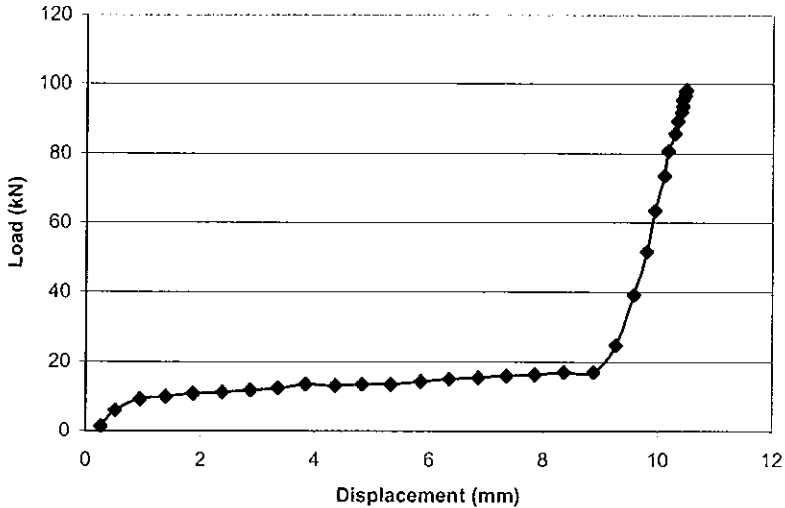


Figure 4.13
Load – Displacement 16 mm Die, 3.0 mm AISI 1010
(Experimental Result)



Figure 4.14
Load – Displacement 16.5 mm Die, 3.0 mm AISI 1010
(Finite Element Result)

4.2. Experimental and FEA results: 6062 Aluminium.

In common with the graphs for steel, the graphs for aluminium , given in figures 4.15 to 4.28 show a clear change from convex to concave format. It will be noted that for both materials, the transition point from convex to concave occurs at the 7.5 mm displacement tooling. It can also be seen that the forces required to form the steel workpieces are larger that those required for aluminium.

4.2.1. Experimental vs. Finite Element results: 3mm 6062 Aluminium, 3.0mm displacement dies.

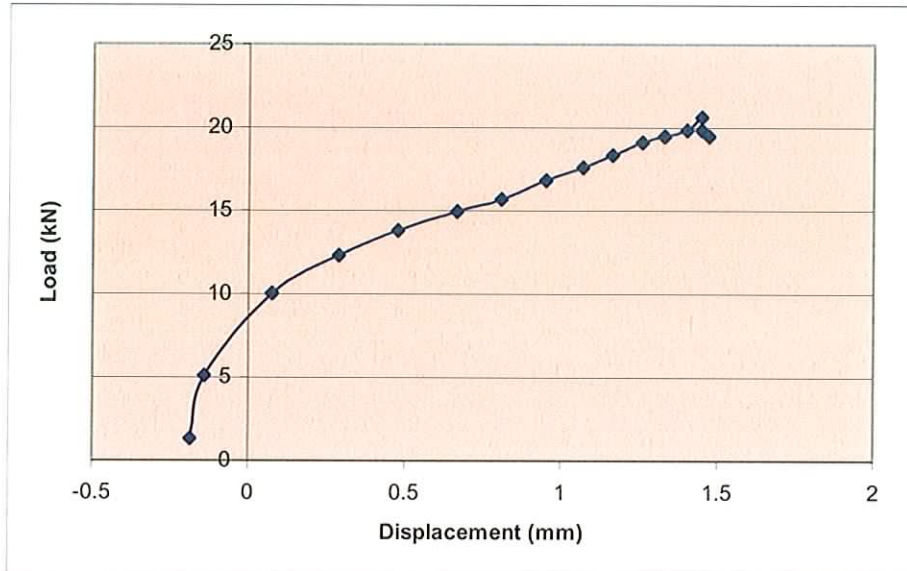


Figure 4.15

Load – Displacement 4.5 mm Die, 3 mm 6062 Aluminium
Experimental Result

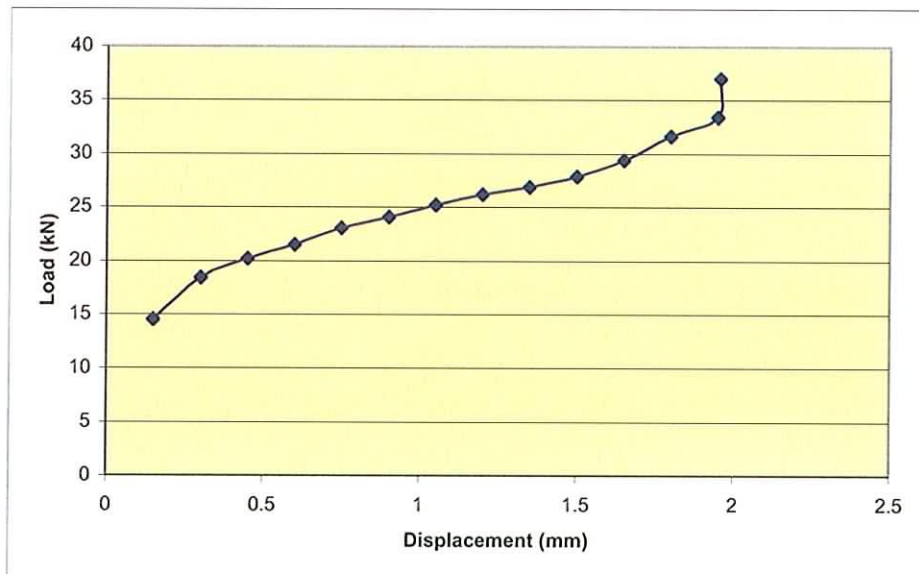


Figure 4.15

Load – Displacement 4.5 mm Die, 3 mm 6062 Aluminium
Finite Element Result

4.2.2. Experimental vs. Finite Element results: 3mm 6062 Aluminium, 6.0mm displacement dies.

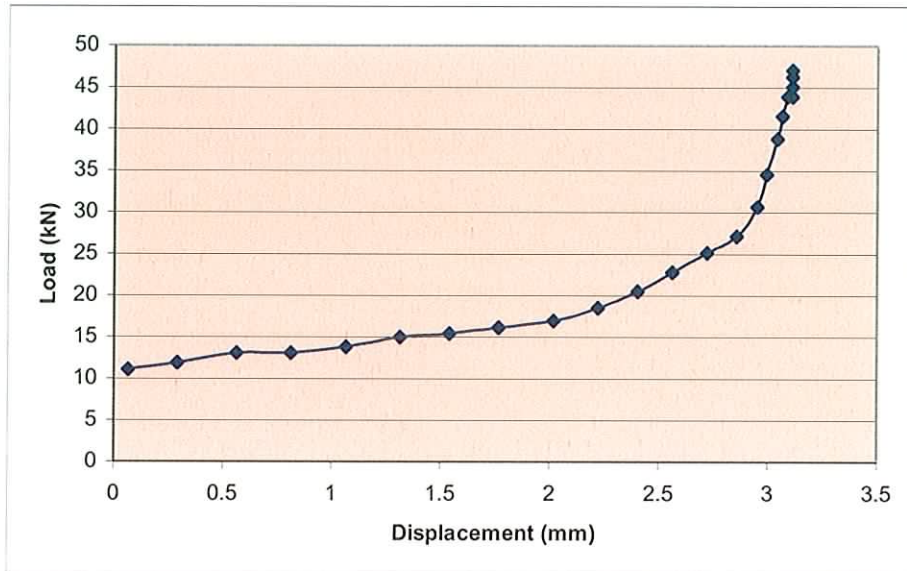


Figure 4.17

Load – Displacement 6.0 mm Die, 3 mm 6062 Aluminium
Experimental Result

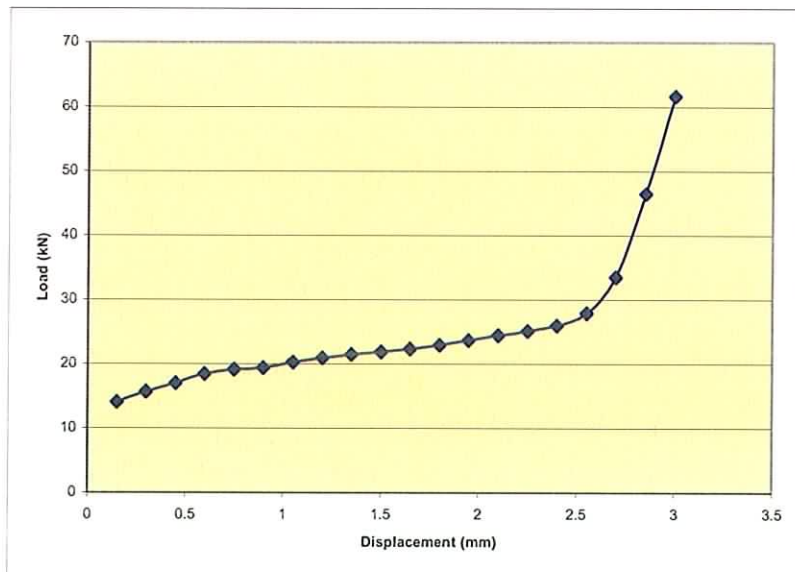


Figure 4.18

Load – Displacement 6.0 mm Die, 3 mm 6062 Aluminium
Finite Element Result

4.2.3. Experimental vs. Finite Element results: 3mm 6062 Aluminium, 7.5mm displacement dies.

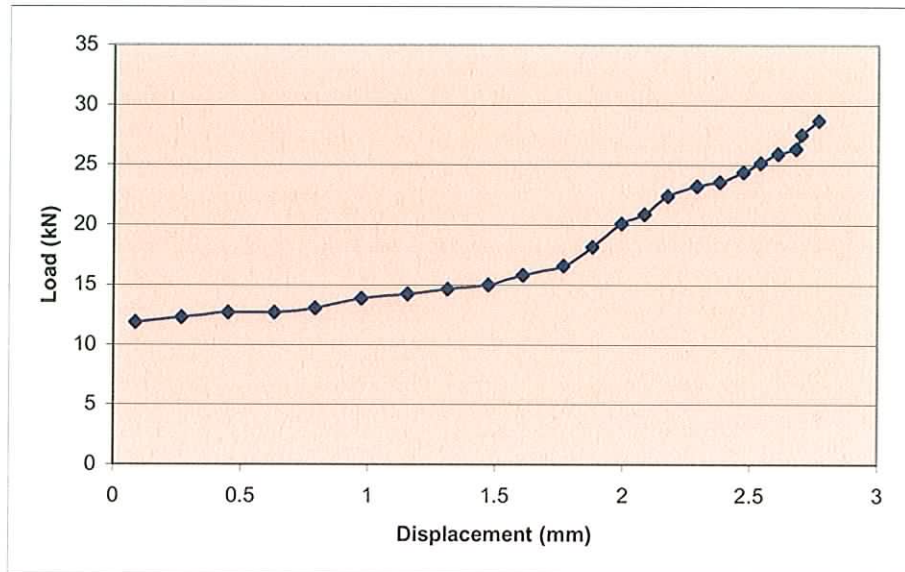


Figure 4.19

Load – Displacement 7.5 mm Die, 3 mm 6062 Aluminium
Experimental Result

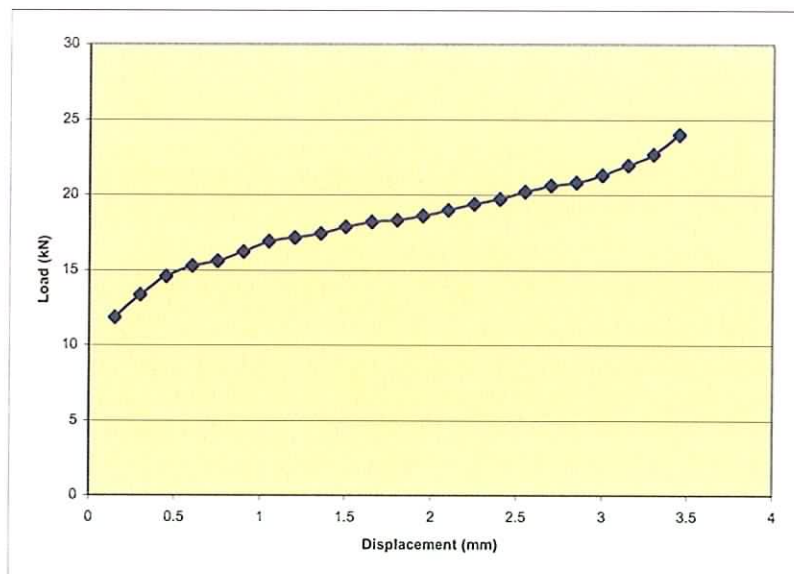


Figure 4.20

Load – Displacement 7.5 mm Die, 3 mm 6062 Aluminium
Finite Element Result

4.2.4. Experimental vs. Finite Element results: 3mm 6062 Aluminium, 9.0mm displacement dies.

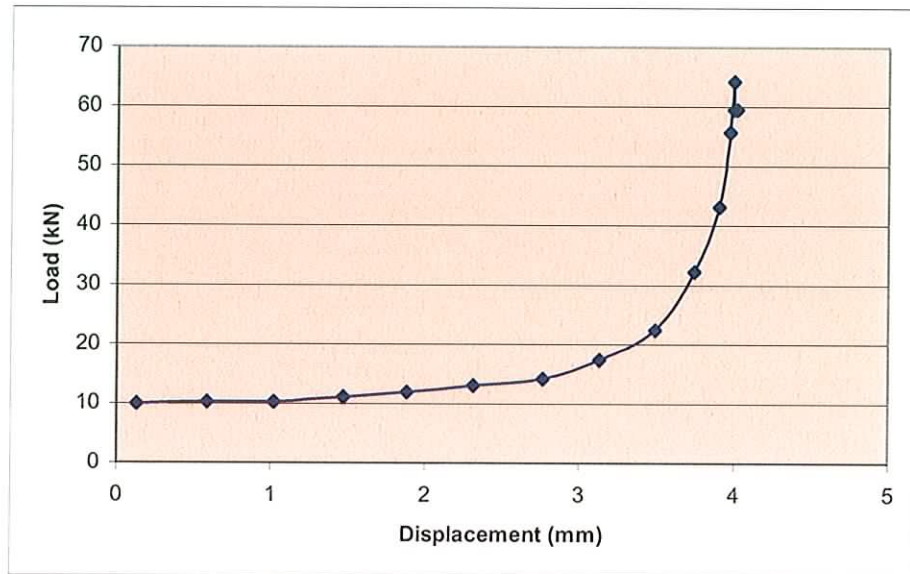


Figure 4.21

Load – Displacement 9.0 mm Die, 3 mm 6062 Aluminium
Experimental Result

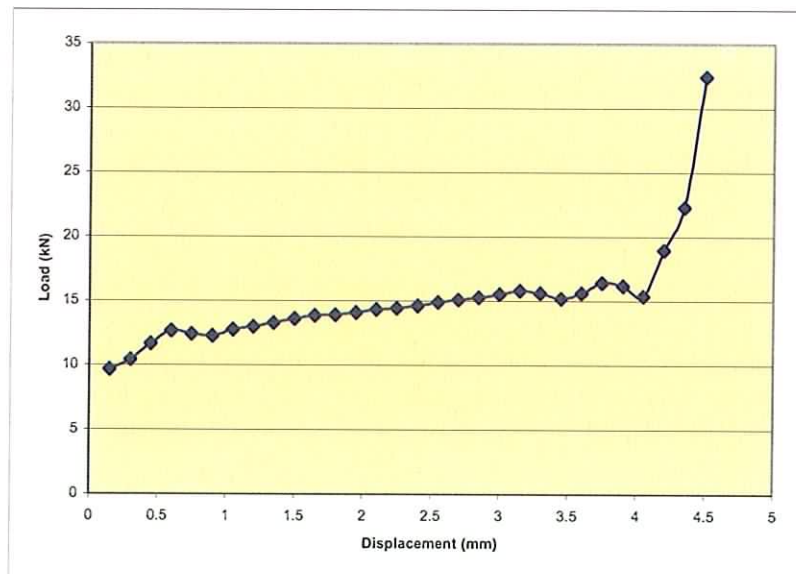


Figure 4.22

Load – Displacement 9.0 mm Die, 3 mm 6062 Aluminium
Finite Element Result

4.2.5. Experimental vs. Finite Element results: 3mm 6062 Aluminium, 10.5mm displacement dies.

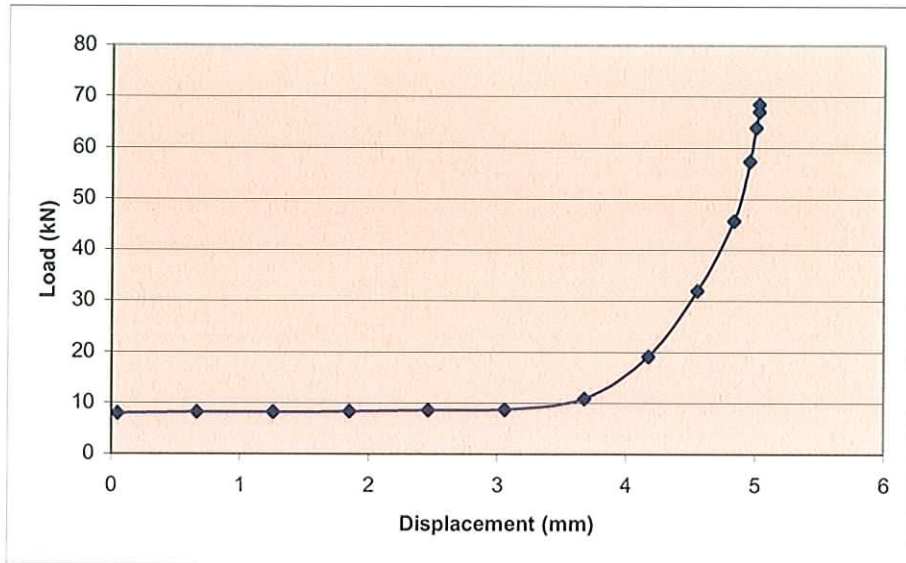


Figure 4.23

Load – Displacement 10.5 mm Die, 3 mm 6062 Aluminium
Experimental Result

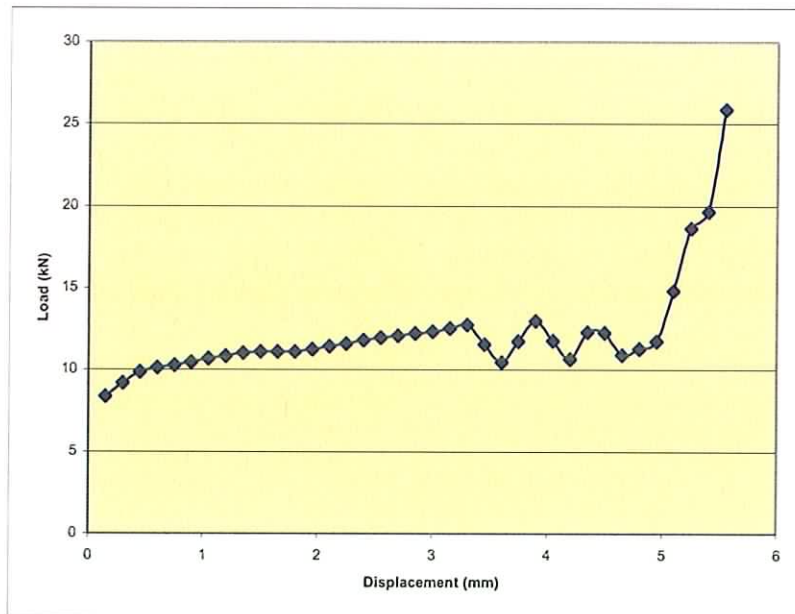


Figure 4.24

Load – Displacement 10.5 mm Die, 3 mm 6062 Aluminium
Finite Element Result

4.2.6. Experimental vs. Finite Element results: 3mm 6062 Aluminium, 12.0mm displacement dies.

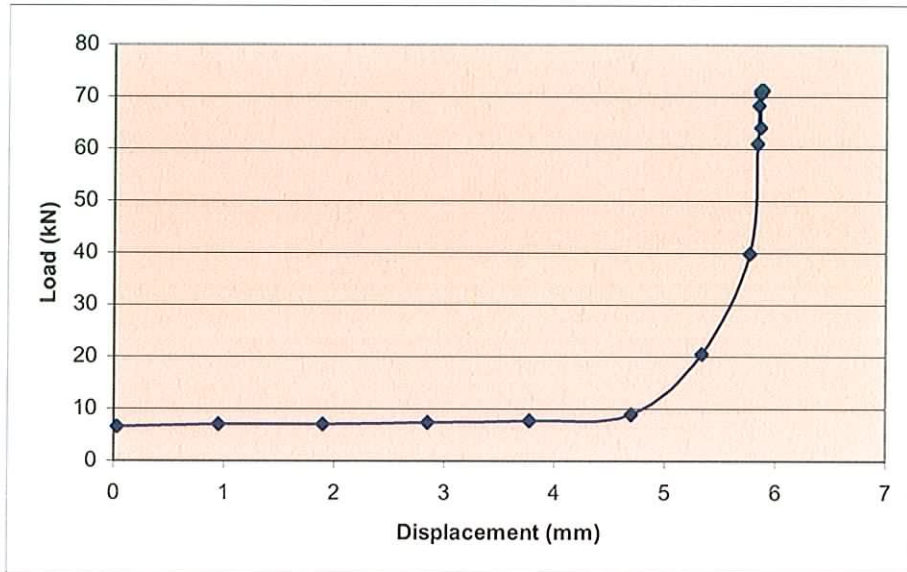


Figure 4.25

Load – Displacement 12.0 mm Die, 3 mm 6062 Aluminium
Experimental Result

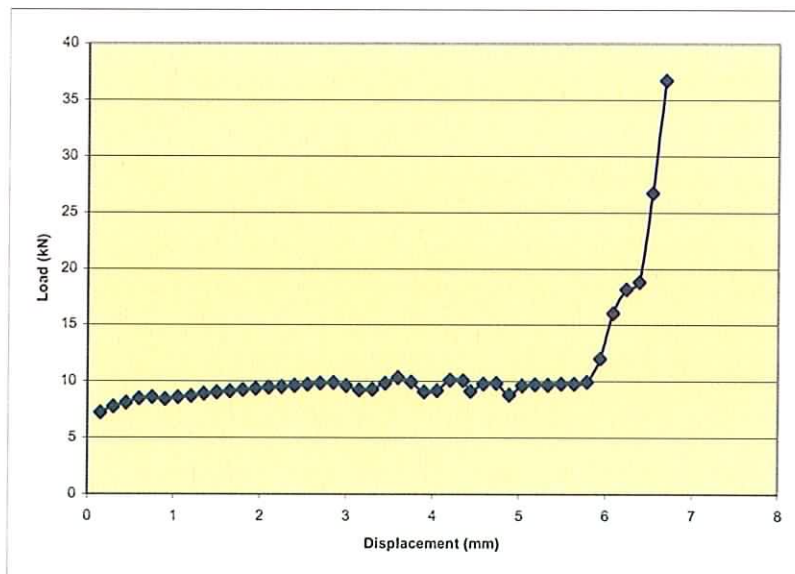


Figure 4.26

Load – Displacement 12.0 mm Die, 3 mm 6062 Aluminium
Finite Element Result

4.2.7. Experimental vs. Finite Element results: 3mm 6062 Aluminium, 16.5mm displacement dies.

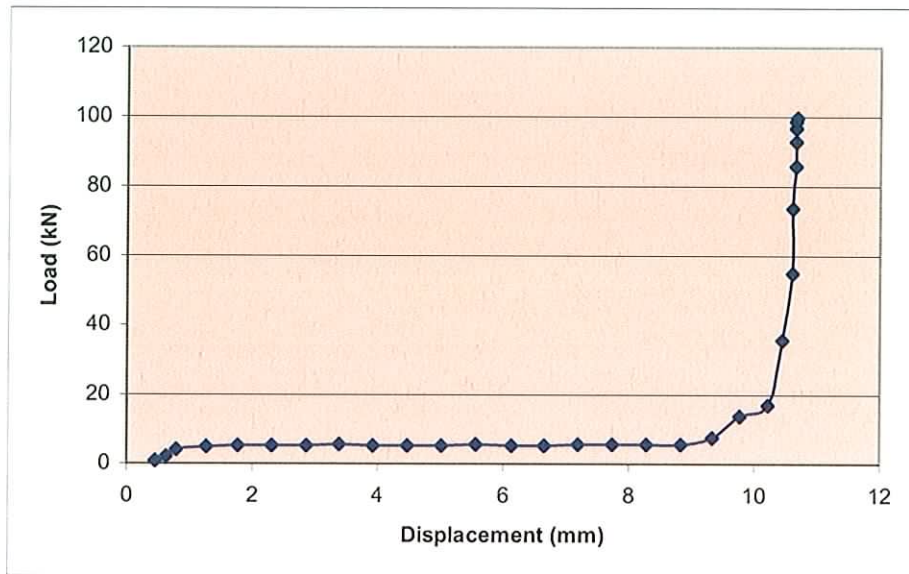


Figure 4.27

Load – Displacement 16.5 mm Die, 3 mm 6062 Aluminium
Experimental Result

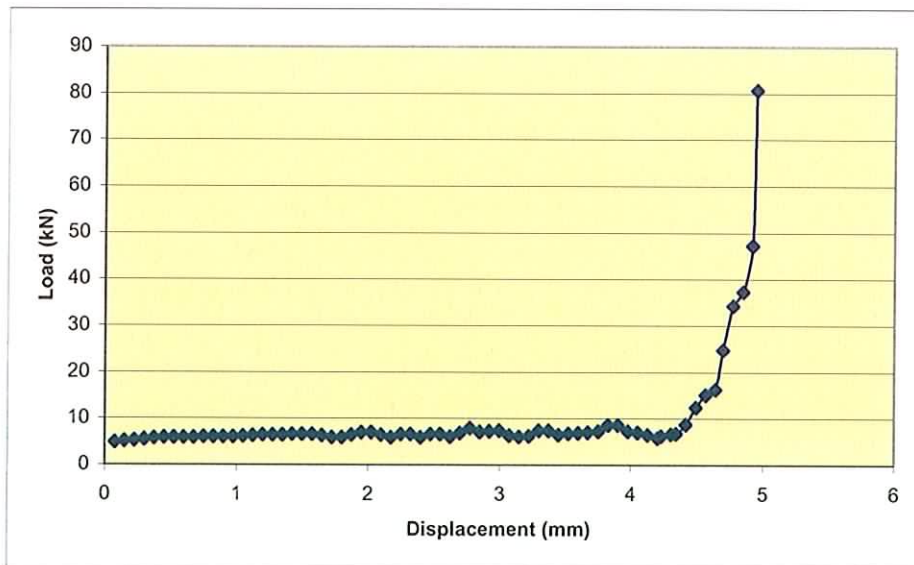


Figure 4.28

Load – Displacement 16.5 mm Die, 3 mm 6062 Aluminium
Finite Element Result

The experimental and finite element graphs show fair correlation in both shape of the load – displacement curves, and the order of magnitude of the forces measured in the experiment and predicted by the analysis. The experimental forming graphs were truncated as necessary for the smaller displacements, as the material of the workpiece exhibited surface damage at the higher forces. This accounts for some of the discrepancies found at higher deformations.

4.3. Discussion of Experimental and FEA results

A finite element analysis of and physical deformation of seven workpieces was carried out. The step height of the dies (i.e., the distance between corresponding faces of the workpieces, see dimension x in figure 4.29), was as follows: 4.5 mm, 6.0 mm, 7.5 mm, 9.0 mm, 10.5 mm, 12.0 mm and 16.5 mm. This series of heights corresponded with the step heights on the tooling manufactured for the experimental work.

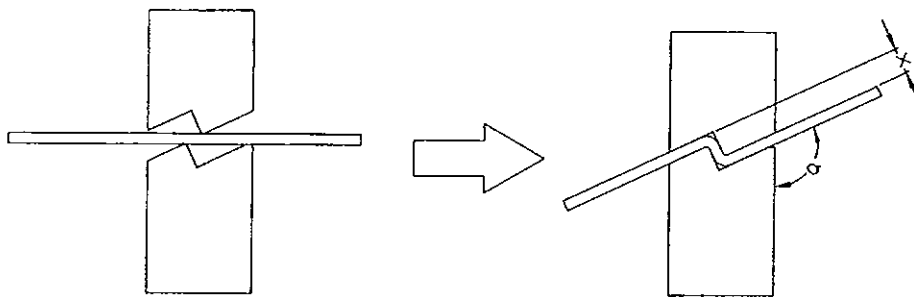


Figure 4.29

The geometry of the workpieces was drawn in AutoCAD and imported into the finite element program, Deform PC Pro, via the .iges file format. The material properties of the workpiece and materials were chosen from the material database that is integral with the program, having first confirmed that the material standards corresponded with the actual material that would be used in the experimental work. Additional criteria, e.g., the co-efficient of friction between the workpieces and the tooling etc., were chosen from the recommended values in the program.

Initially, the strain distributions in the material were computed first, and the stress in the tooling computed using the die stress analysis option in the program. This allows the die stress to be computed at any defined position in the deformation cycle. However, consideration of this method showed that it would be very time consuming, and it was decided to execute the analysis via the coupled problem method, i.e., compute the deformation of the workpiece, its strain patterns, and the die stress analysis, all at the one time.

The analysis cycle takes approximately 4 to 6 hours to complete, depending on the die profile, and taking account of multiple analyses of independent workpiece strain and tooling stress analysis, and a considerable number of practice runs, there totalled over 100 hours of analysis time.

A mesh density of 5000 elements was chosen for the workpiece model, as this is the area of primary concern in the analysis. The mesh density was kept constant. A mesh density of 2900 elements was chosen for the tooling, and the mesh density increased at areas of contact between the tool and the workpiece, as this is the area likely to be subject to increased stress. The Deform PC pro program facilitates variable mesh densities in both workpiece and tooling geometry.

A notable feature of the program is the automatic re-meshing of elements, when required. During the deformation analysis, the aspect ratio of an element may change to such an extent that the accuracy of the output may be compromised. In the event that this happens, the workpiece is automatically re-meshed, transferring the current material properties to the new elements, ensuring that material property changes in flow stress, density etc. are preserved. This ensures a more accurate model.

Appendix 7 presents selected data output from the analyses of the various die profiles for the two materials under consideration. The results are presented using the die profile as the primary classification, thereafter the material type.

The load-stroke diagrams are presented first, showing a characteristic curve for this type of die profile. For the smaller step height dies, the curve is markedly convex up – linear (small slope) – concave up – linear (larger slope), as shown in the example diagram figure 4.30.

A number of the finite element load – displacement profiles have characteristic undulations at various segments the curves, without corresponding undulations in the experimental curves. It is thought that these features may be due to the automatic re-meshing of the finite elements when the material properties of the elements have exceeded predefined limits.

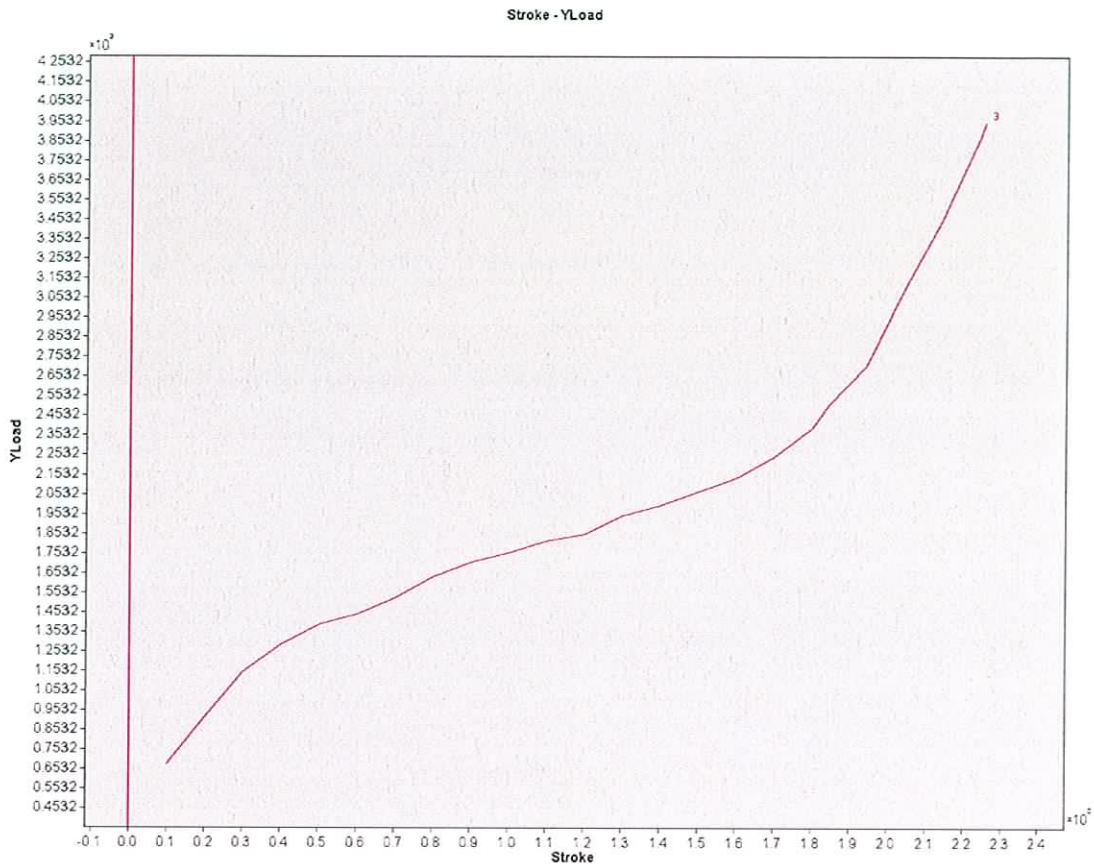


Figure 4.30 Example of graph of Load vs. Stroke, small step height dies, Finite Element Analysis output

The load – stroke diagrams for aluminium are similar to those for steel, with the exception of the actual loads causing similar displacements. These loads are, of course, lower for aluminium. In addition, for aluminium, a vertical ordinate has been drawn indicating the end of the manufacturing process: the excessive loads after this ordinate have caused thinning of the workpiece as opposed to only bending.

As the step height of the dies increases, the load – stroke diagrams start to change shape, i.e., approximately linear, rising very slowly, giving way to a sudden concave up and then sharply rising linear profile, as shown in figure 4.31.

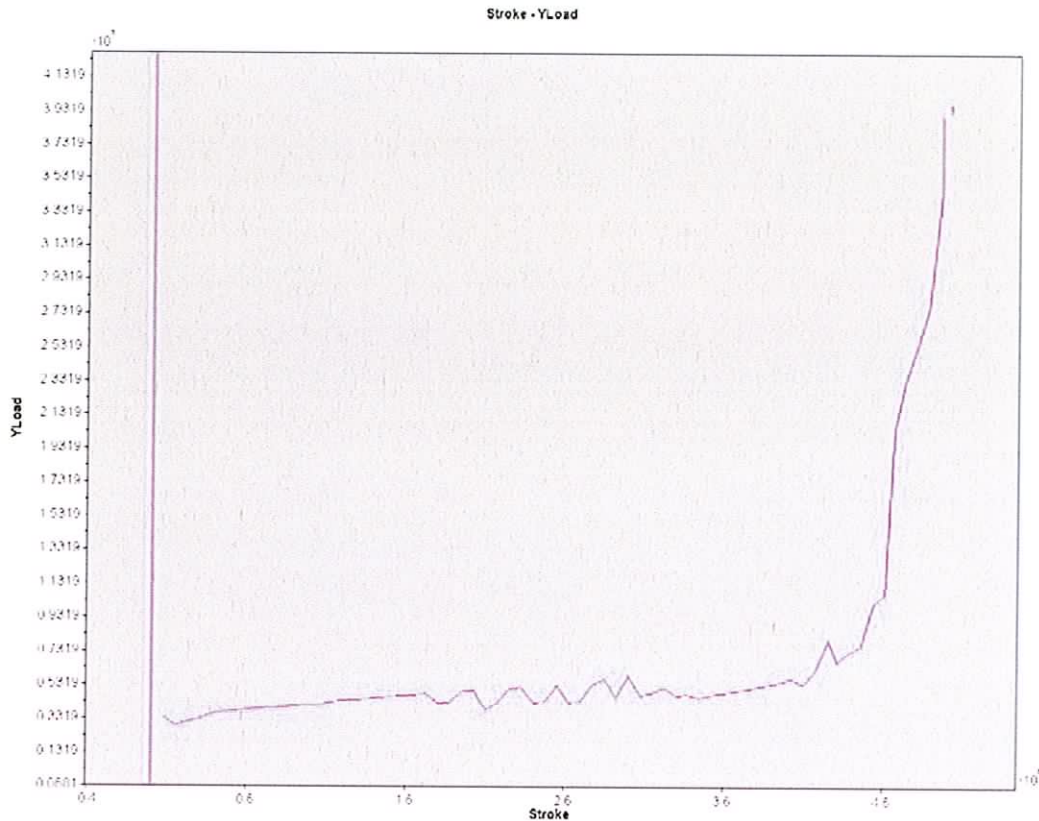


Figure 4.31 Example of graph of Load vs. Stroke, large step height dies, finite element analysis output.

This is thought to be due to the fact that because the step height is increasing, the distance between the load bearing points on the dies is increasing, increasing the effect of the induced bending moment, and decreasing the effect of the shear force. The sudden rise in load for small displacements at the end of the diagram is due to the dies 'shutting out', i.e., the die faces are coming into contact with the workpiece faces, increasing the contact area significantly, hence increasing the force required to produce further displacement.

The general shape of the load – displacement curves are retained across both the finite element results and the experimental results. Both curves are shown for comparison purposes on consecutive pages in Appendix 7, for each die step height and material. The correlation between curve shape and position for each die and material is considered to be reasonable.

The area under the load – displacement curves is indicative of the magnitude of the energy converted during the bending process. The areas under all curves were evaluated, for both finite element and experimental work, in order to compare energy conversion. It should be noted here that due to the fact that it was difficult to anticipate the total loads required to deform the workpieces before the experimentation took place, some workpieces were

deformed beyond the manufacturing requirements. It was therefore necessary to truncate some of the load – deformation curves in order to calculate the energy required to perform the manufacturing process only. The energy requirements are shown in table 4.1:

| Step Height (mm) | Energy for Total Deformation (J) | | | |
|---------------------|----------------------------------|-----------|--------------|-----------|
| | Finite Element | | Experimental | |
| | Steel | Aluminium | Steel | Aluminium |
| 4.5 | 169.5 | 49.2 | 102.5 | 23.5 |
| 6.0 | 182.8 | 75.4 | 127.5 | 54.1 |
| 7.5 | 197.0 | 63.1 | 136.4 | 45.7 |
| 9.0 | 197.0 | 67.7 | 146.9 | 62.0 |
| 10.5 | 105.6 | 65.0 | 138.9 | 63.0 |
| 12.0 | 205.2 | 67.9 | 116.7 | 62.0 |
| 16.5 | 122.3 | 41.8 | 192.5 | 75.4 |

Table 4.1

Comparison of the Step Height Vs. Energy (Total Deformation) curves for AISI 1010 / CR4 steels as shown in figures 4.32 to 4.35 shows a clear minimum in energy requirement of 100J to 120J at a step height of 10.5 to 12.0 mm. This correlates with the total separation of strain fields at the 10.5 mm step height as shown by the finite element strain field graphics, figures 4.36 and 4.37. These figures show that for the smaller step height the strain fields propagate from the bend sites through the short flange and penetrate each other, yielding a single strain field, whereas on the larger die they do not.

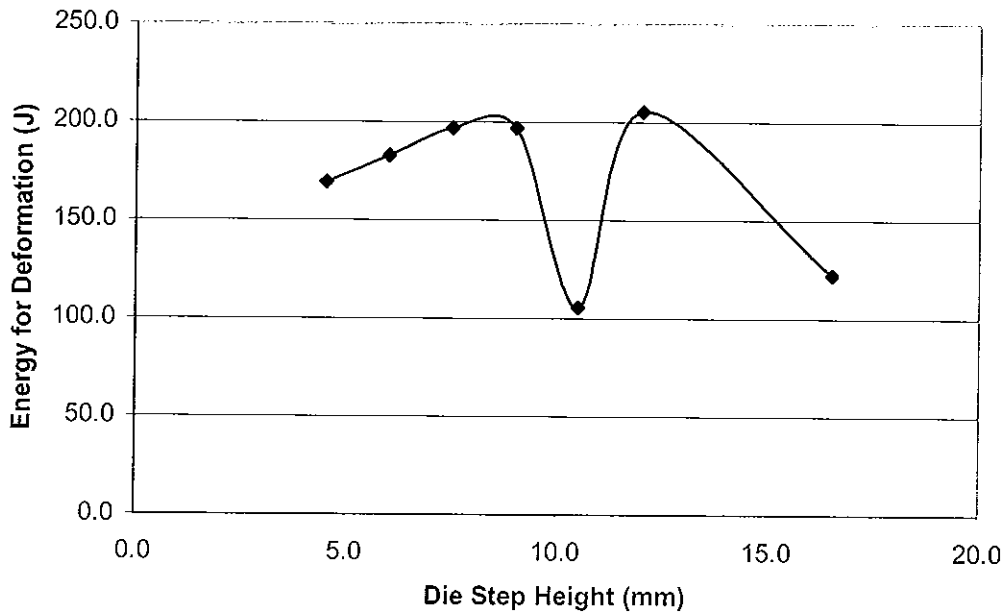


Figure 4.32

Step Height vs. Energy (Total Deformation) Finite Element Analysis Results (AISI 1010 / CR4 Steel)

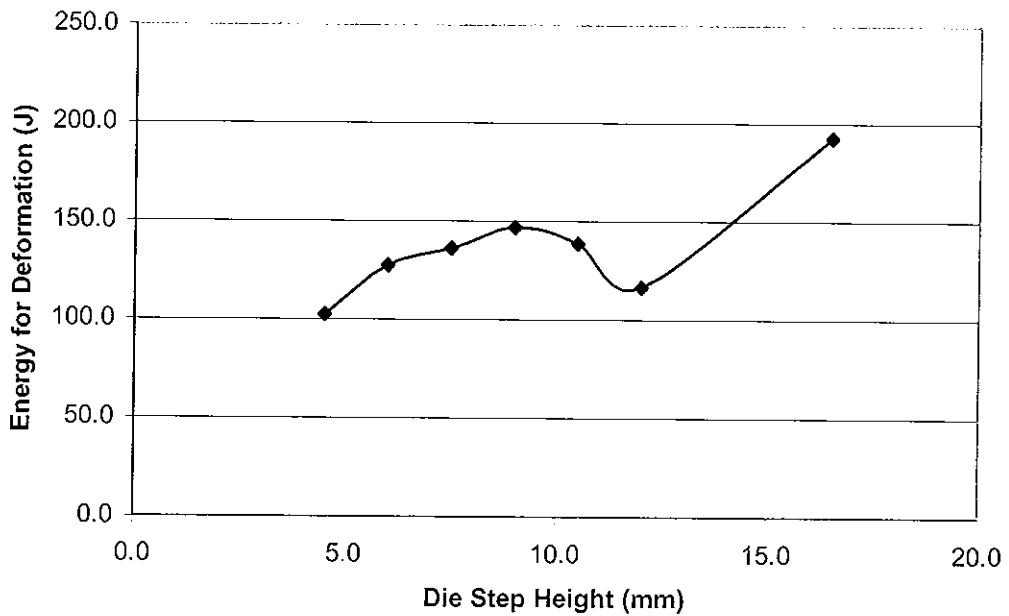


Figure 4.33

Step Height vs. Energy (Total Deformation) Experimental Results (AISI 1010 / CR4 Steel)

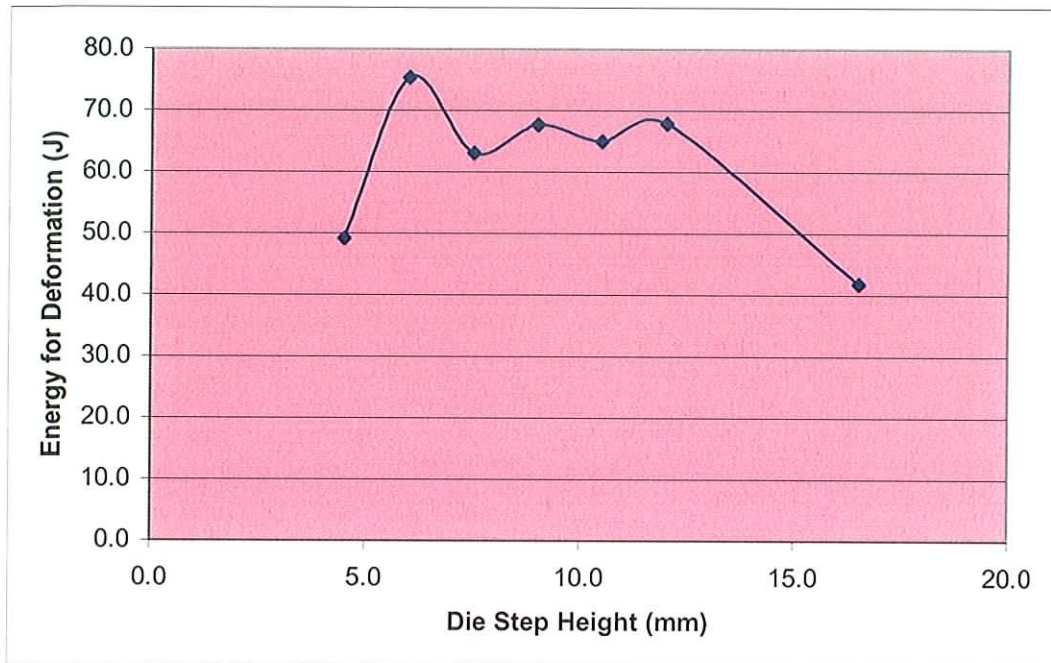


Figure 4.34

Step Height vs. Energy (Total Deformation) Finite Element Analysis Results (Aluminium 6062)

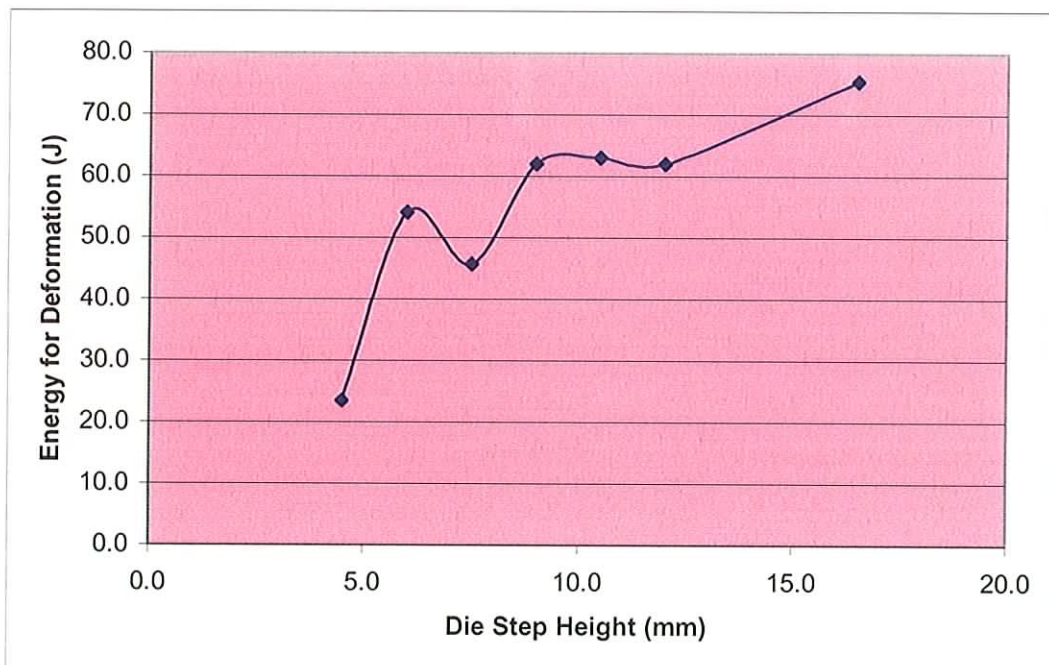


Figure 4.35

Step Height vs. Energy (Total Deformation) Experimental Results
(Aluminium 6062)

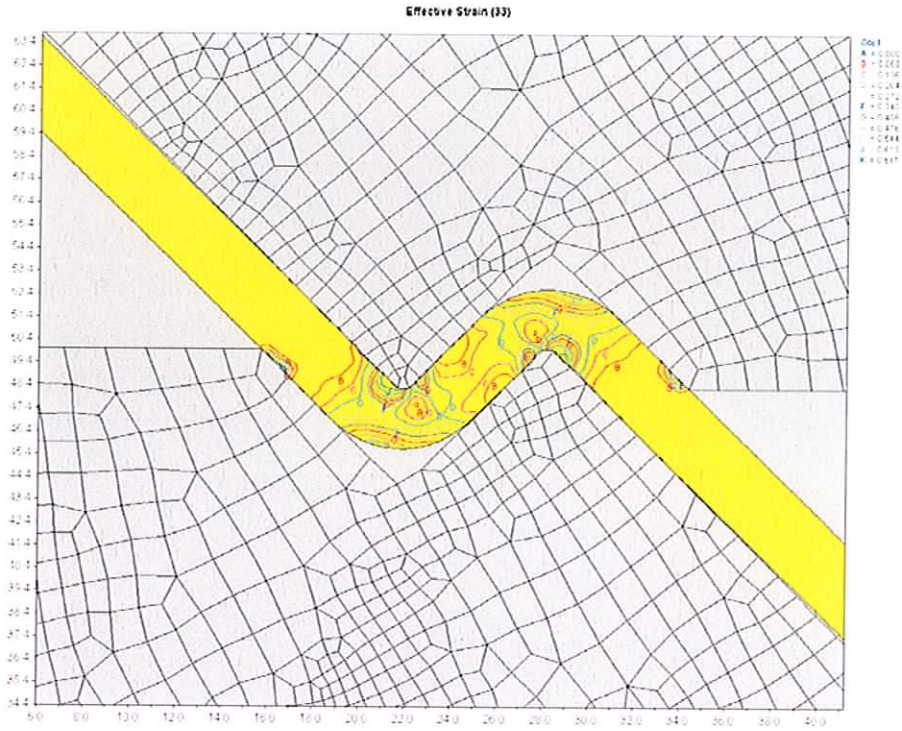


Figure 4.36

9.0 mm Step Height, AISI 1010 / CR4 steel, showing interpenetrating strain fields.

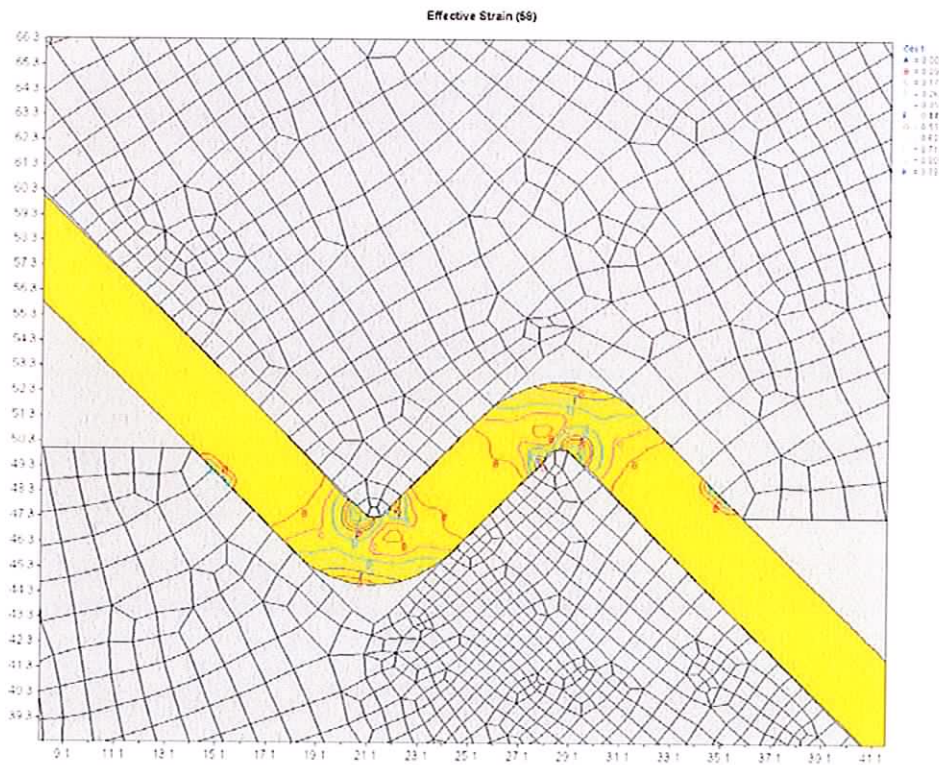


Figure 4.37

10.5 mm Step Height, AISI 1010 / CR4 steel, showing separation of strain fields.

However, it is noted that as the step height rises to 16.5 mm, the FE results and the experimental observations do not correlate.

A correlation is also apparent between the finite element prediction and the observed results in the case of the aluminium workpieces. The finite element analysis shows a local maximum in energy at a 6.0 mm step height, followed by a local minimum at the 7.5 mm die, and then a relatively constant energy requirement thereafter, the general profile of which is matched by the experimental results. However, as with the steel workpieces, the FE and experimental results diverge considerably thereafter.

The deformation characteristics of the FE prediction and the observed results correlate well, as shown in figures 4.34 and 4.35. The small step height reduces the bending moment available for a given force, i.e., because the bending moment is the product of force and perpendicular distance from the force to the fulcrum, a reduction in perpendicular distance causes a reduction in bending moment. Hence to produce a given bending moment for a reduced perpendicular distance, a higher force must be used. In the case in question, it can be seen that the required force is so large that the compressive yield point of the material is reached before the full bend deflection occurs. This can be observed both in the FE prediction and the experimental result for the 4.5 mm step height die.

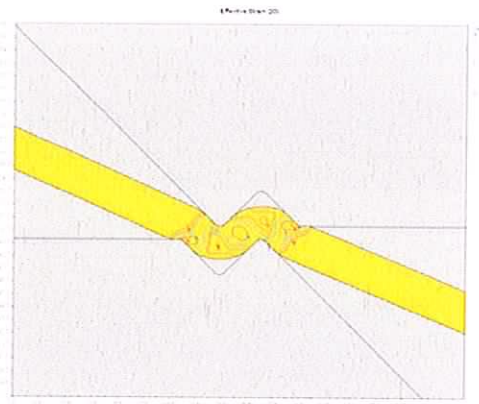


Figure 4.38

Finite Element Graphical Output, 4.5 mm die



Figure 4.39

Experimental Deformation, 4.5 mm die

However, when the die step height is large enough, the surface area under compression increases, and the full deflection is achieved as shown in figures 4.40 and 4.41, FE and experimental results for the 9.0 mm die step height.

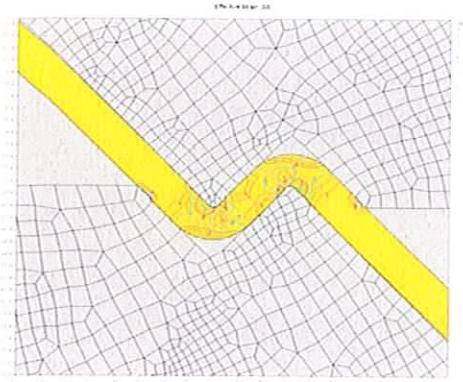


Figure 4.40

Finite Element Graphical Output, 9.0 mm die



Figure 4.41

Experimental Deformation, 9.0 mm die

Die stress analysis was carried out on each of the chosen profiles. Again, these analyses showed characteristic strain fields for the various tooling / workpiece combinations. A sample pair of stress fields (for 7.5 mm dies with AISI 1010 / CR4 steel workpieces) is shown in figures 4.42 and 4.43.

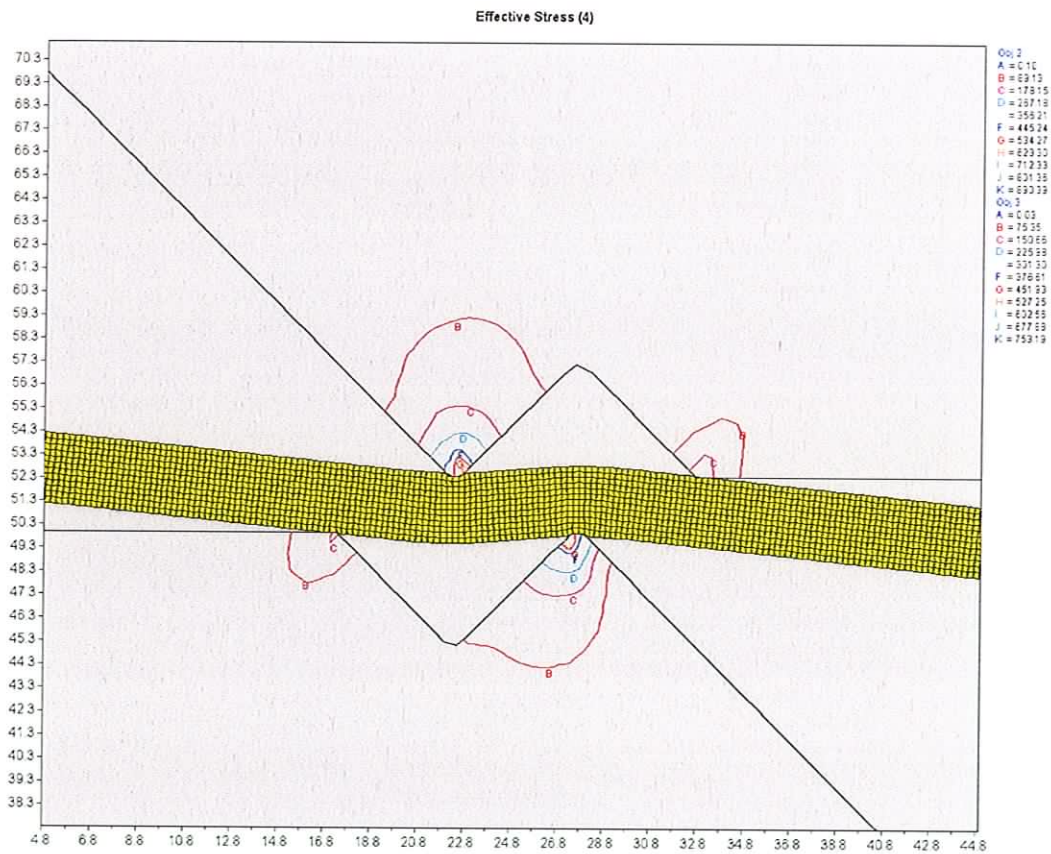
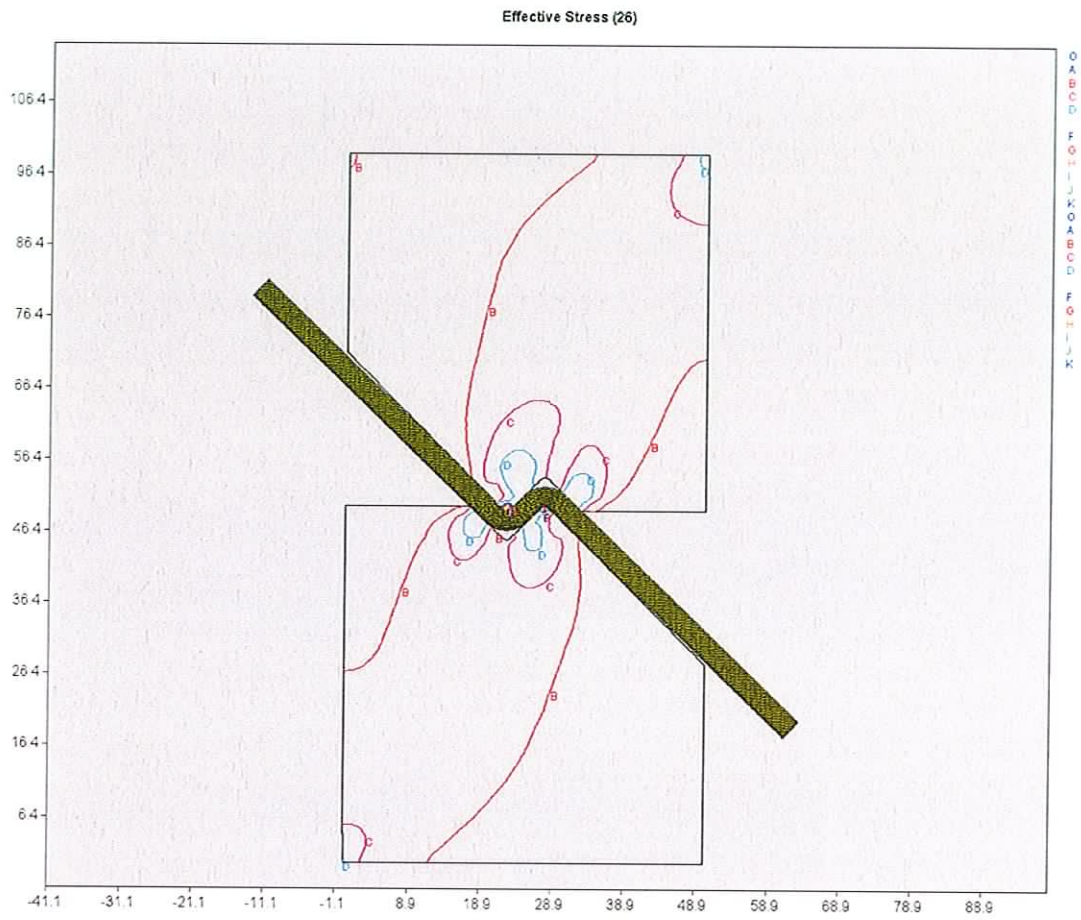


Figure 4.42

Sample stress field, axis dimensions in millimetres



As anticipated, the measurable stresses are limited to the regions of contact during the early part of the deformation process, and only extend to all regions of the tooling when the dies 'shut out' and the forming load reaches the machine capability.

4.4. Experimental results: Displacements vs. time : AISI 1010 steel and 6062 Aluminium.

The graphs given in figures 4.44 to 4.57 show experimental results indicating displacement as a function of time, for both AISI 1010 steel and 6062 aluminium. As can be seen from the graphs the forming process takes place over 2 to 3 seconds, regardless of die profile or of material type. This is due to the fact that the hydraulic ram was throttled in order to provide sufficient time for the process parameters to be recorded, and in addition to provide a safe forming process.

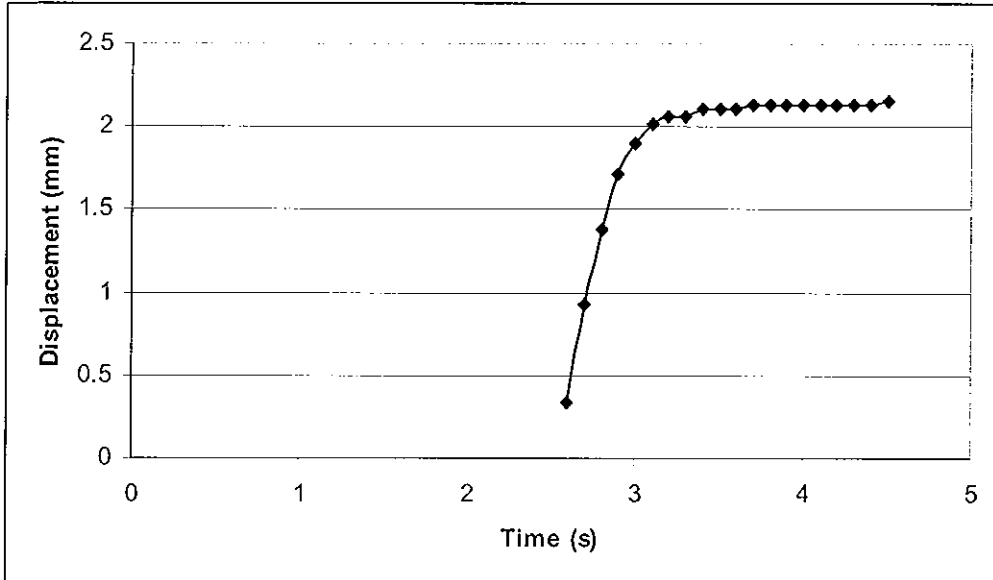


Figure 4.44
 Time – Displacement 4.5 mm Die, 3.0 mm AISI 1010
 (Experimental Result)

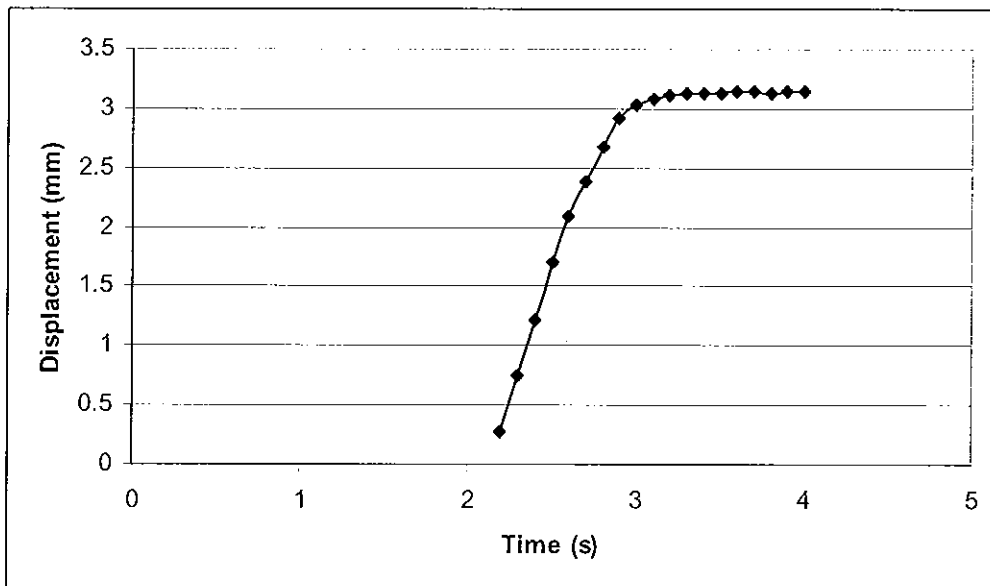


Figure 4.45
 Time – Displacement 6.0 mm Die, 3.0 mm AISI 1010
 (Experimental Result)

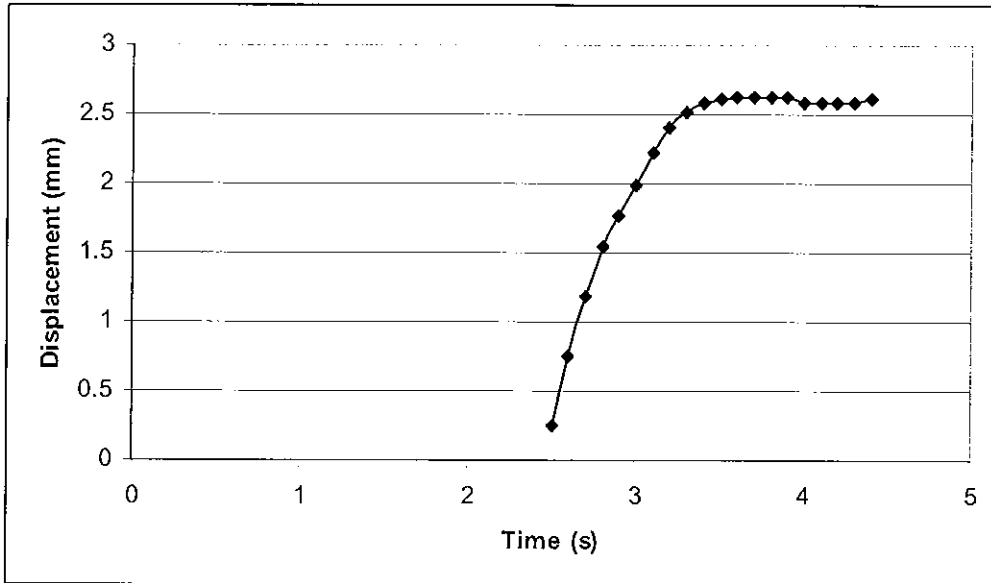


Figure 4.46
 Time – Displacement 7.5 mm Die, 3.0 mm AISI 1010
 (Experimental Result)

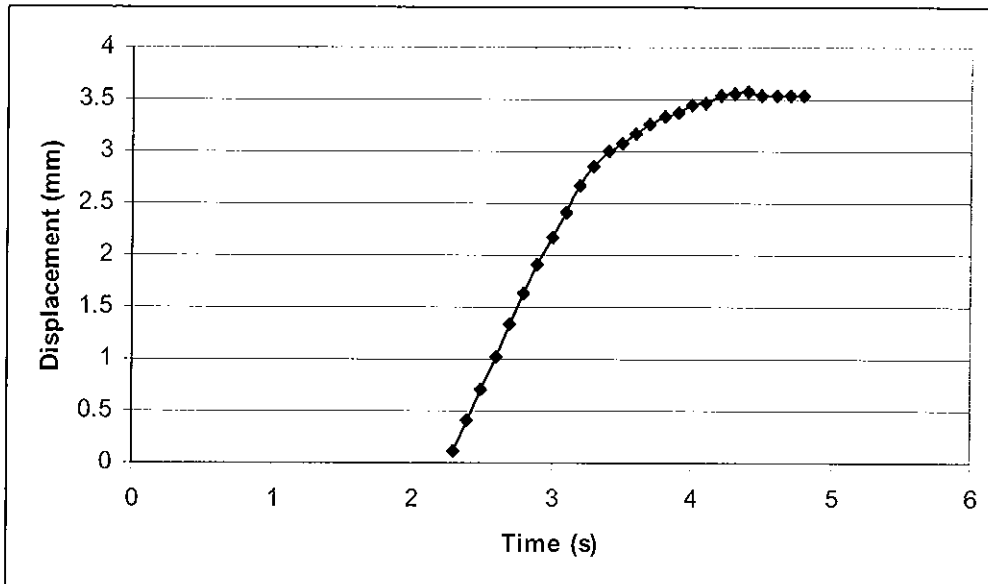


Figure 4.47
 Time – Displacement 9.0 mm Die, 3.0 mm AISI 1010
 (Experimental Result)

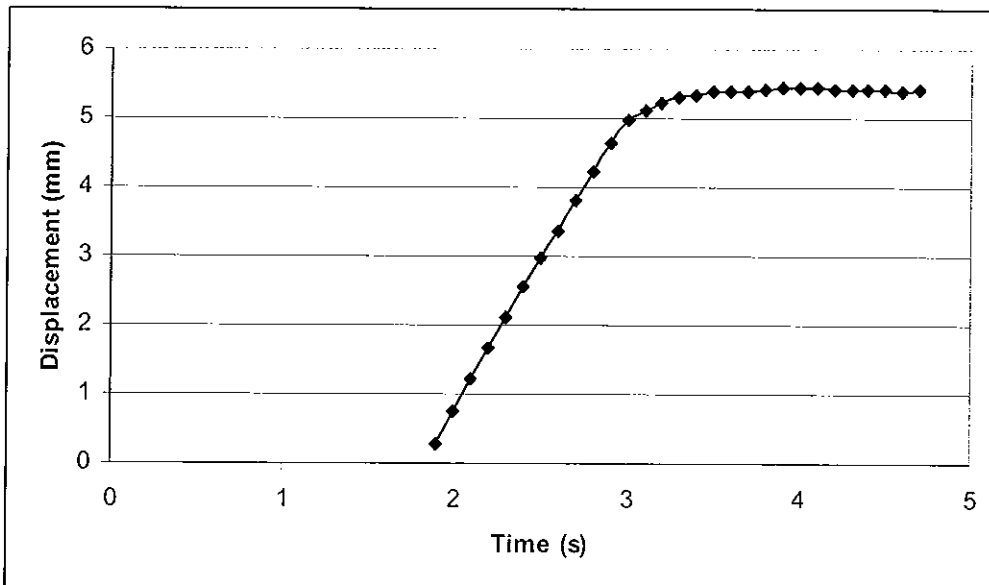


Figure 4.48

Time – Displacement 10.5 mm Die, 3.0 mm AISI 1010
(Experimental Result)

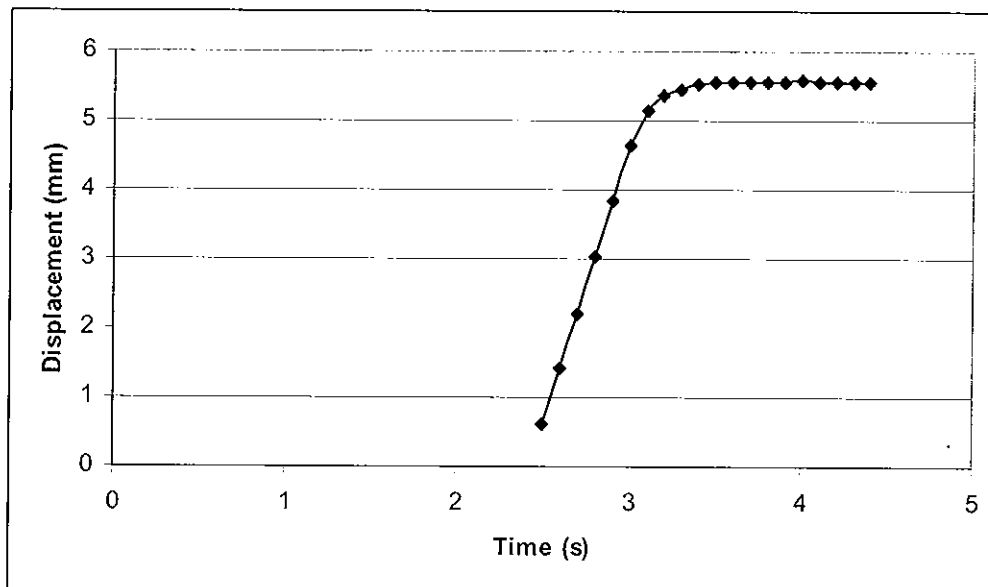


Figure 4.49

Time – Displacement 12.0 mm Die, 3.0 mm AISI 1010
(Experimental Result)

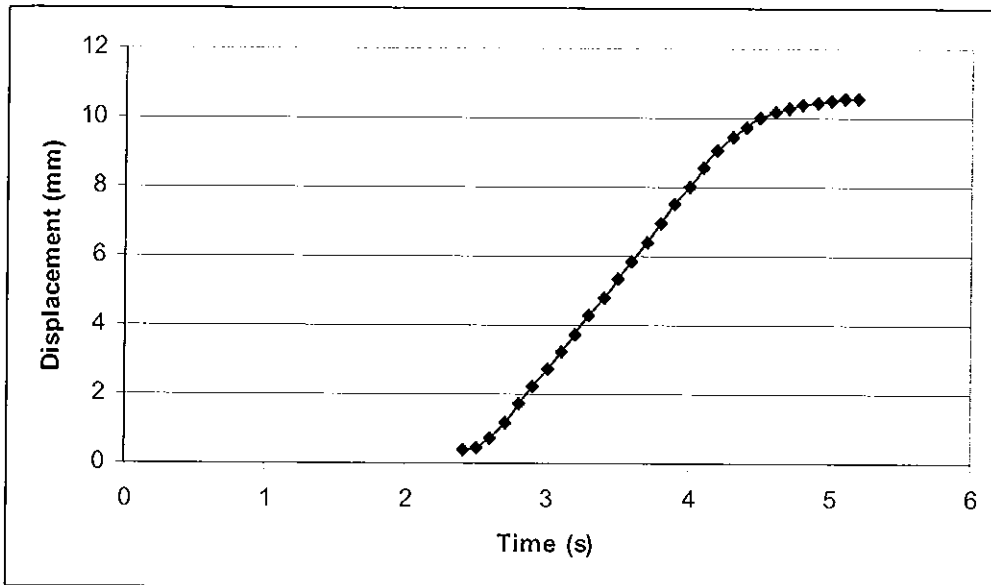


Figure 4.50
Time – Displacement 16 mm Die, 3.0 mm AISI 1010
(Experimental Result)

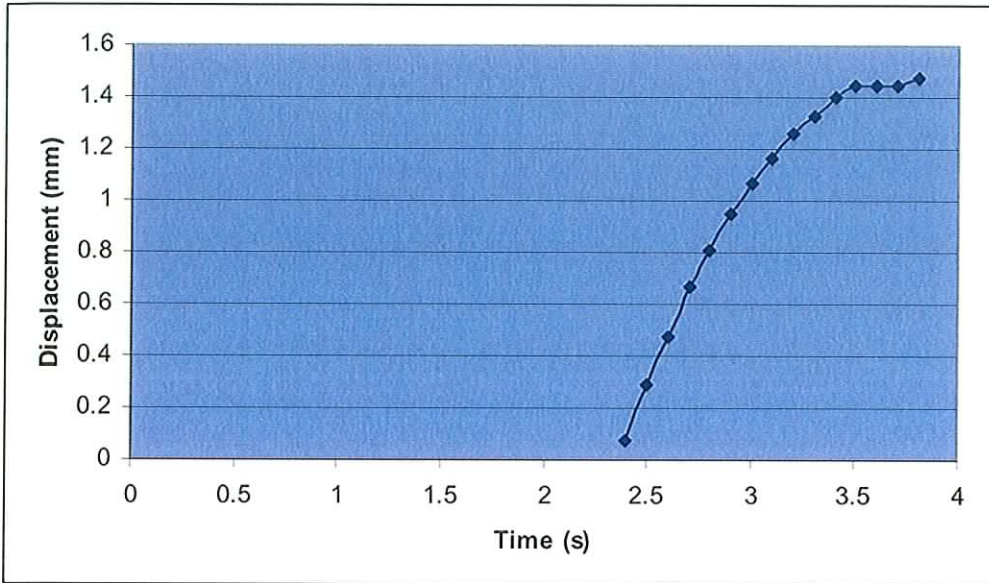


Figure 4.51

Time – Displacement 4.5 mm Die, 3.0 mm 6062 Aluminium
(Experimental Result)

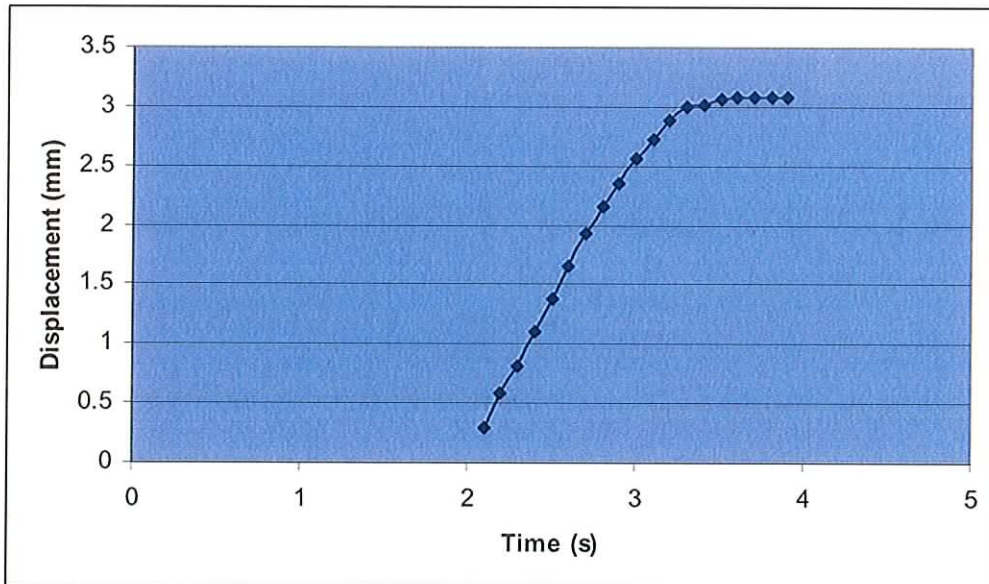


Figure 4.52

Time – Displacement 6.0 mm Die, 3.0 mm 6062 Aluminium
(Experimental Result)

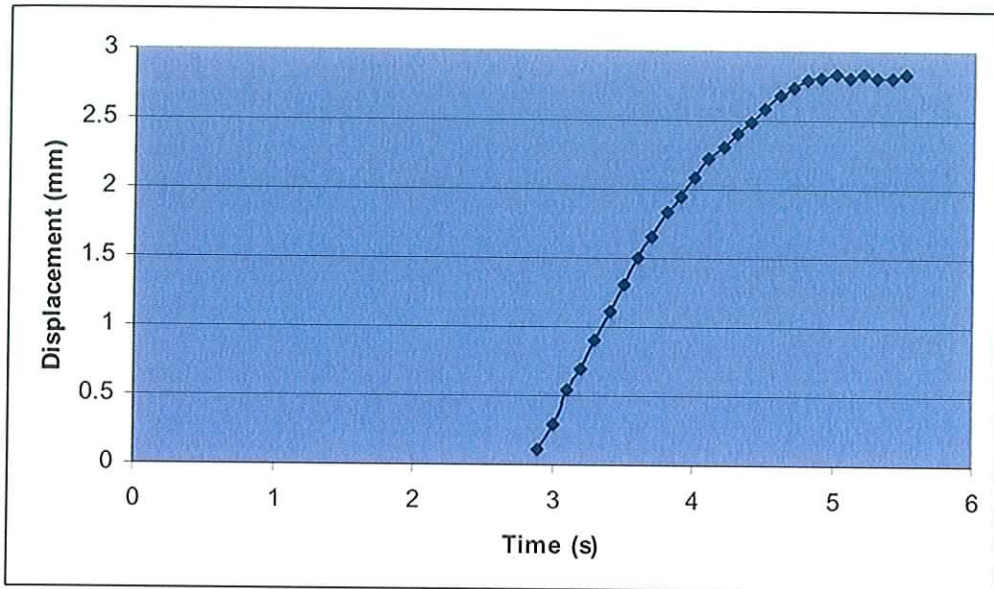


Figure 4.53
 Time – Displacement 7.5 mm Die, 3.0 mm 6062 Aluminium
 (Experimental Result)

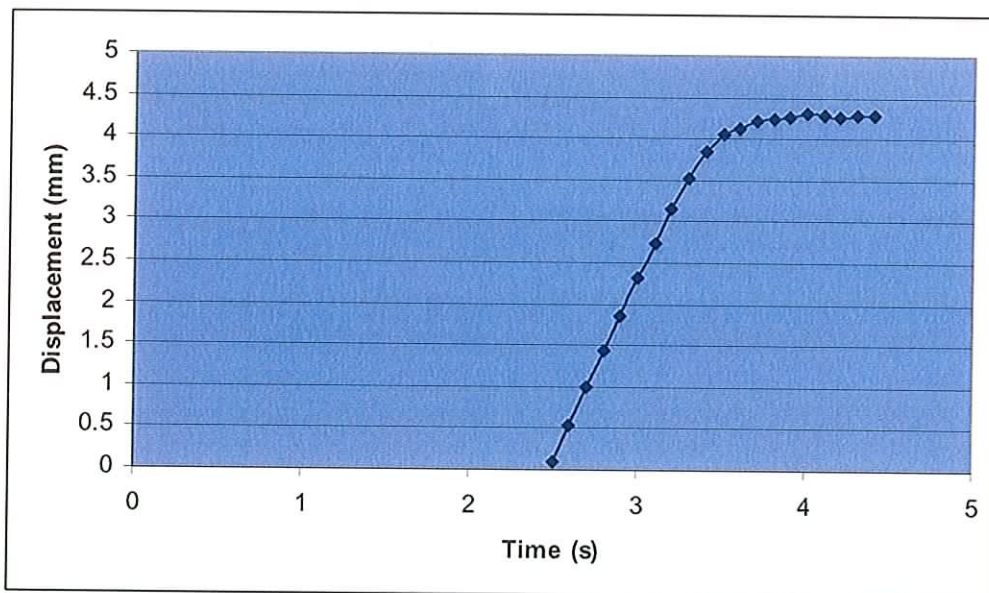


Figure 4.54
 Time – Displacement 9.0 mm Die, 3.0 mm 6062 Aluminium
 (Experimental Result)

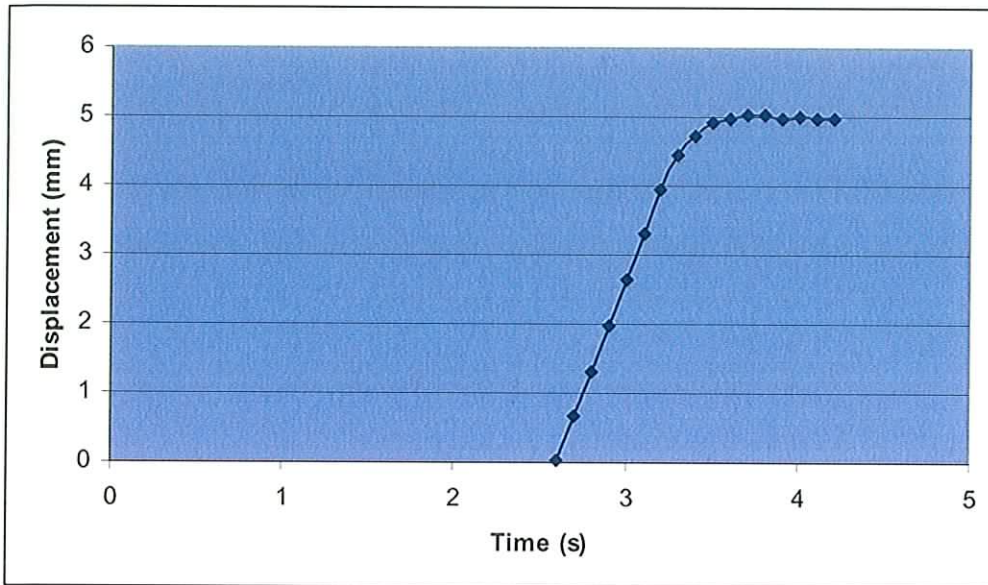


Figure 4.55

Time – Displacement 10.5 mm Die, 3.0 mm 6062 Aluminium
(Experimental Result)

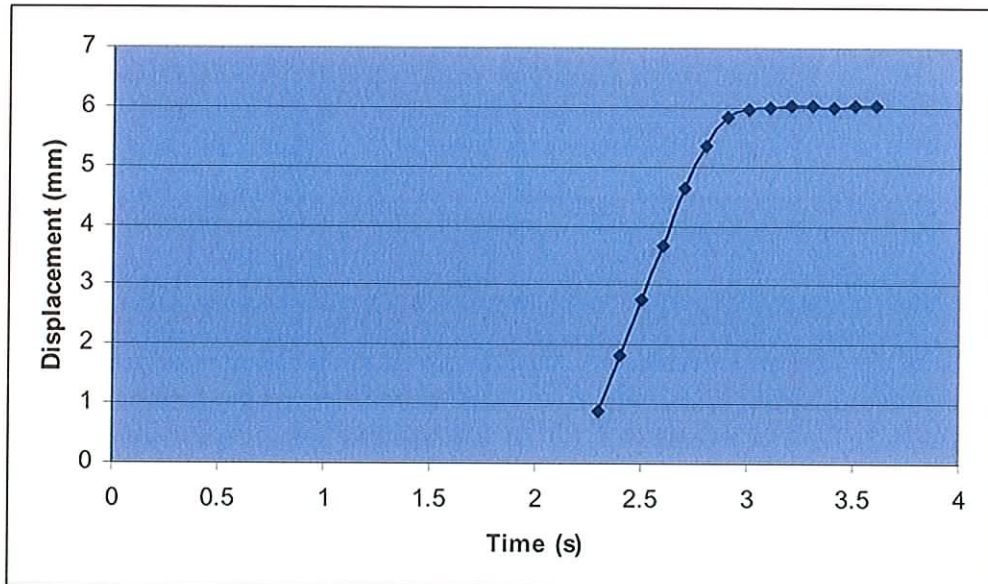


Figure 4.56

Time – Displacement 12.0 mm Die, 3.0 mm 6062 Aluminium
(Experimental Result)

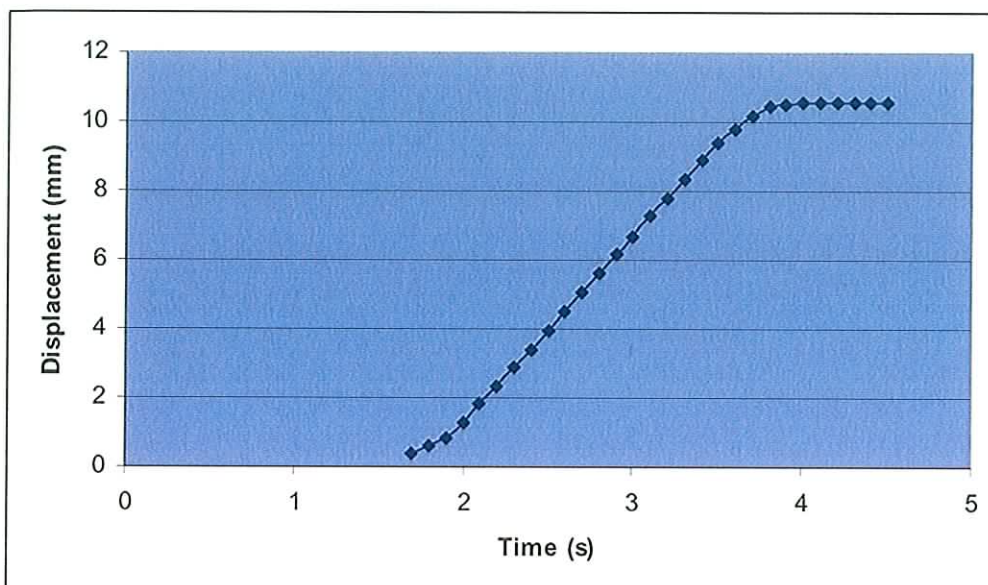


Figure 4.57

Time – Displacement 16.5 mm Die, 3.0 mm 6062 Aluminium
(Experimental Result)

5. Conclusions

5.1 Identification of the relationship between die geometry, die displacement and the forming forces.

The experimental work necessitated the design and construction of both a test rig and series of dies, in order to apply appropriate loads to the workpieces. The test rig was constructed and proved capable of applying the required loads in a controllable and safe manner. The dies, after initial failure, were reconstructed and proved effective. The test rig was calibrated, both in terms of force and displacement, and transducers were used to translate and record data during the forming process. These data were then tabulated. The experimental work demonstrated the following relationships between the displacements of metal forming (joggle) dies, the forces that they are subjected to at various displacements and the die geometry.

5.1.1. Forces vs. Displacements

In general, the force – displacement graphs are concave up, i.e., they are of the shape shown in figure 5.1.

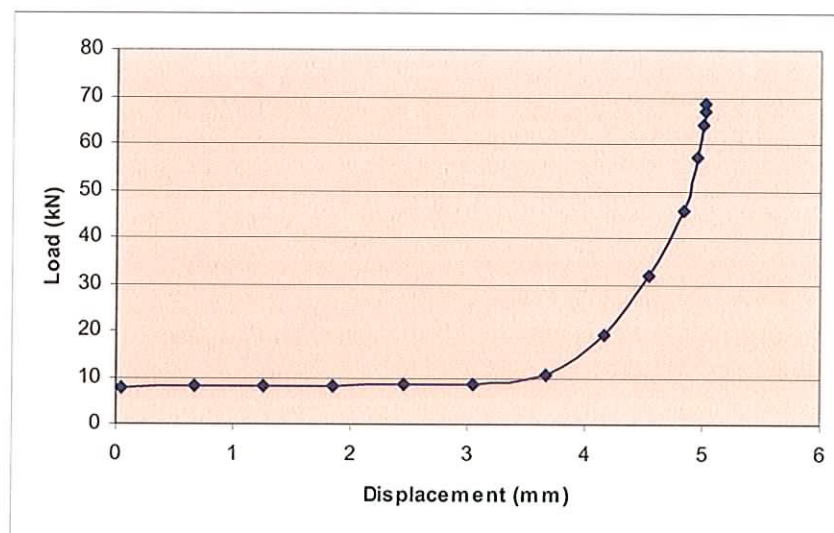


Figure 5.1

General form of Load-Displacement curve (10.5 mm Die, Aluminium 6062 (Experimental Result))

This general shape is explained as follows:

At the early stages of bending and especially for the larger displacement dies, the stresses caused by imposed bending moments are relatively large compared to direct stresses caused by stretching of the material. This means that relatively large displacements occur in the dies for correspondingly low loads. As the deflection increases, the resistance to deflection is increasingly due to the reaction stresses in the material as it is stretched between the die

contact points. The deeper the deflection, the larger the component of force is due to the material stretching. In addition, increasingly larger areas of the material under load have been subjected to work hardening, again leading to increases in force for additional deflection. The combination of these influences lead to the continually rising characteristic of the graph. Finally the resisting load meets the test rig load capacity when the die faces shut out on opposite sides of the workpiece. In this case die displacement ceases, and the manufacturing process has ended.

It is noted here that the reaction forces provided by the aluminium workpiece are of the order of 50% of the forces supplied by the steel workpieces. This is of course due to the fact that the flow stress for aluminium is lower than that of steel.

5.1.2. Forces vs. Die Geometry

Figures 5.2, 5.3 and 5.4, demonstrate the change in the relationship of force and displacement curves, for changing die geometry.

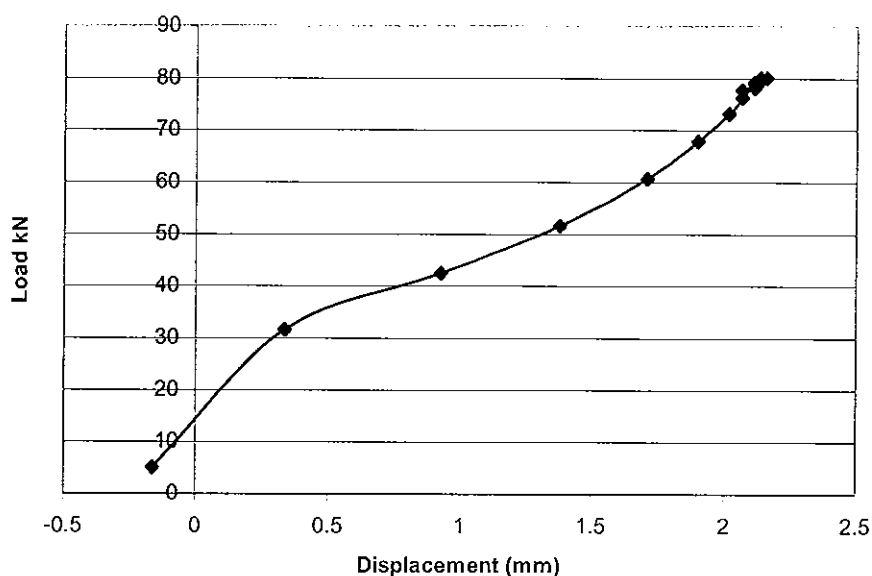


Figure 5.2

Load-Displacement 4.5 mm Die, 3mm AISI 1010 (Experimental Result)

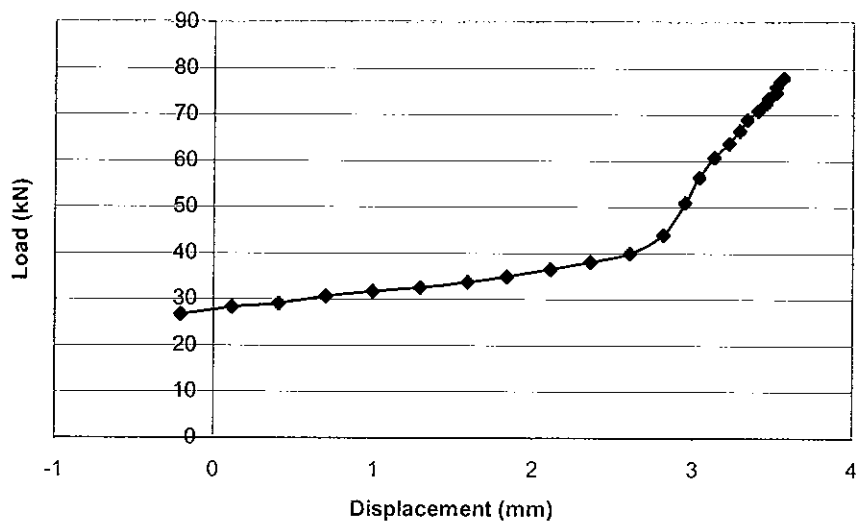


Figure 5.3

Load-Displacement 9.0 mm Die, 3.0 mm AISI 1010 (Experimental Result)

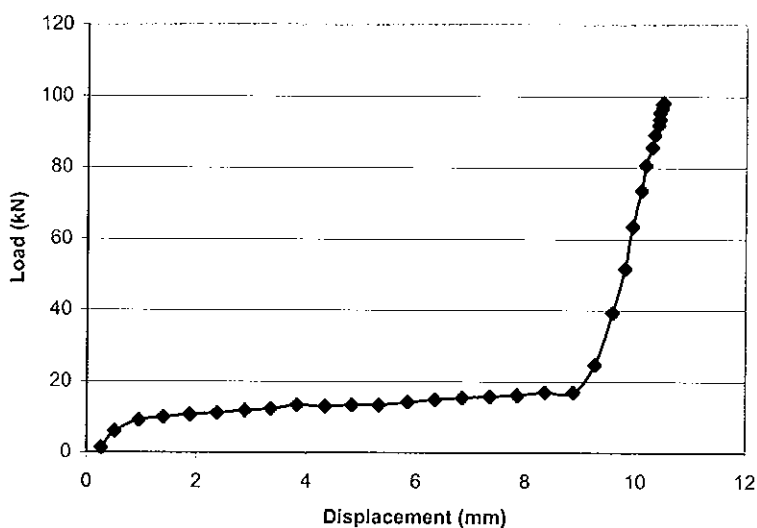


Figure 5.4

Load-Displacement 16.5 mm Die, AISI 1010 (Experimental Result)

It can be seen that there is a general increase in curvature as the die step (dimension x in figure 5.5) rises: the graphs for the smaller step height dies are almost linear in nature leading to a marked concavity in the intermediate dies, and finally to an almost linear (small slope) – linear (large slope) profile for the largest dies.

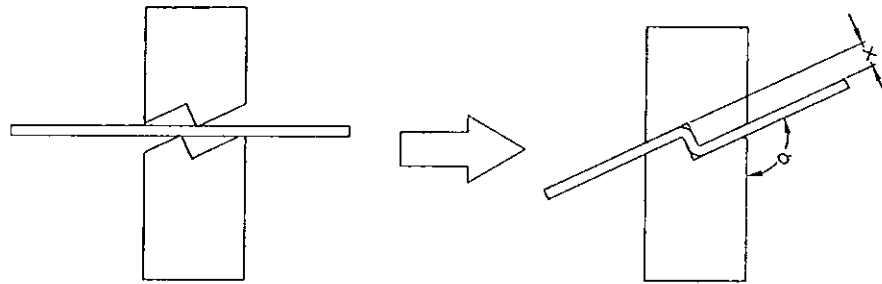


Figure 5.5
Joggle die profile

This general change in shape across die sizes is explained as follows:

For the smaller dies, the distances between the points of contact of the dies with the material are small, i.e., of the order of thickness of the test material itself. This in turn means that the bending moments are smaller than those of the larger dies, and the reaction shear forces in the workpiece are correspondingly more effective in preventing die displacement. Thus higher forces are needed earlier in the displacement profile. These forces continue to increase for increased displacement, culminating in the large forces required to close the dies in the shut off position.

It should be noted here that the data points on the experimental graphs were taken at equal time increments of 10 data points per second. The reducing distance between the data points towards the right hand end of the graphs indicates the reduction in die velocity as it approached the end of its stroke. This effect is equally apparent for both aluminium and steel workpieces.

5.2. The observation and recording of strain distribution on the surfaces of chosen test pieces, by the use of grid circle analysis.

Clear and accurate grid circles were produced on the workpieces, both aluminium and steel. The workpieces were formed in the various dies, and strain distributions noted. As can be seen from figures 5.6 and 5.7 the initial cold rolled steel strip was excessively work hardened before forming and fracture resulted at moderate strains.

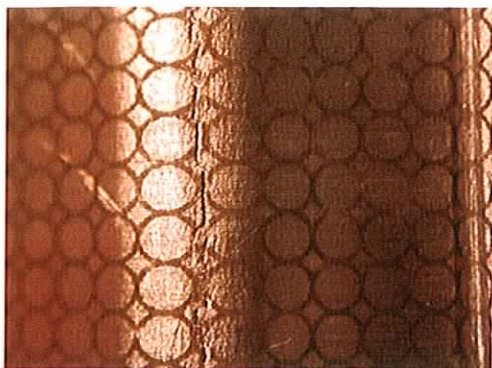


Figure 5.6
Fracture of workpiece

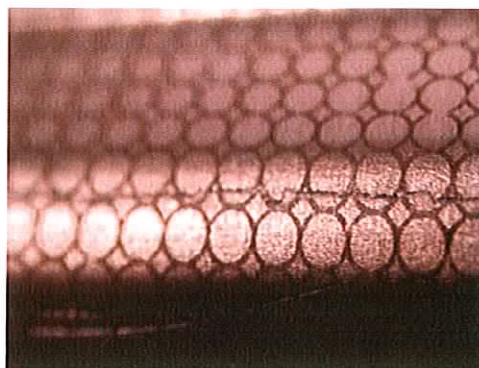


Figure 5.7
Fracture of workpiece

Thereafter AISI 1010 steel and 6062 aluminium were used, and the strain distributions on the material surfaces could easily be seen in all workpieces, as shown in the example figures 5.8 and 5.9.

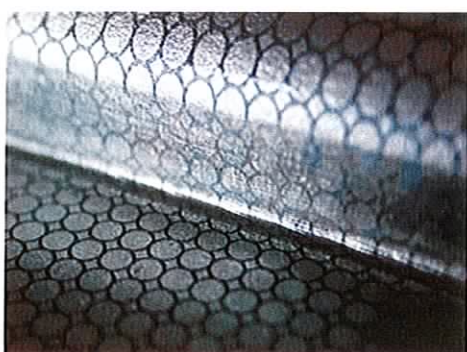


Figure 5.8
7.5 mm Die, 3.0 mm CR4

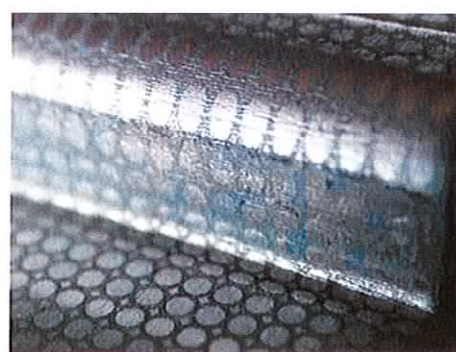


Figure 5.9
7.5 mm Die, 3.0mm Al 6062

It is interesting to note that in all but the smallest (4.5 mm die displacement) dies, the aluminium samples exhibited surface fractures in the areas of large strain.

5.3. The comparison of experimental results with those predicted by Deform PC Pro, a commercial Finite Element forming package.

A comparison of the predicted FE results and the experimental work was carried out for each of the die sizes. In general, a good correlation was achieved, both across die sizes, and across materials. This was true both in terms of the general shapes of the graphs, and the order of magnitude of the forces predicted and observed. In general the correlation improved as the die size increased. This is thought to be due to the larger measured displacement and force differences, between each measurement event, for the larger dies.

Figures 5.10 to 5.15 show the correlation between the experimental and FE results.

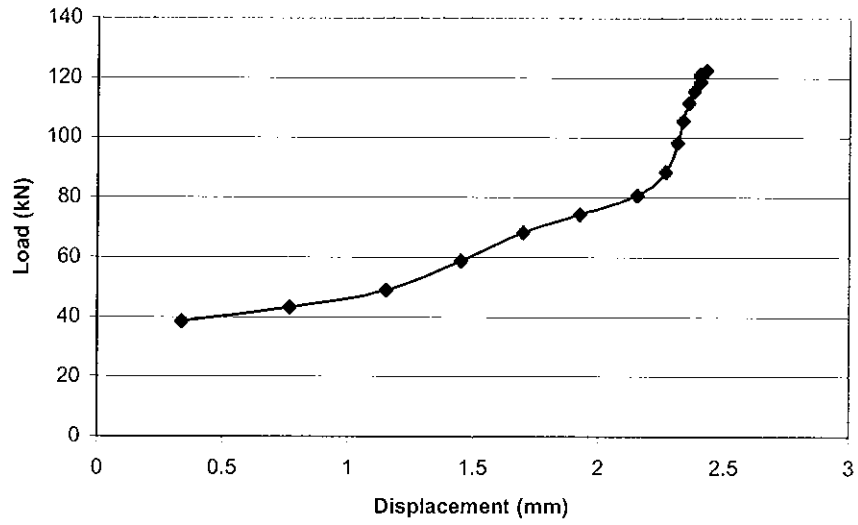


Figure 5.10

Load-Displacement 6.0 mm Die, 3mm AISI 1010 (Experimental Result)

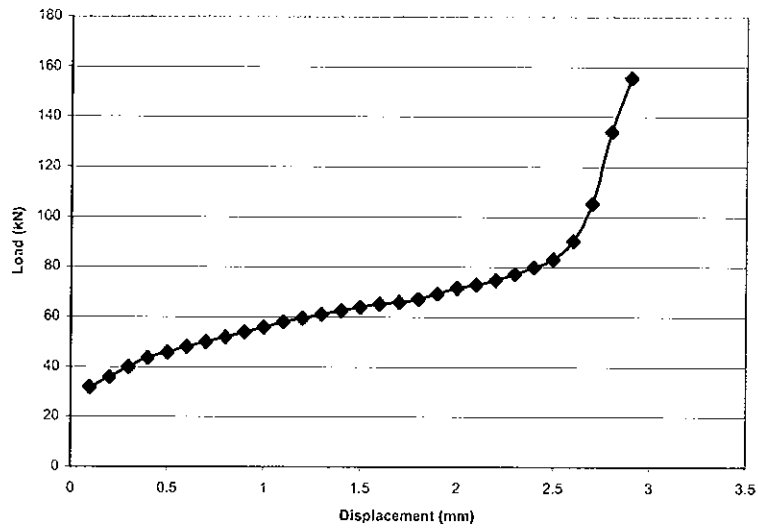


Figure 5.11

Load-Displacement 6.0 mm Die, 3mm AISI 1010 (Finite Element Result)

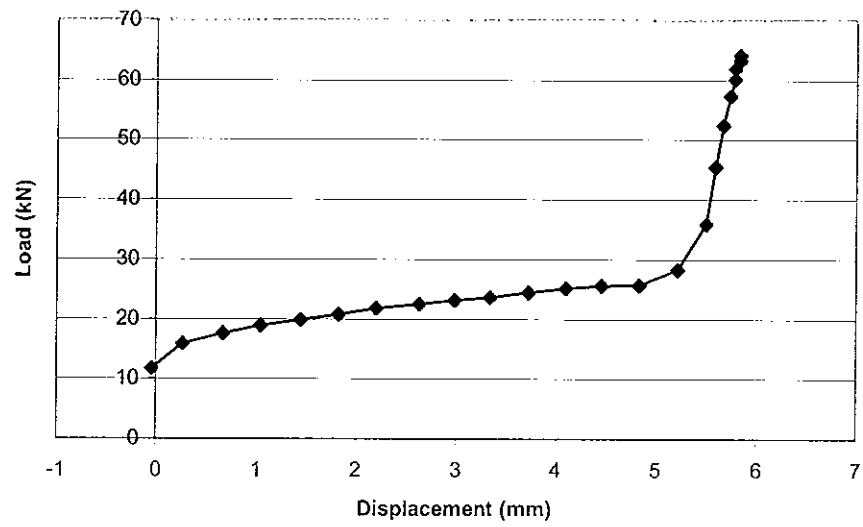


Figure 5.12

Load-Displacement 10.5 mm Die, AISI 1010 (Experimental Result)

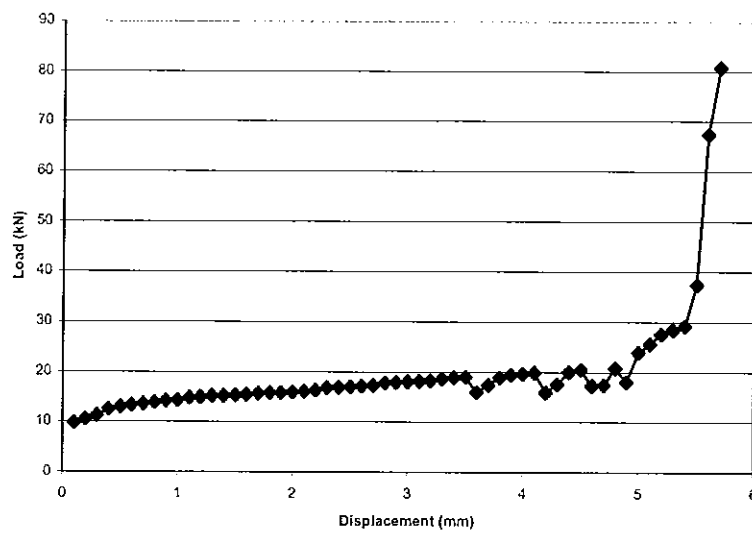


Figure 5.13

Load-Displacement 10.5 mm Die, AISI 1010 (Finite Element Result)

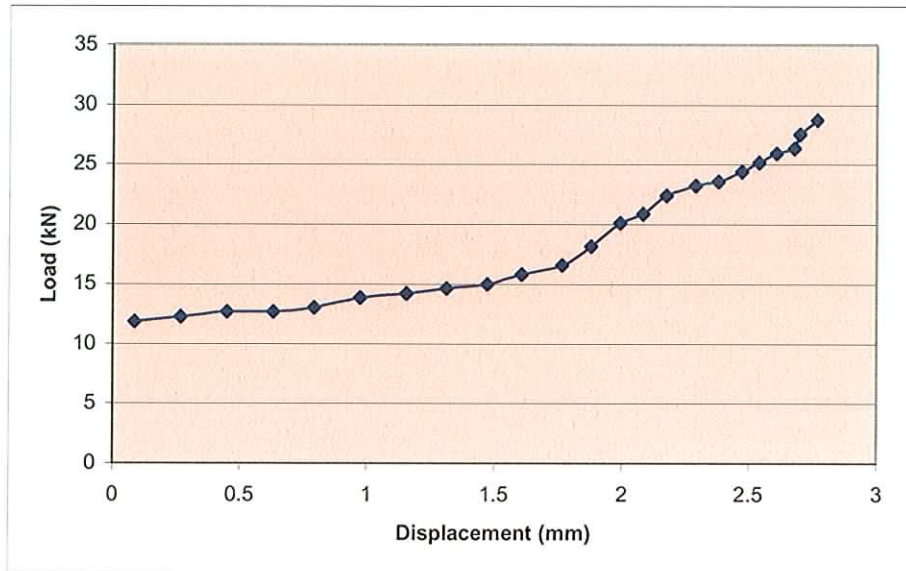


Figure 5.14

Load-Displacement 7.5 mm Die, 3.0 mm Al 6062 (Experimental Result)

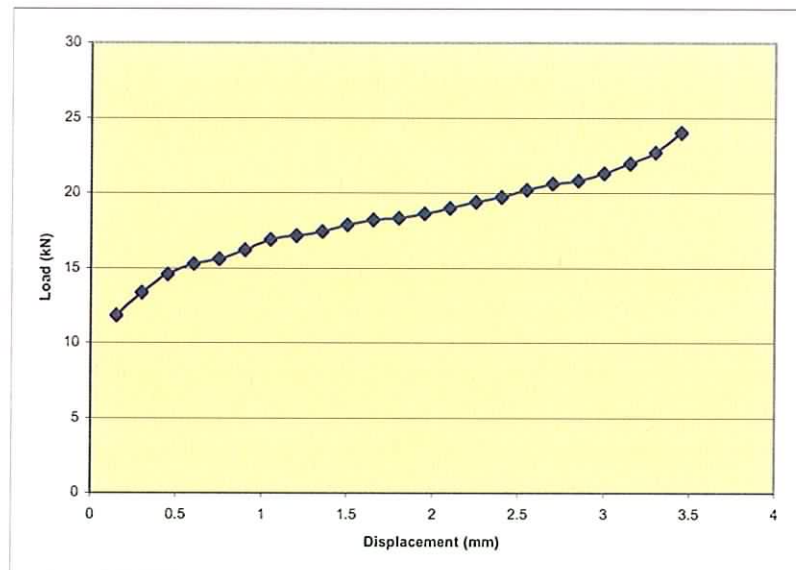


Figure 5.15

Load-Displacement 7.5 mm Die, 3mm Al 6062 (Finite Element Result)

5.4. Determination of the elastic stresses in the dies, and the plastic strains in the workpieces, using the FE package Deform PC Pro.

Finite element analysis of both workpiece strain and die stress analysis were carried out for each material and die size. This was done using the coupled problem method, in order to reduce the time required for the analysis. Even using such a method, this resulted in hundreds of hours of analysis time.

Observation of the results showed some interesting features. For the smaller die sizes, the strain fields at the bends overlap or penetrate each other. As the die size increases, the strain fields no longer interfere with each other. The transition point is the same for both aluminium and steel workpieces, i.e., the transition from 9.0 mm to 10.5 mm dies leads to a clear separation of strain fields in both cases see figures 5.16 to 5.19.

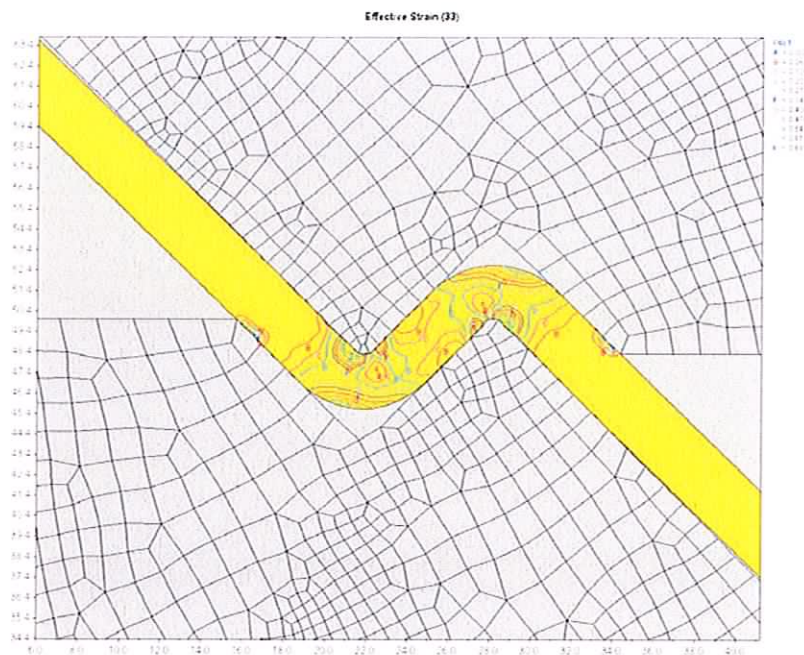


Figure 5.15

AISI 1010 Steel, 9.0 mm Die, Effective Strain, strain fields in contact.

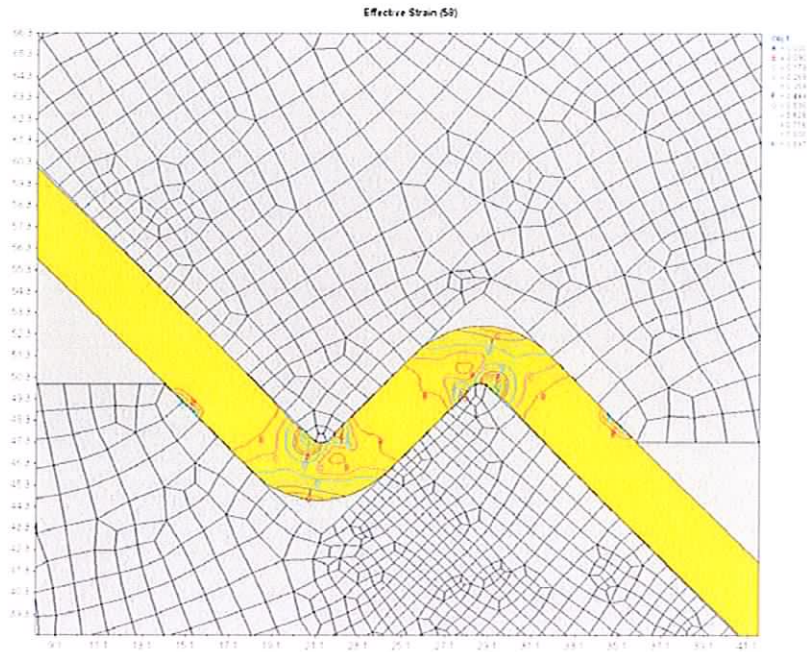


Figure 5.17

AISI 1010 Steel, 9.0 mm Die, Effective Strain, strain fields independent of each other.

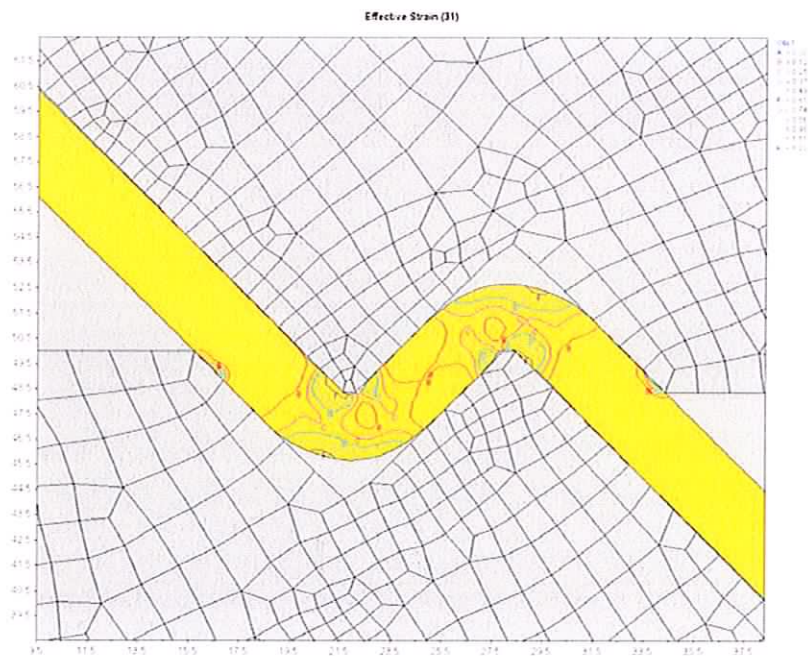


Figure 5.18

6060 Aluminium, 10.5 mm Die, Effective Strain, strain fields in contact.

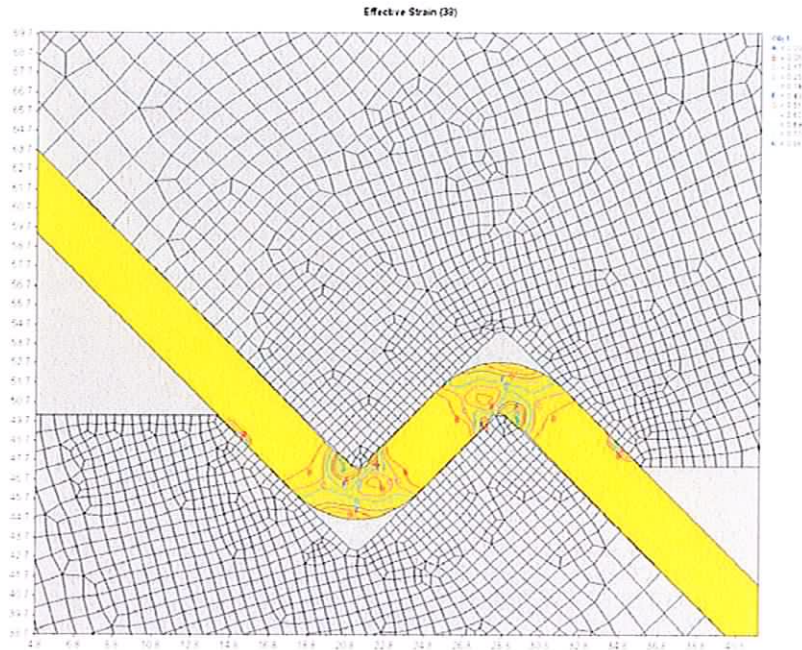


Figure 5.19

6060 Aluminium, 10.5 mm Die, Effective Strain, strain fields independent of each other.

However, in terms of die stress analysis, there was no discernable pattern of changing die stress across die sizes, with the exception of course of the fact that the die stresses for aluminium workpieces were smaller, at about 50% of those for steel.

5.5. General conclusions

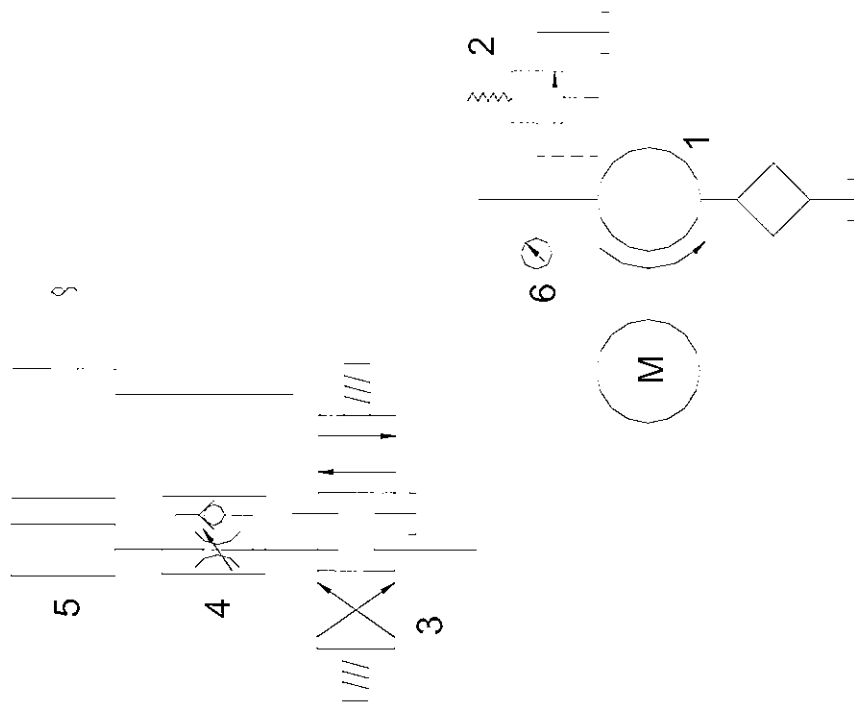
Results show that the joggle forming of both steel aluminium can be performed on a repeatable basis for experimental work, and therefore for production of workpieces. Increasing the step height of the die leads to less interference of the strain fields, leading in turn to an intermediate flange area that is not work-hardened. This suggests that this area may be subjected to additional forming processes if required. In addition, it should be possible to add features such as holes to the area that will remain unstrained, and these features should maintain their dimensions. This means that the component can be punched when it is flat, and formed afterwards, eliminating the need for post forming operations, and therefore reducing cost.

Care should be taken when forming aluminium workpieces, as these tend to exhibit surface cracking when formed with this type of tooling. Only forming grades of steel perform satisfactorily in these types of forming dies, at the given radii of 0.5 mm.

For 3 mm thick materials, die step height should be at least 6 mm and preferably 7.5 mm or more in order to gain the correct joggle profile without excessive pinching and thinning of the workpiece. This is true for both aluminium and steel workpieces.

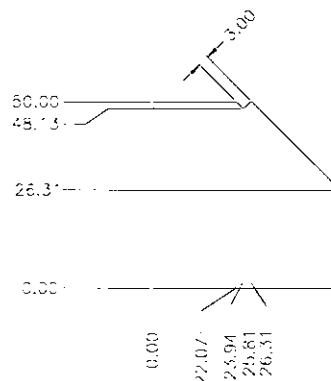
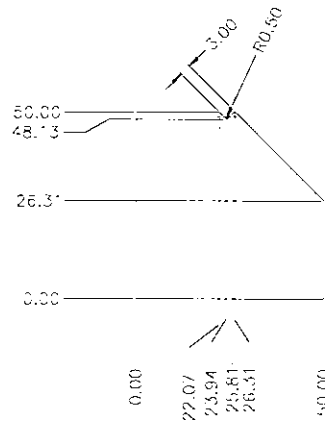
It has been shown that there is a local reduction in the total energy of forming for the steel workpieces in the range of step heights from 10.5mm – 12mm for the forming dies. This means that energy costs should be lower in this range than at other die step heights. The reduction in energy of forming is not so clear for the aluminium workpieces.

The theoretical and experimental work described above is a first analysis of the joggle bending process. It is recommended that further investigation is carried out into the effects of different materials, material thicknesses, tooling profiles and step-height : material thickness ratios in order to further enhance understanding of this process.



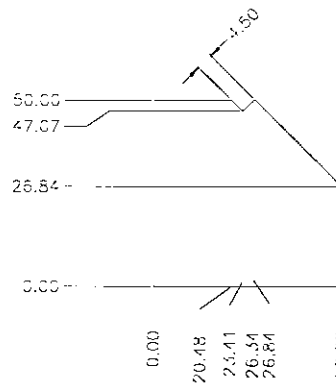
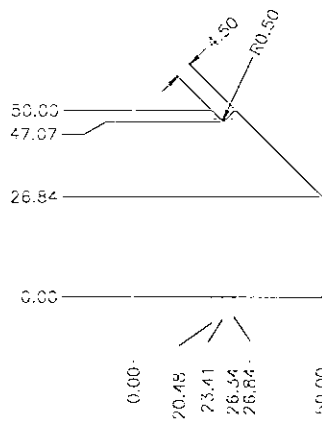
- 1 Pump
- 2 Relief Valve
- 3 Directional Valve
- 4 Flow control Valve
- 5 Cylinder
- 6 Pressure Gauge

Hydraulic Circuit for Test Rig



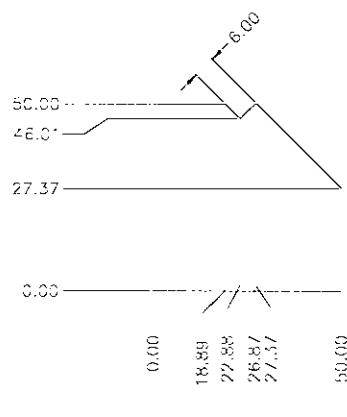
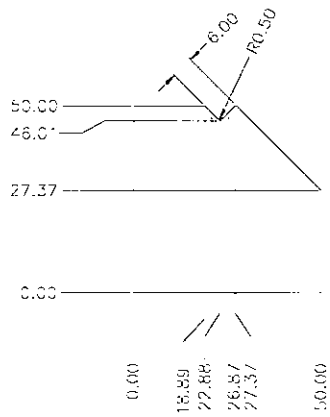
Bottom Tool
 Material: Ground Flat Stock, Harder 55Rc
 Finish: Machine

| | | | |
|--------------|-------------------|-------------|------------|
| Project Name | Hydraulic Press | DATE | 2014-08-18 |
| Project No | 02-11-45 | REVISED | 01 |
| Part Name | Bottom Tool | PROJECTION | |
| Material | Ground Flat Stock | DESIGNED BY | |
| Finish | Machine | CHECKED BY | |
| Scale | 1:1 | APPROVED BY | |
| Drawn By | Water | | |



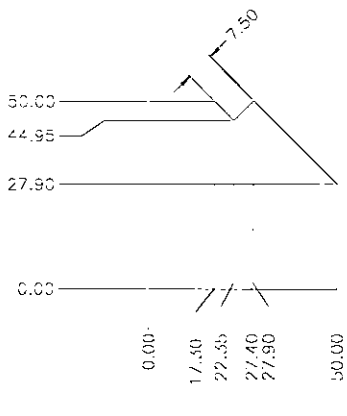
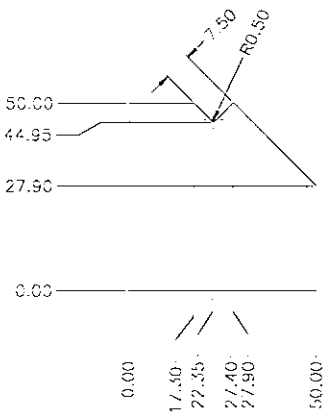
Bottom Tool
 Material: Ground Flat Stock, Harder 55Rc
 Finish: Machine

| | | | |
|--------------|-------------------|-------------|------------|
| Project Name | Hydraulic Press | DATE | 2014-08-18 |
| Project No | 02-11-45 | REVISED | 01 |
| Part Name | Bottom Tool | PROJECTION | |
| Material | Ground Flat Stock | DESIGNED BY | |
| Finish | Machine | CHECKED BY | |
| Scale | 1:1 | APPROVED BY | |
| Drawn By | Water | | |



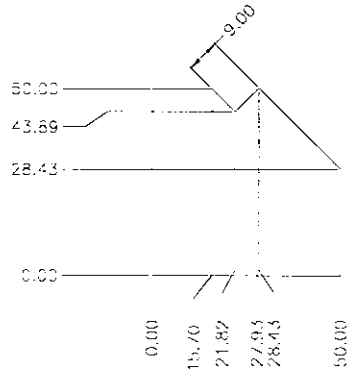
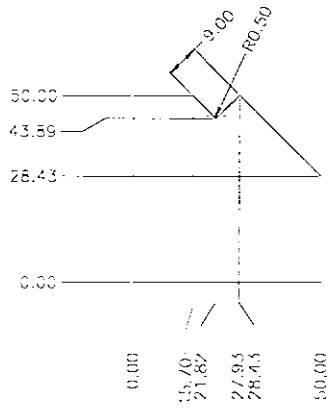
Bottom Top.
 Material: Ground Flat Stock, Harder 55Rc
 Finish: Machine

| | | | |
|--------------|-----------|-----------------|-----|
| Project Name | 123456789 | Sheet No | 1 |
| Product Name | 123456789 | Scale | 1:1 |
| Drawing No | 123456789 | Author | JM |
| Part No | 123456789 | Checker | |
| Material | 123456789 | Quantity | |
| Quantity | 123456789 | Unit | |
| Unit | mm | Manufactured By | |
| Checked By | | Material | |



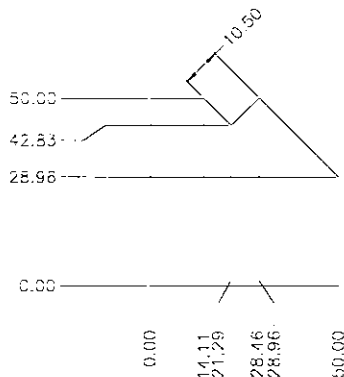
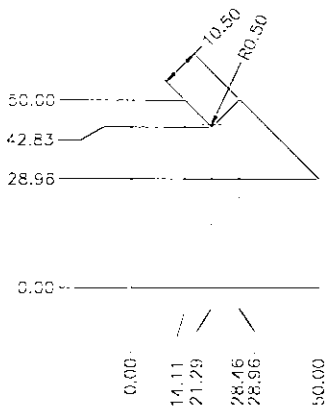
Bottom Top.
 Material: Ground Flat Stock, Harder 55Rc
 Finish: Machine

| | | | |
|--------------|-----------|-----------------|-----|
| Project Name | 123456789 | Sheet No | 1 |
| Product Name | 123456789 | Scale | 1:1 |
| Drawing No | 123456789 | Author | JM |
| Part No | 123456789 | Checker | |
| Material | 123456789 | Quantity | |
| Quantity | 123456789 | Unit | |
| Unit | mm | Manufactured By | |
| Checked By | | Material | |



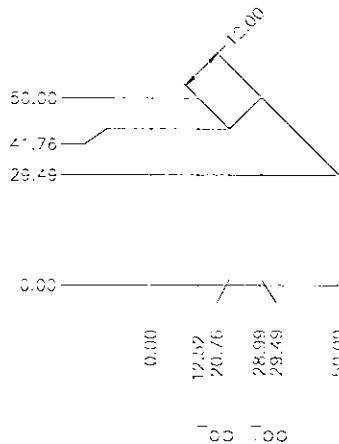
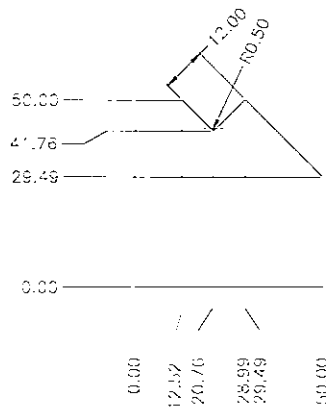
Bottom Tool
 Material: Ground Flat Stock, Harder 55Rc
 Finish: Machine

| | | | |
|--------------|-------------------|--------------|---------------------|
| Project Name | Harder 55Rc | Drawn | W. J. van der Merwe |
| Project No. | 2018-01-01 | Checked | W. J. van der Merwe |
| Part No. | 2018-01-01 | Approved | W. J. van der Merwe |
| Part Name | Bottom Tool | Projection | First Angle |
| Scale | 1:1 | Drawn By | W. J. van der Merwe |
| Material | Ground Flat Stock | Checked By | W. J. van der Merwe |
| Hardness | Harder 55Rc | Approved By | W. J. van der Merwe |
| Finish | Machine | Inspected By | W. J. van der Merwe |
| Notes | | Material | |



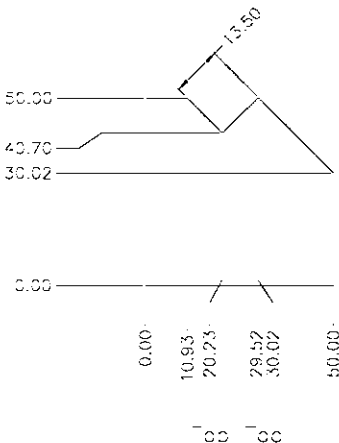
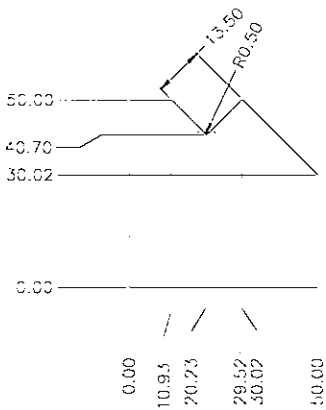
Bottom Tool
 Material: Ground Flat Stock, Harder 55Rc
 Finish: Machine

| | | | |
|--------------|-------------------|--------------|---------------------|
| Project Name | Harder 55Rc | Drawn | W. J. van der Merwe |
| Project No. | 2018-01-01 | Checked | W. J. van der Merwe |
| Part No. | 2018-01-01 | Approved | W. J. van der Merwe |
| Part Name | Bottom Tool | Projection | First Angle |
| Scale | 1:1 | Drawn By | W. J. van der Merwe |
| Material | Ground Flat Stock | Checked By | W. J. van der Merwe |
| Hardness | Harder 55Rc | Approved By | W. J. van der Merwe |
| Finish | Machine | Inspected By | W. J. van der Merwe |
| Notes | | Material | |



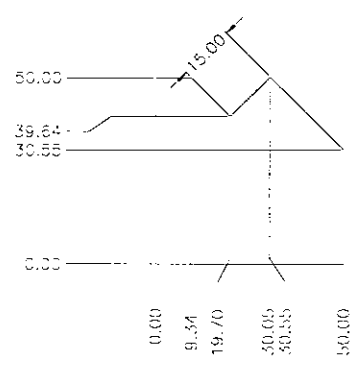
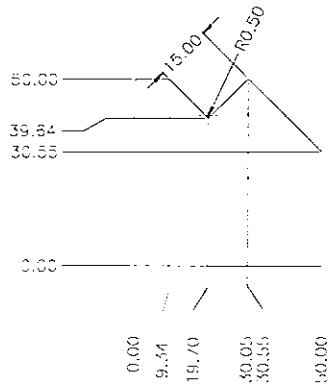
Bottom Tool
 Material: Ground Flat Stock, Harder 55Rc
 Finish: Machine

| | | | |
|------------------|-------------|----------|-----|
| Project Name | Die Profile | Drawn | AKH |
| Project No. | 12 | Checked | AKH |
| Part No. | 12 | Material | AKH |
| Part Name | Die Profile | Quantity | AKH |
| Part Description | Die Profile | Material | AKH |
| Part Material | Die Profile | Material | AKH |
| Part Quantity | Die Profile | Material | AKH |
| Part Material | Die Profile | Material | AKH |
| Part Quantity | Die Profile | Material | AKH |
| Part Material | Die Profile | Material | AKH |
| Part Quantity | Die Profile | Material | AKH |



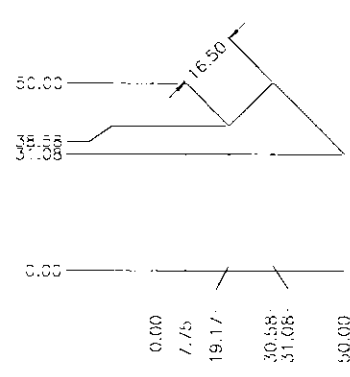
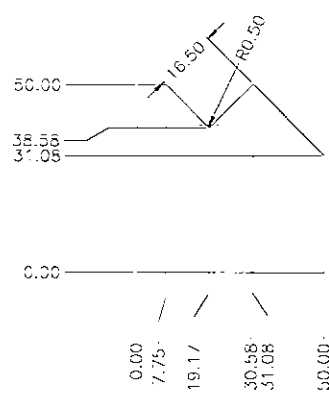
Bottom Tool
 Material: Ground Flat Stock, Harder 55Rc
 Finish: Machine

| | | | |
|------------------|-------------|----------|-----|
| Project Name | Die Profile | Drawn | AKH |
| Project No. | 12 | Checked | AKH |
| Part No. | 12 | Material | AKH |
| Part Name | Die Profile | Quantity | AKH |
| Part Description | Die Profile | Material | AKH |
| Part Material | Die Profile | Material | AKH |
| Part Quantity | Die Profile | Material | AKH |
| Part Material | Die Profile | Material | AKH |
| Part Quantity | Die Profile | Material | AKH |
| Part Material | Die Profile | Material | AKH |
| Part Quantity | Die Profile | Material | AKH |



Bottom Tool
 Material: Ground Flat Stock, Harder S5Rc
 Finish: Machine

| | | | |
|--------------|-----|-------------|-----|
| Project Name | ... | Project No. | ... |
| Part Name | ... | Part No. | ... |
| Material | ... | Quantity | ... |
| Part No. | ... | Quantity | ... |
| Part No. | ... | Quantity | ... |
| Part No. | ... | Quantity | ... |
| Part No. | ... | Quantity | ... |
| Part No. | ... | Quantity | ... |
| Part No. | ... | Quantity | ... |
| Part No. | ... | Quantity | ... |
| Part No. | ... | Quantity | ... |



Bottom Tool
 Material: Ground Flat Stock, Harder S5Rc
 Finish: Machine

| | | | |
|--------------|-----|-------------|-----|
| Project Name | ... | Project No. | ... |
| Part Name | ... | Part No. | ... |
| Material | ... | Quantity | ... |
| Part No. | ... | Quantity | ... |
| Part No. | ... | Quantity | ... |
| Part No. | ... | Quantity | ... |
| Part No. | ... | Quantity | ... |
| Part No. | ... | Quantity | ... |
| Part No. | ... | Quantity | ... |
| Part No. | ... | Quantity | ... |

Transducer Calibration

In order to ensure that the data obtained from the displacement and load transducers was correct, both the transducers were calibrated immediately before use.

The displacement transducer was calibrated using workshop grade gauge blocks, by resting the transducer on increasing known heights of gauge blocks while recording the transducer outputs. The output slope and intercept co-efficients were adjusted so that the transducer output reflected the inputs.

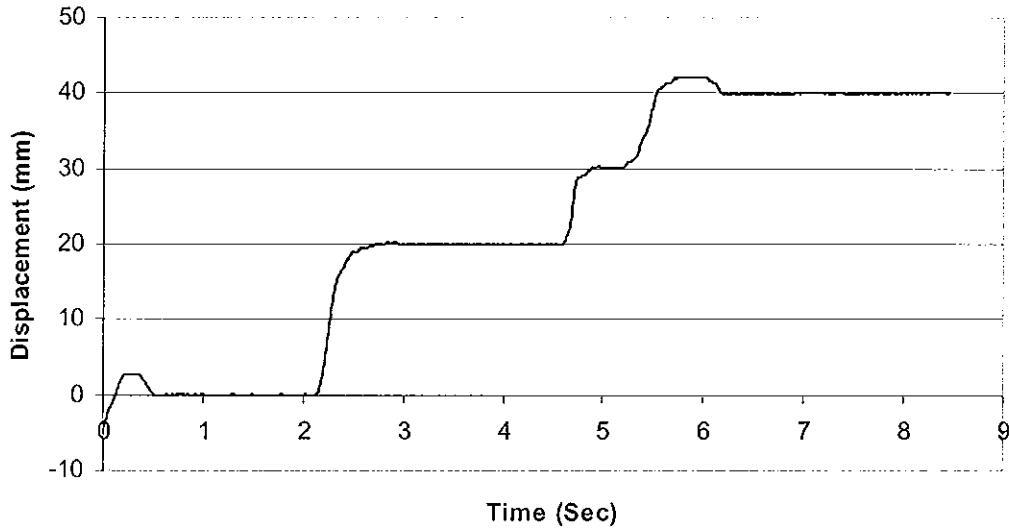
The load transducer was calibrated by using a load measuring system, comprising a calibrated load cell and load output meter. Thus, the load sustained by the rig load cell could be determined at various hydraulic pressure settings and the slope and intercept co-efficients again adjusted so that the rig load cell readings reflected the known inputs.

Graphs of the outputs are on the accompanying documentation: the displacement calibration graph is for inputs of 0mm, 20mm and 40 mm, and the load displacement calibration graph is for inputs of 0kN, 30kN and 60kN loads.

Displacement and load calibration record

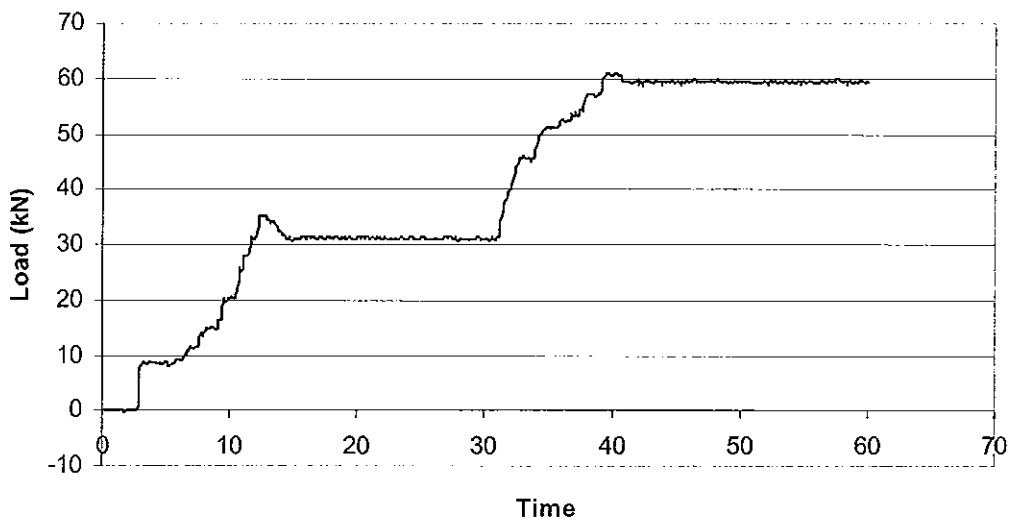
The following graphs represent data recorded from both the displacement (via workshop grade gauge blocks) and load (via a calibrated load cell) transducers immediately before experimental work took place. These outputs verify the accuracy of the transducer outputs during the experimental work.

Displacement Calibration 0-20-40mm



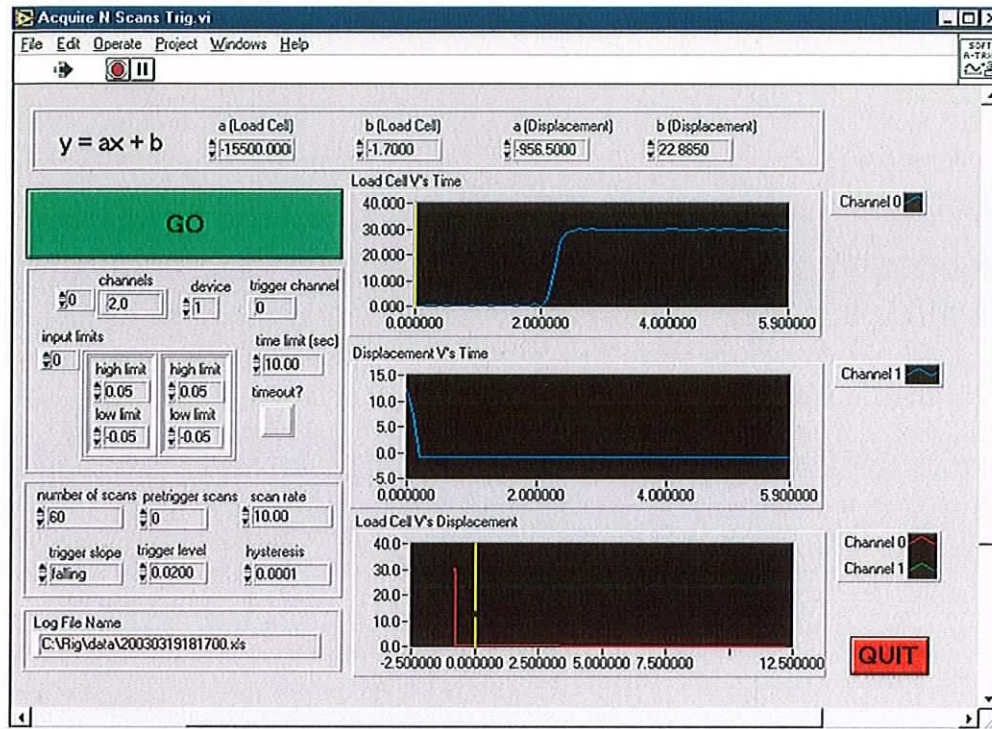
Displacement data

0-30-60 kN Calibration

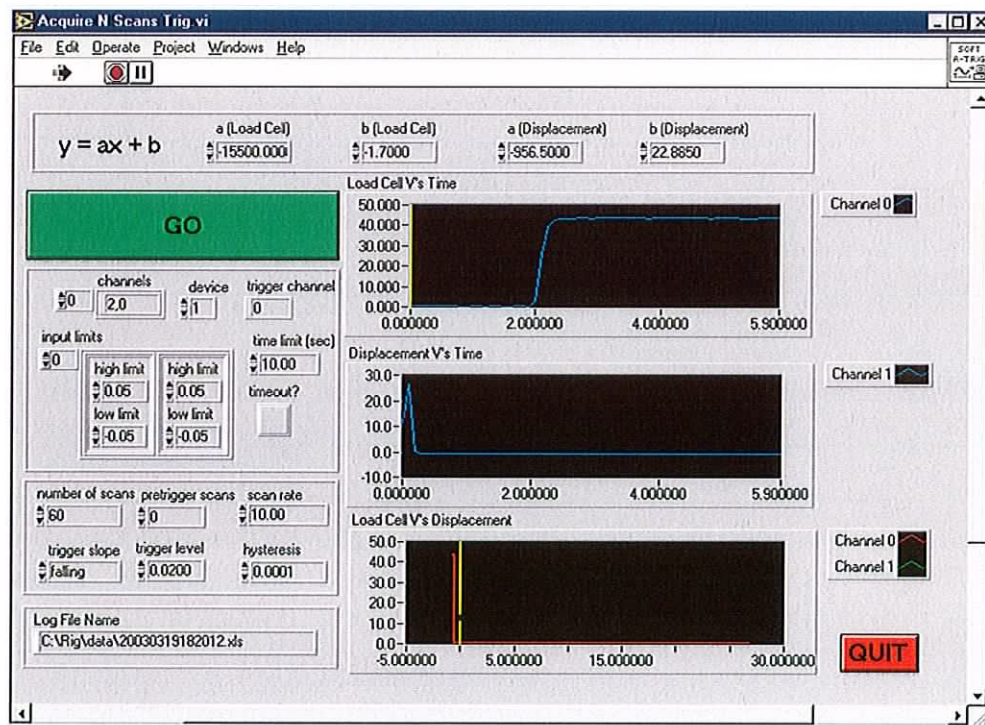


Load data

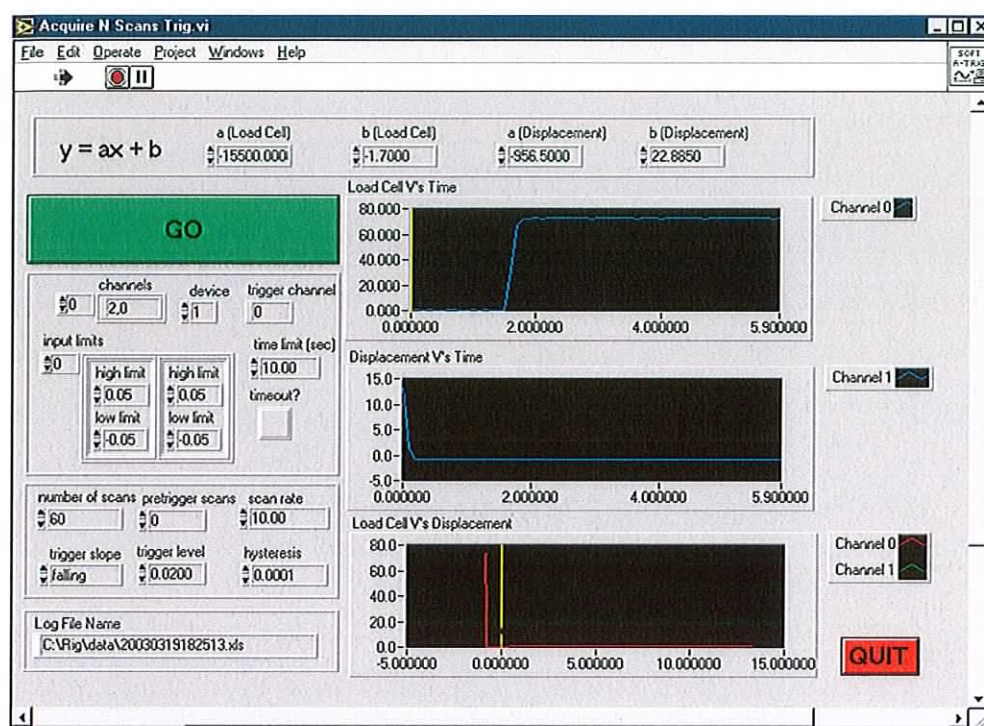
Calibration of Test Rig: Load Cell Calibration.



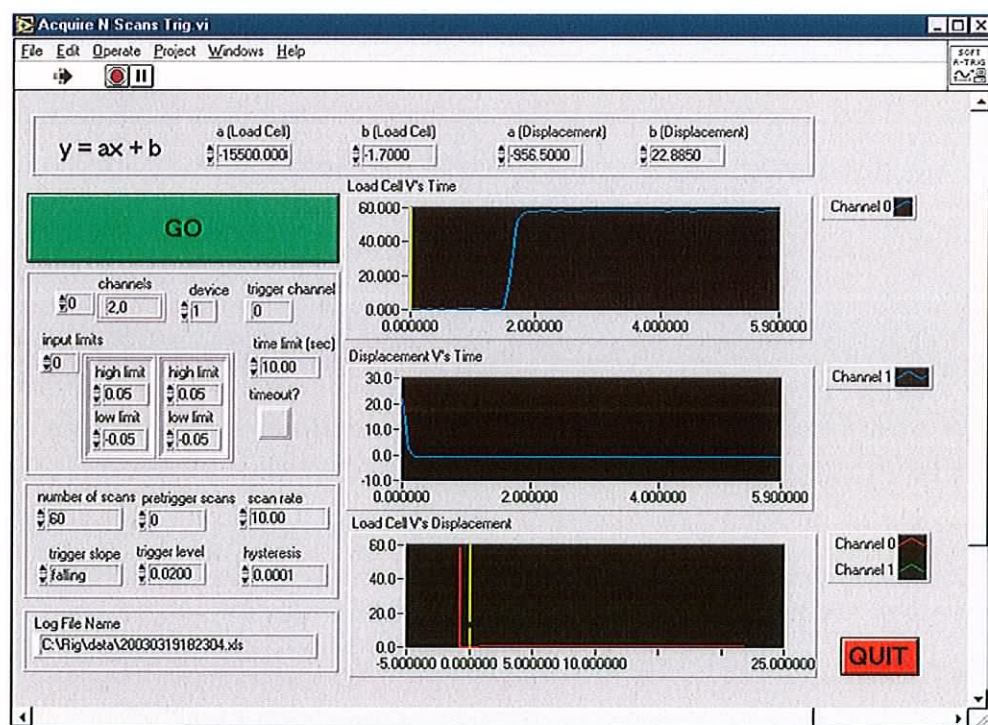
30 kN Calibration



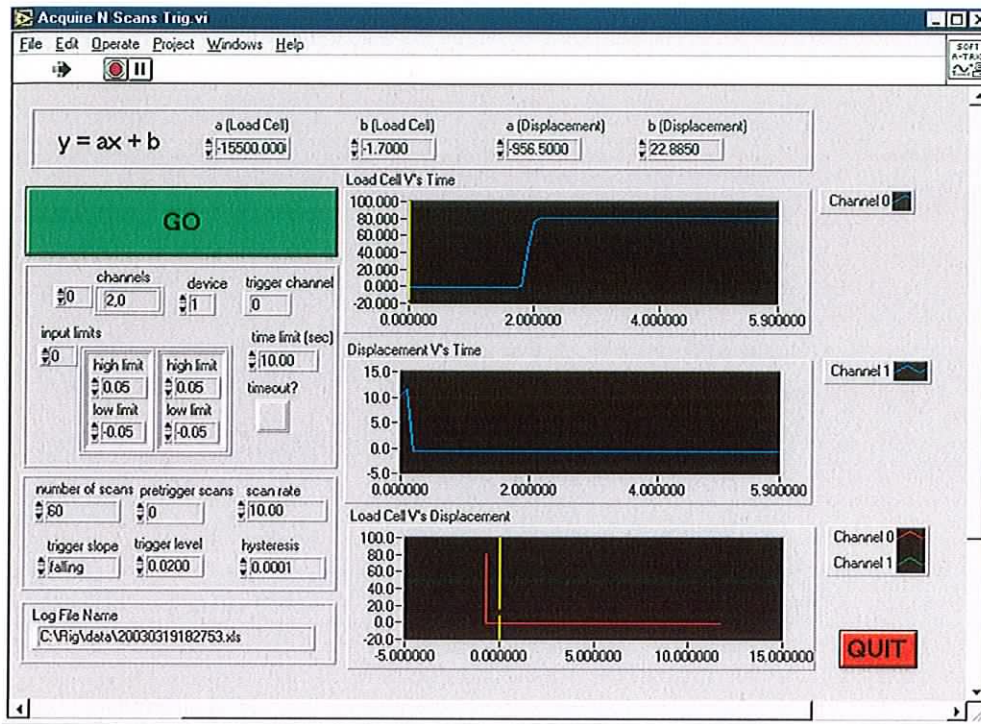
45 kN Calibration



60 kN Calibration



75kN Calibration



90kN Calibration

Calibration standards for steel

In order to confirm equivalence of the steel used for the experimental work and the steel data available in the Deform PC Pro finite element modelling package, documentary evidence of this correspondence was sought. The following pages illustrate copies of relevant pages from the European and National Standards (for steels), furnished by Customer Technical Service, Chorus Steel, UK, and the Engineering Materials Handbook edited by Charles Mantell and published by McGraw Hill.

EUROPEAN AND NATIONAL STANDARDS

| | EUROPE | GREAT BRITAIN | FRANCE | GERMANY | ITALY | NETHERLANDS | SPAIN | SWEDEN | JAPAN | U.S.A. |
|--|----------------|---------------|-----------|----------|----------|-------------|-----------|--------|-----------|-------------|
| | EN 10 130 1991 | BS 1448 | NFA 36291 | DIN 1614 | UNI 1687 | UNE 36-0671 | JIS G3101 | SIS | JIS G3101 | ASTM |
| | F400 | HR14 | OC | | | | | | | 1010 |
| | F401 | HRM | IC | | F4P10 | AP10 | | | | 1008 |
| | F402 | HR1 | 2C | SNW22 | F4P11 | AP11 | | | | 1006 |
| | F403 | HR2 | | SNW23 | F4P12 | AP12 | | | | 1008 (A1 M) |
| | F404 | HR3 | 3C | SNW20 | F4P13 | AP13 | | | | |
| | F405 | HR4 | | | | | | | | |
| | F406 | HR5 | | | | | | | | |
| | F407 | HR6 | | | | | | | | |
| | F408 | HR7 | | | | | | | | |
| | F409 | HR8 | | | | | | | | |
| | F410 | HR9 | | | | | | | | |
| | F411 | HR10 | | | | | | | | |
| | F412 | HR11 | | | | | | | | |
| | F413 | HR12 | | | | | | | | |
| | F414 | HR13 | | | | | | | | |
| | F415 | HR14 | | | | | | | | |
| | F416 | HR15 | | | | | | | | |
| | F417 | HR16 | | | | | | | | |
| | F418 | HR17 | | | | | | | | |
| | F419 | HR18 | | | | | | | | |
| | F420 | HR19 | | | | | | | | |
| | F421 | HR20 | | | | | | | | |
| | F422 | HR21 | | | | | | | | |
| | F423 | HR22 | | | | | | | | |
| | F424 | HR23 | | | | | | | | |
| | F425 | HR24 | | | | | | | | |
| | F426 | HR25 | | | | | | | | |
| | F427 | HR26 | | | | | | | | |
| | F428 | HR27 | | | | | | | | |
| | F429 | HR28 | | | | | | | | |
| | F430 | HR29 | | | | | | | | |
| | F431 | HR30 | | | | | | | | |
| | F432 | HR31 | | | | | | | | |
| | F433 | HR32 | | | | | | | | |
| | F434 | HR33 | | | | | | | | |
| | F435 | HR34 | | | | | | | | |
| | F436 | HR35 | | | | | | | | |
| | F437 | HR36 | | | | | | | | |
| | F438 | HR37 | | | | | | | | |
| | F439 | HR38 | | | | | | | | |
| | F440 | HR39 | | | | | | | | |
| | F441 | HR40 | | | | | | | | |
| | F442 | HR41 | | | | | | | | |
| | F443 | HR42 | | | | | | | | |
| | F444 | HR43 | | | | | | | | |
| | F445 | HR44 | | | | | | | | |
| | F446 | HR45 | | | | | | | | |
| | F447 | HR46 | | | | | | | | |
| | F448 | HR47 | | | | | | | | |
| | F449 | HR48 | | | | | | | | |
| | F450 | HR49 | | | | | | | | |
| | F451 | HR50 | | | | | | | | |
| | F452 | HR51 | | | | | | | | |
| | F453 | HR52 | | | | | | | | |
| | F454 | HR53 | | | | | | | | |
| | F455 | HR54 | | | | | | | | |
| | F456 | HR55 | | | | | | | | |
| | F457 | HR56 | | | | | | | | |
| | F458 | HR57 | | | | | | | | |
| | F459 | HR58 | | | | | | | | |
| | F460 | HR59 | | | | | | | | |
| | F461 | HR60 | | | | | | | | |
| | F462 | HR61 | | | | | | | | |
| | F463 | HR62 | | | | | | | | |
| | F464 | HR63 | | | | | | | | |
| | F465 | HR64 | | | | | | | | |
| | F466 | HR65 | | | | | | | | |
| | F467 | HR66 | | | | | | | | |
| | F468 | HR67 | | | | | | | | |
| | F469 | HR68 | | | | | | | | |
| | F470 | HR69 | | | | | | | | |
| | F471 | HR70 | | | | | | | | |
| | F472 | HR71 | | | | | | | | |
| | F473 | HR72 | | | | | | | | |
| | F474 | HR73 | | | | | | | | |
| | F475 | HR74 | | | | | | | | |
| | F476 | HR75 | | | | | | | | |
| | F477 | HR76 | | | | | | | | |
| | F478 | HR77 | | | | | | | | |
| | F479 | HR78 | | | | | | | | |
| | F480 | HR79 | | | | | | | | |
| | F481 | HR80 | | | | | | | | |
| | F482 | HR81 | | | | | | | | |
| | F483 | HR82 | | | | | | | | |
| | F484 | HR83 | | | | | | | | |
| | F485 | HR84 | | | | | | | | |
| | F486 | HR85 | | | | | | | | |
| | F487 | HR86 | | | | | | | | |
| | F488 | HR87 | | | | | | | | |
| | F489 | HR88 | | | | | | | | |
| | F490 | HR89 | | | | | | | | |
| | F491 | HR90 | | | | | | | | |
| | F492 | HR91 | | | | | | | | |
| | F493 | HR92 | | | | | | | | |
| | F494 | HR93 | | | | | | | | |
| | F495 | HR94 | | | | | | | | |
| | F496 | HR95 | | | | | | | | |
| | F497 | HR96 | | | | | | | | |
| | F498 | HR97 | | | | | | | | |
| | F499 | HR98 | | | | | | | | |
| | F500 | HR99 | | | | | | | | |
| | F501 | HR100 | | | | | | | | |

Entry for CR4 / SAE 1010 in European National Standards Handbook

REF. ENGINEERING MATERIALS
HANDBOOK. CHARLES L. MANTLE,
4-18 ENGINEERING STEELS MCGRAW HILL

Table 4-7. Standard Steels: Ladle Chemical Ranges and Limits for Basic Open-hearth and Acid Bessemer Carbon Steels*

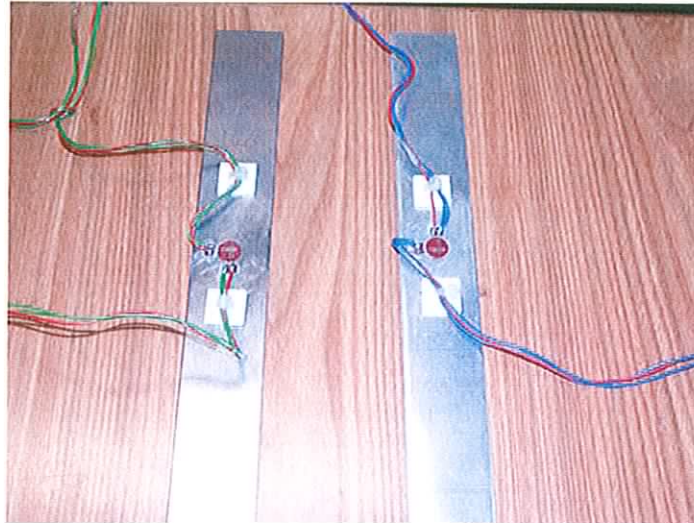
| AISI No. | Chemical composition limits, % | | | | Corresponding SAE No. |
|----------|--------------------------------|-----------|-----------|-------|-----------------------|
| | C | Mn | P max | S max | |
| C1006 | 0.08 max | 0.25-0.40 | 0.040 | 0.050 | 1006 |
| C1008 | 0.10 max | 0.25-0.50 | 0.040 | 0.050 | 1008 |
| C1010 | 0.08-0.13 | 0.30-0.60 | 0.040 | 0.050 | 1010 |
| C1011 | 0.08-0.13 | 0.60-0.90 | 0.040 | 0.050 | |
| C1012 | 0.10-0.15 | 0.30-0.60 | 0.040 | 0.050 | |
| C1015 | 0.13-0.18 | 0.30-0.60 | 0.040 | 0.050 | 1015 |
| C1016 | 0.13-0.18 | 0.60-0.90 | 0.040 | 0.050 | 1016 |
| C1017 | 0.15-0.20 | 0.30-0.60 | 0.040 | 0.050 | 1017 |
| C1018 | 0.15-0.20 | 0.60-0.90 | 0.040 | 0.050 | 1018 |
| C1019* | 0.15-0.20 | 0.70-1.00 | 0.040 | 0.050 | 1019 |
| C1020 | 0.18-0.23 | 0.30-0.60 | 0.040 | 0.050 | 1020 |
| C1021 | 0.18-0.23 | 0.60-0.90 | 0.040 | 0.050 | 1021 |
| C1022 | 0.18-0.23 | 0.70-1.00 | 0.040 | 0.050 | 1022 |
| C1023 | 0.20-0.25 | 0.30-0.60 | 0.040 | 0.050 | |
| C1024 | 0.19-0.25 | 1.35-1.65 | 0.040 | 0.050 | 1024 |
| C1025 | 0.22-0.28 | 0.30-0.60 | 0.040 | 0.050 | 1025 |
| C1026 | 0.22-0.28 | 0.60-0.90 | 0.040 | 0.050 | 1026 |
| C1027* | 0.22-0.29 | 1.20-1.50 | 0.040 | 0.050 | 1027 |
| C1029 | 0.25-0.31 | 0.60-0.90 | 0.040 | 0.050 | |
| C1030 | 0.28-0.34 | 0.60-0.90 | 0.040 | 0.050 | 1030 |
| C1032 | 0.30-0.36 | 0.60-0.90 | 0.040 | 0.050 | |
| C1033* | 0.30-0.36 | 0.70-1.00 | 0.040 | 0.050 | 1033 |
| C1035 | 0.32-0.38 | 0.60-0.90 | 0.040 | 0.050 | 1035 |
| C1036* | 0.30-0.37 | 1.20-1.50 | 0.040 | 0.050 | 1036 |
| C1037 | 0.32-0.38 | 0.70-1.00 | 0.040 | 0.050 | |
| C1038 | 0.35-0.42 | 0.60-0.90 | 0.040 | 0.050 | 1038 |
| C1039 | 0.37-0.44 | 0.70-1.00 | 0.040 | 0.050 | 1039 |
| C1040 | 0.37-0.44 | 0.60-0.90 | 0.040 | 0.050 | 1040 |
| C1041* | 0.36-0.44 | 1.35-1.65 | 0.040 | 0.050 | 1041 |
| C1042 | 0.40-0.47 | 0.60-0.90 | 0.040 | 0.050 | 1042 |
| C1043 | 0.40-0.47 | 0.70-1.00 | 0.040 | 0.050 | 1043 |
| C1045 | 0.43-0.50 | 0.60-0.90 | 0.040 | 0.050 | 1045 |
| C1046 | 0.43-0.50 | 0.70-1.00 | 0.040 | 0.050 | 1046 |
| C1049 | 0.46-0.53 | 0.60-0.90 | 0.040 | 0.050 | 1049 |
| C1050 | 0.48-0.55 | 0.60-0.90 | 0.040 | 0.050 | 1050 |
| C1052* | 0.47-0.55 | 1.20-1.50 | 0.040 | 0.050 | 1052 |
| C1055* | 0.48-0.55 | 0.70-1.00 | 0.040 | 0.050 | |
| C1055 | 0.50-0.60 | 0.60-0.90 | 0.040 | 0.050 | 1055 |
| C1060 | 0.55-0.65 | 0.60-0.90 | 0.040 | 0.050 | 1060 |
| C1065* | 0.60-0.70 | 0.60-0.90 | 0.040 | 0.050 | 1065 |
| C1069* | 0.65-0.75 | 0.40-0.70 | 0.040 | 0.050 | |
| C1070 | 0.65-0.75 | 0.60-0.90 | 0.040 | 0.050 | 1070 |
| C1072* | 0.65-0.76 | 1.00-1.30 | 0.040 | 0.050 | |
| C1075* | 0.70-0.80 | 0.40-0.70 | 0.040 | 0.050 | |
| C1078 | 0.72-0.85 | 0.30-0.60 | 0.040 | 0.050 | 1078 |
| C1080 | 0.75-0.88 | 0.60-0.90 | 0.040 | 0.050 | 1080 |
| C1084 | 0.80-0.93 | 0.60-0.90 | 0.040 | 0.050 | |
| C1085 | 0.80-0.93 | 0.70-1.00 | 0.040 | 0.050 | 1085 |
| C1086* | 0.82-0.95 | 0.30-0.50 | 0.040 | 0.050 | 1086 |
| C1090* | 0.85-0.98 | 0.60-0.90 | 0.040 | 0.050 | 1090 |
| C1095 | 0.90-1.03 | 0.30-0.50 | 0.040 | 0.050 | 1095 |
| B1010 | 0.13 max | 0.30-0.60 | 0.07-0.12 | 0.060 | |

* Grades marked by a star are those less commonly specified.

Silicon promotes the adherence of zinc coating on hot-dipped galvanized wire. Fully killed steels may contain various amounts of silicon up to 0.30% maximum. Silicon is less effective than manganese in increasing strength and hardness. In low-carbon steels it is usually detrimental to surface quality and this condition is more pronounced with the resulfurized grades.

Entry for SAE 1010 / AISI 1010 in Engineering Materials Handbook

As with the tooling materials, the author sought to verify the materials' Poisson's Ratio for the steel and aluminium in question. This was realised by attaching strain gauges to the materials and verifying the longitudinal and lateral strains for various loads.



Aluminium and Steel workpieces with strain gauges attached

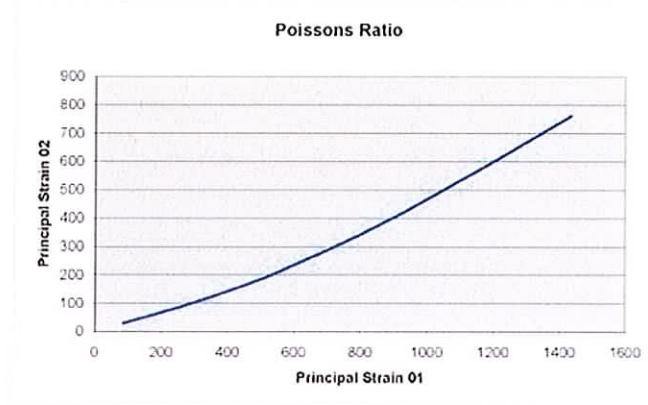
The following page shows diagrams indicating corresponding axial and lateral strains for both steel and aluminium, and the derived values for Poisson's Ratio.

Steel AISI 1010 Workpiece

Units in
Microstrain

| Load kN | Principal Strain 01 | Principal Strain 02 | Poisson's Ratio |
|---------|---------------------|---------------------|-----------------|
| 1 | 84 | 29 | 0.345238 |
| 2 | 145 | 49 | 0.337931 |
| 3 | 208 | 70 | 0.336538 |
| 4 | 261 | 88 | 0.337165 |
| 5 | 308 | 106 | 0.344156 |
| 6 | 355 | 124 | 0.349295 |
| 7 | 406 | 145 | 0.357143 |
| 8 | 466 | 170 | 0.364807 |
| 9 | 530 | 199 | 0.375472 |
| 10 | 600 | 236 | 0.393333 |
| 11 | 695 | 285 | 0.410072 |
| 12 | 791 | 338 | 0.427307 |
| 13 | 930 | 421 | 0.452688 |
| 14 | 1176 | 584 | 0.496509 |
| 150 | 1435 | 762 | 0.53101 |

Average
Poissons
Ratio 0.390584

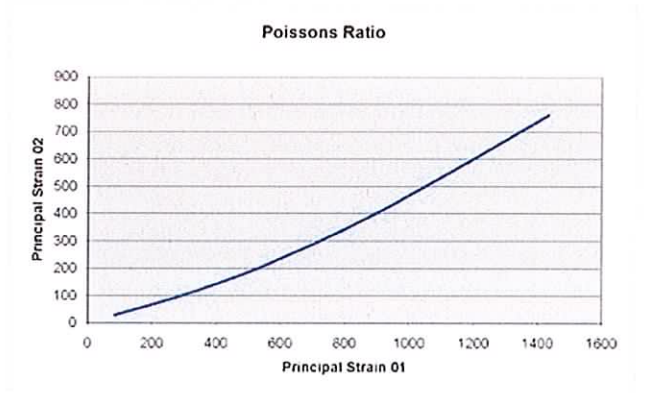


Aluminium Workpiece

Units in
Microstrain

| Load kN | Principal Strain 01 | Principal Strain 02 | Poisson's Ratio |
|---------|---------------------|---------------------|-----------------|
| 0.75 | 148 | 52 | 0.351351351 |
| 1.25 | 230 | 80 | 0.347826087 |
| 1.75 | 325 | 112 | 0.344615385 |
| 2.25 | 412 | 140 | 0.339805825 |
| 2.75 | 504 | 172 | 0.341269841 |
| 3.25 | 606 | 204 | 0.336633663 |
| 3.75 | 693 | 231 | 0.333333333 |
| 4.25 | 756 | 251 | 0.332010582 |
| 4.75 | 833 | 276 | 0.331332533 |
| 5.25 | 893 | 295 | 0.330347144 |
| 5.75 | 964 | 319 | 0.330812863 |
| 6.25 | 1033 | 302 | 0.292352372 |
| 6.75 | 1108 | 365 | 0.329422383 |
| 7.25 | 1175 | 368 | 0.330212768 |
| 7.75 | 1254 | 414 | 0.330143541 |
| 8.25 | 1329 | 440 | 0.331075997 |
| 8.75 | 1416 | 453 | 0.319915254 |

Average
Poissons
Ratio 0.332503584



Transducer Characteristics

Experimental data (Load – Displacement, Load – Time and Displacement – Time) data was acquired in real time. Load data was acquired via a calibrated load cell type Tokyo Sokki Kenkyujo CLC-30A, the characteristics of which are shown in the accompanying document. Displacement data was acquired via a Tokyo Sokki Kenkyujo CDP-50 50mm displacement transducer, again the characteristics of which are shown on the accompanying documentation. The data was logged and analysed by a National Instruments PCI-1200 data acquisition board, running National Instruments LabView on a PC under Microsoft Windows 95.



Certificate of Calibration

Declaration of Conformity
according to ISO/IEC Guide 22 and BS 7514

Manufacturer's Name: National Instruments
Manufacturer's Address: 6504 Bridge Point Parkway
Austin, Texas 78730-5039
USA

The manufacturer hereby declares that the product:

Product Name: Multifunction I/O Board for PCI
Model Numbers: PCI-120C
Product Options: All

conforms to the following standards or other normative documents

- Electromagnetic Emissions:** EN 55011:1997
(by Council Directive 89/338/EEC) CISPR 11:1990
- Electromagnetic Immunity:** EN 50082-1:1992
(by Council Directive 89/336/EEC) IEC 601-2:1991
- IEC 601-3:1991
- IEC 601-4:1988
- Safety:** EN 61010-1:1993
(by Council Directive 73/23/EEC)

- Group 1, Class A
- 4.0 kV by Contact
- 8.0 kV by Air
- 3.0 V/m
- 25 - 1000 MHz
- 0.5 kV Signal Lines
- 3.0 kV AC Power Lines

Supplementary Information

Unshielded cable with non-insulating connectors is used. ESD precautions are required when connecting or disconnecting this type of cable.

When and Where Issued

10 October 1996
Austin, Texas USA

Eric Libbey
Eric Libbey
Compliance Engineer

Marks of Compliance



European Contact
National Instruments Corporation (U.K. Ltd.)
21 Kingfisher Court, Hambroge Road
Newbury, Berkshire RG14 5SJ
Tel (44) 1635 523545
Fax (44) 1635 523154

3012044-01

© Copyright, 1996 National Instruments Corporation. All rights reserved.

October 1996

Board Information

Serial Number: B7817E
Lot Part Number: 18-09451-01
Description: PCI-120C

Certificate Information

Certificate Number: 110597
Issue Period: 10/05/96 - 10/05/99
NI Part Number: 18400-5A-01

Calibration Date: 11-DEC-1999
Calibration Interval: 12 Months
Calibration Due: 11-DEC-2000

Ambient Temperature: 35.1°
Relative Humidity: 35.2%

National Instruments certifies that at the time of manufacture, the above product was calibrated in accordance with applicable National Instruments procedures. These procedures are in compliance with relevant clauses of ISO 9002 and are designed to assure that the product listed above meets or exceeds National Instruments specifications.

National Instruments further certifies that the measurements standards and instruments used during the calibration of this product are traceable to the National Institute of Standards and Technology or are derived from accepted values of natural physical constants.

The environment in which this product was calibrated is maintained within the operating specifications of the instrument and the standards.

For questions or comments, please contact National Instruments Technical Support.


Signed,
Domingo Salcido
Domingo Salcido
Operations Manager



1031994

CDP-50

試験成績書
TEST DATA

| | | | | | |
|---|-------------------------------|----------------------|-------------------|--------------------|---------------------|
| 容 積 Capacity | 50 mm | 試験年月日 Date | 1994.11.15 | 温 度 Temperature | 23 °C |
| 製造番号 Serial No. | 514885 | | | 湿 度 Humidity | 65 % |
| 定格出力 Rated output | | (ひずみ: Strain K=2.00) | 5000 | | $\mu\text{V/V}$ |
| 感 度 Sensitivity | | | 10000 | | $\times 10^{-6}$ |
| 非直線性 Non linearity | | | 200 | | $\times 10^{-4} \%$ |
| | | | 0.1 | | % (R) |
| ブリッジ構成 Bridge configuration | (4ゲージ法) Half bridge method | 入力 Input | 348.7 Ω | 赤 Red(A) | 黒 Black(C) |
| | | 出力 Output | 348.5 Ω | 緑 Green(B) | 白 White(D) |
| 許容印加電圧 Safe excitation | | | 10 | | V (AC or DC) |
| 入出力ケーブル Connection cable | | | 0.3 | | mm |
|  株式会社 東京測器研究所 Tokyo Sokki Kenkyujo Co., Ltd. 140 東京都品川区南大井 6-8-2 TOKYO JAPAN | | 試験者 Tested by | 責任者 Supervised by | | |

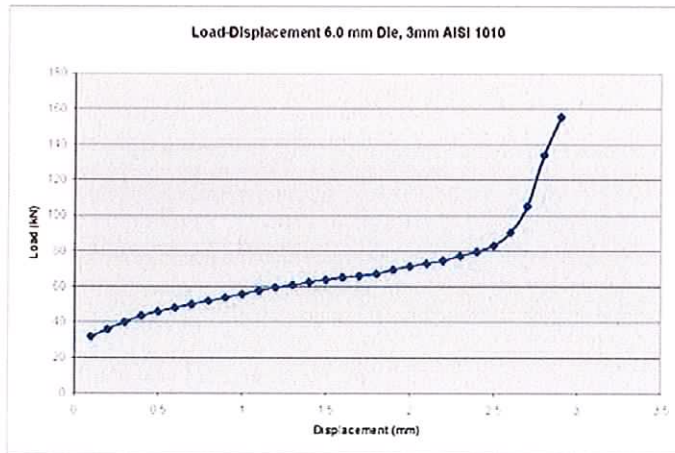
Selected Finite Element and Experimental Work Results

The accompanying documents show the results of selected (6.0 mm die step height) finite element analysis and experimental results of the examination of the double bending process. The complete set of results are organised and available on the accompanying compact disk. The results shown are organised by material type, (AISI 1010 / CR4 Steel, then 6062 Aluminium). Each set of results commences with a load-displacement curve for a unit depth lamina of the appropriate material, as predicted by Deform PC Pro. These results were then outputs as a text file, which itself was used to recreate the results for a 40 mm deep workpiece, both as a spreadsheet and graph. The results of the actual experimental work are then presented, again in spreadsheet and graph form. It can be seen that many of the result sets have reasonable correlation between the finite element predictions and the experimental observations, especially in the shapes of the curves. The effective strain fields are then presented for the workpieces, at fractional amounts of deformation, indicating the nature, position and magnitude of effective strain throughout the workpiece. The effective stress fields on the tooling are then presented, at fractional deformations corresponding to the strain field illustrations. Finally, the transducer outputs are shown for each of three experiments for each material and die set type.

6.0 mm Die, 3.0 mm Steel
 AISI 1010
 Load - Displacement Curve
 Deform PC Pro FEA Results

| | Stroke (mm) | | Force (N) | Incremental Distance (mm) | Average Force (N) per mm width of workpiece | Average Force (kN) for total workpiece width of 40 mm | Force x Incremental Distance (kN-mm) |
|-----|-------------|-----|-------------|---------------------------|---|---|--------------------------------------|
| c0 | 0.1 | h0 | 738.0193512 | 0.1 | 753.3514252 | 31.73405701 | 3.173405701 |
| d1 | 0.2 | h1 | 848.6834992 | 0.1 | 896.4936711 | 35.85974684 | 3.585974684 |
| d2 | 0.3 | h2 | 944.303843 | 0.099964486 | 998.6258057 | 39.94503223 | 3.993084596 |
| d3 | 0.399964486 | h3 | 1052.947769 | 0.1 | 1087.289557 | 43.49158229 | 4.349158229 |
| d4 | 0.499964486 | h4 | 1121.631346 | 0.100000014 | 1146.268522 | 45.85074086 | 4.585074775 |
| d5 | 0.5999645 | h5 | 1170.905697 | 0.1 | 1200.680352 | 48.02761407 | 4.802761407 |
| d6 | 0.6999645 | h6 | 1230.475007 | 0.1 | 1251.720515 | 50.0589206 | 5.00589206 |
| d7 | 0.7999645 | h7 | 1272.966023 | 0.1 | 1297.257602 | 51.89030409 | 5.189030409 |
| d8 | 0.8999645 | h8 | 1321.549181 | 0.1 | 1345.754745 | 53.83018979 | 5.383018979 |
| d9 | 0.9999648 | h9 | 1369.960308 | 0.1 | 1395.111237 | 55.80444949 | 5.580444949 |
| d10 | 1.0999645 | h10 | 1420.262166 | 0.1 | 1447.991957 | 57.91967829 | 5.791967829 |
| d11 | 1.1999645 | h11 | 1475.721748 | 0.099969659 | 1490.116784 | 59.60467136 | 5.958658888 |
| d12 | 1.299934159 | h12 | 1504.51182 | 0.1 | 1524.46944 | 60.97837759 | 6.097837759 |
| d13 | 1.399934159 | h13 | 1544.40706 | 0.1 | 1562.801231 | 62.51204925 | 6.251204925 |
| d14 | 1.499934159 | h14 | 1581.195403 | 0.1 | 1599.216224 | 63.96664895 | 6.396664895 |
| d15 | 1.599934159 | h15 | 1617.237045 | 0.1 | 1627.647066 | 65.10588264 | 6.510588264 |
| d16 | 1.699934159 | h16 | 1638.057087 | 0.1 | 1649.913208 | 65.9965283 | 6.59965283 |
| d17 | 1.799934159 | h17 | 1661.769328 | 0.1 | 1679.481076 | 67.17924302 | 6.717924302 |
| d18 | 1.899934159 | h18 | 1697.192823 | 0.1 | 1735.610549 | 69.42442195 | 6.942442195 |
| d19 | 1.999934159 | h19 | 1774.028274 | 0.1 | 1765.945886 | 71.43783544 | 7.143783544 |
| d20 | 2.099934159 | h20 | 1797.863498 | 0.1 | 1822.037504 | 72.88150016 | 7.288150016 |
| d21 | 2.199934159 | h21 | 1846.21151 | 0.1 | 1864.292349 | 74.57169396 | 7.457169396 |
| d22 | 2.299934159 | h22 | 1882.373188 | 0.099808708 | 1929.329792 | 77.1731917 | 7.702556525 |
| d23 | 2.399742867 | h23 | 1976.286397 | 0.1 | 1992.987065 | 79.7194826 | 7.97194826 |
| d24 | 2.499742867 | h24 | 2009.687733 | 0.1 | 2076.248134 | 83.04992536 | 8.304992536 |
| d25 | 2.599742867 | h25 | 2142.808535 | 0.099081086 | 2258.179934 | 90.32719737 | 8.94887482 |
| d26 | 2.698825953 | h26 | 2373.551333 | 0.1 | 2633.172692 | 105.3269077 | 10.53269077 |
| d27 | 2.798825953 | h27 | 2892.794051 | 0.1 | 3348.911166 | 133.9564466 | 13.39564466 |
| d28 | 2.898825953 | h28 | 3805.028282 | 0.007467138 | 3888.70767 | 155.5463068 | 1.161500621 |
| d29 | 2.906293031 | h29 | 3972.387058 | | | | |

Total Work (kN-mm) 182.9243113
 Total Work (kN-m = kJ) 0.182824311



6.0 mm Die, 3.0 mm Aluminium
6062
Load - Displacement Curve
Deform PC Pro FEA Results

| | Stroke (mm) | | Force (N) | Incremental Distance (mm) | Average Force (N) per mm width of workpiece | Average Force (kN) for total workpiece width of 40 mm | Force x Incremental Distance (kN-mm) |
|-----|-------------|-----|-------------|---------------------------|---|---|--------------------------------------|
| d0 | 0.15 | h0 | 329.6362546 | 0.15 | 351.3550826 | 14.0542033 | 2.109130496 |
| d1 | 0.3 | h1 | 373.0739106 | 0.15 | 393.2622986 | 15.73049195 | 2.35953792 |
| d2 | 0.45 | h2 | 413.4506867 | 0.15 | 427.3312251 | 17.093249 | 2.563987351 |
| d3 | 0.6 | h3 | 441.2117635 | 0.15 | 461.8030375 | 18.4781215 | 2.771418225 |
| d4 | 0.75 | h4 | 482.5943115 | 0.15 | 479.5997938 | 19.18399175 | 2.877598763 |
| d5 | 0.9 | h5 | 476.605276 | 0.15 | 488.6801729 | 19.4640692 | 2.919961038 |
| d6 | 1.05 | h6 | 496.7150698 | 0.15 | 507.5442051 | 20.3017682 | 3.04526523 |
| d7 | 1.2 | h7 | 518.3733403 | 0.15 | 524.9959023 | 20.9993361 | 3.149975415 |
| d8 | 1.35 | h8 | 531.6184647 | 0.15 | 537.2165455 | 21.48866182 | 3.223299273 |
| d9 | 1.5 | h9 | 542.8146262 | 0.15 | 547.4697558 | 21.89879023 | 3.284818535 |
| d10 | 1.65 | h10 | 552.1248894 | 0.15 | 559.0300848 | 22.36120339 | 3.354160509 |
| d11 | 1.8 | h11 | 565.9352842 | 0.15 | 573.682788 | 22.94731152 | 3.442096728 |
| d12 | 1.95 | h12 | 581.4302917 | 0.15 | 593.1422476 | 23.7256899 | 3.558853486 |
| d13 | 2.1 | h13 | 604.8542035 | 0.15 | 612.2771028 | 24.49108439 | 3.673662659 |
| d14 | 2.25 | h14 | 619.700016 | 0.15 | 627.7337166 | 25.10934882 | 3.788402294 |
| d15 | 2.4 | h15 | 635.7674153 | 0.15 | 651.1332163 | 26.04532865 | 3.906799298 |
| d16 | 2.55 | h16 | 666.4990173 | 0.15 | 696.6273783 | 27.86509513 | 4.17976427 |
| d17 | 2.7 | h17 | 726.7557392 | 0.15 | 838.2270803 | 33.52908321 | 5.029362482 |
| d18 | 2.85 | h18 | 949.6984215 | 0.15 | 1162.46264 | 46.4985056 | 6.97477594 |
| d19 | 3 | h19 | 1375.228858 | 0.15 | 1540.444652 | 61.61778649 | 9.242667973 |
| d20 | 3.15 | h20 | 1705.662466 | | | | |

Total Work (kN-mm) 75.43259165
Total Work (kN-m = kJ) 0.075432594



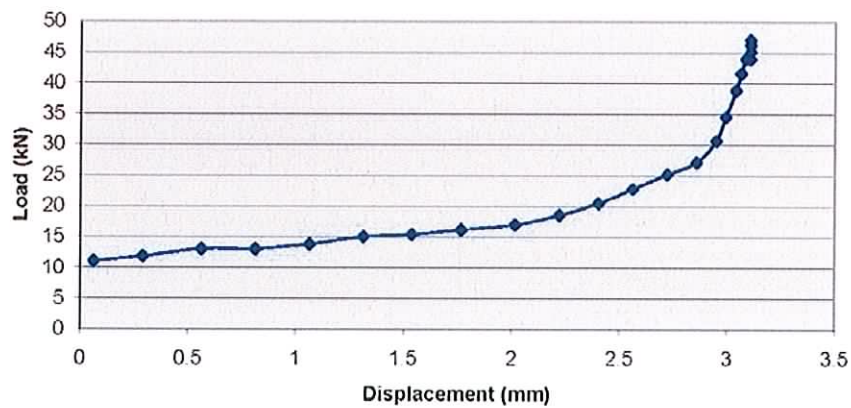
6.0 mm Die, 3.0 mm Al 6062
Load - Displacement Curve
Experimental Results

| Time (sec) | Displacement (mm) | Load (kN) | Incremental Displacement | Average Load | Average Load x Incremental Displacement |
|------------|-------------------|-----------|--------------------------|--------------|---|
| 2.4 | 0.064 | 11.109 | 0.227 | 11.5 | 2.6105 |
| 2.5 | 0.291 | 11.891 | 0.272 | 12.477 | 3.393744 |
| 2.6 | 0.563 | 13.063 | 0.25 | 13.063 | 3.26575 |
| 2.7 | 0.813 | 13.063 | 0.25 | 13.4535 | 3.363375 |
| 2.8 | 1.063 | 13.844 | 0.249 | 14.43 | 3.59307 |
| 2.9 | 1.312 | 15.016 | 0.227 | 15.211 | 3.452897 |
| 3 | 1.539 | 15.406 | 0.227 | 15.7965 | 3.5858055 |
| 3.1 | 1.766 | 16.187 | 0.25 | 16.578 | 4.1445 |
| 3.2 | 2.016 | 16.969 | 0.205 | 17.75 | 3.63875 |
| 3.3 | 2.221 | 18.531 | 0.181 | 19.5075 | 3.5308575 |
| 3.4 | 2.402 | 20.484 | 0.159 | 21.656 | 3.443304 |
| 3.5 | 2.561 | 22.828 | 0.159 | 24 | 3.816 |
| 3.6 | 2.72 | 25.172 | 0.136 | 26.1485 | 3.556196 |
| 3.7 | 2.856 | 27.125 | 0.091 | 28.883 | 2.628353 |
| 3.8 | 2.947 | 30.641 | 0.045 | 32.594 | 1.46673 |
| 3.9 | 2.992 | 34.547 | 0.046 | 36.6955 | 1.687993 |
| 4 | 3.038 | 38.844 | 0.023 | 40.211 | 0.924853 |
| 4.1 | 3.061 | 41.578 | 0.022 | 42.75 | 0.9405 |
| 4.2 | 3.083 | 43.922 | 0.023 | 44.508 | 1.023684 |
| 4.3 | 3.106 | 45.094 | 0 | 45.68 | 0 |
| 4.4 | 3.106 | 46.266 | 0 | 46.6565 | 0 |
| 4.5 | 3.106 | 47.047 | 0 | 45.4845 | 0 |
| 4.6 | 3.106 | 43.922 | | | |

Total Work (kN-mm) 54.066862

Total Work (kN-m = kJ) 0.054066862

Load-Displacement 6.0 mm Die, 3.0 mm Al 6062

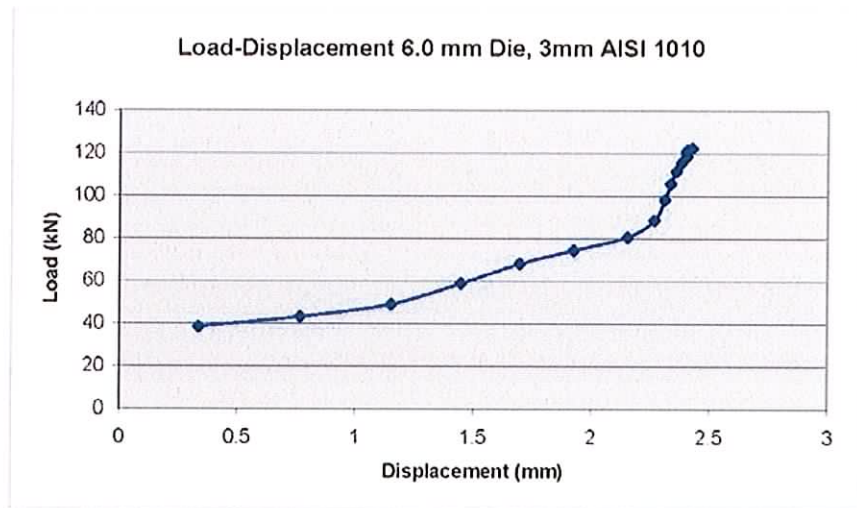


6.0 mm Die, 3.0 mm Steel
 AISI 1010
 Load - Displacement Curve
 Experimental Results

| Time | Displacement (mm) | Load (kN) | Incremental Displacement | Average Load | Average load x incremental displacement |
|------|-------------------|-----------|--------------------------|--------------|---|
| 2.3 | 0.336 | 38.453 | 0.431 | 40.797 | 17.583507 |
| 2.4 | 0.767 | 43.141 | 0.386 | 46.0705 | 17.783213 |
| 2.5 | 1.153 | 49 | 0.296 | 53.883 | 15.949368 |
| 2.6 | 1.449 | 58.766 | 0.249 | 63.4535 | 15.7999215 |
| 2.7 | 1.698 | 68.141 | 0.227 | 71.266 | 16.177382 |
| 2.8 | 1.925 | 74.391 | 0.227 | 77.516 | 17.596132 |
| 2.9 | 2.152 | 80.641 | 0.114 | 84.547 | 9.638358 |
| 3 | 2.266 | 88.453 | 0.045 | 93.336 | 4.20012 |
| 3.1 | 2.311 | 98.219 | 0.023 | 101.93 | 2.34439 |
| 3.2 | 2.334 | 105.641 | 0.023 | 108.5705 | 2.4971215 |
| 3.3 | 2.357 | 111.5 | 0.022 | 113.453 | 2.495966 |
| 3.4 | 2.379 | 115.406 | 0.023 | 116.9685 | 2.6902755 |
| 3.5 | 2.402 | 118.531 | 0 | 119.5075 | 0 |
| 3.6 | 2.402 | 120.484 | 0 | 120.875 | 0 |
| 3.7 | 2.402 | 121.266 | 0.023 | 121.8515 | 2.8025845 |
| 3.8 | 2.425 | 122.437 | | | |

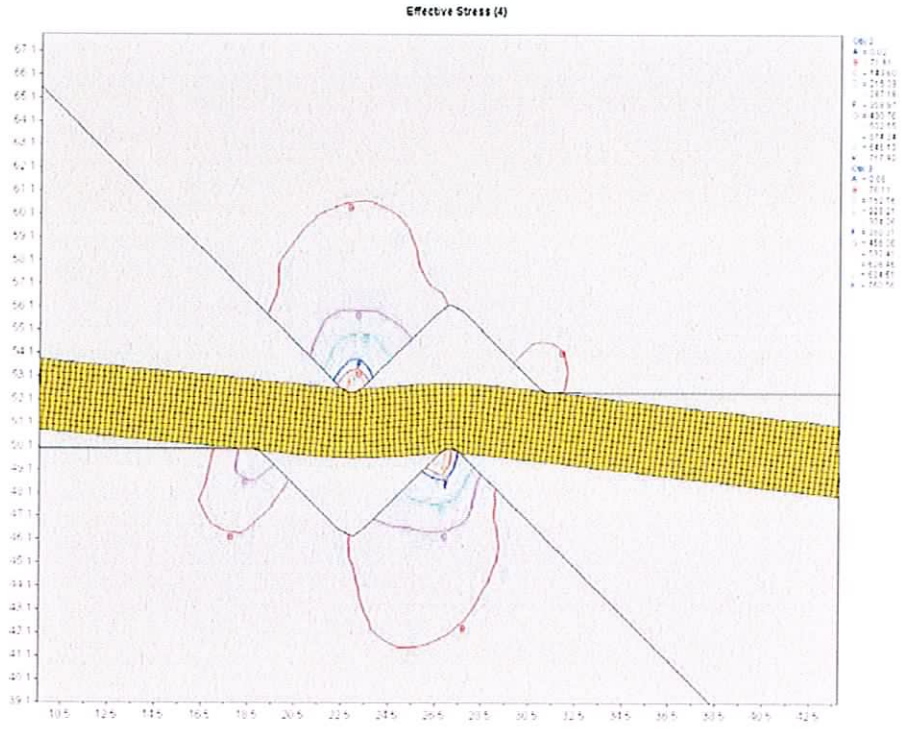
Total Work (kN-mm) 127.558339

Total Work (kN-m = kJ) 0.127558339

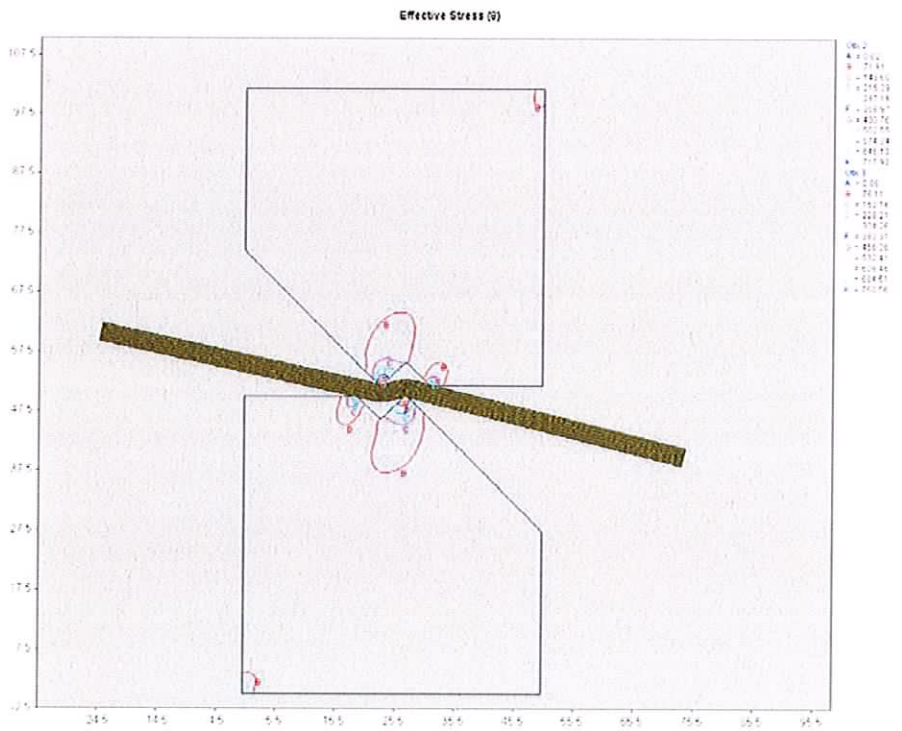


6.0mm Die
Material: AISI 1010 Steel
Effective Die Stress at defined step numbers.

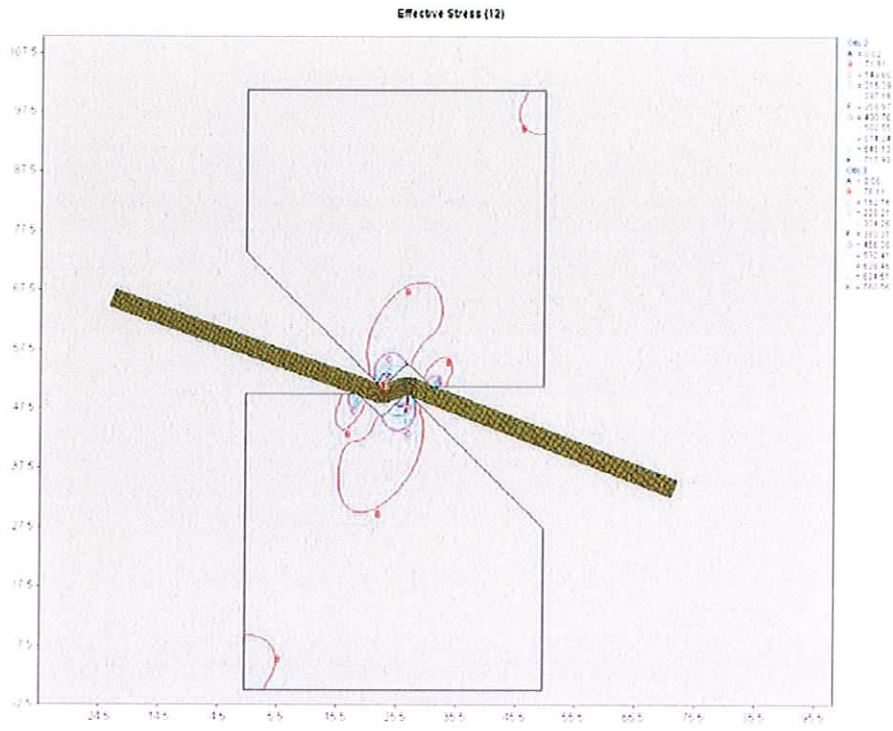
Step 4



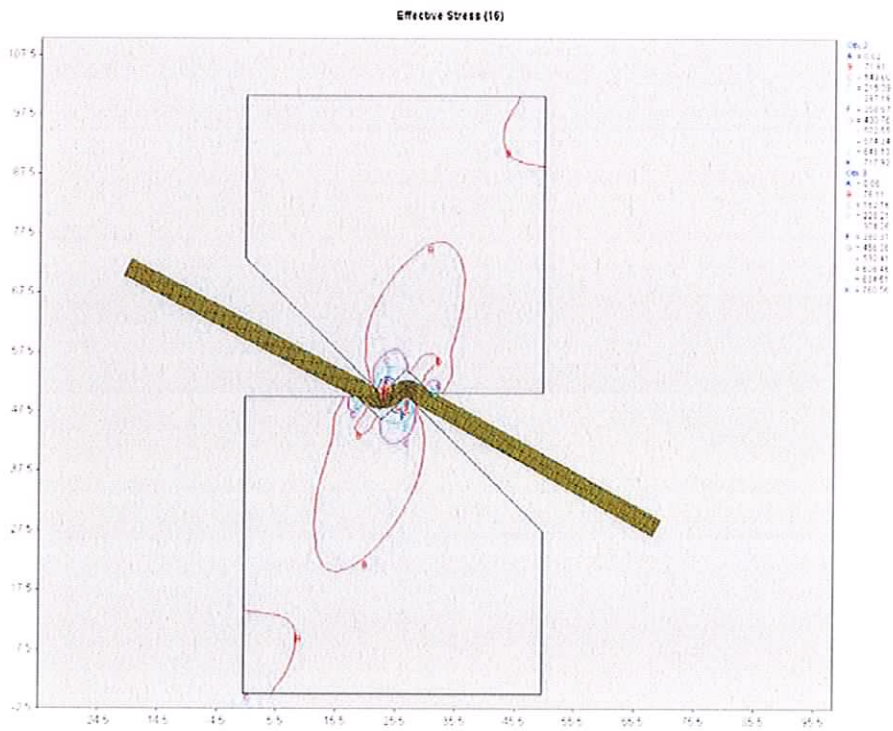
Step 8



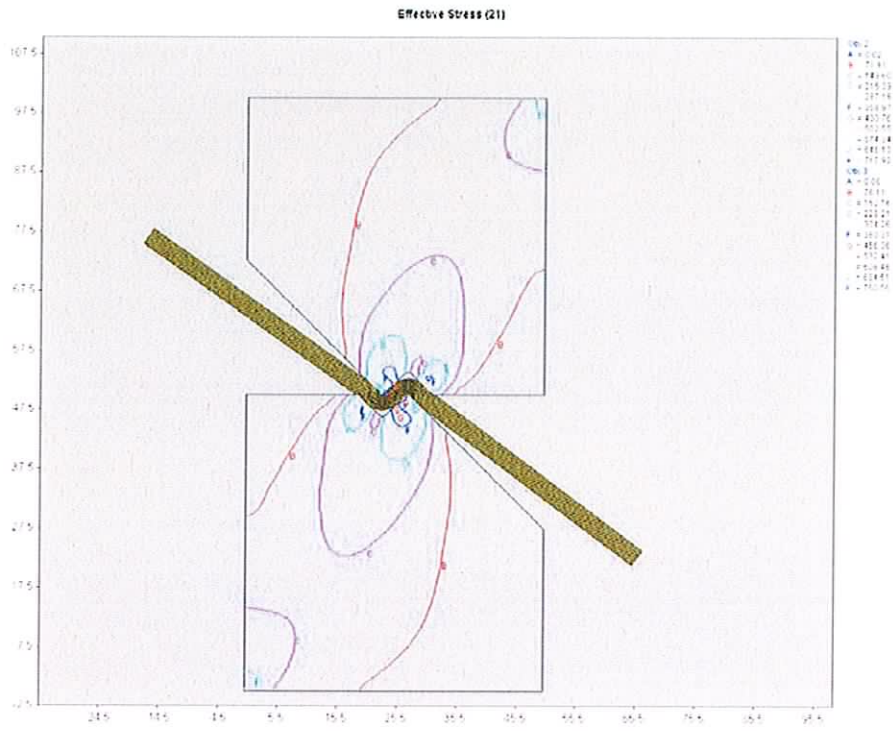
Step 12



Step 16

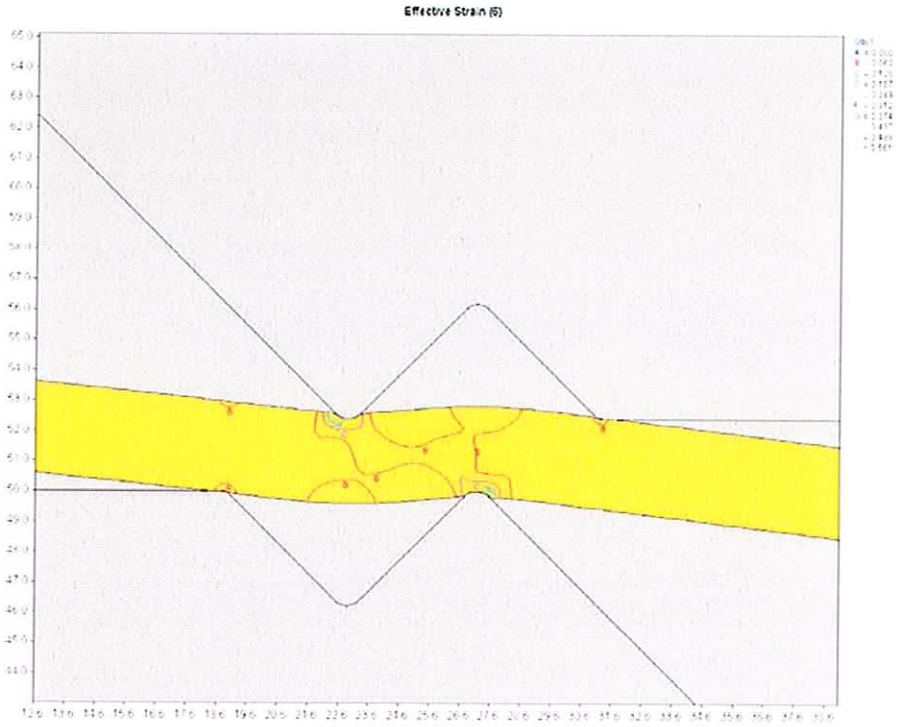


Step 21

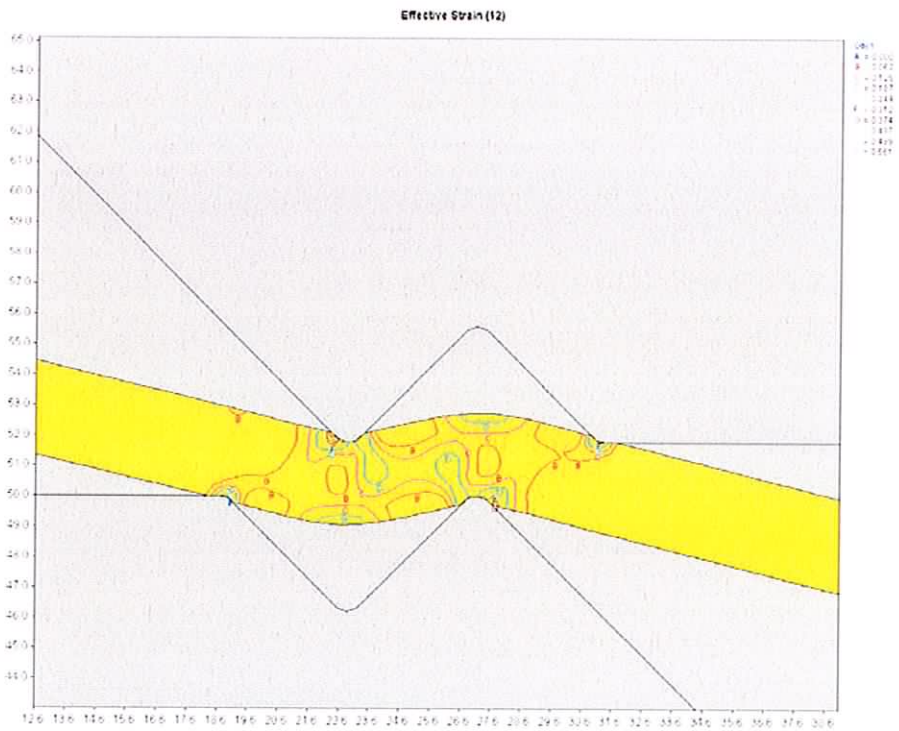


6.0mmDie
Material: AISI 1010 Steel 3.0 mm
Effective Strain at defined step numbers.

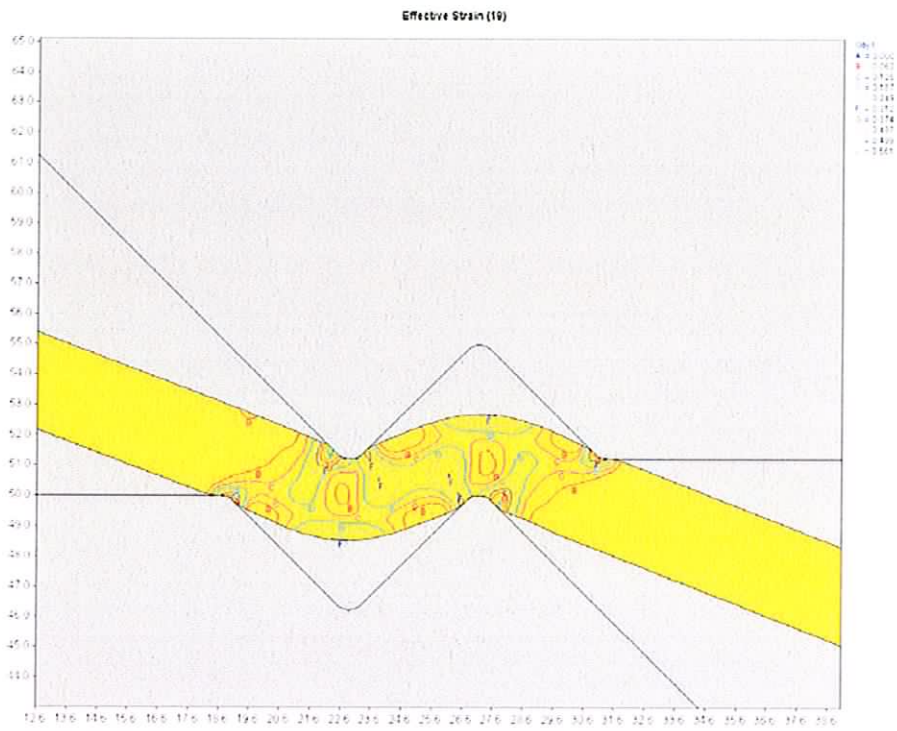
Step 6



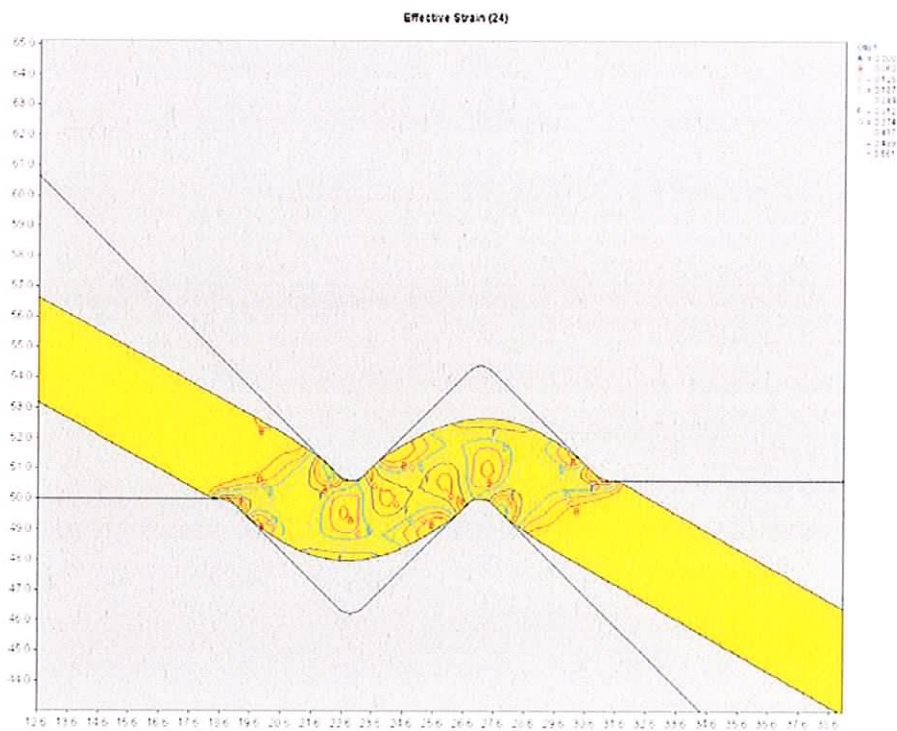
Step 12



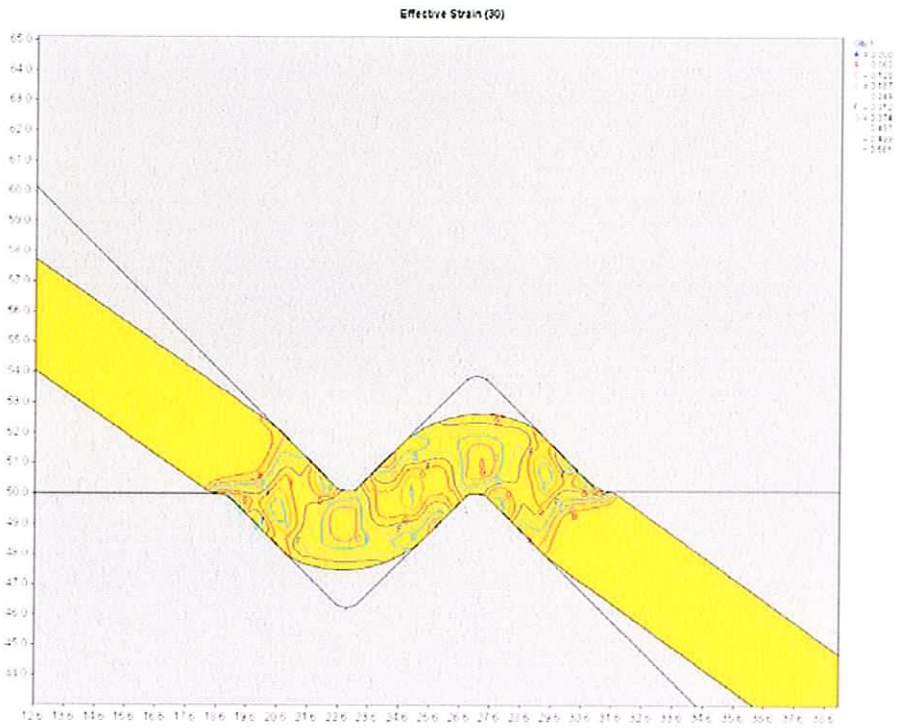
Step 18



Step 24

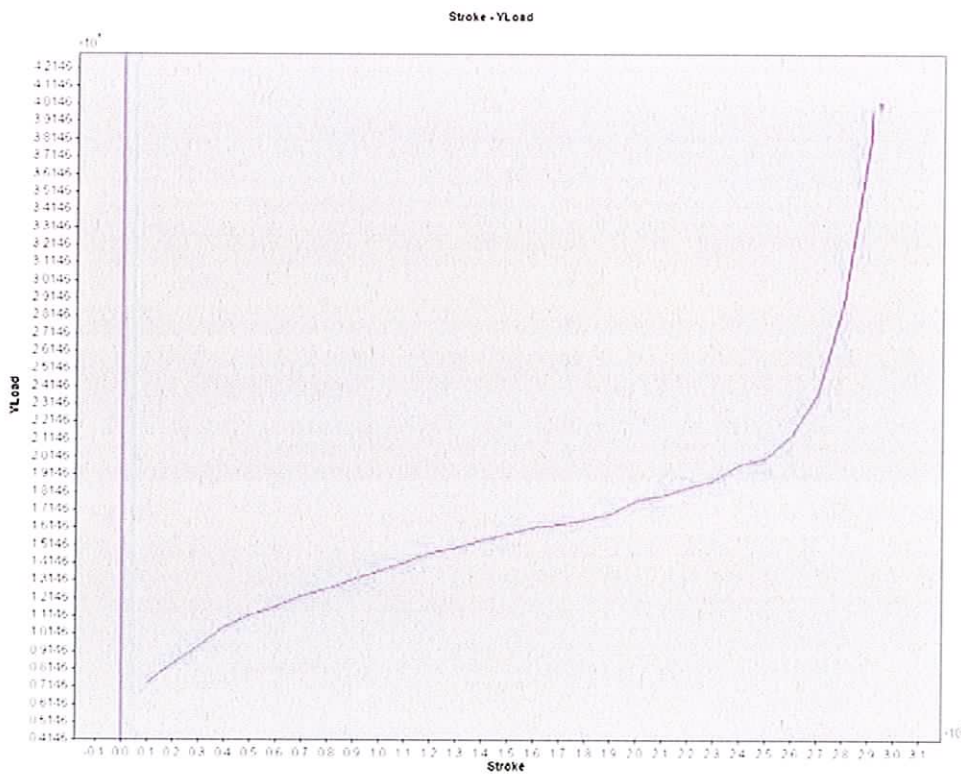


Step 30



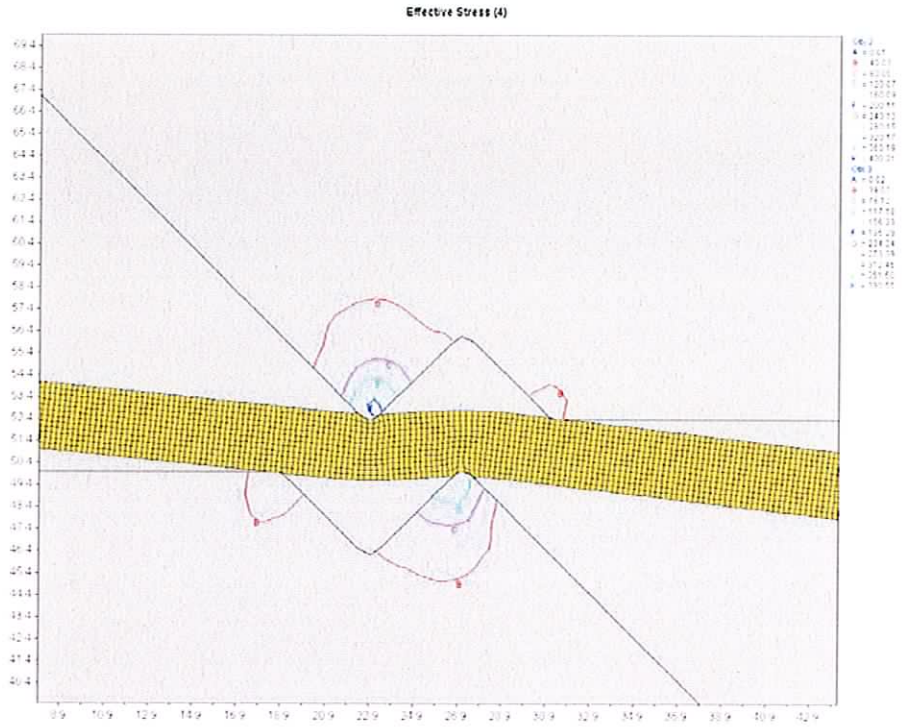
6.0mm Die, 3.0 mm, Steel AISI 1010

Load / Stroke curve (Deform PC Pro)

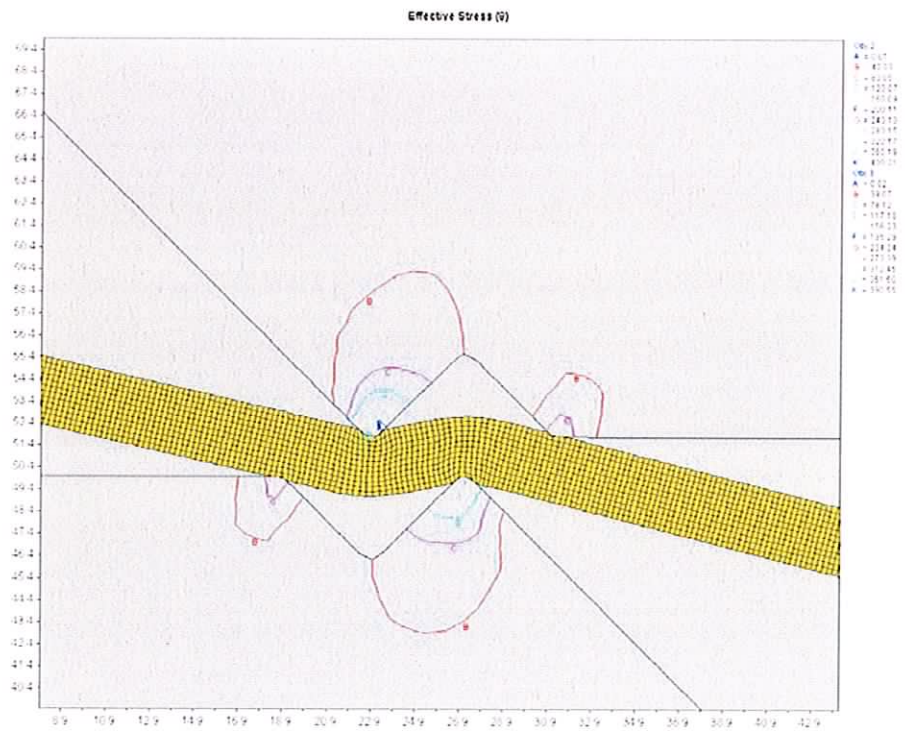


6.0mm Die
Material: 6062 Aluminium
Effective Die Stress at defined step numbers.

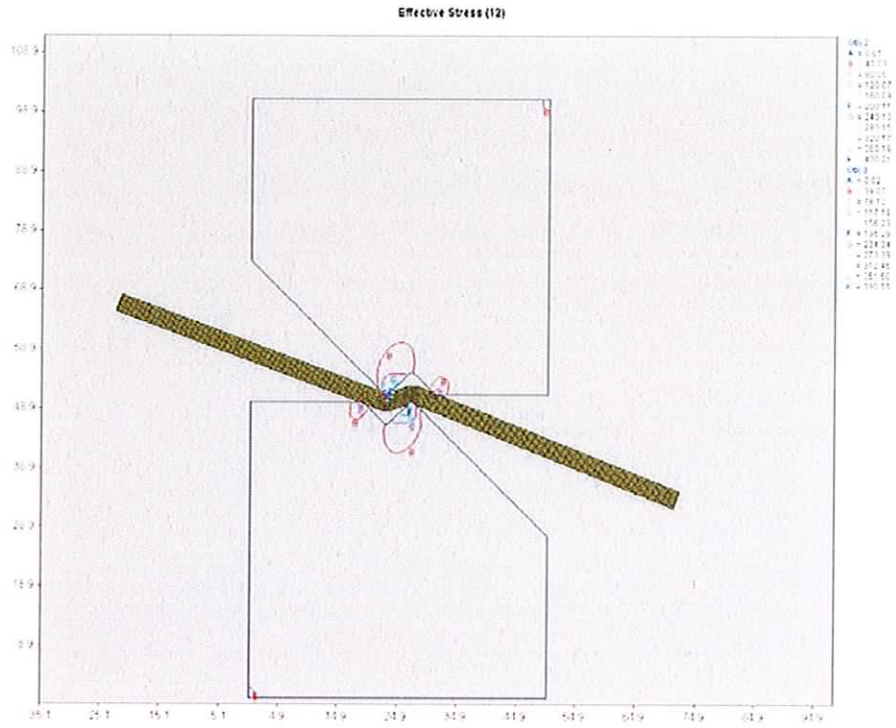
Step 4



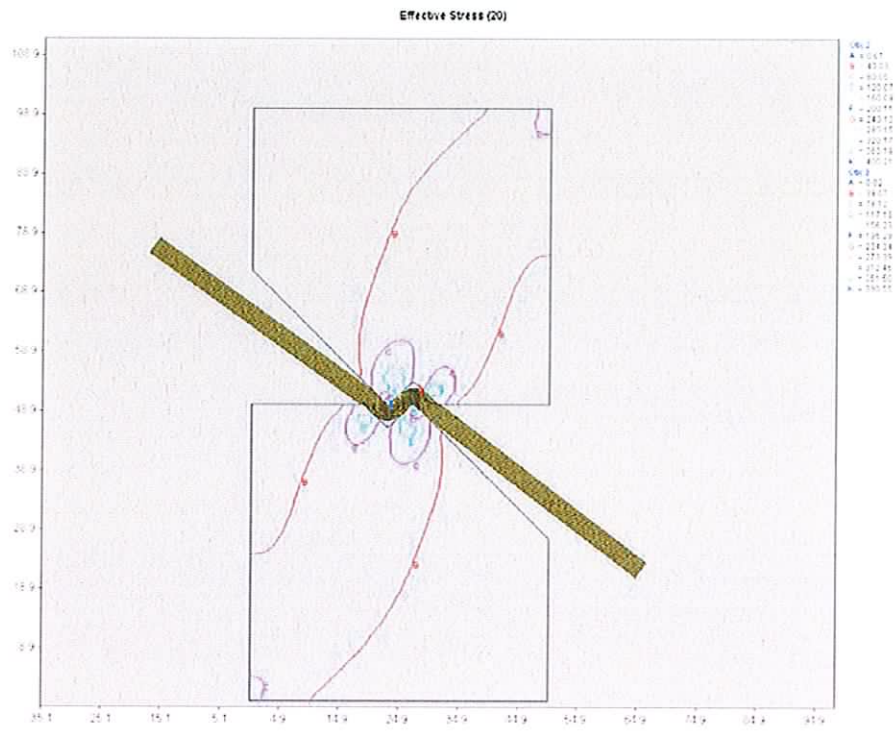
Step 8



Step 12

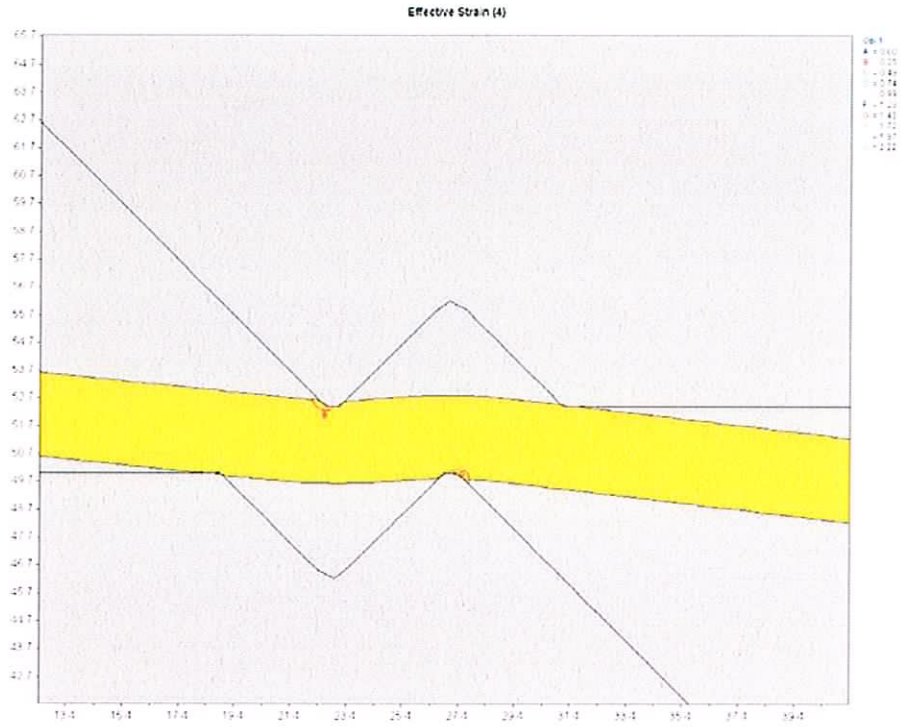


Step 20

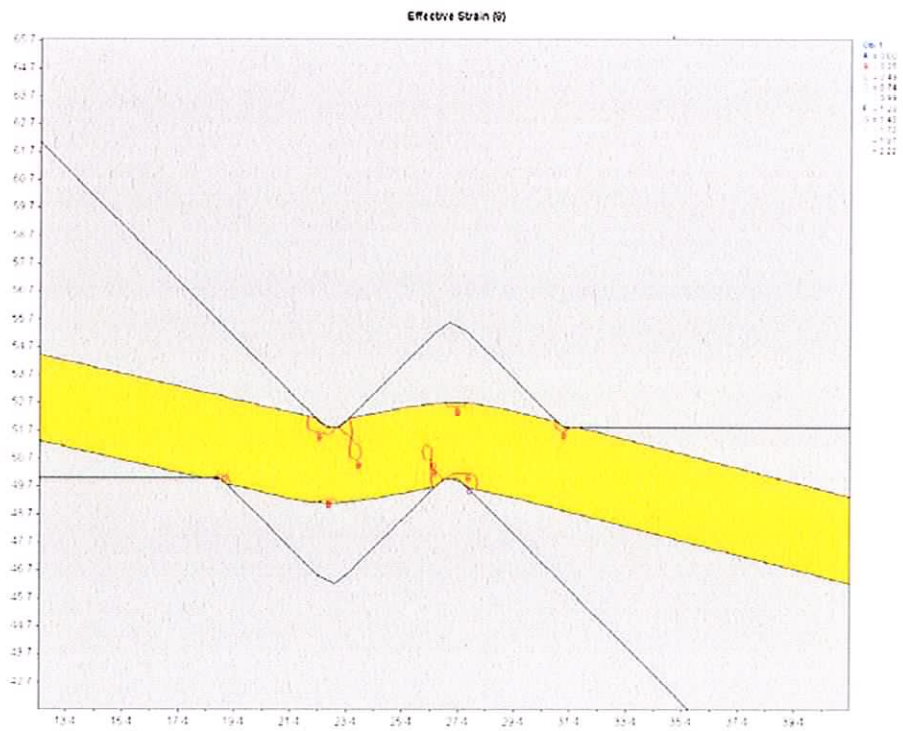


6.0mm Die
 Material: 6062 Aluminium
 Effective Strain at defined step numbers.

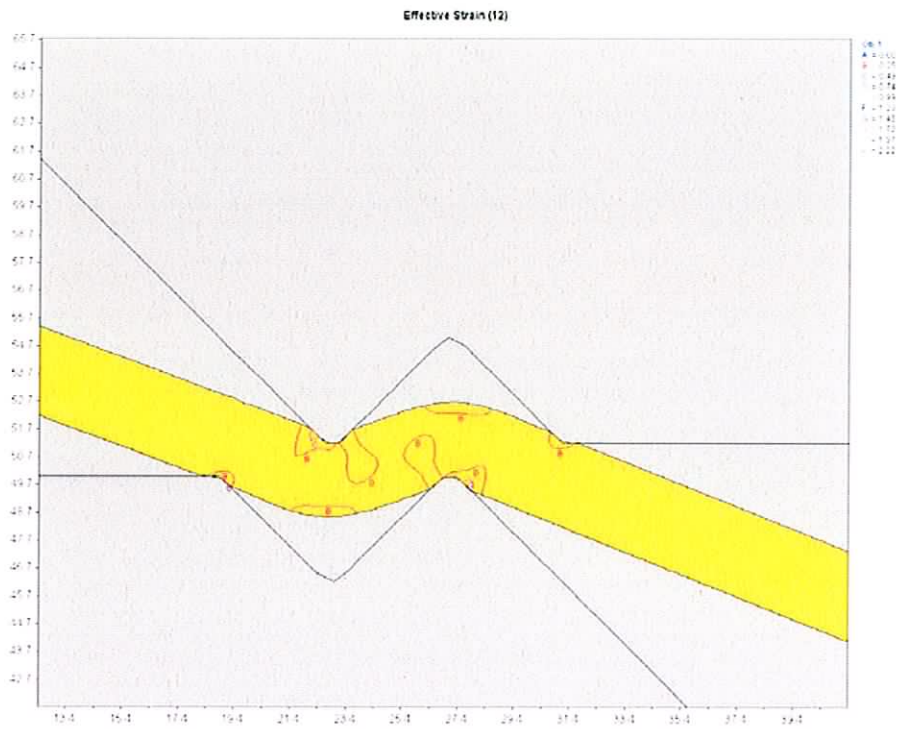
Step 4



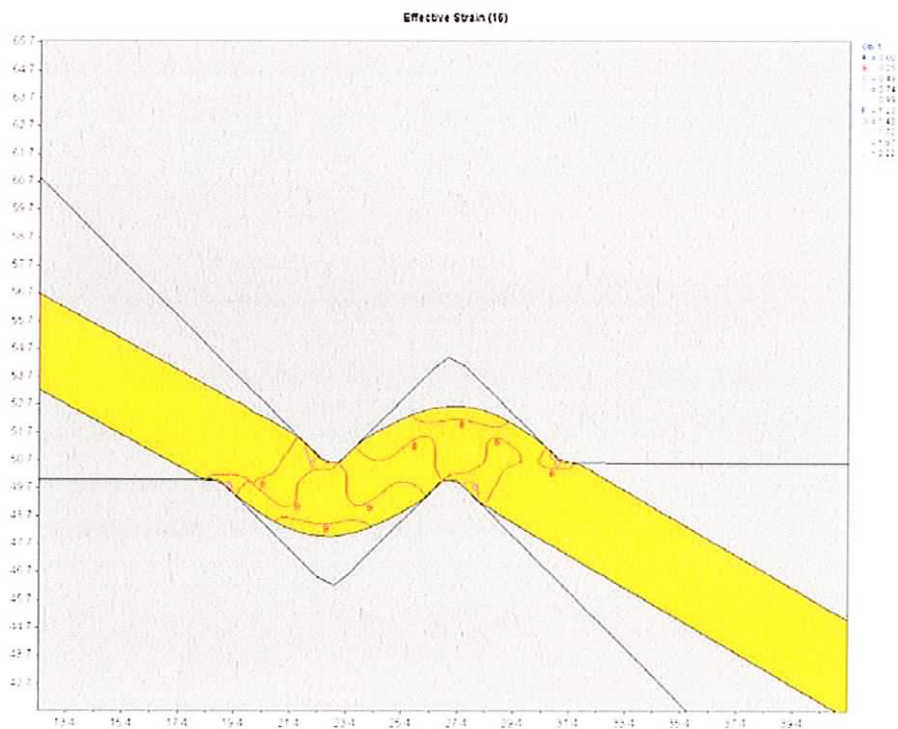
Step 8



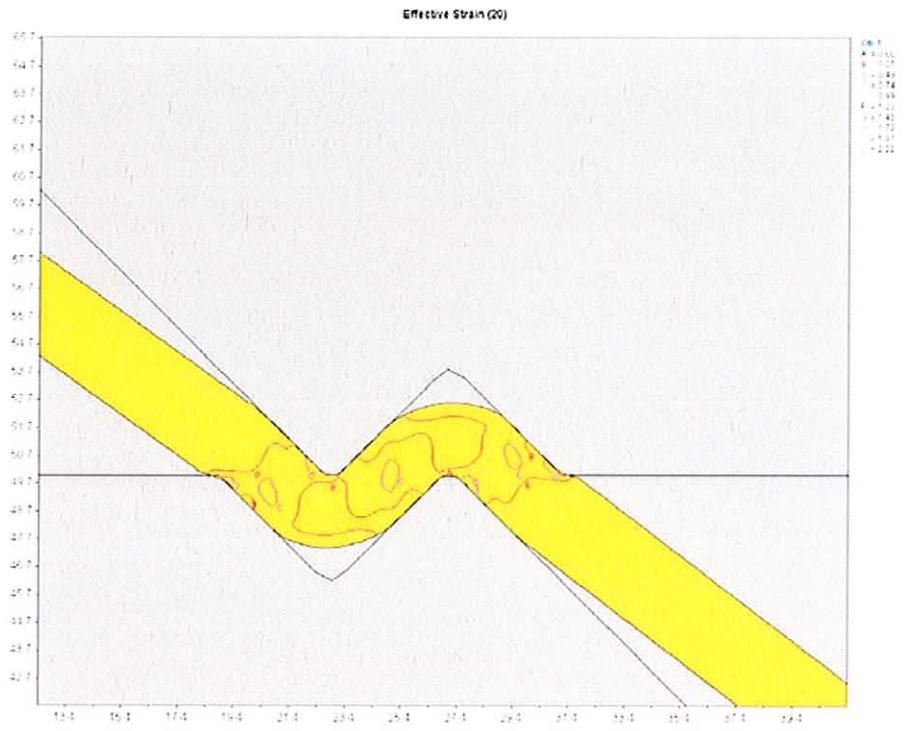
Step 12

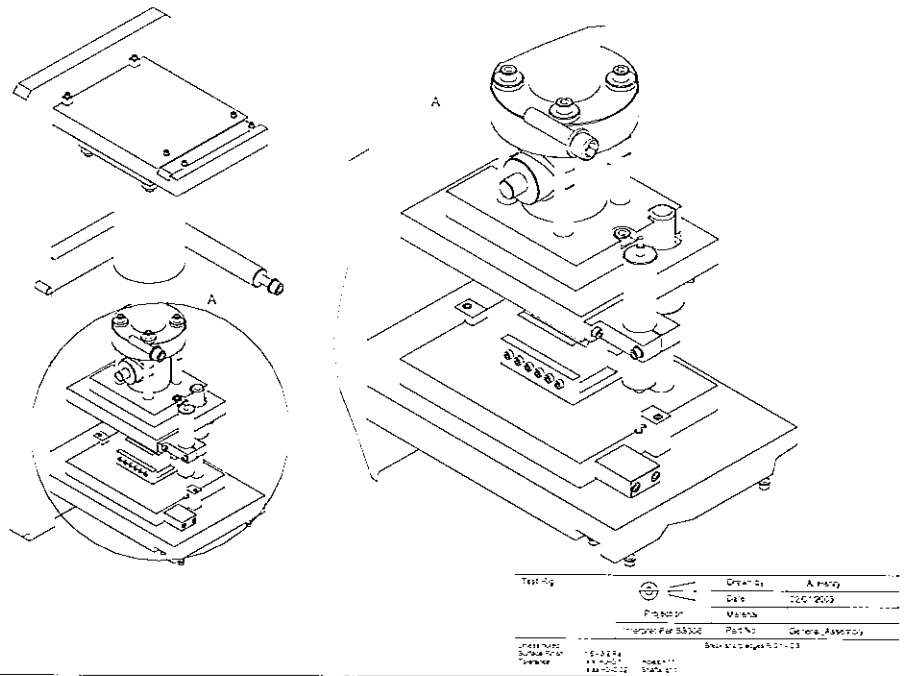
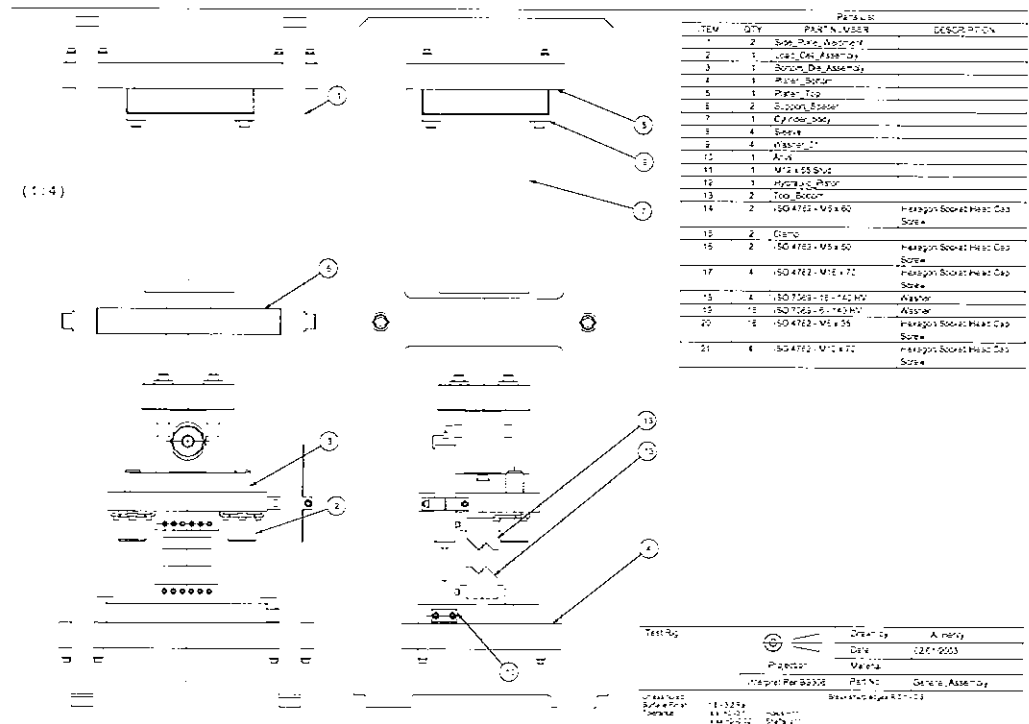


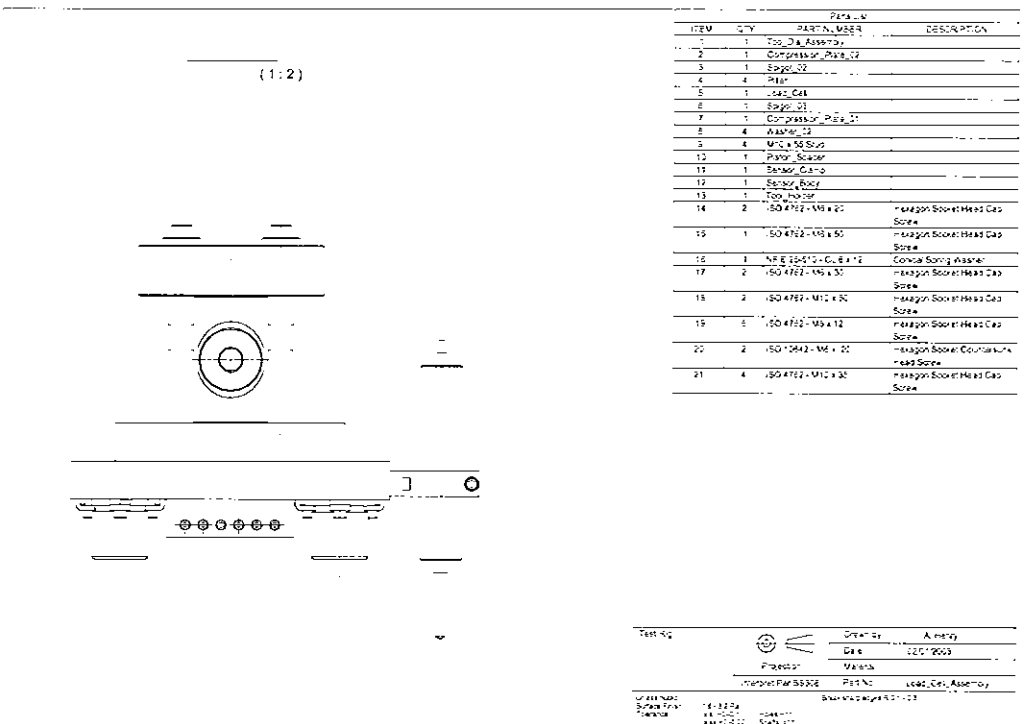
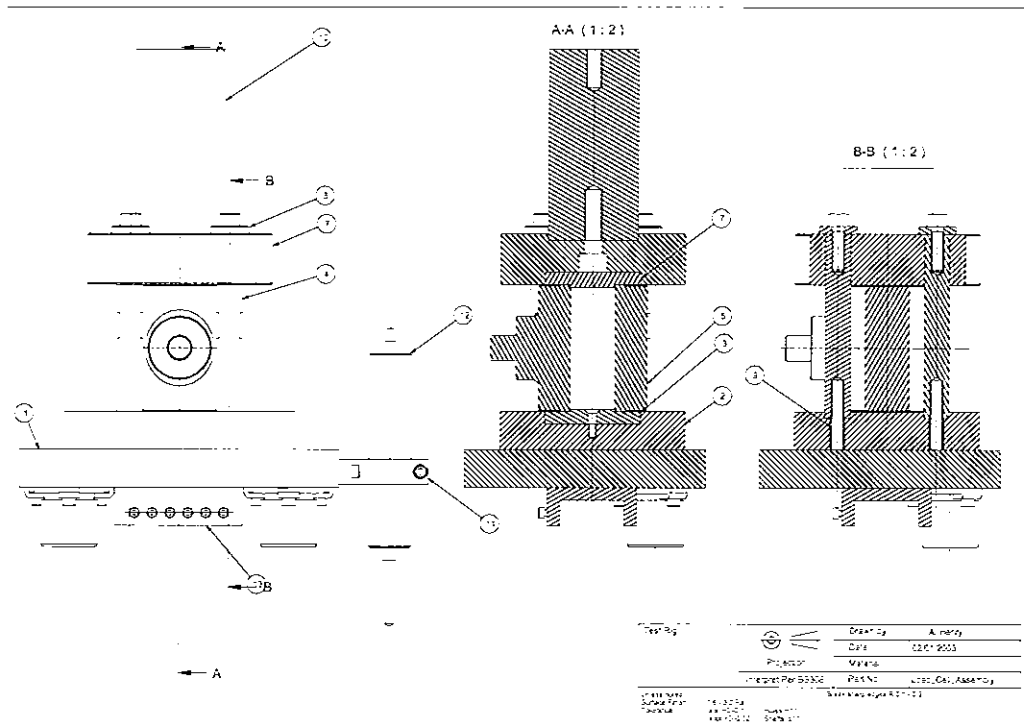
Step 16

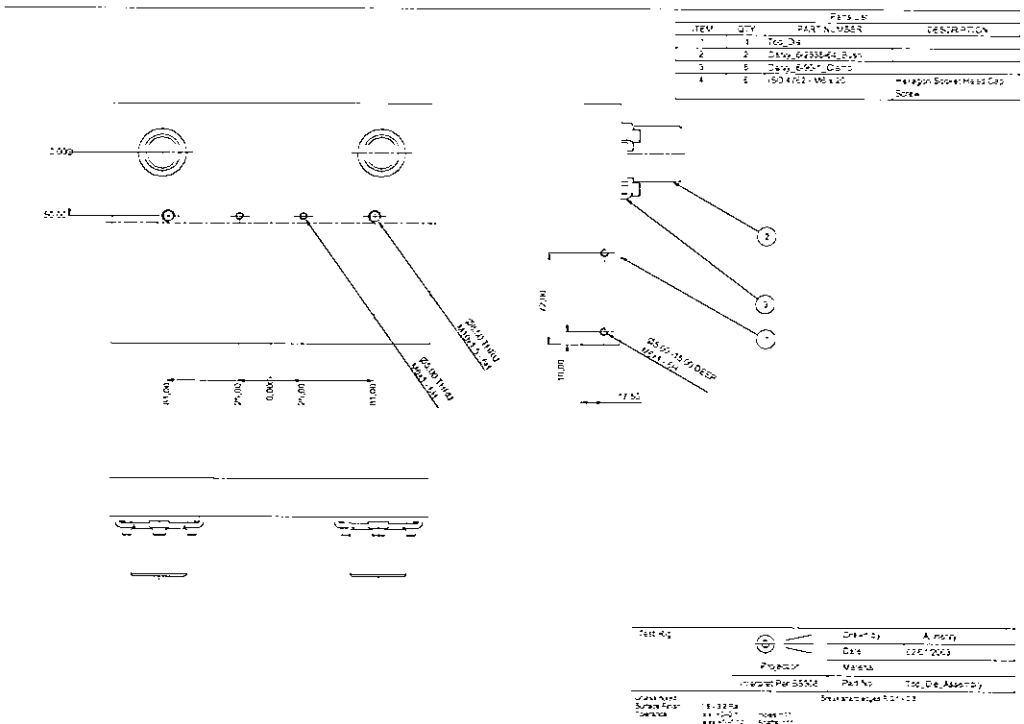
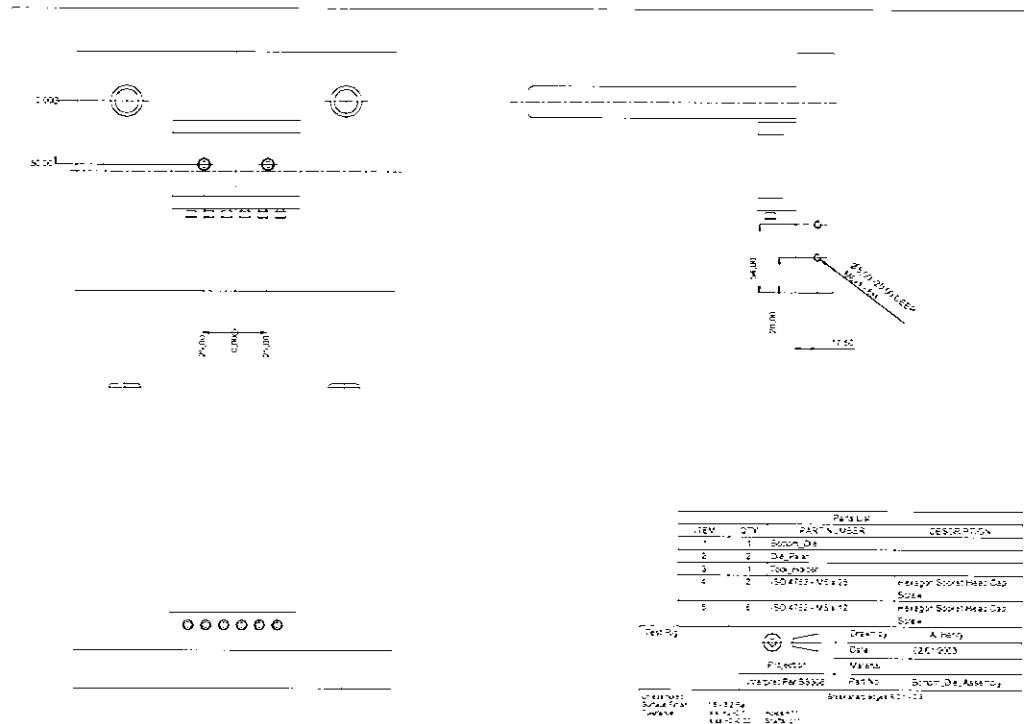


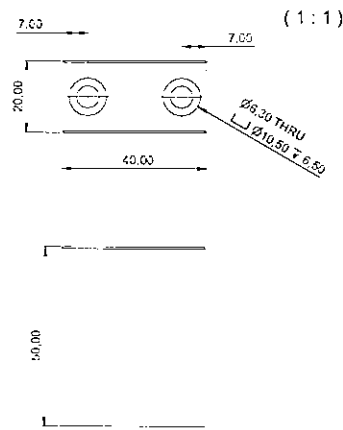
Step 20



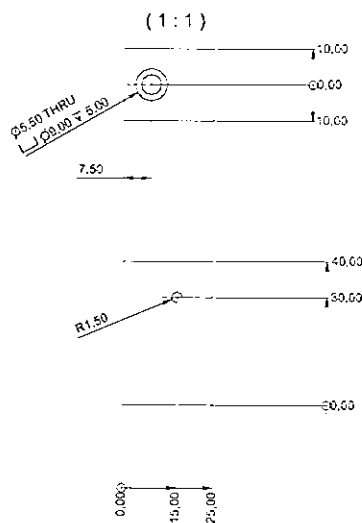




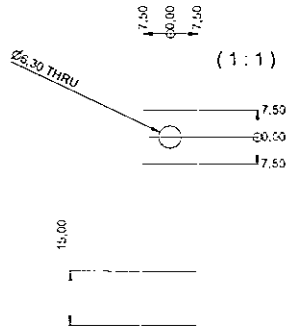




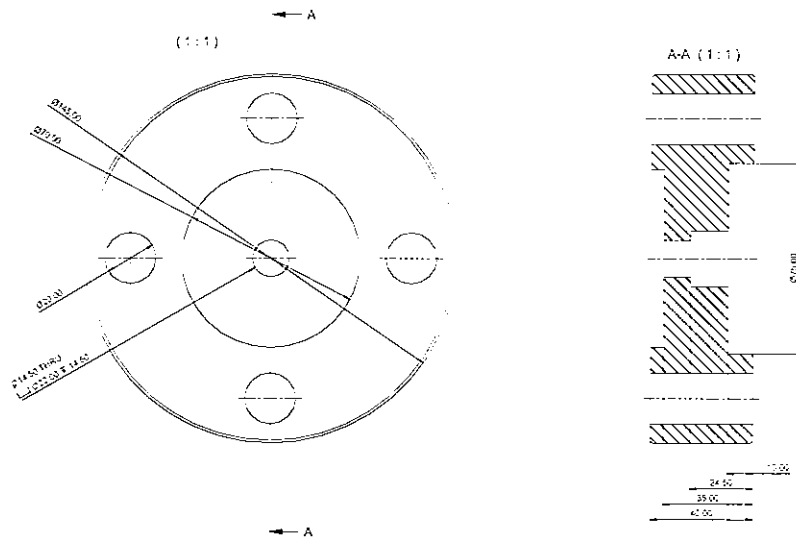
| | | | |
|---|---------------------------------|-----------------------|-------------------------------|
| Test Rig | | Drawn by | A. Henry |
| | | Date | 02.01/2003 |
| | Projection | Material | Steel, Mild |
| | Interpret Per BS5333 | Part No. | Any |
| Unless noted Surface Finish Tolerance | 1.6 - 3.2 Ra ± 0.1 ± 0.02 | Process Shaft: c11 | Blank sharp edges R 0.1 - 0.3 |



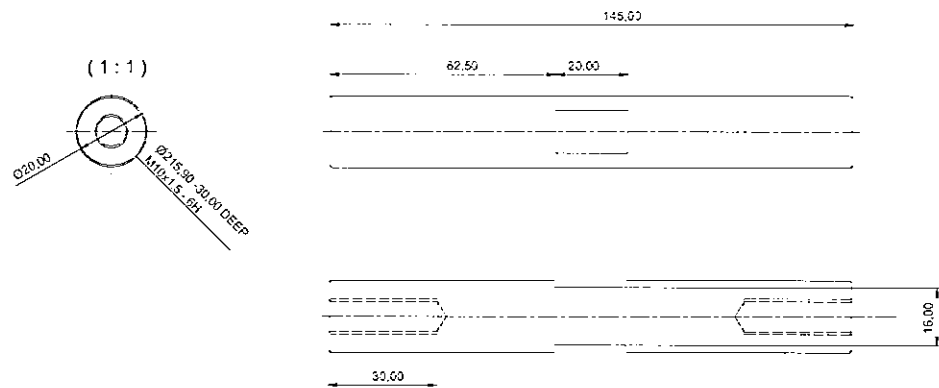
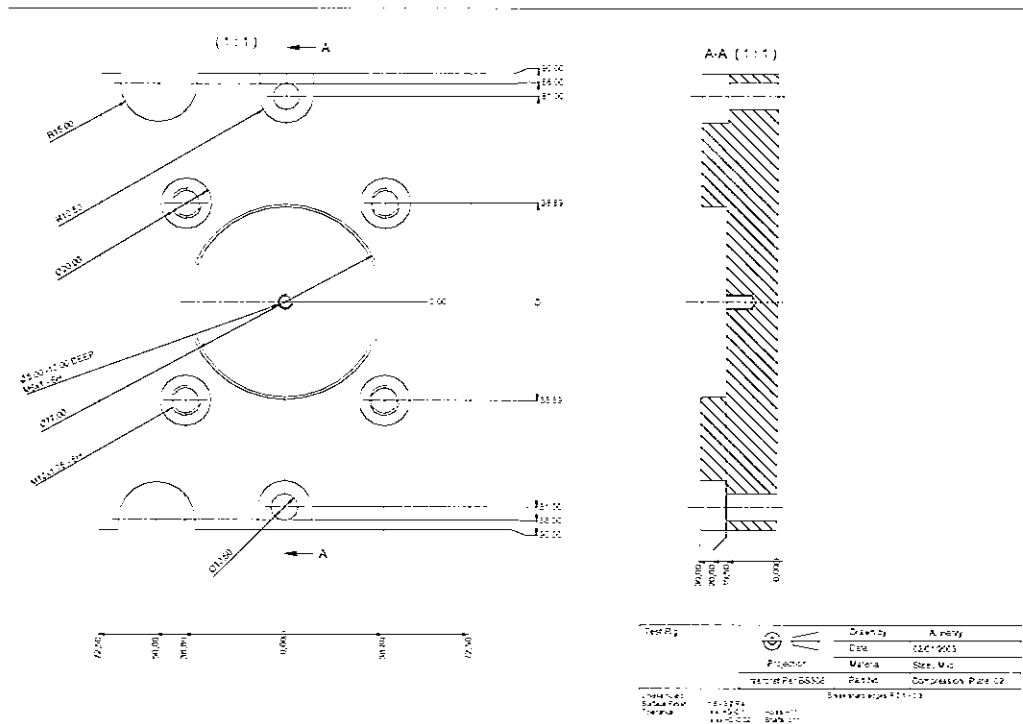
| | | | |
|---|---------------------------------|-----------------------|-------------------------------|
| Test Rig | | Drawn by | A. Henry |
| | | Date | 02.01/2003 |
| | Projection | Material | Steel, Mild |
| | Interpret Per BS5333 | Part No. | Camp |
| Unless noted Surface Finish Tolerance | 1.6 - 3.2 Ra ± 0.1 ± 0.02 | Process Shaft: c11 | Blank sharp edges R 0.1 - 0.3 |



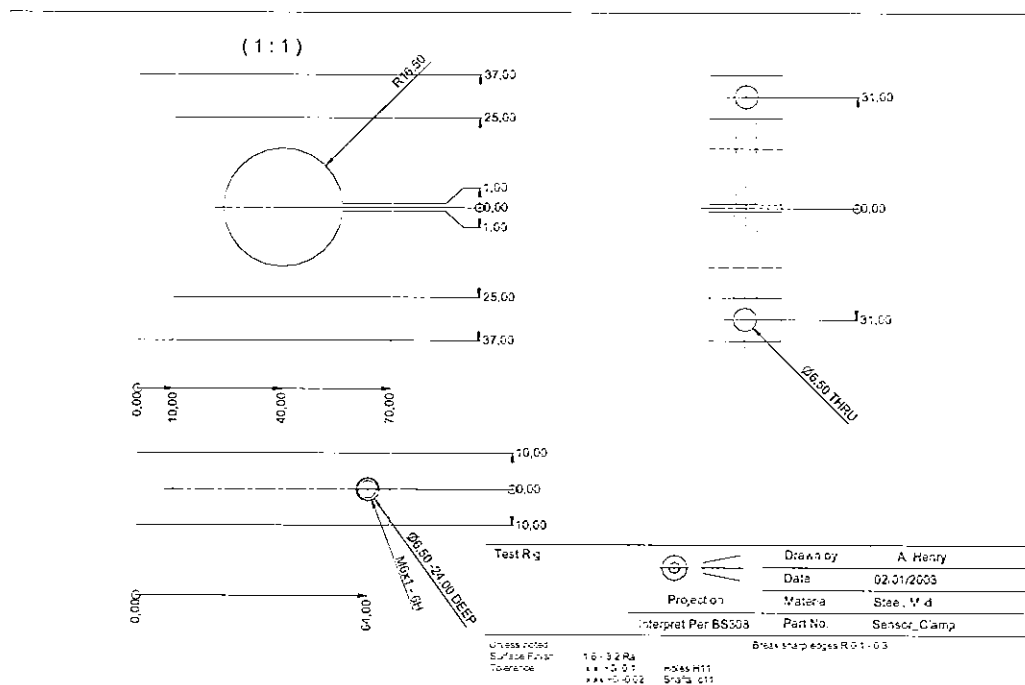
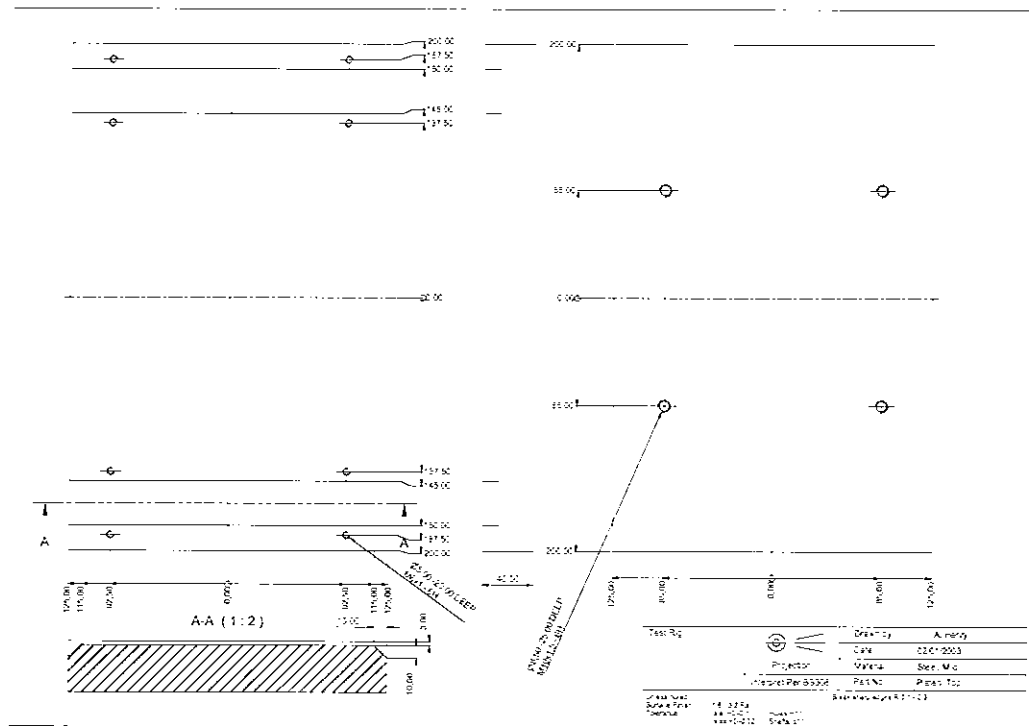
| | | | |
|----------------|--------------------------|----------|-------------|
| Test Rig | Projection | Drawn by | A. Henry |
| | Interpret Per BS5503 | Date | 02.01.2003 |
| | | Material | Steel, M. d |
| | | Part No. | Camp_Boock |
| Class notes | Shank shapes R 0.1 - 0.3 | | |
| Surface Finish | 1.6 - 3.2 Ra | Notes | 111 |
| Tolerance | ± 0.05 | Shank | 111 |

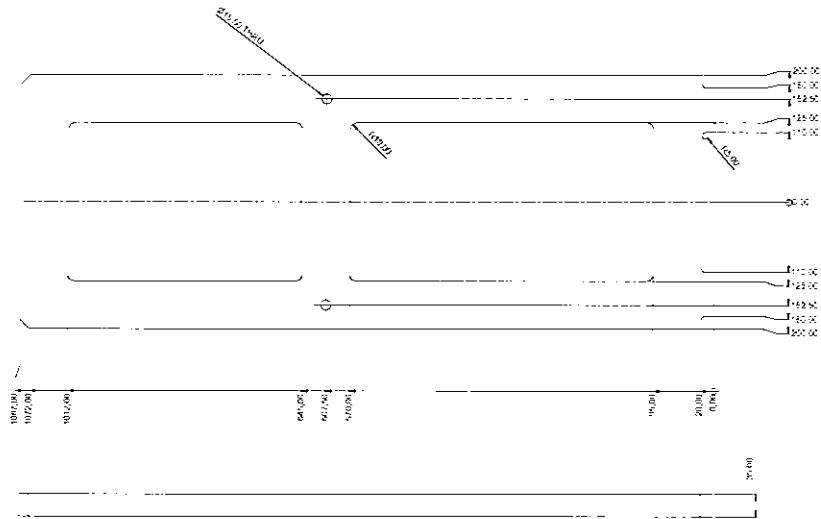


| | | | |
|----------------|--------------------------|----------|---------------------|
| Test Rig | Projection | Drawn by | A. Henry |
| | Interpret Per BS5503 | Date | 02.01.2003 |
| | | Material | Steel, M. d |
| | | Part No. | Compression, Part 2 |
| Class notes | Shank shapes R 0.1 - 0.3 | | |
| Surface Finish | 1.6 - 3.2 Ra | Notes | 111 |
| Tolerance | ± 0.05 | Shank | 111 |

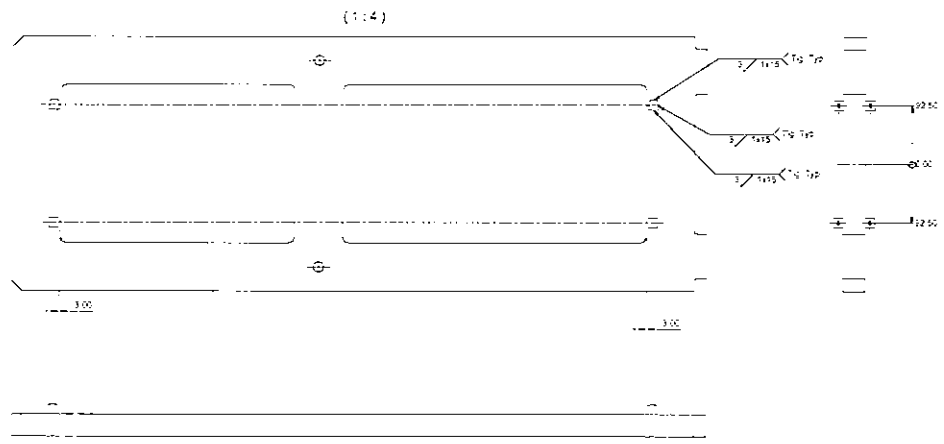


| | | |
|-----------------------------|--------------|-------------|
| Test Rig | Drawn by | A. Henry |
| | Date | 02/01/2003 |
| | Material | Steel, Mild |
| | Part No. | P 01 |
| Interpret Per BS503 | | |
| Engr. sharp edges R 0.1-0.3 | | |
| Unless noted | 1:6 - 3:2 Ra | ISO 9001 |
| Surface Finish | 1:4 - 2:0 R | ISO 9001 |
| Tolerance | ±0.02 | ISO 9001 |

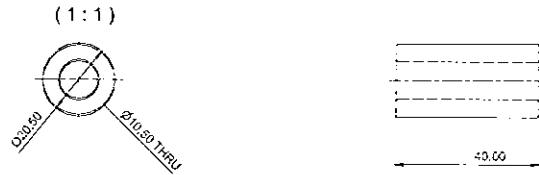




| | | | |
|-----------|-----------|-------------|----------|
| Test No: | 1000000 | Drawn by: | A. Kelly |
| Scale: | 1:1 | Date: | 22/05/03 |
| Project: | Per 65502 | Material: | See M.C. |
| Part No: | 508 Part | Part No: | 508 Part |
| Drawn by: | A. Kelly | Checked by: | A. Kelly |
| Scale: | 1:1 | Date: | 22/05/03 |



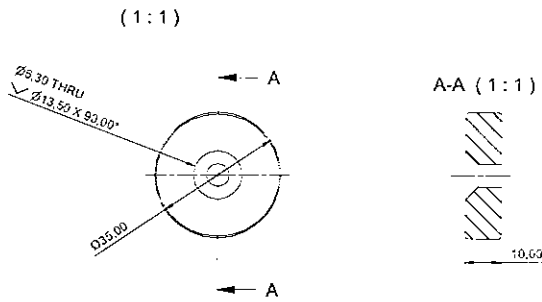
| | | | |
|-----------|-----------|-------------|----------|
| Test No: | 1000000 | Drawn by: | A. Kelly |
| Scale: | 1:1 | Date: | 22/05/03 |
| Project: | Per 65502 | Material: | See M.C. |
| Part No: | 508 Part | Part No: | 508 Part |
| Drawn by: | A. Kelly | Checked by: | A. Kelly |
| Scale: | 1:1 | Date: | 22/05/03 |



| | | | |
|----------|---------------------|----------|-------------|
| Test Rig | | Drawn by | A. Henry |
| | | Date | 02/01/2003 |
| | Projection | Material | Steel, Mild |
| | Interpret Per BS308 | Part No. | Sieve |

Unless noted
Surface Finish 1.6 - 3.2 Ra
Tolerance ± 0.1 Holes m11
 ± 0.02 Shims c11

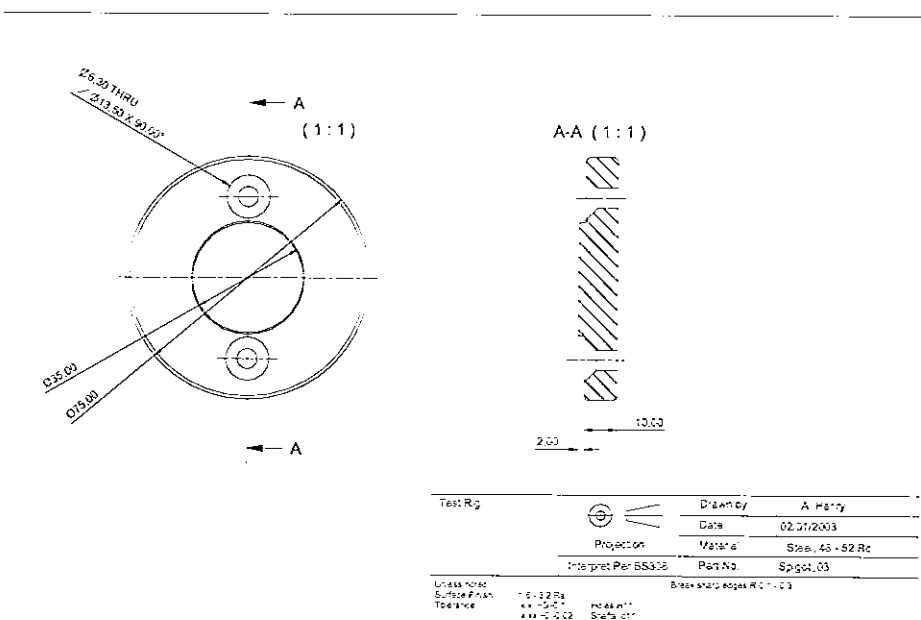
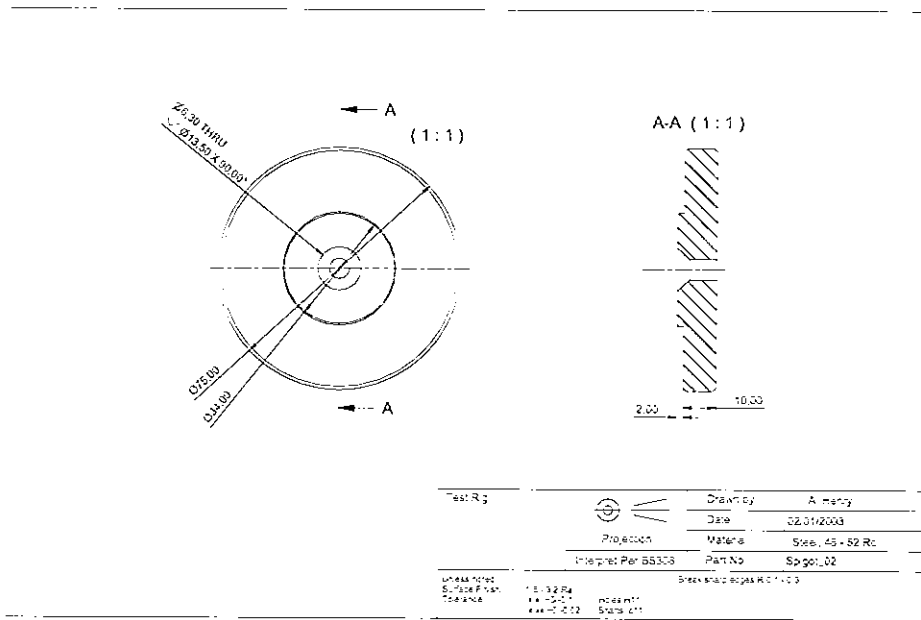
Break sharp edges R0.1-0.3

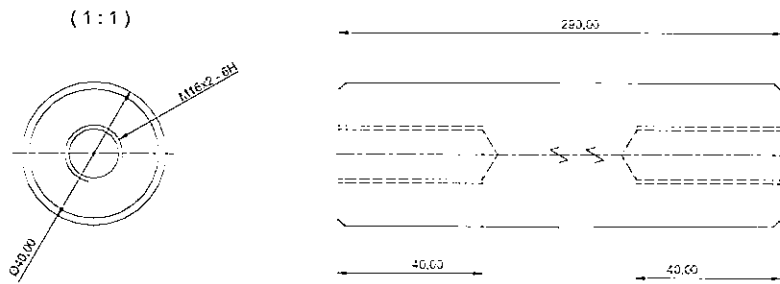


| | | | |
|----------|---------------------|----------|-------------------|
| Test Rig | | Drawn by | A. Henry |
| | | Date | 02/01/2003 |
| | Projection | Material | Steel, 48 - 52 Rc |
| | Interpret Per BS308 | Part No. | Spigot |

Unless noted
Surface Finish 1.6 - 3.2 Ra
Tolerance ± 0.1 Holes m11
 ± 0.02 Shims c11

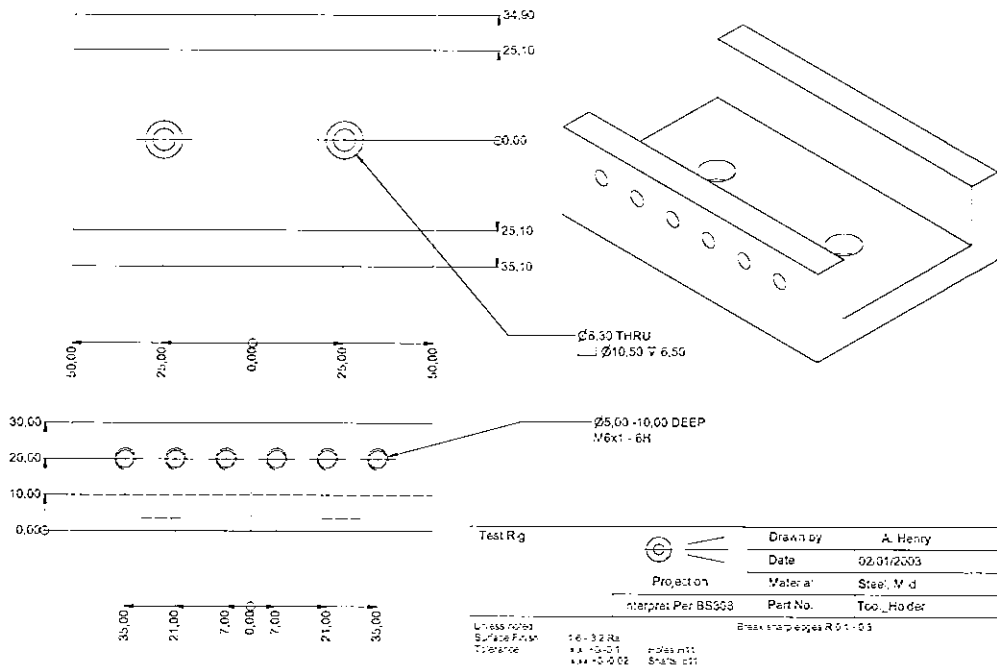
Break sharp edges R0.1-0.3



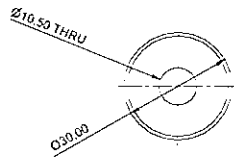


| | | |
|---------------------|----------|----------------|
| Test Rig | Drawn by | A. Henry |
| | Date | 02.01.2003 |
| | Material | Steel, M d |
| | Part No. | Support_Spacer |
| Interpret Per BS303 | | |

Unless noted Surface Finish: 1.6 - 3.2 Ra
 Tolerance: ± 0.10 / ± 0.02
 Break sharp edges R 0.1 - 0.3
 Holes m11
 Slots c11



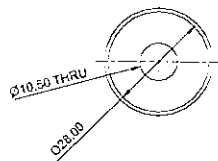
(1:1)



11.00

| | | | |
|----------------|----------------------|---------------------------|------------|
| Test Rig | | Drawn by | A. Henry |
| | Projection | Date | 02.01/2003 |
| | Interpret Per BS5503 | Material | Steel, V.d |
| | | Part No. | Washer_01 |
| Unless noted | | Breaks in pages R 01 - 03 | |
| Surface Finish | 1.6 - 3.2 Ra | Process | HT |
| Tolerance | *** -0.01 | Shape | c11 |
| | *** -0.02 | | |

(1:1)



6.00

| | | | |
|----------------|----------------------|---------------------------|------------|
| Test Rig | | Drawn by | A. Henry |
| | Projection | Date | 02.01/2003 |
| | Interpret Per BS5503 | Material | Steel, V.d |
| | | Part No. | Washer_02 |
| Unless noted | | Breaks in pages R 01 - 03 | |
| Surface Finish | 1.6 - 3.2 Ra | Process | HT |
| Tolerance | *** -0.01 | Shape | c11 |
| | *** -0.02 | | |

Steps to create and use the Deform PC Pro Finite Element Simulation Package:**(1) Create geometry in AutoCAD**

All tools and materials should be in their correct relative positions with respect to the origin. Make sure all polylines are exploded, all geometry is on layer 0, and all layers, linetypes etc. are purged.

Save drawings of individual parts as separate drawing files:- top tools, bottom tool, and material.

Create .igs files of all parts.

(2) Open Deform PC Pro

At this stage set up the default paths for deform to find the iges files for geometry usage, and the path in which to store the problem files. Remember, the problem title in deform is used to create a directory in which to place the files. To do this,

Options → problems → directories Set the radio buttons to point to the correct place for the problem files to be written to. The iges files that are required should be kept in either deform/iges or the problem directory. This saves having to look for them each time.

File → New → Enter Problem Title (and directory if required) → OK

(3) Set up Units

In the controls window, set up units to SI, and make sure to set profile to plane strain and problem type to isothermal.

(4) Create Geometry

Create new problem file: for each part (tool, material), using part #1 as the material, part #2 as the bottom die, and part #3 as the top (primary) die, as follows:

Object → add new → set whether rigid, plastic etc.

Geometry → import → load iges file via dialogue box. When the file is imported, it is shown in the Iges file window.

If the hatching is outside the profile, then the geometry is illegal. Click 'Edit Geometry' button, click 'Reverse Order' button. Then check geometry (allows deform to correct the geometry). If necessary, check the geometry via the table option.

To check the geometry at any time, Object → make required object current → geometry → table → check → correct (if required). Also, you have the option to reverse (i.e. if the hatching is on the outside) the geometry here.

Ensure that the start point on the geometry loop is not a contact point in the problem. In order to change this, click on the button 'edit objects', and then click the button 'first point' (a '1' on the toolbar), and click on the new start point.

(5) Assign Material

Import the material for the workpiece from the Deform standard library. Initially, use AISI-1035 Cold. (NB The steel supplied to Peterson Manufacturing is CR4, i.e., SAE 1010 = ASTM 366) In order to do this, objects → import → set 'files of type' to .mdb → open 'deform.mdb', and copy over the material types required.

(6) Generate Mesh

Generate mesh for material

Preprocessor → Object → (select material object (#1)) → mesh →

Max size between elements = 1
 Number of elements = 5000
 Generate

NB set the auto-remeshing criteria here.

Generate mesh for dies

Preprocessor → Object → (select material object (#2)) → mesh →

Number of elements =500
 Select user defined mesh density
 Select mesh density window

Put numbers around periphery of tool to represent mesh density (put the relative mesh density point in the dialogue box first, then choose the position of the point on the geometry).

Note: if mistake is made, use delete points (to left hand corner)

Repeat for second tool (object #3)

(7) Define boundary conditions

Not required in this case, but would be required in axisymmetric loading, for example deep drawing, where (due to symmetry), there should be no axial displacement of nodes from their original position.

(8) Assign velocity to primary die

Preprocessor → Objects → Select #3 → Movement → set radio buttons as follows:

Translational

Down

Speed

Set speed = constant = 0.5 mm / sec

(9) Confirm Inter-object Positioning

Because the objects were drawn in the correct position via AutoCAD and the .iges out translator, they will be in almost the correct position when imported into Deform. However, they will work more predictably when they interfere slightly (0.001% ?). To do this:

Positioning Type → Interference

Object to position (set as required)

Reference object (set as required)

Direction → Down or Up as required

Position.

Complete the cycle again so that the top tool interferes slightly with the material, and the material interferes slightly with the bottom tool.

(10) Setup deformation pre-processing motion controls

Preprocessor → controls → main control →

| | | |
|----------------------------------|--|--|
| Starting step | | -1 |
| Number of simulation steps | | 20 |
| Increment to save in database | | 1 |
| Solution Steps definition | | Equal die displacement 0.1mm or equal amounts of time. Nb: if these increments are too small, it may cause 'non positive stiffness matrix' problem, hence set a boundary constraint of velocity = 0 in the x direction for about the first five steps. In addition, use the maximum strain criterion = 0.025 per element, as an additional step control. |
| Advanced stop control → max load | | 3.9kN (From calculations of cylinder area and available hydraulic pressure). |

(11) Establish inter-object Interface.

Preprocessor → Inter-object Interface →

Assign Inter Object Friction.

For each object pair, (i.e., material (object #1) to each die in turn (i.e., objects #s 2, 3)) assign slave → master relationships and assign inter object friction ($\mu = 0.08$, type = Shear)

(12) Establish inter-object boundary conditions

Generate (If required, initialize and regenerate) boundary conditions. (A series of Xs should appear on the interface lines). If this does not happen, it may be because the mesh size in the workpiece (or the tooling ?) is too small.

(13) Create database:

Preprocessor → interface → database → Generate database. Remember, each time you redefine the problem, make sure to regenerate the database.

(14) Run the simulation.

Simulation → start

Viewing the results

Post processor → Graphics

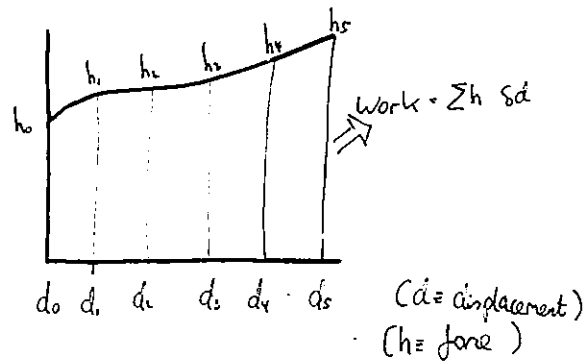
Postprocessor graphics:

Each icon on the RHS of the postprocessor graphics screen is additive, i.e., use the mesh button to determine whether to show mesh, boundary or mesh and boundary, and the contour plot to determine which contour (if any) to add, etc.

Use the point tracking to find to where points are displaced. This will enable the determination of the amount of sliding that will take place over the die faces for the large dies, and what way the material is pinched in the small dies.

In order to yield a graph of load sustained by the dies, click the x-y plot button, set the checkmark for the "Bottom Die", and set the variable for y-load as a function of time. (This is the only setting that will work).

In order to find the total work done under the graph, when the graph is displayed, save the file as a text file, allowing Deform PC pro to know which information (i.e., from which object you wish to save information) that you wish to output. Output it as a tab delimited file. Then, import it into excel (open --> file type --> .txt) and use the file input wizard to import the info into two columns. Then, find the area under the graph thus:



$$\text{Area} = \frac{1}{2} \left[(d_1 - d_0) (h_1 + h_0) \right] + \frac{1}{2} \left[(d_2 - d_1) (h_2 + h_1) \right] + \dots$$

$$+ \frac{1}{2} \left[(d_n - d_{n-1}) (h_n + h_{n-1}) \right]$$

NB - do not use last row of output, i.e.
no of areas = no of ordinates - 1

(15) Produce AVI files

When saving video outs an .avi files, ensure that they are in the following format:

The .avi file will only record what is shown on the screen, therefore is useful to zoom to the area of interest first.

| | |
|---------------------|--|
| Size | 1024 x 768 (or suitable size) |
| Video Compression | Microsoft Video 1 or Autodesk FLC compressor (seems the best). |
| Compression Quality | 100% |
| Configure | Temporal Quality Ratio = 100% |

(16) General Notes:

You can only save the problem in the preprocessor option.

E Steel = 206,000 MPa. The SI unit for E in Deform PC pro is MPa (=N/mm²)

Stopping Controls:

To set the stopping controls for the top die:

Make the top die the primary die: this is the one the stopping controls refer to.

None of the movement controls for the top die effect stopping.

Only the stopping controls in the main controls dialogue box effect the stopping of the die. If multiple stopping controls are set (dialogue box data = 0 → stopping control not set), then the simulation stops when the first stopping criterion is reached.

(17) Die Stress Analysis:

For die stress analysis, the load from the workpiece is transferred to the dies at a particular stage of the process, and the stress is thus calculated.

To execute a die stress analysis problem:

Create a new problem in the appropriate directory (same directory as problem from which you will obtain the data to run the stress analysis problem). Set up the problem parameters to be 'Isothermal die stress analysis', 'plane strain' and set the units to ISO.

A dialogue box will open, indicating that you should load data from a database. Use the database of the problem that you wish to analyse.

Define meshes for both the top and bottom die if not already done.

Define the BCCs of both the top and bottom die. Set both velocity in the x and y direction on the top and bottom surfaces of the dies. This will simulate them being clamped in the die set. For each die, when setting the BCCs, set the Additional BCC to Interpolate. Interpolate from the appropriate database file.

Assign material elastic data for the dies.

Write the database.

Run the simulation

Post Process the results:

| | |
|---------------|---------------------|
| Type of plot: | Contour |
| Display type: | Shaded without mesh |
| Variable: | Effective Stress |

(18) Changing conditions, i.e., motion controls, etc., part way through a simulation.

Run the simulation up to the required point. If the simulation goes past the required point, the required point may be identified from the graphics screen, by watching the graphic output and noting the step number from the top of the screen.

Go to the preprocessor page, and load → database and choose the appropriate step number to load from. Then, in the controls dialogue box, set the starting step to – (last step number +1), e.g., if the last step was 16, then the new starting step is – (16+1) = -17.

Re-set whatever controls etc have to be changed, and continue the simulation. When the simulation is run in the graphics section, it will contain the entire database, i.e., the beginning stage and the subsequent stages. In the event that you need to re-run the problem from the start, reload the database from the first step, and change the controls as required, and the new database will overwrite the old one.

In order to speed up the simulation using when using the springback criterion, model the experiment in the plastic mode first, until you reach near the end of the stroke. Then, change the material to elastoplastic, reload the database, and finish the stroke. Then, reload the database again, and move the top die up a few steps to observe springback.

(19) Coupled Analysis: Combined stress analysis of both dies and workpiece.

Create a new problem in its own directory.

Load the database from the relevant directory, i.e., if using a type xxx tool / workpiece setup, then load the type xxx database from the type xxx folder.

Check for correctness of geometry of the workpiece – this may have to be corrected by Deform, and the mesh re-built.

Change the die material type to elastic and choose a suitable material from the material database. Make sure to add in the material elastic properties, (these are not kept in the database)

Create appropriate meshes for both of the dies: NB use only the standard method of making meshes: the user density method seems to crash the program. Create a mesh of about 3000 elements for each die.

Ensure that the simulation mode is isothermal.

Make sure to reset the inter-object boundary conditions.

The displacement of the top die is given via boundary conditions; make sure the bottom die is constrained on its lower surface by $V_x = V_y = 0$. For the top die, ensure $V_x = 0$ and $V_y = -0.5$ (say). Type the number in the box first, and then select the points anticlockwise. The direction arrows should turn blue to indicate a non-zero velocity. The actual velocity can be shown on the die by clicking the radio button.

Use equal time increments (0.3 sec) for die displacement, (not equal stroke lengths: this is because the die is elastic).

Make sure to restrain the workpiece in the x direction with a node set at $V_x=0$ for the first few steps. When reloading the database, make sure that the correct (i.e., current) database is used, and remember to free the node set above.

Tooling material properties

In order to determine the properties of the tools (end effectors) used to deform the material workpieces, experimental work was carried out to determine Poisson's ratio and Young's modulus. This involved the installation of strain gauges on to the body of a sample tool, and the subjection of the tool to known loads via a tensile / compression testing machine. The strain gauge installation process is illustrated below, as is the load application:



Figure 1 Abrade the tool surface to clean off any oxide from the hardening and tempering process

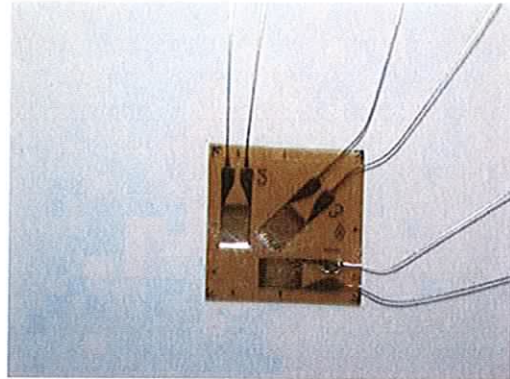


Figure 2 Select appropriate strain gauges

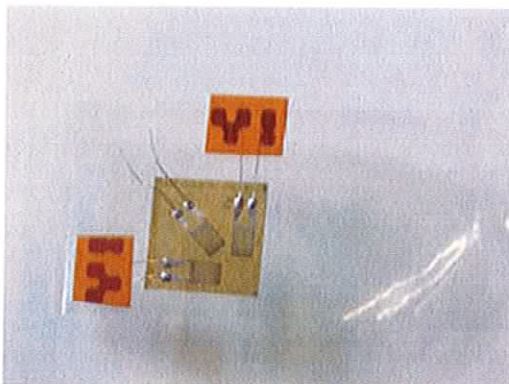


Figure 3 Use adhesive tape to secure relative positions of strain gauges and electrical contacts

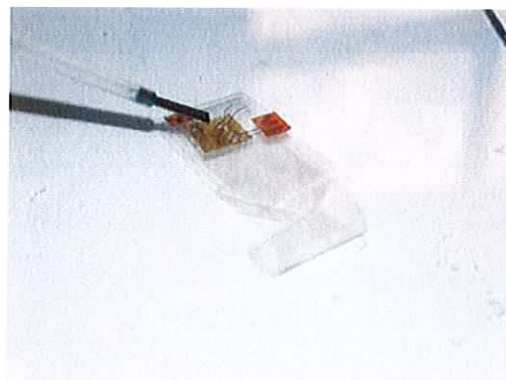


Figure 4 Brush on adhesive activator

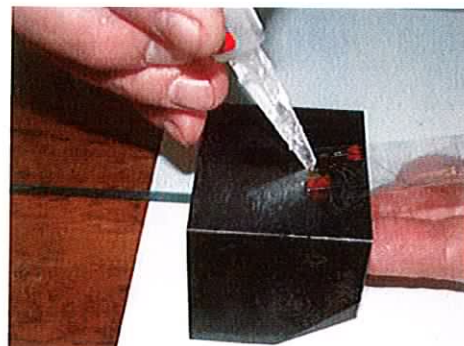
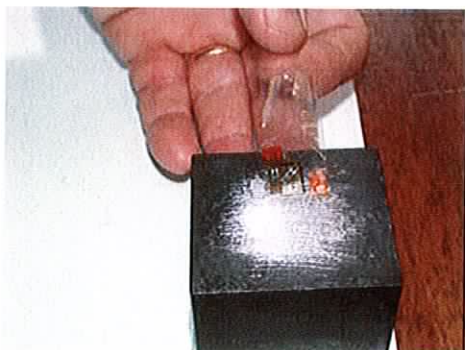


Figure 5 Install gauges, peel back adhesive tape, exposing surface of gauges, connectors and workpiece

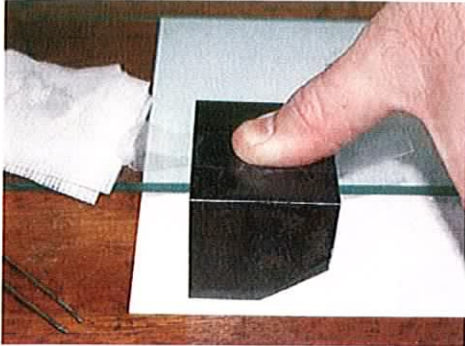


Figure 6 Deliver adhesive to adhesive tape / workpiece interface



Figure 7 Keep thumb pressure on gauge for 2 minutes to allow adhesive to set

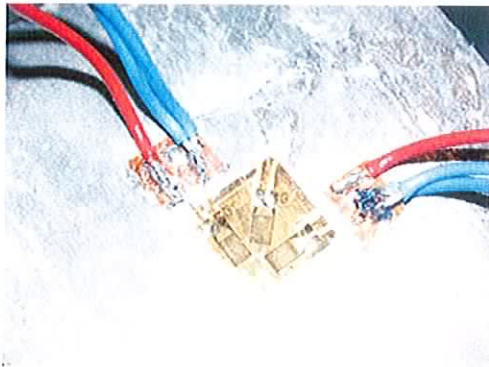


Figure 8 Strain gauge and connectors in place.

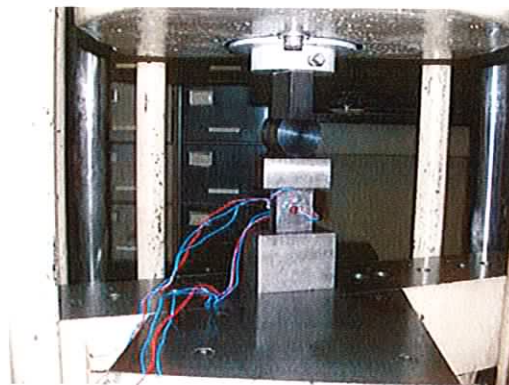


Figure 9 Electrical connection in place

Figure 10 Application of load to tooling

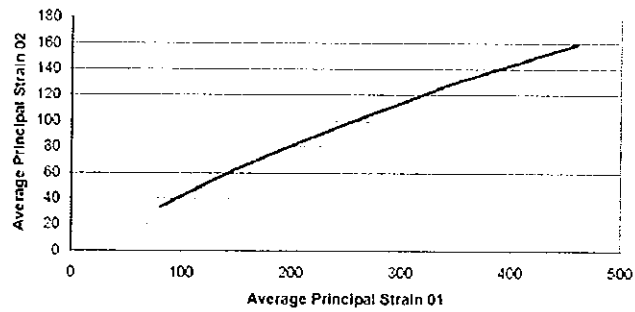
Experimental values for Poisson's ratio are shown in the following table. These show some deviation from the theoretical value of Poisson's Ratio for the tooling material, and therefore the theoretical value was used. In addition, the experimental values for Young's modulus was also far removed its expected value, so the theoretical value of Young's Modulus was also used in the finite element analysis.

**Tooling: Gauge Plate,
Hardened 55Rc**

Units In
Microstrain

| Load kN | Principal Strain 01 Sample 1 | Principal Strain 01 Sample 2 | Average Principal Strain 01 | Principal Strain 02 Sample 1 | Principal Strain 02 Sample 2 | Average Principal Strain 02 | Poisson's Ratio | |
|---------|------------------------------|------------------------------|-----------------------------|------------------------------|------------------------------|-----------------------------|-------------------------------|-------------------|
| 10 | 80 | 82 | 81 | 33 | 34 | 33.5 | 0.41358025 | |
| 20 | 139 | 140 | 139.5 | 60 | 57 | 58.5 | 0.41935484 | |
| 30 | 183 | 184 | 183.5 | 74 | 76 | 75 | 0.40871935 | |
| 40 | 227 | 227 | 227 | 90 | 90 | 90 | 0.38847577 | |
| 50 | 266 | 266 | 266 | 103 | 103 | 103 | 0.38721805 | |
| 60 | 307 | 306 | 306.5 | 116 | 116 | 116 | 0.37846656 | |
| 70 | 346 | 343 | 344.5 | 129 | 128 | 128.5 | 0.37303435 | |
| 80 | 384 | 381 | 382.5 | 139 | 138 | 138.5 | 0.3620915 | |
| 90 | 423 | 420 | 421.5 | 149 | 149 | 149 | 0.35349941 | |
| 100 | 463 | 458 | 460.5 | 160 | 159 | 159.5 | 0.34636265 | |
| | | | | | | | Average Poissons Ratio | 0.38357727 |

Poissons Ratio



-
- (1) E. Paul DeGarmo
Materials and Process in Manufacturing
5th Edition 1979 pp 405 - 408
Collier MacMillan International Edition
 - (2) Serope Kalpakjian
Manufacturing Engineering & Technology 3rd Edition
3rd Edition 1995 pp. 459 - 468
Addison Wesley
 - (3) S.A. Urry and P.J. Turner
Solution of Problems in Strength of Materials and Mechanics of Solids
4th Edition 1981 pp. 1 - 20, 241 - 270
Pitman
 - (4) S.P. Timoshenko and J.N. Goodier
Theory of Elasticity
3rd Edition 1982 pp. 1 - 33
McGraw-Hill
 - (5) J.C., K.D. Leaver J.M. Alexander and R.D. Rawlings
Materials Science
2nd Edition 1982 pp. 149 - 161, 175 - 197
Thomas Nelson and Sons Ltd.
 - (6) Raymond A. Higgins
Engineering Metallurgy
5th Edition 1983 pp. 78 - 90
Edward Arnold
 - (7) C. R. Calladine
Plasticity for Engineers
1st Edition 1985 pp. 15 - 88
Ellis Horwood Ltd.
 - (8) W. Johnson & P.B. Mellor
Engineering Plasticity
1st Edition 1973 pp. 13 - 17
Van Nostrand Reinhold
 - (9) Z. Marciniak & J. Duncan
Mechanics of Sheet Metal Forming
1st Edition 1992 pp. 33 - 35, 59, 69 - 70,
Edward Arnold
 - (10) Robert D. Cook Et. Al.
Concepts and Applications of Finite Element Analysis 3rd Edition
3rd Edition 1989 pp. 1-25
John Wiley and Sons Inc.
 - (11) Constantine C. Spyrakos
Finite Element Modeling in Engineering Practice
1st Edition 1994 pp. 33 - 74
West Virginia University Press

-
- (12) National Agency for Finite Element Methods and Standards
Guidelines to Finite Element Practice
2nd Edition 1986 pp. 1 - 15
Department of Trade and Industry, National Engineering Laboratory, UK.
- (13) S.I. Krishnamachari
Applied Stress Analysis of Plastics
1st Edition 1993 pp. 449 - 544
L.J. Broutman & Associates Limited
- (14) Bajpai Mustoe and Walker
Specialist Techniques in Engineering Mathematics
1st Edition 1980 pp. 245 - 304
John Wiley and Sons
- (15) Alan Jeffrey
Mathematics for Engineers and Scientists
6th Edition 2005 pp. 464 - 503
Chapman and Hall
- (16) I.S. Sokolinkoff & R.M. Redheffer
Mathematics of Physics and Modern Engineering
1st Edition 1958 pp 367 - 370
McGraw-Hill Book Company, Inc.
- (17) B. Kroeze, A.H. Streppel and D. Lutters
Tools and accessories for press brakes.
Research paper
SheMet Conference 1994
- (18) A. Erman Tekaya
State of the Art of Simulation of Sheet Metal Forming
Research paper
SheMet conference, 1998.
- (19) Dr. Ir. F Hollander
Metal sheet: a dedicated resource.
Research paper
SheMet conference, 1996
- (20) Klingenberg, Singh, Urquhart.
A finite element simulation of free bending:
Research paper
SheMet conference: 1994
- (21) DeVin, Klingenberg, Singh
Air bending of sheet to large radii.
Research paper
SheMet conference: 1996
- (22) H. Hagenah, F. Backes.
Computer aided estimation of the achievable accuracy for bending parts.
Research paper
SheMet Conference, 1998
- (23) Dr-Ing. W. Heckel
In process measurement and spring back in sheet metal bending
Research paper
SheMet conference, 1996
-

-
- (24) L.J. DeVin, W. Urquhart, U.P. Singh
Adaptive control in the air bending.
Research paper
SheMet conference 1996.
- (25) D. Lutters, A.H. Streppel, B. Kroeze, H.J.J Kals.
Adaptive press brake control in air bending.
Research paper
SheMet conference, 1997
- (26) A.B.Perduijn, S.M. Hoogenboom.
The pure bending of sheet.
Research paper
SheMet Conference 1996
- (27) K. Anokye-Siribor, U.P. Singh.
Physical modelling of the air bending process.
Research paper
SheMet conference 1997.
- (28) A.G. Leacock, K.R. Gilmour, I.T. Laurenson, W. Urquhart.
An empirical model for the description of strain distribution during the punch stretch test.
Research paper
SheMet Conference, 1998.
- (29) Prof. Dr.-Ing. Klaus Siegert.
Tendencies in presses and dies for sheet metal forming processes.
Research paper
SheMet conference, 1998
- (30) J. Ferreira Duarte, A. Dias dos Santos, A. Barata da Rocha.
Formability analysis in sheet metal forming testing equipment.
Research paper
SheMet conference, 1994